Durham University

Durham E-Theses

STRUCTURAL STYLE AND TECTONIC EVOLUTION OF THE NORTHWEST SIRT BASIN–CRETACEOUS- TERTIARY RIFT, LIBYA

KHALIFA M. ABDUNASER KHALIFA

How to cite:

KHALIFA, KHALIFA M. ABDUNASER (2012) STRUCTURAL STYLE AND TECTONIC EVOLUTION OF THE NORTHWEST SIRT BASIN–CRETACEOUS- TERTIARY RIFT, LIBYA. Doctoral thesis, Durham University.

Use policy

The full-text may be used and/or reproduced, and given to third parties in any format or medium, without prior permission or charge, for personal research or study, educational, or not-for-profit purposes provided that:

- a full bibliographic reference is made to the original source
- a https://etheses.durham.ac.uk/id/eprint/4452/ is made to the metadata record in Durham E-Theses
- the full-text is not changed in any way

The full-text must not be sold in any format or medium without the formal permission of the copyright holders.

Please consult the full Durham E-Theses policy for further details.

Academic Support Office, The Palatine Centre, Durham University, Stockton Road, Durham, DH1 3LE
e-mail: e-theses.admin@durham.ac.uk Tel: +44 0191 334 6107
https://etheses.durham.ac.uk

DEPARTMENT OF EARTH SCIENCES, UNIVERSITY OF DURHAM

STRUCTURAL STYLE AND TECTONIC EVOLUTION OF THE NORTHWEST SIRT BASIN–CRETACEOUS-TERTIARY RIFT, LIBYA

A thesis submitted to the University of Durham
for the degree of Doctor of Philosophy in the
Faculty of Science

Khalifa Abdunaser

2012

ABSTRACT

The Cretaceous-Tertiary northwest-trending Sirt Basin system, Libya is a rift/sag basin formed on Pan-African to Paleozoic-aged basement of North Africa. This study is an investigation of the rift-basin architecture and tectonic framework of the western Sirt Basin. A combination of several geological and geophysical methods (remote sensing interpretation supported by surface geologic maps, borehole data analysis, from about 300 deep wells, extensive seismic reflection profiles and maps, and paleostress analysis), have been used to construct geological cross sections, and surface and subsurface geology maps that have proved particularly useful in identifying various regional and local structures in the study area. Indication of the relative timing of structures and movement along faults has been determined where possible.

We recognize six lithostratigraphic sequences (phases) in the area's stratigraphic framework. A Pre-graben (Pre-rift) initiation stage involved the Pre-Cretaceous sediments formed before the main Sirt Basin subsidence. Then followed a Cretaceous to Eocene graben-fill stage that can divided into four structurally-active and structurally-inactive periods, and finally a terminal continental siliciclastics-rich package representing the Eocene post-rift stage.

Late Eocene rocks exposed in the western part of the basin exhibit a complex network of branching segmented normal and strike-slip faults, generally with a NNW-SSE structural grain. Many surface structural features have been interpreted from satellite images which confirm sinistral strike-slip kinematics. Relay ramp structures, numerous elongate asymmetric synclines associated with shallow west limbs and steeper dipping east limbs are developed in the hangingwalls adjacent to west downthrowing normal faults. These structural patterns reflect Cretaceous/Tertiary extensional tectonics with additional control by underlying pre-existing Pan-African basement fabrics and ENE-WSW trending Hercynian structures.

The interpretation of a large volume of two-way time seismic data has allowed the construction of long regional seismic cross sections and resultant time structure contour and thickness maps, thus enabling an understanding of the structural and stratigraphic relationships on a regional scale.

Six major fault systems were identified initially from the remote sensing study and was subsequently expanded to seven on the basis of interpretation of 2D seismic data. These

fault systems dissect the study area into geomorphological elevated blocks and depressions. Most of the oil fields present in the study area are associated with structural hinge zones and adjoining highs.

A new kinematic and structural conceptual model is proposed here for the evolution of NW Libya (Jifarah Basin and the Nafusah Uplift) and Hun Graben during Late Eocene times.

The multidisciplinary approach used in this study has resulted in good surface and sub-surface structure correlation and future petroleum prospectivity has been identified in this study.

We relate the Sirt Basin rift development as exemplified in our study area to the break-up of Gondwana represented by the structural evolution of the West-Central African rift system and the South and Central Atlantic, the Tethys and the Indian Oceans.

TABLE OF CONTENTS

CHAPTER 1: INTRODUCTION 1

1.1 Review of hydrocarbon exploration and production history of Libya 1

1.2 Study aims 5

1.3 Location of the study area 5

1.4 Database and methodology 6

1.4.1 Remote sensing data 7

1.4.2 Borehole data 8

1.4.3 Seismic Data 10

1.4.4 Paleostress analysis 10

1.5 Summary 12

CHAPTER 2: TECTONO-STRATIGRAPHIC EVOLUTION 14

2.1 Regional Stratigraphy and Structures of Libya 14

2.1.1 Regional Stratigraphy of Sirt Basin 18

2.1.1.1 Surface geology 18

2.1.1.2 Subsurface Stratigraphy 20

2.1.1.3 Stratigraphy of the study area 28

2.1.2. Regional structure of Sirt Basin 32

2.1.3 Discussion and synthesis of published models 36

2.2.0 Summary 40

CHAPTER 3: PETROLEUM GEOLOGY OVERVIEW 42

3.1 Introduction 42

3.2. Petroleum Geology 48

3.3. Sirt Basin 50

3.4. Study area (western Sirt Basin) 53

3.4.1 Geochemistry of the source rocks 53

3.4.2 Sirte Shale source rock characteristics 53

3.4.3.1 Pre-Upper Cretaceous reservoirs 57
3.4.3.2 Gargaf quartzitic sandstone 57
3.4.3.3 Upper Cretaceous reservoirs 57
3.4.3.4 Paleocene reservoirs 59
3.4.3.5 Eocene reservoirs 61
3.4.4 Traps 61
3.4.5 Seals 63
3.4.6 Migration 63
3.5 Summary 64
CHAPTER 4: REMOTE SENSING DATA INTERPRETATION 66
4.1 Introduction 66
4.2 Surface structures 70
4.3 The major fault systems 72
4.3.1 Gedari fault system 72
4.3.2 Hun Graben fault system 77
4.3.3 East Waddan Uplift fault system 79
4.3.4 Qarat Ash Shush fault system 79
4.3.5 Ar Raqubah fault system 85
4.3.6 Zallah fault system 85
4.4 Basin elements and Geotectonics of the Area 88
4.4.1 Zallah Trough 90
4.4.2 Dur al Abd Trough 93
4.4.3 Az Zahrah-Al Hufrah Platform 95
4.4.4 Hun Graben 97
4.4.5 Waddan Uplift 98
4.4.6 Gattar Ridge 101
4.4.7 Maradah Trough 102
4.4.8 Al Hulayq Ridge 102

4.4.9 Al Qargaf Arch 104

4.5 Orientation analysis of the structural features 104

4.6 Relative timing and age of the structures within the study area 106

4.7 Significance of surface structure features for petroleum exploration in the study area 107

4.8 Summary 109

CHAPTER 5: SUBSURFACE (BOREHOLE DATA) ANALYSIS 111

5.1 Introduction 111

5.2 Contour maps interpretation 113

5.2.1 Basement map 113

5.2.2 Lower Cretaceous thickness map 114

5.2.3 Upper Cretaceous thickness map 115

5.2.4 Paleocene thickness map 116

5.2.5 Eocene thickness map 118

5.2.6 Oligocene-Miocene sediments 120

5.2.7 Cross section constructed from well data 120

5.3 Rifting phases 122

5.3.1 Pre-rift (Pre-Cretaceous) phase 122

5.3.2 Graben-fill phases 123

5.3.3 Rift initiation (Early Cretaceous) phase 123

5.3.4 Main syn-rift (Late Cretaceous) phase 125

5.3.5 Basin downwarping (Paleocene) phase 125

5.3.6 Fault reactivation (Eocene) phase 126

5.3.7 Basin tilting and volcanic eruption (Post-Eocene) phase 127

5.4 Discussion of Sirt Basin sub-surface structure and rifting 127

5.5 Summary 128

CHAPTER 6: SEISMIC DATA INTERPRETATION AND RESULTS 130
6.1 Introduction 130
6.2 Dataset 132
6.3 Well Correlations 133
6.4 Interpretation workflow and products 133
6.4.1 Principal horizons of the study area 134
6.4.2 Fault identification and analysis 136
6.4.2.1 Major seismic fault population 139
6.5 Seismic and geological cross sections correlation 139
6.5.1 Cross-section A-A' 140
6.5.2 Cross-section B-B' 145
6.5.3 Cross-section C-C' 149
6.5.4 Cross-section D-D' 152
6.6 Seismic subsurface maps 155
6.6.1 Time structure maps 156
6.6.1.1 Near base Kalash 156
6.6.1.2 Near top Dahra 157
6.6.1.3 Near top Hon 160
6.6.2 Isochron maps 160
6.6.2.1 Near top Satal to near base Kalash (Late Cretaceous to Early Paleocene) 162
6.6.2.2 Near top Harash to near top Zelten (Middle Paleocene to Late Paleocene). 163
6.6.2.3 Near top Hon to near top Facha (Late Lower Eocene to Early Upper Eocene). 164
6.6.3 Velocity analysis and isopach (Thickness) maps 164
6.6.3.1 Velocity analysis 166
6.6.3.1.1 Average velocity to the near base Kalash surface 166
6.6.3.1.2 Average velocity to the near top Hon surface 168

6.6.3.2 Isopach (Thickness) maps....168

6.6.3.2.1 Near top Satal (base Kalash to top Satal) (Late Cretaceous to Early Paleocene)....169

6.6.3.2.2 Near top Hon to near top Facha (Late Lower Eocene to Early Upper Eocene)....172

6.7 Summary....172

CHAPTER 7: PALEOSTRESS ANALYSIS....174

7.1 Introduction....174

7.2 Data processing and results....176

7.2.1 Stress inversion techniques....176

7.2.2 Fault geometry analysis....177

7.2.3 Stress analysis....177

7.2.3.1 Simple shear tensor average....177

7.3 Testing regional tectonic models....178

7.3.1 Previous results from the Hun Graben, western Sirt Basin....182

7.4 The present study results....184

7.4.1 Inversion procedures....185

7.4.2 Whole Hun Graben....185

7.4.3 Paleostress tensor analysis along Eastern Fault Zone (EFZ):....188

7.4.4 Paleostress tensor analysis along West Fault Zone (WFZ)....189

7.4.5 Summary and discussion of Hun Graben....190

7.5 Northwest Libya (Jifarah Basin and Nafusah Uplift)....194

7.6 The present study results....196

7.6.1 Inversion Procedures....197

7.6.2 Whole study area....197

7.6.3 Paleostress tensor analysis along Al Azizyah fault zone (AZFZ), site 1 & 2....198

7.6.4 Paleostress tensor analysis of Jabal Nafusah escarpment fault zone (JEFZ), sites 3 & 4....199

7.6.5 Paleostress tensor analysis of Jabal Nafusah uplift along Gharyan fault zone (GFZ), sites 5 to 9 200

7.6.6 Paleostress tensor analysis of Jabal Nafusah uplift along Wadi Ghan fault zone (WFZ), site 10 200

7.7 Summary and discussion of northwest Libya 201

7.7.1 Extension regimes 203

7.7.2 Compressional regime 204

7.8 Summary 206

CHAPTER 8: DISCUSSION 207

8.1 Introduction 207

8.2 Major structural elements in the western Sirt Basin 207

8.3 Fault and fold geometries, ... 211

8.4 Rift basin infill model for the NW Sirt Basin 215

8.4.1 Mesozoic rifting and continental break-up 216

8.4.1.1 Permo Triassic rifting 216

8.4.1.2 Cretaceous rifting 218

8.4.1.3 Latest Cretaceous and Cenozoic evolution: thermal sag, fault reactivation and inversion. 221

8.5 Hun Graben and northwest Libya (Jifarah Basin and Nafusah Uplift) relationship 223

8.6 Geometry and kinematic model for the NW Libya in response to Hun Graben, W. Sirt Basin 226

8.7 Surface and sub-surface structure correlation and their petroleum prospectivity. 229

CHAPTER 9: CONCLUSIONS AND FUTURE WORK 232

9.1 Conclusions 232

9.2 Future work 234

APPENDIX 1 236

Teknica seismic data reprocessing 236

Mis-tie derived seismic interpretation problems 236

General overview of mis-ties 237

Seismic survey static correction parameters: The datum plane and elevation or replacement velocity 240

The datum plane adjustment algorithm (with examples).....242

Summary of mis-tie resolution 243

Mis-tie recommendations.....244

REFERENCES.....245

LIST OF FIGURES

Fig. 1.1 Generalized tectonic map of Libya... 2
Fig. 1.2 Data used in this study.. 8
Fig. 1.3 Simplified surface geologic map. 9
Fig. 1.4 Generalized tectonic map of the western Sirt Basin. 11
Fig. 1.5 Data from Google EarthTM imagery 12
Fig. 1.6 MrSid images of the study area. 13
Fig. 2.1 Geological map of Libya. 14
Fig. 2.2 Digital shaded-elevation model (DEM) map of Libya 15
Fig. 2.3 Generalized structural map and the main sedimentary basins of Libya.. 16
Fig. 2.4 Surface and subsurface columnar stratigraphy for the study area. 23
Fig. 2.5 3D perspective image shows depth to basement of the structural domains of the Sirt Basin 24
Fig. 2.6 Generalized structural map of the Sirt Basin. 25
Fig. 2.7 The tectonic framwork of Sirt Basin. 34
Fig. 2.8 The three subsurface arms define a large triple junction. 35
Fig. 2.9 Rifting episodes of Sirt Basin. 39
Fig. 2.10 Major structural elements of Libya. 40
Fig. 3.1 Sirte Shale thickness map of Sirt Basin. . 45
Fig. 3.2 Sirte Shale thermal maturity map of Sirt Basin.. 50
Fig. 3.3 Western Sirt Basin oil kitchen and migration directions map. 52
Fig. 3.5 Gross thickness map of the Sirte Shale in the study area. 55
Fig. 3.4 Gross thickness map of the Sirte Shale of the study area. 55
Fig. 3.6 Map of the thermal maturity for three wells in the study area 56
Fig. 3.7 Map of source rock richness (TOC). 56
Fig. 3.8 Subsurface columnar stratigraphy for the study area 58
Fig. 3.9 Generalized tectonic map of the western Sirt Basin shows the location of the main oil and gas fields. 60
Fig. 4. 1 Data from Google EarthTM imagery covers the study area 66
Fig. 4.2 MrSid imagery covers the study area.. 67
Fig. 4.3 Structural interpretation map of surface faults and folds. 69
Fig. 4.4 Overview structural map of the major faults with established sense of displacement and folds.. 70
Fig. 4.5 Location map for images presented later. 71
Fig. 4.6 Location map of the main interpreted fault systems and folds. 71
Fig. 4.7 Examples of fault related folds. 74
Fig. 4.8 Example of basalt lavas eruptions 76
Fig. 4.9 S Segmented normal faults with relay ramp structures associated with horsetail splay faults 78
Fig. 4.10 (A): Example of sinistral strike-slip faults. Left lateral horizontal displacement of strata. 80
Fig. 4.10 (B): Example of sinistral strike-slip faults. Wadis (valleys) horizontal displacement. 81
Fig. 4. 11a Example of relay ramp structures 82

Fig. 4. 11b Example of relay ramp structures with adjacent elongated synclines. 83
Fig. 4.12 Segmented faults bounding the Hun Graben. 84
Fig. 4.13 Satellite imagery interpretation of the northern end of the western margin of the Hun Graben..... 85
Fig. 4.14 Satellite imagery and it's interpretation of the southern portion of the Hun Graben 86
Fig. 4.15 Anticlines and synclines belong to the southern tip of the Waddan Uplift. 87
Fig. 4.16 Example of horse-tail structures. 89
Fig. 4.17 Synclines and anticlines located in the south Ar Raqubah area. 91
Fig. 4.18 Map of Zallah Trough structural subdivisions.. 92
Fig. 4.19 Large triangular bedding facets or 'flat-irons'..... 94
Fig. 4.20 Map of the early opening phase of the South Atlantic. 97
Fig. 4.21 Satellite (MrSid) imagery of the northern end of Az Zahrah-Al Hufrah Platform. 99
Fig. 4.22 Satellite (MrSid) imagery of the combination of the NNW-SSE and ENE-WSW trending faults.. 100
Fig. 4.23 Satellite (Google Earth) imagery of wadis along the eastern margin of the Hun Graben.. 101
Fig. 4.24 Satellite (MrSid) imagery showing the shape of wadis (valleys). 103
Fig. 4.25a-e 4.25a-e Rose diagrams in various parts of the study area..... 105
Fig. 5.1 Stratigraphical Comparison of two deep wells..... 112
Fig. 5.2 Contour map of the top of the basement of the study area.. 113
Fig. 5.3 Isopach and structural thickness map of Lower Cretaceous time for the study area..... 115
Fig. 5.4 Isopach and structural thickness map of Upper Cretaceous time for the study area..... 117
Fig. 5.5 Isopach and structural thickness map of Paleocene time for the study area.... 119
Fig. 5.6 Isopach and structural thickness map of Eocene time for the study area. 121
Fig. 5.7 Geological cross section. 124
Fig.6.1 The major faults interpreted from seismic data overlaid on simplified tectonic elements map of the study area..... 131
Fig.6.2 Some sonic wells used as well to seismic correlation. 134
Fig. 6.3 Typical workflow for interpreting horizons 136
Fig.6.4 Workflow for interpreting faults..... 138
Fig.6.5 Map of fault cuts on a series of 2D-seismic lines.. 138
Fig.6.6 Seismic cross section A-A'..... 144
Fig. 6.7 Geological cross section A-A'). 144
Fig. 6.8 Seismic cross section B-B'. 146
Fig. 6.9 Geological cross section B-B' 146
Fig. 6.10 Seismic cross section C-C' 151
Fig. 6.11 Geological cross section C-C'. 151
Fig. 6.12 Seismic cross section D-D'..... 154
Fig. 6.13 Geological cross section D-D'..... 154

Fig. 6.14 The time contour map of near base Kalash.....158
Fig. 6.15 The time structure contour map of near base Kalash.....158
Fig. 6.16 The time contour map of near top Dahra.....159
Fig. 6.17 The time structure contour map of Near Top Dahra.....159
Fig. 6.18 The time contour map of near top Hon.....161
Fig. 6.19 The time structure contour map of near top Hon.....161
Fig. 6.20 The near top Satal to near base Kalash isochron contour map. 162
Fig. 6.21 The near top Harash to near top Zelten isochron contour map.....164
Fig. 6.22 The near top Hon to near top Facha isochron contour map.....165
Fig. 6.23 The average velocity to the near base Kalash surface contour map. 169
Fig. 6.24 The average velocity to the near top Hon surface contour map. 170
Fig. 6.25 The near base Kalash to near top Satal thickness contour map. 171
Fig. 6.26 The near top Hon to near top Facha thickness contour map.....171
Fig. 7.1 Geological map of Hun Graben).....179
Fig. 7.2 Generalized tectonic map for the northwestern Libya.....179
Fig. 7.3 Interpretation of Sirt Basin relative to the Sabratah Basin and Cyrenaican Platform. 180
Fig. 7.4 Results of different stress phases of Hun Graben. System 1: Left normal dip-slip faults.....187
Fig. 7.5 Results of different stress phases of Hun Graben. System 2: Normal dip-slip faults.. 188
Fig. 7.6 Results of different stress phases of the Eastern Fault Zone (EFZ) of Hun Graben. System 3: Left Normal strike-slip faults.....189
Fig. 7.7 Results of different stress phases of the Eastern Fault Zone (EFZ) of Hun Graben. Left Normal strike-slip faults 190
Fig. 7.8 Results of different stress phases of Hun Graben. The Eastern Fault Zone (EFZ) of Hun Graben without area 1&2.. 191
Fig. 7.9 Results of different stress phases of Hun Graben. The West Fault Zone (WFZ). 192
Fig. 7.10 Results of different stress phases of northwest Libya (Jifarah Basin and Nafusah Uplift). System 1: Normal dip-slip faults.....198
Fig. 7.11 Results of different stress phases of northwest Libya (Jifarah Basin and Nafusah Uplift). System 2: Right normal dip-slip faults.....200
Fig. 7.12 Results of different stress phases of northwest Libya (along Al Azizyah fault zone (AZFZ), site 1&2, Jifarah Basin). Areas 1&2.....201
Fig. 7.13 Results of different stress phases of northwest Libya (Jifarah Basin and Nafusah Uplift). Areas 3&4.). 202
Fig. 7. 14 Results of different stress phases of northwest Libya (Jifarah Basin and Nafusah Uplift). Areas 5 to 9.....203
Fig. 7.15 Results of different stress phases of northwest Libya (Jifarah Basin and Nafusah Uplift). Area 10.. 204
Fig. 7.16 Results of different stress phases of northwest Libya (Jifarah Basin and Nafusah Uplift). All NW Libya data after misfit.....205
Fig. 7.17 The phases of the pure extension and compression of NW Libya.....205

Fig. 8.1 (A) Schematic E-W cross section of Sirt Basin.....208
Fig. 8.2 Geological cross sections.....210
Fig.8.3 The main boundaries of the geomorphological elevated blocks and depressions of the study area.....211
Fig. 8.4 Polyphase tectonic model for the study area. 217
Fig. 8.5 The hypothezed structural model of the NW Libya and Hun Graben. 225

LIST OF TABLES

Table 2.1 The exposed sedimentary rocks of the study area.....19
Table 3.1 The principal petroleum systems in Libya. 43
Table 3.2 Libya Total Oil Reserves by Region.....44
Table 3.3 Libya, Total Oil Reserves, by Reservoir Age. 44
Table 6. 1 The interpreted horizons. 135
Table 6.2 The seismic and geological data used to construct cross sections. 141
Table 6.3 The sonic wells used to calculate velocity and depth to near base Kalash surface.....166
Table 6.4 The sonic wells used to calculate velocity and depth to near top Hon surface. 167
Table 7.1 Results of the reduced Paleostress tensors from fault-slip data of the Hun Graben. 187
Table 7.2 Results of the reduced Paleostress tensors from fault-slip data of NW Libya 199
Table 8.1 Tectonosedimentary events and its influence on Sirt Basin 219

Acknowledgements

Firstly I would like to express my thanks and appreciations to my supervisor, Ken McCaffrey for his support guidance and encouragement, and also for his honest criticisms, during my project. I'd also like to extend my thanks to Richard Hobbs, for all of his help, especially when he managed to get well data tied to the nearest seismic lines. To the Management of Libyan Petroleum Institute and National Oil Corporation, Libya for their support throughout the study and for allowing me to use the seismic and well data and sponsorship during my study. My gratitude goes to my colleagues Abdulbaset Abadi and Laila Gamberlu at Libyan Petroleum Institute, for providing me with their paleostress data used as a part of this work.

Thanks of course to all my friends and colleagues at Durham and all of the other people I have met in the department. These people really were the supporters that gave me patience to complete this thesis.

A big thanks to my family (wife, and my children) for helping me whenever I needed and for giving me moral and constant support during the most difficult moments of this project and I am sincerely indebted to them all.

At the end, I give thanks to God for giving me the means, the skills and the courage to complete my thesis and my degree.

Declaration

No part of this thesis has previously been submitted for a degree at this or any other university. The work described in this thesis is entirely that of the author, except where reference is made to previously published or unpublished work.

Khalifa M. Abdunaser
University of Durham
Department of Earth Sciences
July 2012

Copyright © by Khalifa M. Abdunaser

The copyright of this thesis rests with the author. No quotation or data from it should be published without the author's prior written consent and any information derived from it should be acknowledged.

CHAPTER 1: INTRODUCTION

Libya is the second-largest oil producer in Africa but remains "highly unexplored" according to reports by *Wood Mackenzie*, with only around 25 percent of Libya covered by exploration agreements with oil companies. It is well known that sedimentary basins related to extensional tectonics contain a significant volume of the world's oil reserves (e.g., North Sea, Gulf of Suez; Harding and Lowell, 1979; Harding, 1983) and the Sirt Basin of Libya is one of these important oil basins. For example, oil reserves discovered to the end of 2006 in Libya are reported as 41 billion bbls (*Oil and Gas Journal OGJ 2007)* and the Sirt Basin represents almost 87% of the total oil reserves for all the producing basins in Libya. Moreover, the Libyan national corporation (NOC, 2007) estimates the future undiscovered oil potential for all of the Sirt Basin to be at 24 billion bbls OOIP and 10% of it will probably be provided by the western part of the Sirt Basin (study area). The Sirt Basin is therefore the most prolific petroleum province located within the North African passive (Fig. 1.1) continental margin and is considered to be a holotype of a continental rift (extensional) area and is referred to as part of the Tethyan rift system (Futyan and Jawzi, 1996; Guiraud and Bosworth, 1997). Recent detailed studies on a number of continental margin rifts have shed considerable light on the architecture and evolution of these types of basins (e.g., Rosendahl, 1987; Morley, 1995).

This study, and resultant report, contributes new findings based on an integrated approach utilizing data from the various disciplines of geology and geophysics. The aim of the study is to critically review the existing body of knowledge on the petroleum geology of the western part of the Sirt Basin and to build a new understanding based on my own interpretations of seismic data, remote sensing and borehole data. These new insights provide a basis for a new exploration strategy that could stimulate future exploration activities in the study area.

1.1 Review of hydrocarbon exploration and production history of Libya

It is reported that the first show of hydrocarbons in Libya was a gas flow from shallow depths in a well drilled in 1914 at Sidi Missri, near Tripoli (Waddams, 1980). Non productive gas and oil shows were reported from shallow wells drilled in Miocene strata in the Tripoli area since 1914 (Crema, 1926). Knowledge of the geology of the country became clearer after the independence by the United Nations in 1951.

The 1950's saw active exploration in eastern Algeria and western Libya. At this time aerial photography and airborne magnetometer surveys were used extensively over most of Libya alongside topographic surveys and intensive field geology programmes.

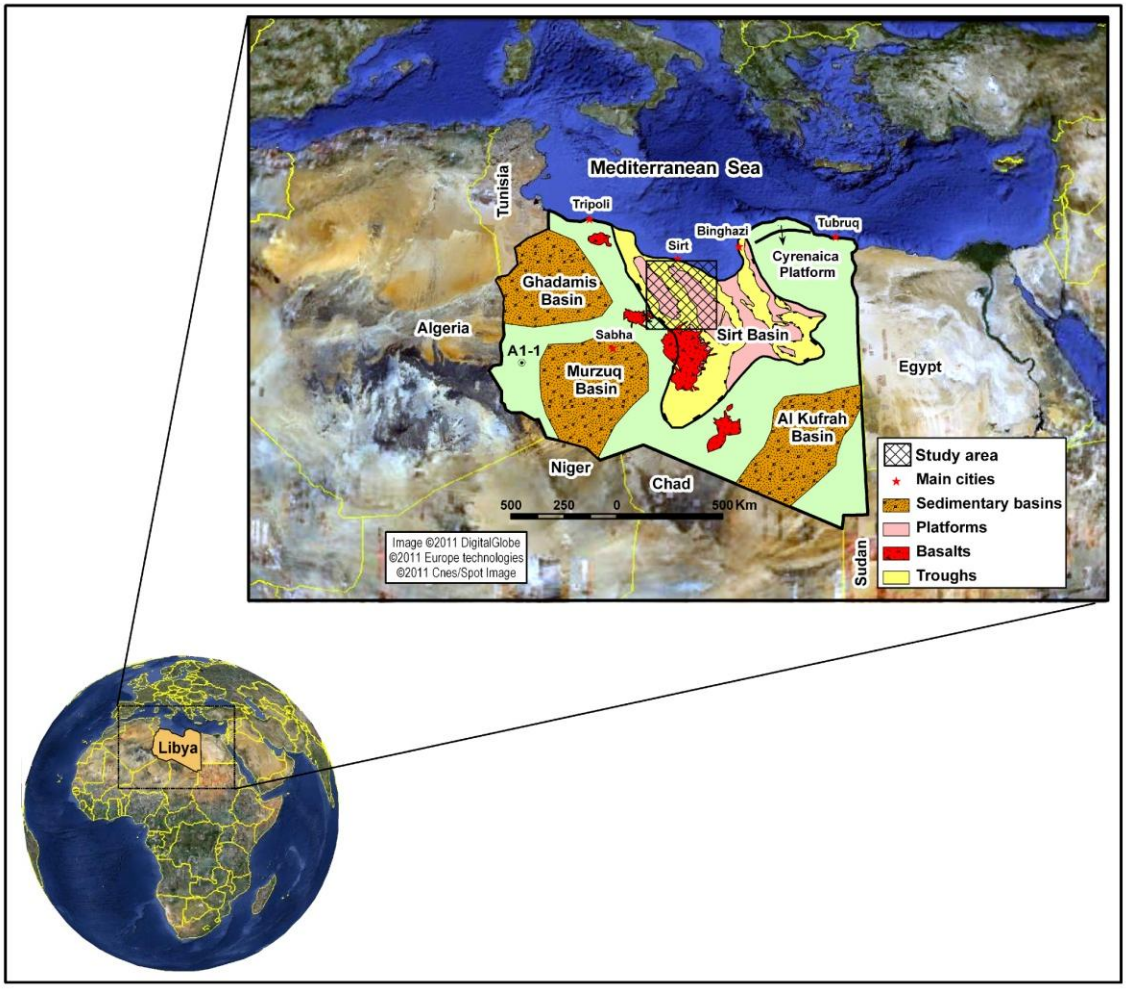


Fig. 1.1 Generalized tectonic map of Libya as located in the north central Africa showing the major structural elements and main sedimentary basins of Libya (modified after Mouzughi, and Taleb1981 and Abadi, 2002). Marked box represents the study area. Well A1-1 is shown in the northwestern Murzuq Basin.

This set the stage for Libya to initiate a policy for the exploration of hydrocarbon reserves. The passing of the Petroleum Law No. 25 by Libya in 1955, established a policy for foreign oil companies to obtain concessions to perform exploration activities in the search for oil and gas reserves.

In 1956, gravity and ground magnetometer surveys commenced and much of Libya was covered, and seismic techniques were also used for the first time. The first grant of concessions occurred in 1955/6 where nine operators applied successfully for a total of 489 concessions covering 36% of the entire country. Subsequent annual grants were made and by late 1962 about 60% of the territory of Libya was under concession. Exploration activities started in the western part of the Ghadamis Basin, where

prospective geologic trends were extrapolated from the adjoining Algerian discoveries of Zarzaitine and Tiguentourine oifields.

Esso Standard in 1958 made the first oil discovery in Devonian age sandstones in the Atshan area (A1-1 well). This well is located in Concession 1 in western Libya adjacent to and just across the border from eastern Algeria (Fig. 1.1). According to Fraser (1967) this well produced oil at the rate of 508 barrels per day on test. The discovery, however, did not generate much interest amongst the oil industry because it was some 660 kilometers from the coast and 730 kilometers from Tripoli. Also in 1958, the first significant oil discovery was made in the Sirt Basin by the OASIS Oil Company in their A1-32 well. The well discovered oil in the Upper Cretaceous Bahi Sandstone that was later developed as the Bahi and Az Zahrah Fields.

Following these successes, the industry concentrated on the Sirt region, which resulted in the discovery, in 1959, of Zelten in the C1-6 well in Concession 6 in the Sirt Basin. Well C1-6 tested 17,500 barrels of oil per day and Libya's destiny as a major oil producing country was demonstrated (Fraser, 1967). After the success of these discoveries, there was an increase in exploration activities in the Sirt Basin with drilling programs continuing into the late 1950s and beyond. In the 3 year period 1959 to 1962, a total of 247 new field wildcat wells resulted in 51 oil discoveries. Of a total of 534 wells of all types drilled, 248 were successful. Each year for 5 years after the discovery of Zelten, a billion barrel oil field was discovered in the Sirt Basin. Success to some degree was gained by all of the original 9 concessionaires. During the 1960s several oil deposits were discovered in western Libya, but only the El Hamra and Tigi fields of the Ghadamis Basin were commercial. The first shipment of Libyan crude to world markets was made from the Zelten Field in 1961. By 1962 crude shipments (from this and other fields) averaged 236,000 BOPD. In 1963, the peak exploration drilling rate (120 wells per annum) was achieved. By the end of 1963 more than 20 billion barrels of recoverable oil had been discovered. Production increased annually until 1970 when a peak of 3.3 million barrels of oil per day was reached and Libya was the fourth largest oil exporter in the world. During this period at least 30 exploration wells were drilled per annum. By 1969, 33 billion barrels of recoverable oil had been discovered.

During the 1970s and 1980s, the National Oil Corporation (NOC) established additional petroleum laws aimed at exercising control over the petroleum industry in Libya, including the nationalization of several foreign oil companies followed by a name change (e.g., BP became AGOCO and Amoseas became Umm Al Jawaby). Also at that time, the NOC signed partnership agreements with other oil companies, for example,

getting 51% ownership of Esso (in Libya) through the establishment of the Sirte Oil Company (SOC).

Following these changes production declined at an average annual rate of 14% for many years. During the 1970s average production was 1.8 million barrels of oil per day. From 1982 until the present, production rates have no longer been primarily determined by technical production capacity but by OPEC quotas; during this period production rates have been between 1 and 1.5 million barrels per day. In the 1980's geological and exploration activity was undertaken by local, eastern European and Russian scientists. The Romanians and Bulgarians made discoveries in the Ghadamis and Murzuq basins leading ultimately to the development of the El Sharara Field in the Murzuq. Trading sanctions were imposed early in the 1980s and then, following the ban by the United States government on the operation of American oil companies in Libya in 1986, exploration and production activities were mainly carried out by the NOC and its joint venture companies Agoco (ex BP), Veba Exploration (ex Mobil Libya), Zueitina Oil Company (ex Oxy Libya), Waha Oil Company (ex Oasis) and Sirte Oil Company (ex Esso). European oil companies became increasingly active and in the 1990s. Lundin's oil company discovered and developed a field in the Sirt and LASMO discovered the Elephant field in the Murzuq. International sanctions continued to restrict commercial activity in Libya, however, throughout the 1990s and in 2000 the UN sanctions were lifted. US legislation (the Iran Libya Sanctions Act –ILSA) placed restrictions on trading partners of the US as well, so its effects were comprehensive. The lifting of the US State Department restrictions on US companies working in Libya resulted in a rapid growth in exploration and production activity in the country.

Libyan authorities in 1999 decided to extend their future production profile resulting in the offer to international oil companies of a chance to acquire vast areas of unlicensed acreage in all of the oil-producing basins in Libya. In 2000, the block divisions were announced and included 70 blocks in the Sirt Basin, 20 in Ghadames, 16 in Murzuq, 10 on the Cyrenaican Platform, 3 in the Tripolitanian Basin and 17 Offshore. New play concepts developed between 1979 and 2000 have undoubtedly contributed to recent successes, through fruitful collaborations between oil companies and academia.

A new phase in the exploration of this vast country has been marked by the return of Libya to the international exploration arena with bid rounds in 2005 and 2006 and the arrival of new major international oil companies. Infrastructure developed over recent years, including a subsurface gas pipeline to Italy and, most recently, an upgrade to refining facilities by International Oil Companies, meaning that emerging basins will be

well served and are thus become increasingly attractive. Many international surveys conducted in the last seven years have consistently ranked Libya as one of the top destinations for International Oil Companies for new oil exploration.

1.2 Study aims

The aim for the present study is to understand the detailed structure and tectonic development of the western part of Sirt Basin, using an extensive geological and geophysical database to investigate the significance of surface lineaments and fractures, their correlation with subsurface structures and their ability to delineate oil and gas reservoirs in the area.

The main objectives are:-

1) Conduct interpretation of seismic data (i.e., horizons, faults, sequence boundaries).
2) Prepare regional geologic cross-sections (structural and stratigraphic) showing stratigraphic correlations, major sequences and structures.
3) Prepare maps showing regional structural trends and their sedimentary responses.
4) Integrate a large amount of surface lineaments, surface major fracture zones, surface fracture traces, and seismic lineaments, and Precambrian basement fault systems.
5) An orientation analysis of these surface and subsurface linear features will be performed to detect the basic structural grain in the region.
6) Correlation between surface linear features and subsurface oil and gas traps will be assessed.
7) Construct conceptual tectonic models to explain the data.

1.3 Location of the study area

The Sirt Basin in north-central Libya (Fig. 1.1) covers an approximately 600 000 km² area that is bordered to the east by the block-faulted region of the Cyrenaican Platform, including AI Jabal al Akhdar, and extend as far as the Dakhla Basin in Egypt. It is bounded to the south by the Tibisti Mountains and the Al Kufrah Basin to the south, to the west by the Nafusah and Al Qargaf Arch, and the Ghadamis-As Sawda and Murzuq Basin, and the Mediterranean Sea to the north. This study is focusing mainly on north western Sirt Basin, Libya between 15°00’ E to 18°30’ E and 28°00’ N to 31°30’ N (Fig. 1.1).

1.4 Database and methodology

A large database containing information about structural features such as faults, folds and fractures was produced in the form of GIS thematic layers enabling interpretation and analysis. This information was then integrated using GIS software and used to construct a range of thematic maps. Seismic reflection profiles and well logs, plus other data such as remote sensing imagery, scaled and co-registered with the interpretation, using ArcGIS software were the main datasets used in this project. The inter-relationship between surface structural features, seen mainly in the horizontal plane (satellite imagery), and subsurface features seen mainly in the vertical plane (seismic in addition to well data) was established and showed good consistency.

The large amount of data that is collected in a typical exploration area, such as data from remote sensing, boreholes, geophysical (seismic lines), geological and topographical maps, etc. mean it is necessary to use some sort of geospatial database system. Geographical Information Systems (GIS) have proved to be ideal for that purpose (Gustafsson, 1993). A GIS can be used for data capture, storage, analyses, prognostication, presentation, and follow-up and constitutes an excellent tool for modelling work. It is important to start building the GIS database at an early stage of any project, enabling data interpretation and prognostication as soon as enough data have been entered into the system.

Once the core of the database is established, it is easy to complement the data or add new types of data, with immediate data interpretation and subsequent improvement of prognoses. It is important to regard the GIS as a dynamic or "live" database, reflecting the present knowledge of a project area, rather than just a tool for producing colourful maps and impressive data tables in the final stages of a project (Gustafsson, 1993).

In this study the following data have been incorporated into the ArcGIS database:

- Formation tops, lithology, many of them reach to basement
- 500 oil and gas wells
- 2D seismic data consisting of 252 lines totalling approximately 5000 km.
- 8 sonic logs and density logs existed for 4 wells
- Satellite Imagery
- Surface geology map (scale 1:250,000)
- Base maps showing the location of these datasets

The project also had access to the following reports courtesy of the Libyan Petroleum Institute (LPI):

- Geochemical study by Robertson Research, 1989.
- Geochemical study by LPI, 1985
- Published geological papers
- Surface geology maps and explanation booklets by Industrial Research Centre

Map data compiled for the GIS database (Fig. 1.2) include nine 1:250,000-scale of Industrial Research Centre, Libya. The geological maps were digitally trimmed and sliced seamlessly together, then geographically registered to provide an accurate base map for the geology and for borehole locations. This led to the production of a regional surface geology map of the study area (Fig. 1.3) which also complimented the remote sensing interpretation.

The GIS database provides the capability of automatically displaying borehole locations and attributes in relation to seismic line distribution, geology, or any other mapped features, and for quickly retrieving and displaying boreholes selected to constrain geological cross-sections (Fig. 1.4).

1.4.1 Remote sensing data

The main purpose of conducting a remote sensing interpretation is to identify faults and fractures as well as major stratigraphic boundaries. Data from Google Earth™ imagery that covers the study area were used for the remote sensing component of this study because it provided the highest resolution data and is available free (Fig. 1.5). Most areas are covered in satellite imagery with a resolution of about 15 m per pixel. This base imagery is 30m multispectral Landsat™ which is sharpened with 15m [panchromatic] Landsat imagery. However, Google™ is actively replacing the base imagery in this region with 2.5m SPOT™ data. MrSid images (Fig. 1.6) covering the area were also used to provide more information on structural phenomena in the study area.

The structural interpretation was performed digitally on-screen using ArcGIS software and then summarized as major faults in the region. The interpretation benefited from the fault/fracture information that was derived from the high resolution SPOT satellite imagery. This helped to identify faults and fractures not visible on the Landsat TM optical imagery. The satellite imagery provided effective images on which to map the surface geological structure and geomorphology of the region and therefore enables validation of existing geological mapping.

In addition to the satellite imagery, 1:250,000 scale published geological maps and accompanying reports were also used during the interpretation. The maps were scanned and geo-referenced to the satellite imagery.

An orientation analysis was performed, and correlations between surface and subsurface structures as well as between surface structures and subsurface oil and gas traps were investigated. The significance of using surface faults and fracture analysis for delineating additional traps in the region was assessed.

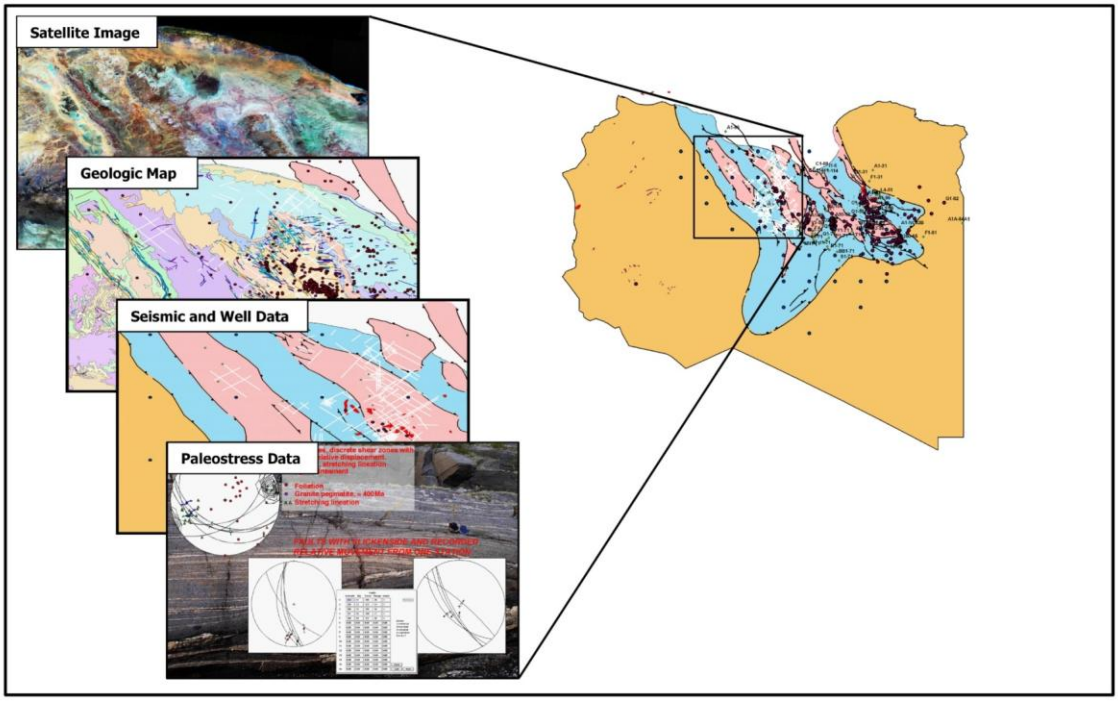


Fig. 1.2 Map of Libya shows the location of study area and data types used in this study.

1.4.2 Borehole data

All oil and gas borehole data were used in this study provided by Libyan Petroleum Institute and national oil companies. A database of formation tops of 500 wells was made available to the author. Well formation tops are markers that specify where a well intersects stratigraphic horizons, faults or other structural features. After eliminating many wells which were either very close to each other, or very shallow, a total of 300 wells were analysed and used. Eight sonic logs with full stratigraphical column are located randomly within the study area (Fig. 1.4). These were converted to synthetic seismograms that were tied to the nearest seismic lines and this distant correlation was very productive.

The well headers and formation tops were primarily used in this project to associate the position of the wells with the interpreted reflective horizons that were mapped on the seismic lines in the Landmark Seisworks/2D software. The well headers are ASCII files

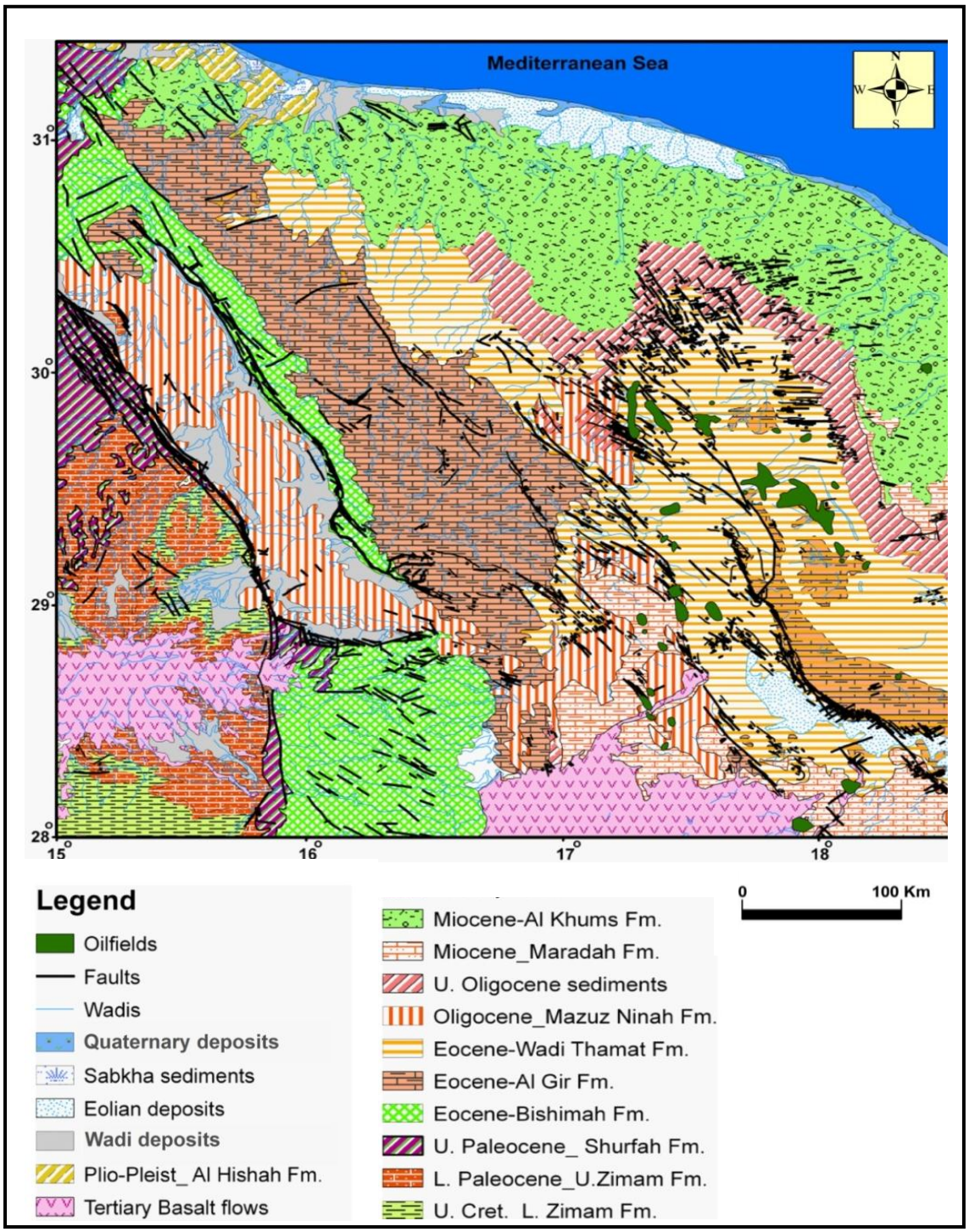


Fig. 1.3 Simplified surface geologic map of study area shows the exposed rock units, wells, and oil fields compiled after Vesely, (1985), Jurak, (1985) and Anketell and Kumati, (1991b).

containing the well's top position (X-Y-Z), length of the well path (measured depth or MD), well name and optionally a well symbol. The wells did not have any path deviation and were vertical upon import in Landmark Seisworks/2D software.

Numerous subsurface geologic maps (Isopachs, structural and contour maps) were constructed based on the available well data to determine the distribution of rock layers, their thickness variations, and their attitudes (structure).

1.4.3 Seismic Data

One of the main objectives of the project was to integrate the surface and subsurface geology in the western Sirt Basin by correlating the seismic dataset with the well data. The combined dataset was used for seismic analysis and interpretation in Landmark Seisworks/2D software to define the subsurface structural configuration of the study area.

The 2D seismic dataset used for this seismic interpretation was made available through the Libyan Petroleum Institute and were extracted from many surveys acquired between the mid-1960's and the late 1990's, by different oil companies.

For the purpose of this study, a total of 253 seismic lines of 2D data totaling approximately 5000 km from the survey were interpreted with the majority of them running in an east-west trend, orthogonal to the strike of the basin's major fault system (Fig. 1.4). Geologic information became sparse as the seismic interpretation was pushed westward through the complex basin due to a lack of seismic data. This placed some limitation on the accuracy of picking horizons across the entire study area, especially across syn-depositonal faults.

1.4.4 Paleostress analysis

The qualitative and quantitative analyses of brittle structures can provides a reliable key to understanding the distribution and evolution of paleostress fields through successive tectonic events (Angelier, 1989). Thus a paleostress reconstruction provides an interpretation of the stress conditions in the past. The method involves determining the stress axes directly from field observations and measurements. Thus, making detailed observations of fault-slip data on available outcrops based allows the reconstruction of some major characteristics of the tectonism. This study presents paleostress results from fault-slip data collected by Abadi (2002) & Gamberlu, (2007) on U. Cretaceous-Tertiary sediments in the western portion of Sirt Basin and the NW Libya (Jifarah Basin and Jabal Nafusah Uplift). The two datasets provides an opportunity to perform a correlated

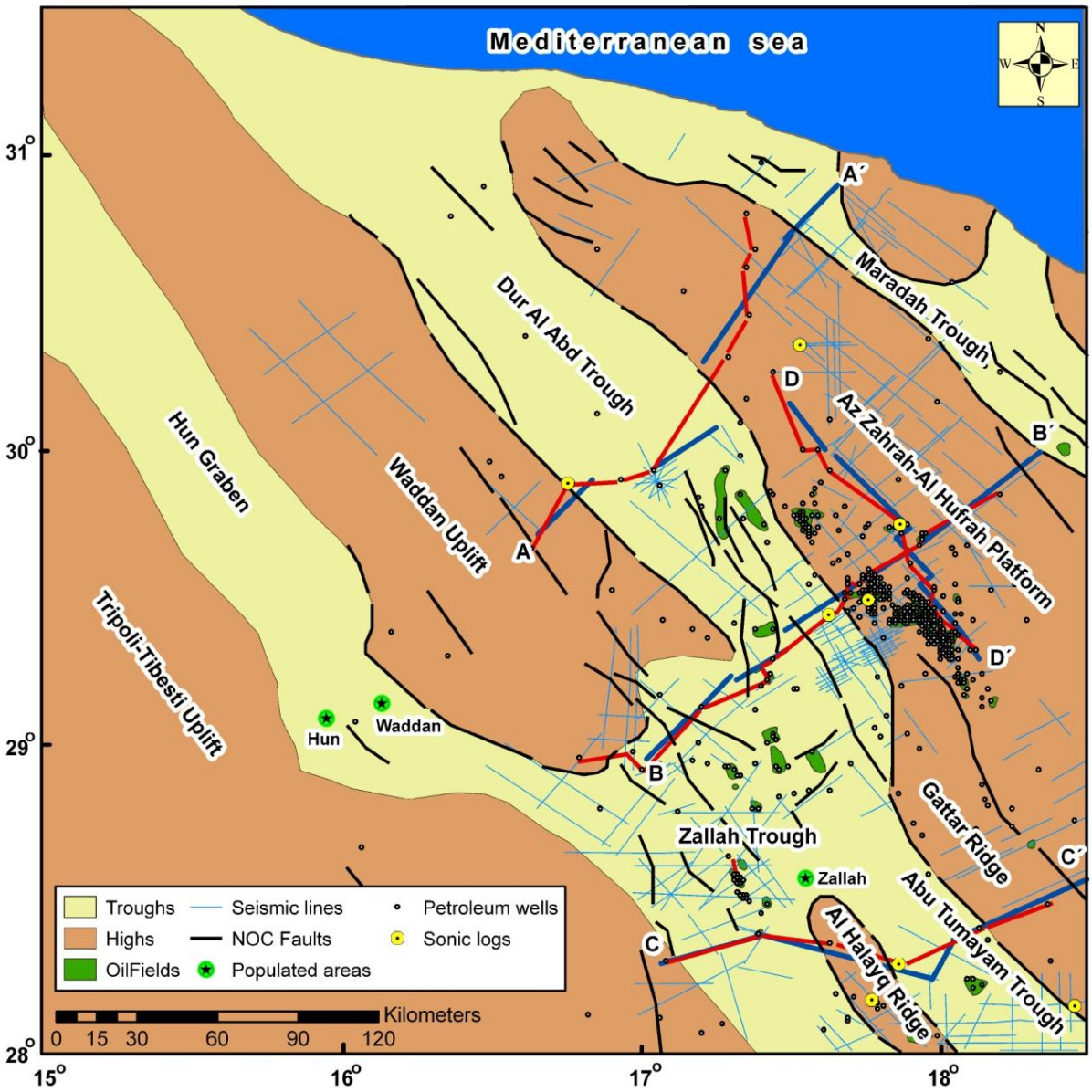


Fig. 1.4 Generalized tectonic map of the western Sirt Basin showing the location of seismic and well data in addition to oil and gas fields used in this study overlaid on National Oil Corporation (NOC) tectonic elements (modified after Mouzughi, and Taleb1981 and Abadi, 2002).

study to define the relationship between these two areas – one inside the Sirt Basin and one outside. Analysis of petroleum exploration data supplemented by outcrop-derived paleostress data informed the development of the conceptual tectonic models and provides insights into the origin of the deformation observed in the study area.

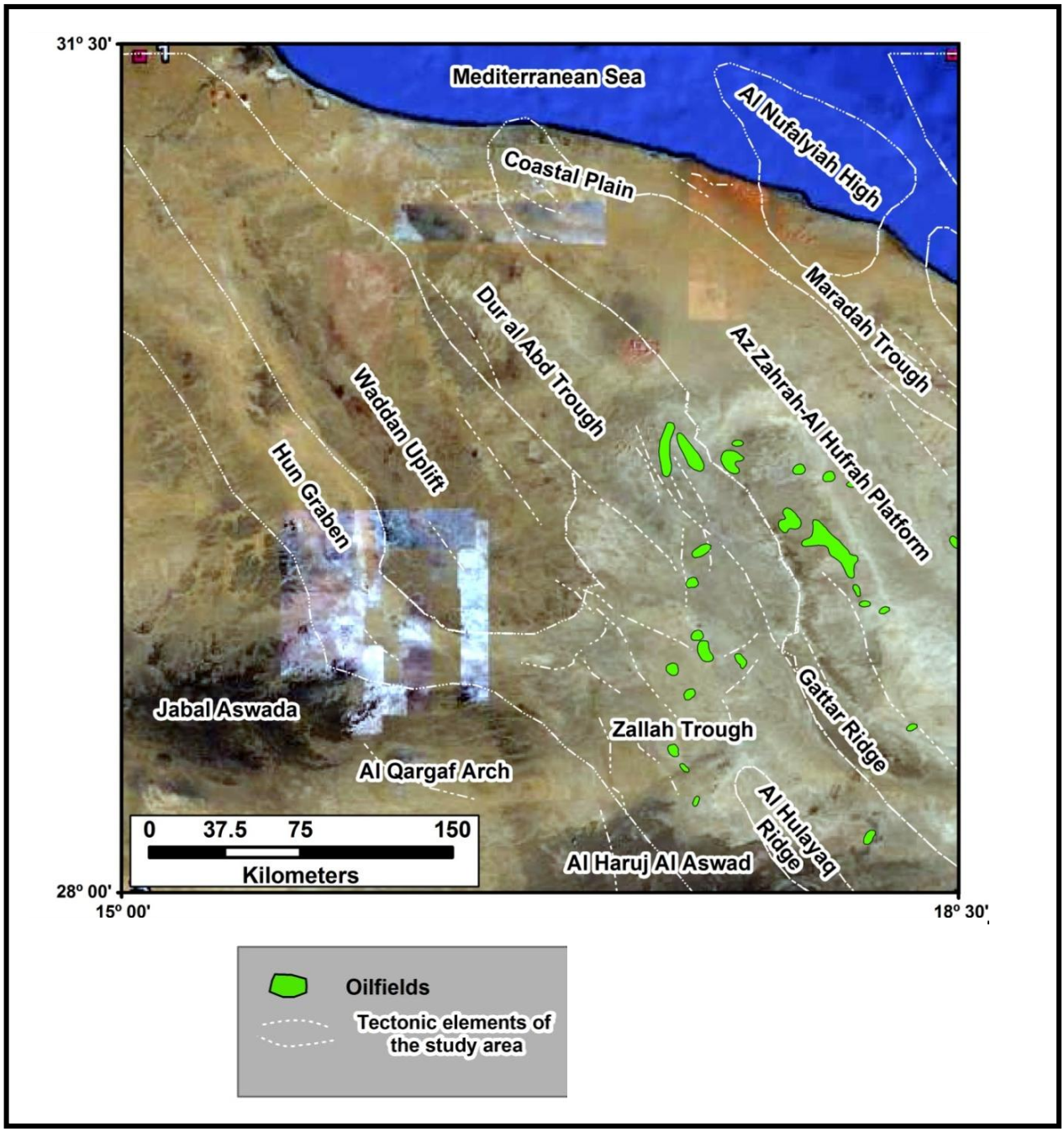


Fig. 1.5 Data from Google Earth™ imagery that covers the study area were used for the remote sensing component of this study.

1.5 Summary

Libya is the second-largest oil producer in Africa and the Sirt Basin is the most prolific petroleum province and one of its most important oil basins. The hydrocarbon exploration and production history of Libya has been reviewed in this chapter.

The study sims to understand the detailed structure and tectonic development of the western part of Sirt Basin, using an extensive geological and geophysical database to

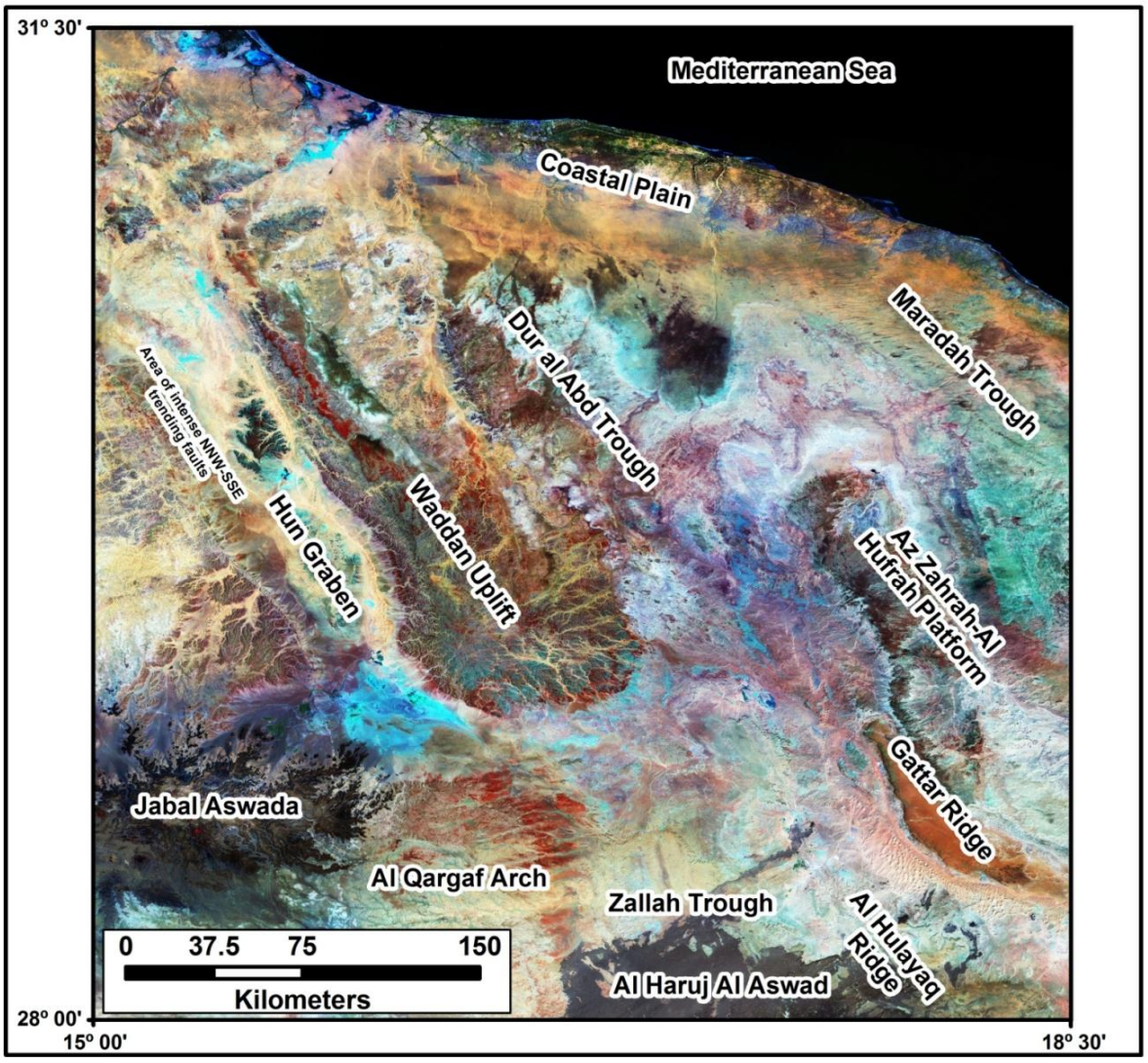


Fig. 1.6 MrSid images covering the area were also used to provide more information on structural phenomena in the study area.

investigate the significance of surface lineaments and fractures, their correlation with subsurface structures and their ability to delineate oil and gas reservoirs in the area.

This study is focusing mainly on Western Sirt Basin, Libya between 15°00’ E to 18°30’ E and 28°00’ N to 31°30’ N (Fig. 1.1).

A large database containing information from formation tops of 500 oil and gas wells, 2D seismic data consisting of 252 lines totalling approximately 5000 km and satellite imagery were utilized in this study. This study also presents paleostress results from fault-slip data on U. Cretaceous-Tertiary sediments in the western portion of Sirt Basin and the NW Libya (Jifarah Basin and Jabal Nafusah Uplift).

CHAPTER 2: TECTONO-STRATIGRAPHIC EVOLUTION

2.1 Regional Stratigraphy and Structures of Libya

Libya is located on the Mediterranean foreland of the African Shield and extends over a platform of cratonic basins, covering an area of approximately 1.75 million square kilometers (Fig. 1.1).

Although Libya has relatively simple surface geology, (Fig. 2.1) it has a very complex subsurface geology and geological history. Morphologically the country has its highest elevations in the south, generally gently sloping northwards to the Mediterranean Sea (Fig. 2.2). The higher grounds are generally indicative of older rock units (Fig. 2.1).

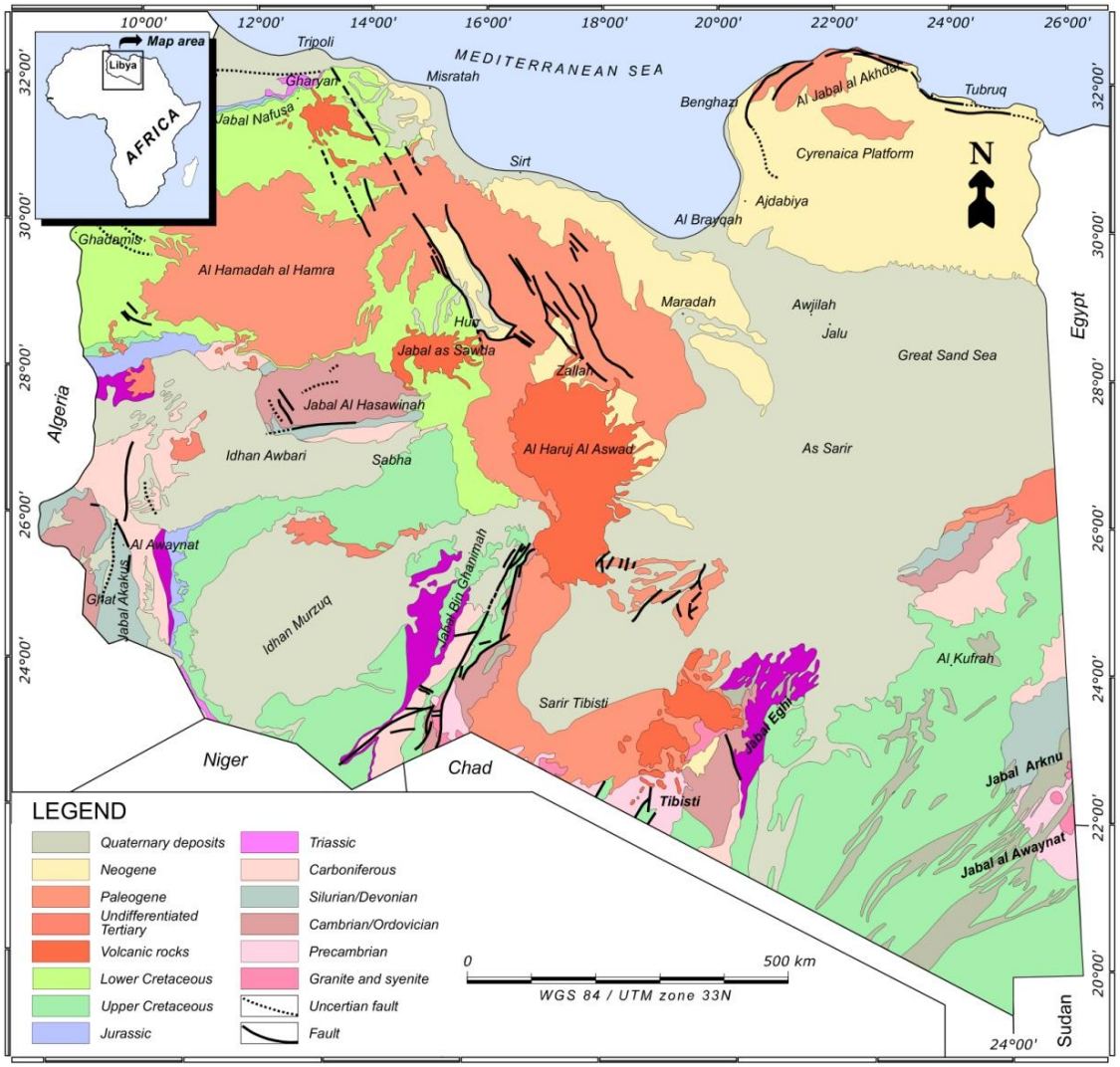


Fig. 2.1 Geological map of Libya. Modified after Conant, and Goudarzi, (1977).

Tectonically Libya is divided into two geologic provinces that are reflected by the main faulting patterns of the sedimentary basins, which seem to have been ultimately

controlled by the configuration of stable cratonic cores since the Precambrian. Each province includes a number of sedimentary basins (Fig. 2.3). The southern province, which lies within a stable cratonic area, was controlled by the evolution of Pangaea during Paleozoic and Mesozoic times and includes the Paleozoic Ghadamis and Murzuq Basins to the west separated by the Tibisti crystalline basement massif from the Paleozoic Al Kufrah Basin in the east.

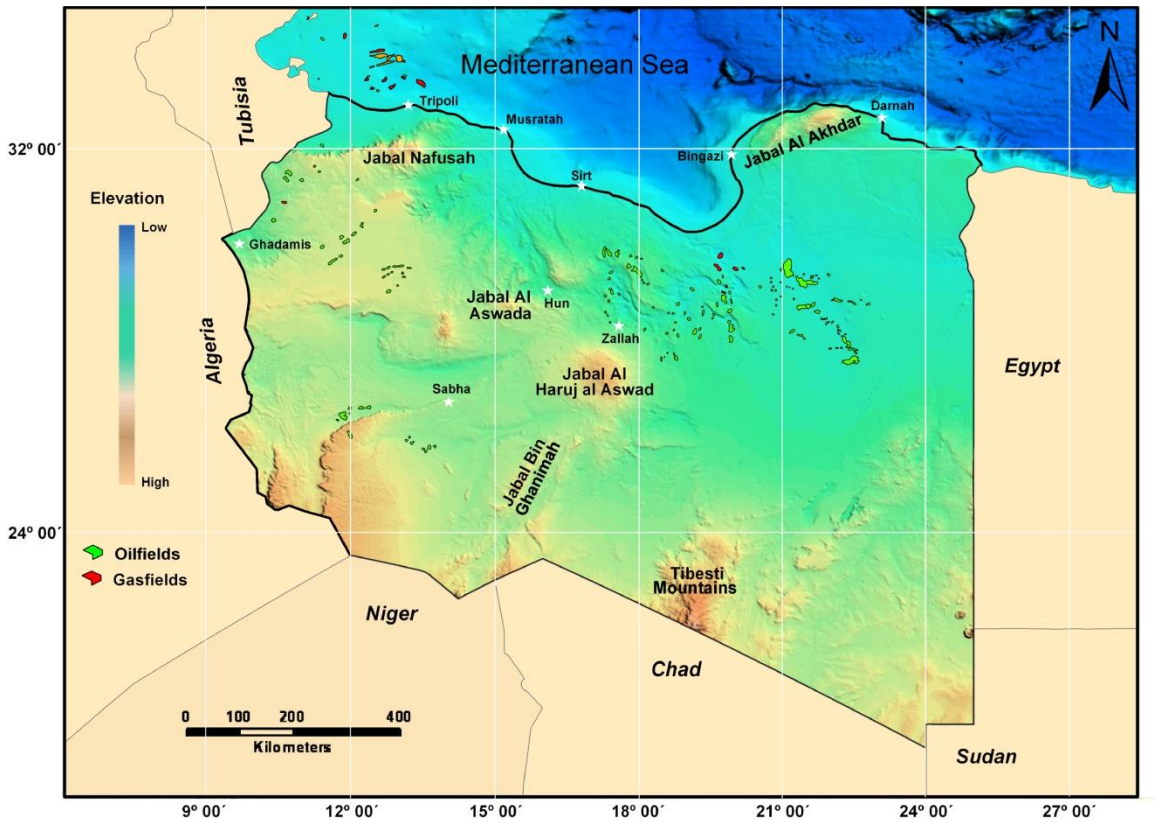


Fig. 2.2 Digital shaded-elevation model (DEM) map of Libya generated from SRTM, 3 arc seconds (90 m) resolution. It shows the highest topographic regions and the oil and gas fields.

The northern province of the country is situated on a tectonically active subsiding margin (Gumati, et al., 1996) controlled by the evolution of Tethys and the Mediterranean during the Late Mesozoic and Cenozoic, and includes from west to east Late Mesozoic and Cenozoic, the Sabratah Basin, Benghazi Basin, Sirt Basin and Cyrenaica Platform. The province was referred to as an extensional continental rift area and believed to be part of the Tethyan rift system (Hallet, 2002).

The position of the country at the edge of the African plate has caused the Libyan sedimentary basins to have been affected by several successive phases of continental collision and plate divergence (Pickford, 1991).

The regional geology and the structural framework has been highly influenced by the Caledonian, Hercynian, and Alpine tectonic events which led the country to become a site of deposition of large sheets of continental clastics, and several transgressions and regressions episodes with consequent accumulation of a wide variety of sedimentary rocks.

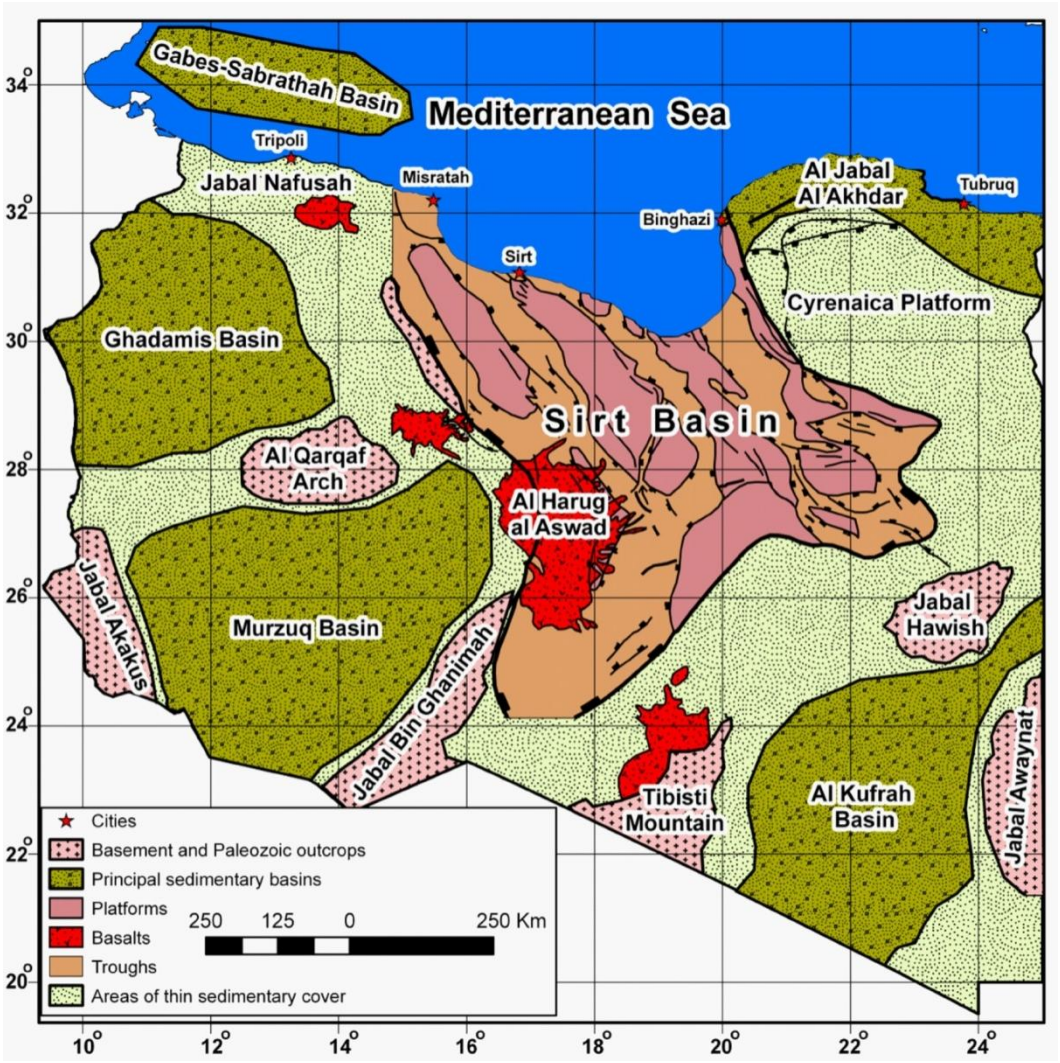


Fig. 2.3 Generalized structural map and the main sedimentary basins of Libya. Modified after Conant, and Goudarzi, (1977) and Bellini and Masa, 1980.

The area has undergone discontinued periods of uplift and subsidence (folding and consolidation) in the Precambrian, which started with the Pan African Orogeny (Anketell, 1996). It was accompanied by intense metamorphism which led to remobilization of the old cratonic margins, (Hallet, 2002).

Throughout the Paleozoic, the whole area was characterized by a low subsidence caused a local depocentres of intra-cratonic sags of Murzuq, Ghadamis, and Al Kufrah Basins, separated by thinning or erosion over the Late Silurian Caledonian E-W Gargaf and N-S Tibesti-Sirt Arches.

Along the northern margin, Paleozoic sedimentation took place particularly in the Cyrenaica area northwards and, with uncertain distribution, in parts of northern Sirt Basin with volcanic episodes. Areas in southern Cyrenaica, northwest Libya and in places on the Tibesti-Sirt Arch were not submerged, or were later stripped by erosion.

At the end of Carboniferous, a Hercynian reactivation produced further uplift with erosion over the arches represented by the formation of Nafusah Uplift, Al Qargaf Arch, Tibesti-Sirt Arch, Ennedi-Alawaynat Uplift and their associated troughs, (Fig. 2.3), (Hallet, 2002).

Thereafter, the Tibesti-Sirt Arch underwent progressive collapse from the north during the Mesozoic which established a series of horsts and grabens trending NNW-SSE to NW-SE cross-cutting the Paleozoic structures. Post-Hercynian deposition was more extensively developed north of the cratonic areas, with intra-cratonic sedimentation restricted mainly to the Murzuq Basin and, diminishingly, the Al Kufrah Basin. Major hydrocarbon discoveries have been made in the Paleozoic sequence of the Ghadamis and Murzuq Basins, and the Mesozoic and Cenozoic sequence in the Sirt and Sabratah Basins.

In general, geological studies from different sources such as (Klitzsch, (1963 and 1971), Mickbel (1979), Anketell, (1996), Hallet, (2002), Abadi, (2002), and others have revealed four main structural trends of Libya:

1. a N-S Trend which is a deep basement trend, related to the Pan-African Orogeny as stated above;
2. an E-W trend with an origin yet to be determined, but thought to be characterized by tensional/strike-slip activity during the Mesozoic. It was reactivated and inverted during the Alpine Orogeny;
3. a WSW-ENE Trend which is considered to be of Hercynian origin consisting mostly of normal faults, that may have been reactivated during the Alpine phase as contractional faults;
4. a NW-SE Trend that originated in the Caledonian Orogeny, which was intensively reactivated during the Cretaceous and Middle Paleocene. Generally, the structures present in the Mesozoic are dominantly characterized by inversion due to the compressional force associated with the Alpine Orogeny. This inversion is more pronounced at normal faults and at the intersection of ENE-WSW and E-W fault trends.

2.1.1 Regional Stratigraphy of Sirt Basin

The structural and palaeotopographic configuration, and tectonic development since the Upper Jurassic - Lower Cretaceous were the main factors controlling sedimentation, stratigraphy and palaeogeography of the Sirt Basin area. The stratigraphy of the Sirt Basin has been established mainly on the basis of subsurface and partially on outcrops in the western part of the basin. Oil companies in many cases have adopted their own classification and formation names. Sirt Basin stratigraphic succession consists of a variety of lithologies ranging from Pre-Cambrian crystalline basement to recent sedimentation episodes. Sedimentary lithologies exceed 6400.8 m in the deepest parts of the troughs, mostly of Cretaceous and Tertiary age, diminishing in thickness to 1219.2 m on the regional highs and on the southern most shelf area. Mesozoic and Tertiary lithologies are extremely variable, reflecting the tectonic and structural evolution of the Sirt Basin, which is closely related to the opening of the Atlantic Ocean and evolution of the Tethyan margin.

2.1.1.1 Surface geology

The surface geology of the study area is dominated by sedimentary rocks ranging in age from Late Cretaceous to Tertiary (Fig. 1.3 and Table 2.1).

- **Mesozoic**

Generally, the oldest exposed sedimentary rocks are located in the northwestern part of the area and the youngest in the east and northeast (Burollet, 1963, Barr and Weegar, 1972, Said, 1981 and Abdshakoor and Shagrouni, 1984). The Late Turonian-Coniacian age, Qasr Tigrinnah Formation, is the oldest sedimentary unit exposed in the study area. The Campanian age Mizdah Formation (Mezuzah and Thala Members) conformably overlies the Qasr Tigrinnah Formation and is also restricted to the northwestern part of the study area consisting of limestone, marly limestone and gypsiferous sediments.

- **Tertiary**

The Zimam Formation (Tar and Had Members) consists dominantly of marl, marly limestone and calcareous dolomite to dolomitic limestone where the lower part of this formation belongs to the Maastrichtian, the upper part of the formation is Danian in age (Abdshakoor and Shagrouni, 1984). The overlying Thanetian Shurfah Formation (Said, 1981) contains three members Bu Ras, Qaltah and Ammur, which consist of limestone, marl, marly limestone, calcarenite and calcilutite. The Bishimah Formation overlies the Shurfah Formation and is Thanetian-Ypresian in age.

It consists of the Khayir, Wadi Zakim, and Rawaghah Members. The formation has significant variations in thickness and lateral facies changes from east to west across the study area.

ERA	PERIOD		EPOCH	UNIT NAME
CAINOZOIC	QUATERNARY		RECENT	FLUVIO-EOLIAN AND RECENT WADI DEPOSITS
			HOLOCENE	SABKHA DEPOSITS
			PLEISTOCENE	ANCIENT WADI TERRACES
	TERTIARY	PLIOCENE	PLEISTOCENE	AL HISHAH FM.
		MIOCENE	LANGHIAN	AL KHUMS FM.
		OLIGOCENE	CHATTIAN	U.MB.OF MAZUL NINAH FM.
			RUPELIAN	L.MB.OF MAZUL NINAH FM.
		EOCENE	LUTETIAN-PRIABONIAN	WADI THAMAT FM.
			YPRESIAN-LUTETIAN	AL JIR FM.
			THANETIAN-YPRESIAN	BISHIMA FM.
		PALEOCENE	THANETIAN	SHURFAH FM.
			DANIAN	U.MB.OF ZIMAM FM.
MESOZOIC	CRETACEOUS		MAASTRICHTIAN	L.MB.OF ZIMAM FM.

Table 2.1 The exposed sedimentary rocks of the study area (after Vesely,1985; Jurak, 1985).

In the eastern part, it is represented by complete sections of the three members while to the northwest, it changes in lithology and has reduced thickness (Said, 1981). Lithologically it consists of gypsiferous marl to marlstone, dolomite, chalky dolomite and limestone. The Al Jir Formation overlies the Bishimah Formation and is composed of chalky to marly dolomite and dolomitic limestone. It is Ypresian-Lutetian in age. The overlying Wadi Thamat Formation (Al Gata and Wadi Thamat al Qasur Members) consists of marl, limestone and dolomitic limestone of Lutetian-Priabonian age. During the Oligocene, the depositional environment changed and sedimentation was dominated by continental deposits of the Mazul Ninah Formation. These sediments are very clear in the Hun Graben where the basin is filled by a considerable thickness of clastics of the Mazul Ninah Formation. They consist of gypsum, marl, sandy limestone and marly

limestone (Abdshakoor and Shagrouni, 1984). In the eastern part of the study area (Fig. 1.3 and Table 2.1) Mazul Ninah Formation is overlaid by thin layers of sediments of the Umm ad Dahiy and Bu Hashish formations which is composed of marly dolomite and gypsified fine grained marly sandstone.

Miocene stratigraphy is represented by limestone, marly limestone and calcarenite of Maradah and Al Khums Formations. The youngest Tertiary stratigraphic unit in the area is Al Hishah Formation. This consists mainly of fine grained gypsiferous marl, calcarenite, and sandy clay of Pliocene in age (Said, 1981).

- **Tertiary volcanics**

Tertiary volcanic rocks are well-exposed in the study area forming the northerly continuation of the basaltic flows of Jabal Al Haruj Al Aswad and the lava massif of Jabal Asawda occurs in the southern part of the study area (Fig. 1.3 and Table 2.1). The volcanics are localised at the intersection of the NW-SE to NNW-SSE trending Pan-African lower Paleozoic structural arch and the WSW-ENE trending Hercynian Late Palaeozoic to Mesozoic uplifts.

- **Quaternary and recent sediments**

Quaternary deposits are found in the coastal plain, wadi floors and low-lying areas. They can be divided into sabkha, wadi deposits, and fluvio-eolian deposits associated with lithic fragments, sand, silt, clay and gypsum (Said, 1981 and Abdshakoor and Shagrouni, 1984).

2.1.1.2 Subsurface Stratigraphy

The Sirt Basin consists predominantly of rock formations whose nomenclature comes from the subsurface. The stratigraphy of the subsurface has been the subject of many publications and summary volumes (e.g., Barr and Weegar, 1972; Megerisi and Mamgain, 1980; Banerjee, 1980; Anketell and Kumati, 1991a; Gumati and Kanes, 1985 and Bezan, 1996). The Barr and Weegar (1972) stratigraphic nomenclature has essentially been adopted in the present study (Fig.2.4) with minor modifications by Gumati and Kanes (1985).

- **Precambrian (Basement)**

Several types of igneous and metamorphic rocks, comprising mainly Precambrian granites and volcanics floor the Sirt Basin. Goudarz (1980) showed, on his top-basement structure contour map of the Sirt Basin, that the surface drops rapidly from 3500 m a.s.l. in the southern part adjacent to the Tibesti mountains to more than 7500 m b.s.l towards the Mediterranean in the Ajdabiya Trough. The basement configuration of the Sirt Basin

can be clearly illustrated in Fig.2.5. In the study area, the basement is deepens rapidly from about 330 m b.s.l. in the southwestern part on Al Qargaf Arch to more than 3,300 m b.s.l in Central Zallah Trough and Maradah Trough (Fig.2.5).

Rocks forming the basement of the Sirt Basin ranges in age from Neo-Proterozoic to Cambrian (540 to 665±25 Ma), (EI Makhrouf, 1996) and it resulted from the Pan African Orogeny that consolidated a number of proto-continental fragments into an early Gondwanaland.

Generally within the Sirt rift complex the basement is predominantly made up of phyllites, schists and gneisses into which granitoids and subordinate gabbros are intruded (Busrewil, et al. 2009).

The basement consists of two suites,

1- An orogenic rock suit composed of pyroxene gabbro, gabbro, diorite and granodiorite,

2- Post-orogenic rock suit composed of coarse hornblende and biotite granite, quartz syanite and rhyolitic porphyry. The metamorphic rocks on the other hand are composed of banded gneiss and chlorite schist, as well as metasediments ranging from coarse grained greywacke and fine grained siltstone and phyllites.

- **Paleozoic**

A Cambro-Ordovician succession of clastics, which are largely sandstones occur in the subsurface of the Sirt Basin immediately above the basement and have an upper boundary marked by the unconformable contact with the overlying continental to transitional (Triassic, Jurassic and Lower Cretaceous) or marine (Upper Cretaceous and Lower Paleocene) strata (Fig.2.4).

The Cambro-Ordovician System (Amal and Hofra formations) are widespread throughout the Sirt Basin and they are dominated by cyclic sequences of thick, regionally-extensive, transgressive, fluvial and estuarine sands which pass up into shallow marine sandstones and maximum flooding shales. They possibly are thicker in the troughs and also drape over most of the positive tectonic elements. The unconformably overlying Silurian marine shales are known from only a few localities. Investigations to date have revealed the presence of thick (177m) marine graptolitic shales of Silurian age in the subsurface of the northern Az Zahrah-Al Hufrah Platform (D1-32; Fig. 2.6) (Banerjee, 1980, p.137) and Q1-31, and in several wells drilled to the south of the present coastline of the Gulf of Sirt.

These Early Paleozoic rocks are unconformably overlain by sandstones of possibly Devonian age and the presence of Devonian strata is expected, since other Palaeozoic

strata have already been identified from various locations in the basin. Thick sandstones are found immediately overlying the Silurian graptolitic shale at D1-32 (Fig. 2.6) and over northern parts of the Az Zahrah-Al Hufrah Platform they include white-gray, very fine to coarse grained, silty and at times quartzitic sandstones with quartz fragments assigned to Devonian age.

To-date there is little available data to suggest presence of Carboniferous and Permian sediments although they are well developed in the nearby Ghadamis Basin as well as the Cyrenaican Platform. Their presence or otherwise, however, remains very speculative since large parts of the troughs are yet not sampled.

In view of the foregoing it appears very reasonable to conclude that the Sirt Basin witnessed deposition of sediments during the Silurian, Devonian and possibly, the Carboniferous as well. In all probability, basement arching was rejuvenated sometimes during the Carboniferous and most strongly during the Permian period. The older sediments were uplifted and subjected to widespread erosion which obliterated or eliminated most of their imprints in the basin. This uparching could be related to the Hercynian tectonic phase, which is well established in the adjoining Ghadamis Basin (Bellini and Massa, 1980).

- **Mesozoic**
  - **Triassic- Jurassic**

In the general area of, the broad Tibesti-Sirt Arch, basement and Cambrian-Ordovician rocks are exposed at the Hercynian surface, and this area remained positive until the Late Jurassic. In discrete peripheral areas, sediments dated as Middle Triassic (Ladenian-Anisian) microspore and pollen assemblages are known from the subsurface of the Maragh Trough which fringes the eastern margins of Rakb High in the eastern part of Sirt Basin. These have been reported by Brugman et al. (1985) and Brugman and Visscher (1988) from the Amal Formation in the eastern Sirt Basin. These, however, seem to have been largely eroded.

Late Middle Jurassic claystone and shales from well 4D1-59 contain a diverse humic kerogin rich microflora. Similar lithologies of Middle Jurassic age were also described from well A1-96 (Barr and Weegar, 1972).

- **Cretaceous**

Two extremely diverse palaeotopographic and palaeogeographic settings resulted in different sedimentary sequences, which distinguish the Upper and Lower Cretaceous Series.

The first stirrings of formation of the Sirt Basin probably occurred prior to the Cretaceous (Wennekers, et al 1996).

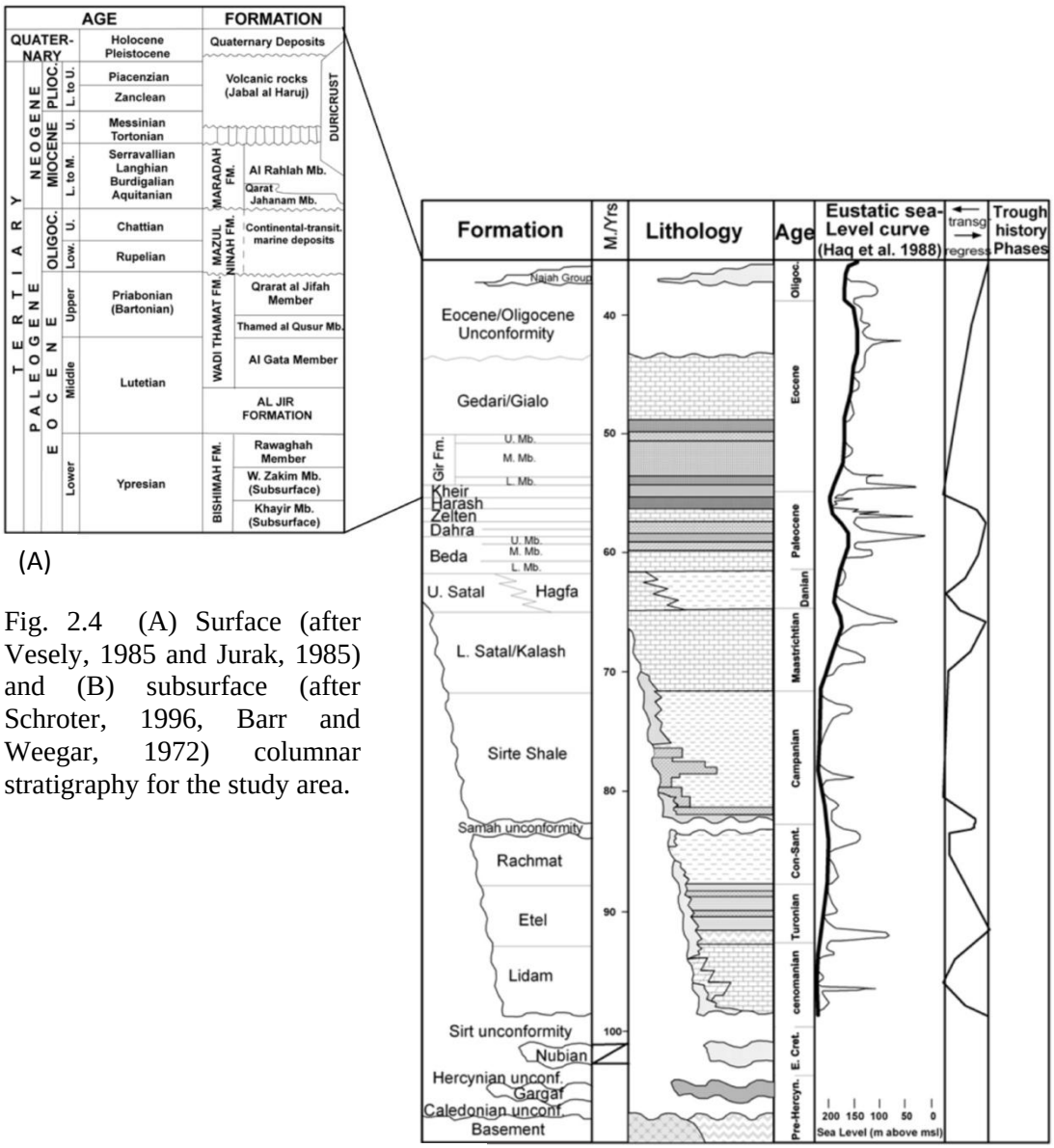


Fig. 2.4 (A) Surface (after Vesely, 1985 and Jurak, 1985) and (B) subsurface (after Schroter, 1996, Barr and Weegar, 1972) columnar stratigraphy for the study area.

It developed on a substratum of basement rock and sedimentary strata of Palaeozoic, Triassic and Jurassic age. The Lower Cretaceous section developed between the late Kimmerian and Austrian orogenic events, while the Upper Cretaceous section developed between the Austrian and the Laramidian orogenic events. The latter section also contains evidence of the sub-Hercynian orogenic event. Ages of several associated intrusives and extrusives have been recognized in the Sirt Basin. The resulting rift terrain and fault block topography formed an exposed, irregular landscape. Over and around this landscape mainly continental deposition occurred in the Early Cretaceous.

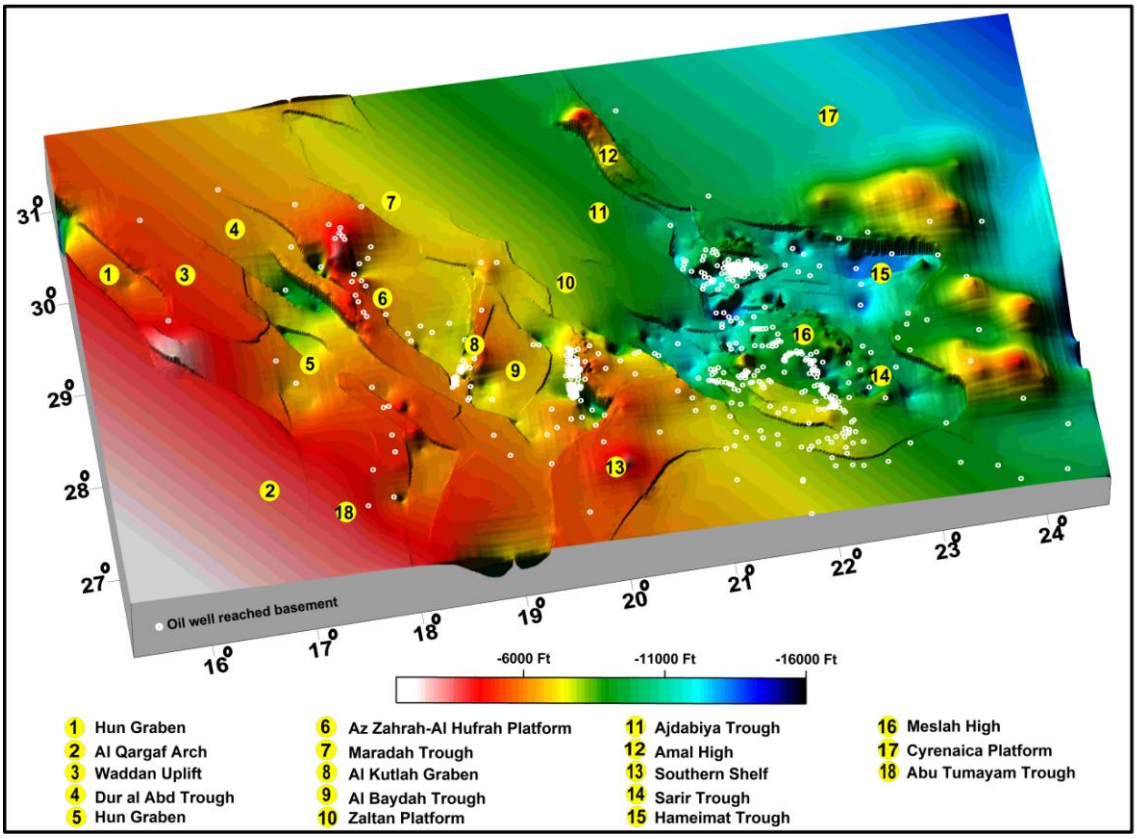


Fig. 2.5 3D perspective image shows depth to basement of the structural domains of the Sirt Basin based on well data overlaid over major faults of Sirt Basin.

It is clear from geological studies of the area that the Lower Cretaceous oil fields are located almost entirely within the eastern Sirt Basin, while the bulk of Upper Cretaceous production is from the central Sirt Basin and some of later ages located in the western portion. Reservoirs in the Lower Cretaceous are present in non-marine clastics of Late Early Cretaceous age while the Upper Cretaceous contains reservoirs in both clastics and carbonates from all stages of that series.

- **Lower Cretaceous**

The end of the Triassic-Jurassic witnessed widespread positive tectonism and lowering of sea levels and consequently, uplift and erosion followed by continental transgression leading to deposition of mainly non-marine clastics. Barr and Weegar (1972) applied the name Nubian Sandstone, or Formation, for "a variety of inter-bedded non-marine lithofacies including sandstones, siltstones and conglomerates", in the subsurface which they assigned to an Early Cretaceous age. The Nubian Formation which is resoluble into three lithologic units. The lower and upper units comprise non-marine gray and medium to coarse grained argillaceous sandstones with rare to very rare levels of shales. The

middle unit includes multicoloured, variegated, greenish, reddish, buff and greenish gray shales.

In general, the Nubian Formation is poorly fossiliferous and the mineralogical and textural similarities mean that differentiation and age dating is difficult. As a result of this, Jones (1992) grouped all the pre-Maastrichtian quartzites and sandstones under the informal term ‘Sirte Basin siliciclastic succession’. This problem is also mentioned by others (Gillipse and Sandford, 1967; Viterbo, 1969; Sandford, 1970; Barr, 1972 and Clifford et al., 1980) where they believe that the lower age limit could extend into the Late Jurassic although most of the unit may be of Early Cretaceous age and is referred to in the literature under a variety of names such as the Sarir Sandstone, Nubian, Calanscio or Pre-Upper Cretaceous Sandstone (Gras and Thusu, 1998).

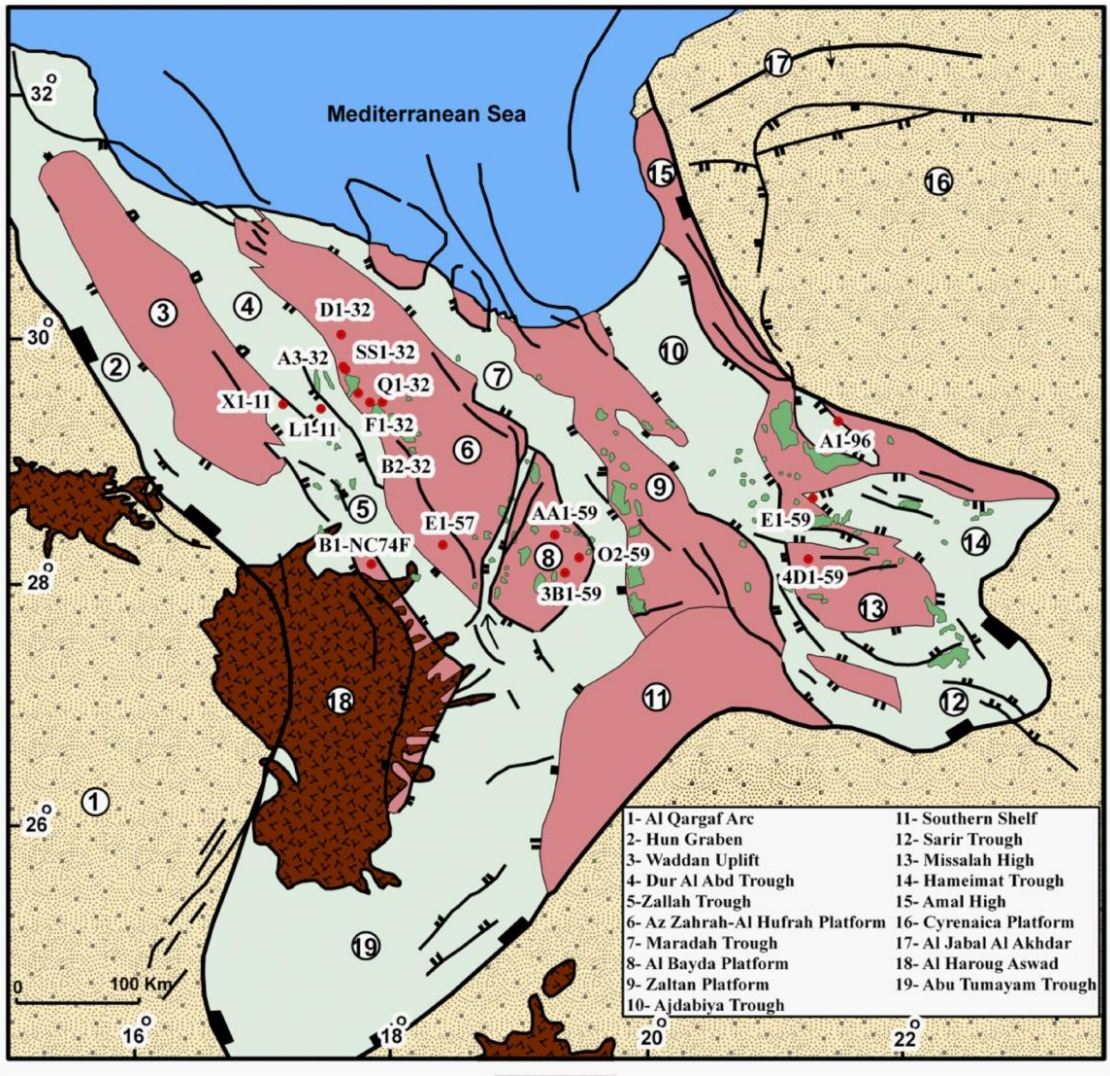


Fig. 2.6 Generalized structural map of the Sirt Basin (showing the locations of the principal wells studied, and boundaries of the oil and gas fields within the study area. Modified from Mouzughi and Taleb, (1981). For legend see figure 2.7.

The Nubian Formation on the horst blocks is thinner than that present in the grabens. The Austrian orogenic event resulted in a complex Early Cretaceous structural/stratigraphic relationship. It caused widespread emergence and the deposition of a major regressive section during Early Cenomanian time in the northern Sirt Basin. Then, a Mid-Cenomanian uplift and erosion was followed by a major marine transgression from the north during late Cenomanian time.

- **Upper Cretaceous**

The Upper Cretaceous is characterized by widespread faulting in the form of a pattern of horsts and grabens that trend generally NW-SE (Conant and Goudarzi, 1967; Van Houten, 1983), concurrently with a mega cycles of transgression caused the deposition of a sequence of Cretaceous through Miocene sediments on Pre-Upper Cretaceous with differential movements on horsts and grabens accounting for very thick deposits in the troughs, and much thinner sections on the fault-block highs.

However, locally, as a consequence of structural differentiation, resulting partly from tectonism that occurred prior to and alongside deposition, thick accumulations of deep-marine shales and deep-water carbonates formed in the grabens, while shallow-marine carbonates were deposited on the highs. These vary from deep marine shales to salt deposits. During this age a rapid increase in the rate of subsidence of the basin occurred during the Campanian and reached a maximum during the Eocene (Gumati and Kanes, 1985; Gumati and Nairn, 1991), even though it was initially slow in the beginning of Upper Cretaceous. As a result of the differential tectonic movements in the pre-rift and syn-rift, the juxtaposition of high-energy reservoir rocks and low-energy source beds developed that allowed the generation of the best prospects for oil formation and entrapment and accounts for the impressive volume of Upper Cretaceous production in the basin.

The Upper Cretaceous marine carbonate and shale section, termed the Lidam, Etel, Argub, Rachmat, Sirte, Kalash, Samah and Waha Formations (Barr and Weegar, 1972). These are floored by basal units (mainly sandstone and conglomerates) named the Bahi, and Maragh Formations (Barr and Weegar, 1972). The formations are unfossiliferous, and are assumed to be non-marine. They represent a fluvial environment which was ultimately covered by the late Cretaceous marine transgression, but at differing times depending on the local palaeogeography.

- **Tertiary**

Tertiary strata occur throughout the Sirt Basin. The Paleocene sequence of the Sirt Basin consists of open shelf carbonates and deep marine shales that reach a total thickness of 750 to 1000 m and closely follow the underlying structure with thickening in troughs and thinning on platforms, which indicates that faulting along trough edges was probably contemporaneous with deposition. Spatially, carbonates are confined to the structurally higher platform areas while shales occupy the troughs.

Hydrocarbon production is from both upper (Thanetian) and lower (Danian) Palaeocene carbonates and oil has been found in both structural and stratigraphic traps or a combination of both. The late Palaeocene was a time of widespread reef growth in the basin and it is in such features that much oil is found.

During the Eocene, subsidence in Sirt Basin had ceased and the carbonate environment was dominant. Carbonates and evaporites were the major constituents of the Lower Eocene. Nummultic and biomicritic facies form the main composition of the Middle Eocene, which changes abruptly to shales in Upper Eocene. The thickness of the Eocene sequence as a whole is 500 m as developed in the troughs and thins out slightly on the highs.

The Oligocene was a time of major tectonic events that were attributed to the uplift of the African plate, which in turn left a significant signature on the stratigraphic record of sediment infill within the North African basins (EI Hawat, 1997). In the western part of Sirt Basin, these events led to the formation of a mixed sedimentary sequence of non-marine clastic rocks in the southwest that gradually intermixes with shallow marine strata to the northeast.

The initiation of volcanic activities in the AI Haruj al Aswad area and along the Tripoli-Tibesti tectonic line also occurred, as did the marine regression within the Sirt embayment and increased siliciclastic sedimentation along the basinal margin along the NW-SE trending troughs. In the central and eastern segments of the basin the Oligocene deposits consist of fluvial sandstones with shale intercalations and lenses. The thickest development of the Oligocene sequence is in north central Sirt Basin (northern Ajdabiya) where it exceeds 1300 m, thinning gradually to 350 m toward the southeast.

Miocene rocks, partially because of their shallow depth of burial, do not, form reservoirs in the Sirt Basin nor do they offer high exploration potential and like the Oligocene. The Miocene section presents a mixed lithologic assemblage of fluvial, littoral and nearshore deposits forming part of a regressive sequence.

Additionally, outcrop and thickness patterns and facies distribution emulate the underlying Oligocene, indicating that the rate of subsidence and therefore centres of deposition were to some degree continuous. In the Sirt Basin, strata belonging to this age are assigned to the Maradah and Al Khums Formations. These rocks have been extensively studied particularly by Magnier, (1969) Selley, (1971) El Hawat, (1980a) and Benfield and Wright, (1980)

2.1.1.3 Stratigraphy of the study area

- **Pre Cretaceous time**

Most of the authors who dealt with the stratigraphy of Sirt Basin considered the sediments of Paleozoic to Lower Cretaceous as a pre-rift megasequence. Initially the igneous basement was probably covered by Paleozoic sediments of Cambro-Ordovician to Carboniferous age. In Late Paleozoic to Triassic time, a Late Hercynian event caused the development of an uplifted arch in the Sirt Basin area as mentioned in the previous paragraphs. It is possible that an earlier uplift already existed in Paleozoic section toward the time, as indicated by some thinning of the Paleozoic cover.

Much of Paleozoic section from the west was eroded over this high during Lower Mesozoic time and this influence may have extended into the offshore area, as shown by the absence of most of the Paleozoic in wells around the Gulf of Sirt (Fraser 1967). The flanks of this arched complex lay in the northern and eastern Cyrenaica and in the southern shelf of the basin and eastern Ghadamis Basin areas respectively. Here much of this Paleozoic cover is still preserved together with Triassic, Jurassic and Lower Cretaceous sediments. Except in early graben areas Paleozoic and Triassic to Lower Cretaceous sediments are very thin over the Sirt Arch.

- **Early Upper Cretaceous**

This age is comprised of Bahi, Lidam, Argub formations as proposed by Barr and Weegar (1972) for an interval of clastics, which occur between Campanian (Rachmat Formation) and Nubian sandstones of Early Cretaceous time in the Waha A3-32 well. They consist of sandstone, dolomite, anhydrite, and shale. They also are overlain by the Campanian (Rachmat Formation) with an abrupt contact and unconformably overlie various lower Paleozoic formations.

The Lidam is an oil reservoir in the northern part of the Bahi Field. The Argub Formation is only recognizable in the northern half of the study area and onlaps the Az Zahrah-Al Hufrah Platform from the north. The Argub Formation is an oil reservoir in the northern part of the Mabruk Field and in the southern part of the Bahi Field (SS1-

32). The Etel Fm is recognizable only across the south half of the study area and onlaps the Az Zahrah-Al Hufrah Platform from the south.

- **Rachmat Formation and Sirte Shale (Maastrichtian to Campanian)**

These two formations have been proposed by Barr and Weegar (1972). The Rachmat Formation is an interval of shale with subordinate thin limestone, sandstone and dolomite interbeds which occurs between Etel Formation and Sirte Shale in the Waha O2-59 well. The Sirt shale is a widespread unit and it is predominantly shale (calcareous mudstone) with siltstone and limestone intrabeds between the Rachmat and Kalash formations. It is the main source rock in Sirt Basin. The type section is about 100 km east of the west Sirt Basin study area. The Sirt Shale is absent over the highest parts of the Az Zahrah-Al Hufrah Platform. In the study area these two formations are thickest in the central part of Zallah Trough, south western of Dur al Abd Trough and on the eastern boundary of Dur al Abd Trough with Az Zahrah-Al Hufrah Platform while they absent or very thin on the other parts of the study area.

The Sirt-Rachmat Shale sequence, which includes minor amounts of carbonates (Tagrifet Limestone) with variable source potential, varies in thickness from 1000 ft to more than 3000 ft. The total organic carbon (TOC) of this sequence ranges from 0.5% to 8%, averaging 1.5–4% (Parsons et al., 1980; Hamyouni et al., 1984; Baric et al., 1996).

- **Kalash Formation (Maastrichtian to lowermost Paleocene)**

It is proposed by Barr and Weegar (1972) for an interval of calcilutite which occurs between the Sirte and the Hagfa Shale units at the top of Maastrichtian in the Mobil E1-57 well. The lithology at the type location is argillaceous calcilutite with some dark grey calcareous shale intrabeds.

The Kalash Formation is the most regionally mapable unit, but is absent or very thin on the highest parts of the Az Zahrah-Al Hufrah Platform and on the north western part of Waddan Uplift, and Hun Graben.

In the Zallah Trough area, the Kalash thins and is more argillaceous. Well picks in this area are tentative. They are based on limited biostratigraphic data and previous interpretations made by operating companies. Towards the western margin of the basin the Kalash is equivalent to the upper part of the Lower Tar Member of the Zmam Formation (Eliagoubi and Powell, 1980) which is exposed at the surface. The Kalash Formation contains limestone layers that form an oil reservoir in the Abeter and Fidda Fields as well as in the KK1-32 well north of the Bahi Field.

- **Hagfa Shale (Formation) (Lower Paleocene)**

Hagfa Shale is proposed by Barr and Weegar (1972) for an interval of shale with siltstone and limestone interbeds between the Kalash and Beda Formations in the Waha Y1-59 well. The Hagfa Shale is widespread in the southern part of the basin. It is thought to be (in part) the time equivalent of the Satal Carbonates of Danian age (Barr and Weegar, 1972).

- **Satal Formation (Lower Paleocene)**

A rock unit that comprises calcilutite and calcarenite that occurs between the Sirte Shale and the Thalith Member of the Beda Formation in the Waha B2-32 well. On the highest parts of the Az Zahrah-Al Hufrah Platform the Satal rests unconformably on clastics belonging to either the Bahi or Gargaf formations. The Satal Formation is an oil reservoir in the Bahi, Dahra, Almas, Ali, and Arbab Fields.

- **Beda Formation (Thalith and Rabia Shale), (Middle Paleocene)**

Beda Formation is an interval of calcarenite and calcilutite which occurs between the Hagfa shale and Dahra Shale in the Waha 3B1-59. In the western part of the study area (Waddan Uplift, Hun Graben) the Beda stratigraphic interval is composed mainly of dolomite, anhydrite and limestone and correlations are tentative. In the Hun Graben it is extremely difficult to separate Eocene from Paleocene strata because of similar lithologies, and lack of biostratigraphic information.

The Beda Formation is an important oil reservoir in the Zallah Trough area. (Abrag, Daba, Facha, Ghani, Sabah, Tagrifet, and Zenab Fields)

- **Dahra Formation (Paleocene)**

This formation is composed of Limestone with dolomite and shale interbeds which occur between Rabia Shale and Khalifa Formation in the Waha F1-32 well. The Dahra Formation shales out to the north and east on the Az Zahrah-Al Hufrah Platform as do most of the Paleocene carbonates. It appears to be absent on the periphery, and over the northeast of the study area. In the western part of the study area (Waddan Uplift and Hun Graben) the Dahra cannot be distinguished, as discussed previously under Beda Formation. The Dahra Formation is the main reservoir in Az Zahrah, Al Hufrah, and Mabruk Fields.

- **Khalifa Formation (Paleocene)**

An interval of shale and calcilutite which occurs between the Beda Formation and Zelten Limestone in the waha AA1-59 well. The type section is approximately 90km east of the study area. At this location, part of the interval assigned to the Khalifa is equivalent to Dahra Formation.

- **Zelten Formation (Upper Paleocene)**

It contains mainly limestone which occurs between Khalifa and Harash formations in the Waha AA1-59 well. The Zelten Limestone shales out to the north and to the east on the Az Zahrah-Al Hufrah Platform, and is absent towards the northeast. The distribution is similar to the Dahra Formation.

- **Harash Formation (Upper Paleocene)**

This formation is proposed by Barr and Weegar (1972) for an interval of calcilutite and shale between Zelten Limestone and Kheir Formation in the waha AA1-59 well.

Lithologically at the type location is composed of interbedded limestone and shale with a thicker limestone cap unit. Its thickness exceeds 400 feet in the central part of Zallah Trough while less than 50 feet or absent on the northwestern part of Hun Graben, Waddan Uplift, and Dur al Abd Trough

- **Kheir Formation (Upper Paleocene to Lower Eocene)**

Barr and Weegar (1972) proposed to elevate the Kheir Marls, described by Burollet (1960) from the surface outcrops of the Hun Graben, to the formational status. The subsurface reference section of the Kheir Marls (Formation) has been designated in the Waha E1-59 well (Barr and Weegar, 1972).

In the type section at the surface the Kheir Formation is predominantly marlstone with some calcilutites. In the subsurface, the formation is represented predominantly by shale with some clay and limestone. Within the study area, the lithology of the interval between the Harash Formation and the overlying Facha dolomite is quite variable. In the southern part of the Zallah Trough area this interval consists of mainly of interbedded argillaceous limestones and shales, with the occasional thick clean limestone bed.

- **Gir Formation (Facha Dolomite, Hon Evaporite and Mesdar Members) (Lower Eocene)**

The name Gir Gypsum was originally introduced by Burollet (1960) to designate a member of the Gabal Waddan Formation in the Waddan area. Abugares (1996) delivered a comprehensive account of the sedimentology and correlation of the Gir Formation. The formation is a succession of dolomites, anhydrites with a subordinate amount of limestone and shale. It has been subdivided into three members: Facha Dolomite, Hon Evaporite and Mesdar Limestone This three fold subdivision of the formation can be made over a large part of the Western Sirt Basin exception of the northeastern end of the Az Zahrah-Al Hufrah Platform.

- **Facha Dolomite**

The lithology consists almost entirely of dolomite, with only occasional interbeds of anhydrite and it is identifiable over most of the study area, except for the northeast part of the Az Zahrah-Al Hufrah Platform. The Facha dolomite is an oil reservoir in many fields in the southern part of the study area. These include Abrag, Aswad, Fidda, Ghani, Hakkim, Hamama, Zallah, and Zenab. The Hon Dolomites produce oil in many fields including, Aswad, Facha, Ghani, Hamama, and Karim.

- **Hon Evaporite**

The lithology consists mainly of interbedded dolomite and anhydrite where the Halite is an important constituent in the southwest part of the Zallah Trough and it is the approximate lateral extent of the Halite facies which is referred to as the Zallah Sub-Basin. Abugares (1996) indicates that the top of the Hon is a major unconformity in the deeper parts of the basin in wells B1-NC74F, X1-11 and L1-11. The Hon dolomites produce oil in many fields including, Aswad, Facha, Ghani, Hamama, and Karim.

- **Mesdar Limestone**

At the type section, it is 78 ft thick and composed of dolomitic calcarenite. In the basinal parts of the study area, and particularly within the Zallah Trough, the Mesdar is a transitional unit between the underlying evaporites of the Hon and the overlying shale. The lithology varies upward from anhydritic dolomite, to dolomite, to limestone and finally to argillaceous limestones with interbedded calcareous shale. Over the western part of Az Zahrah-Al Hufrah Platform and Gattar Ridge areas, the Mesdar is significantly thinner and the lithology is mainly dolomite and dolomitic limestone. On the northeastern part of Az Zahrah-Al Hufrah Platform, the top of the Mesdar is characterized by a clean relatively thick, tight limestone bed.

- **Post-Gir Formations (Mid-Late Eocene to Miocene)**

The Gir Formation passes up into the Gialo Limestone Formation. This is a Nummilitic limestone that is also laterally continuous across much of the Sirt Basin. In addition to the Gialo Formation, the following formations: Gedari, Augila, Arida, Diba and Maradah are referred to in the present study as the post-Gir Formations of Mid-Late Eocene to Miocene age. Information about the post-Gir formations from the subsurface western Sirt Basin is rather limited because they mainly are exposed at outcrop.

2.1.2. Regional structure of Sirt Basin

The tectonic evolution and stratigraphy of the Sirt Basin has been studied by many

authors, most of whom believe that it represents an intracratonic basin constructed on the northern margin of African Plate. The primary structural pattern of the Sirt Basin (Anketell, 1996) are NW trending horsts and grabens with NE-, ENE-, and E-W-trending clusters of faults and/or fault blocks present mainly in the SE part, around the southern edge of the Cyrenaica Platform (Fig. 2.7).

Key studies on the Sirt Basin are summarized in approximate chronological order in the following sections.

Conant and Goudarzi (1967) suggested that the Sirt Basin formed during the Late Cretaceous due to large-scale subsidence and block faulting that continued until at least the Miocene and possibly, also to the present. According to Klitzsch (1971), east-west shearing movements were responsible for the formation of Sirt grabens during the Late Cretaceous. Burke and Dewey (1974) regard the horst and grabens of this basin to have been formed during the Early Cretaceous by widespread extension between two African sub-plates during Early Cretaceous time, when the African continent was stationary or slow moving with respect to underlying mantle plume resulting in the collapse of the " Tibesti-Sirt Arch". According to this model, the Sirt Basin formed the northern end of a fracture zone which extended south through the Chad depression into the Benue Trough separating a Saharan plate to the northwest from an East African plate. Mickbel (1979) concluded that the NNW-SSE striking graben and horst structures of the Sirt Basin were initiated during the Upper Cretaceous. According to Clifford et al., (1980), the Sirt Basin represents a Mesozoic to Tertiary cratonic rift formed by crustal extension of the Suez type as an interior fracture basin, but near the plate margin.

In contrast, Kingston et al. (1983a) has classified the Sirt Basin as an interior fracture basin originating from divergence and tension within a continental block. Goudarzi, (1980) maintained that the "Sirt Basin generally remained a positive element until near the end of Cretaceous, at which time movements and deformation took place in western Libya, and the Sirt area gradually submerged, probably for the first time since Early Palaeozoic time. Large scale subsidence and block faulting that began in Late Cretaceous times continued intermittently into the Miocene". Parsons et al., 1980, indicated that the horsts are often tilted eastwards to form half grabens in the hanging wall of faults that started movement in the Late Cretaceous and ended in the Middle Eocene. Van Houten (1983) considers the collapse of the "Tibesti-Sirt Arch" to have been caused by drift of the African plate and the resulting movement of north-central Libya over a fixed mantle hot-spot during the Early Cretaceous. A time when a significant shift in plate motion took place. The shift in the direction of the plate led to a

change from extensional to compressional stresses within the African plate and to the

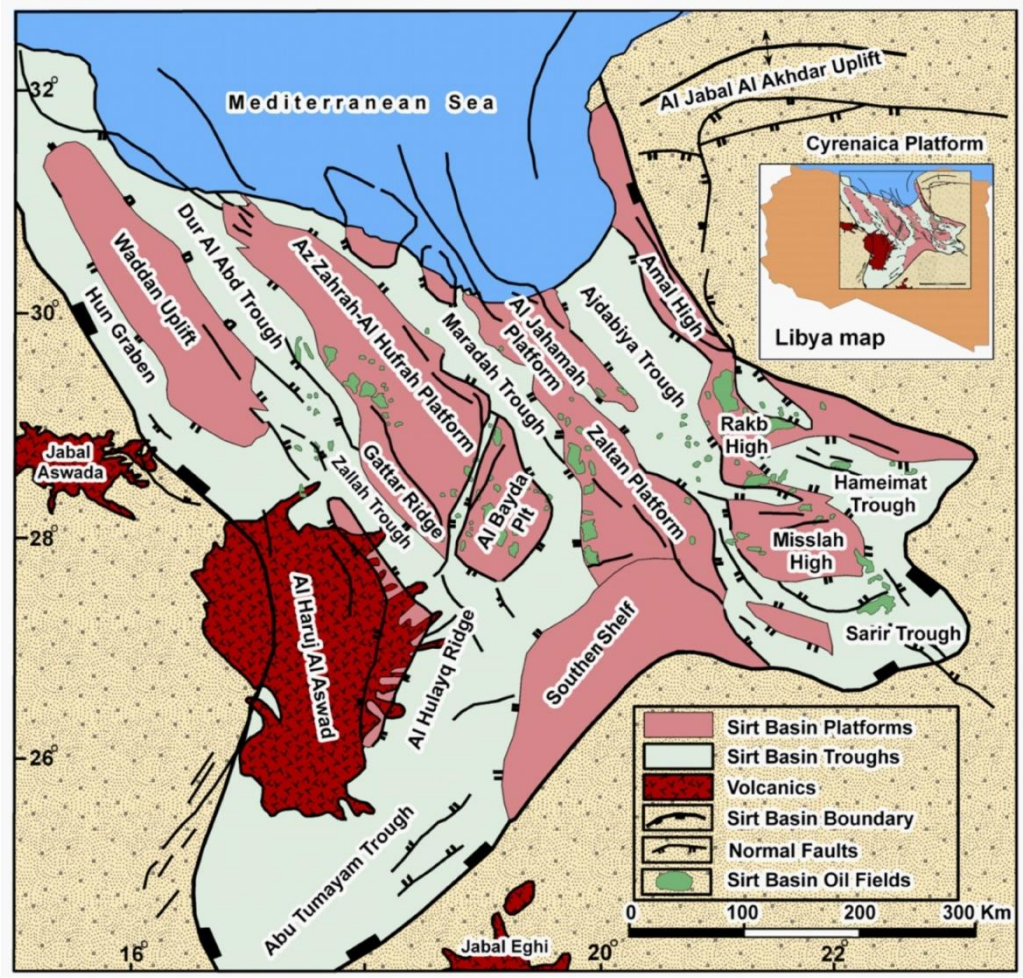


Fig. 2.7 The tectonic framwork of Sirt Basin, shows that the basin is differentiated into several positive and negative tectonic elements delimated by normal faults. (Modified after Mozoughi and Taleb, 1981; Bellini and Masa, 1980). Insert map of Sirt Basin in Libya

fragmentation of the thinned lithosphere. Harding (1984) has pointed out the similarity between the Viking Graben, the Gulf of Suez and the Sirt Basin that comprising three arms define a large triple junction, including the Sirt Basin deep which represents the NW arm, the Abu Tumayam Trough which represents the southern arm, and the Sarir-Hameimat Trough which represents the eastern arm (Fig. 2.8). The idea of the three arms (Sirt Basin) rift was first postulated by Parsons et al. (1980).

Gumati and Schamel (1988) considered the Sirt Basin to be the youngest rifted intracratonic basin of Libya and were formed by "active subsidence and block-faulting accompanying the collapse of the Tibesti-Sirt Arch in the Late to Early Cretaceous time". Lewis (1990) has commented that such basins are caused by extensional shear forces, an idea initially postulated by Klitzsch (1971). Gumati and Nairn (1991), however, observe that lithospheric extension at the beginning of Late Cretaceous caused

faulting and differential subsidence. In an earlier study, Gumati and Kanes (1985) concluded that the maximum subsidence occurred during the Palaeocene and Eocene times and that during the last decade great progress has been made in working out the stratigraphy of the Palaeozoic rocks of Libya.

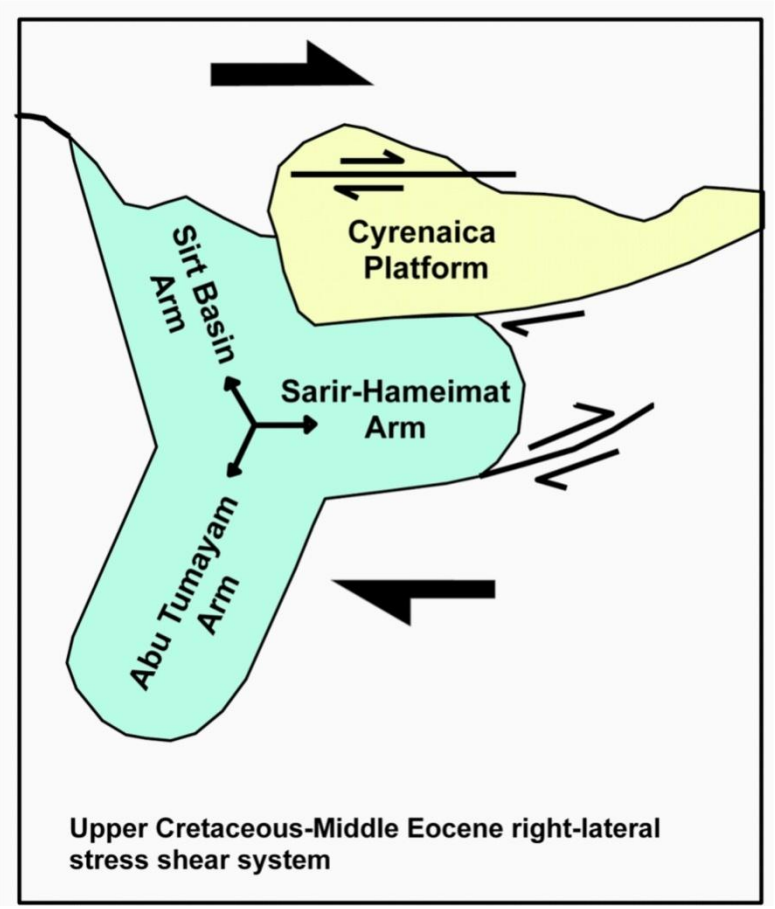


Fig. 2.8 The three subsurface arms define a large triple junction, including the Sirt Basin deep trending features which represent the NW arm, the Abu Tumayam Trough which represents the southern arm, and the Sarir-Hameimat Trough which represents the eastern arm. Modified from Harding, (1984).

Baird et al, (1996) suggest that the basin formed during the Late Cretaceous and has been subjected to four different tectonic stages or phases. Tectonic phase I includes the geohistory of the area from the Precambrian to the end of the Early Cretaceous (96 Ma), tectonic phase II extends from about the beginning of the Cenomanian to the Maastrichtian (97-74 Ma), tectonic phase III extends from the Maastrichtian to the end of the Eocene (74-36 Ma), and tectonic phase IV, extends from the earliest Oligocene to the Recent (36 Ma-Present). The collapse of the Tibesti-Sirt Arch initially occurred during the Pre-Early Cretaceous (Hallett, 2002). Rift valleys probably began to form in the Jurassic times (Hallett and El-Ghoul, 1996; Guiraud, 1998); According to Westaway (1996), the Sirt Basin is an active oblique extension area which can be regarded as

internal deformation of the African Plate that adjust its motion sense from northward to northeastward relative to Eurasia.

Anketell (1996) presented the most comprehensive synthesis of the tectonics of the Sirt Basin. He explained the structural configuration of the basin including the Sabratah Basin and the Cyrenaica Platform as a response to large-scale strike-slip movements along a South Atlas basement megashear that feathered eastwards as it extended into Tunisia and Libya. He also postulated that later structures within Sirt Basin are a result of major dextral and sinistral strike-slip movements on basement faults in concert with different rates of movement of the Western (Saharan) and Arabian (Nubian) sub-plate boundaries in response to differring times and rates of opening of various regions of the Atlantic Ocean. Gras, (1996) believes the formation of Sirt Basin is closely related to the opening of the Atlantic Ocean and to Tethyan convergence in Mesozoic and Tertiary times.

Jerzykiewicz, et, al. (2002) suggests that the formation of the Sirt Basin was due to polyphase extensional tectonics initiated in the Early Cretaceous time, that divided the basin into NW-SE trending platforms alternating with troughs. Gruenwald, (2001) proposed that rifting had ceased by the Mid-Cretaceous, but Alpine-related tectonic pulses in the Late Eocene resulted in northward tilting of the basin.

Recently Capitanio, et al. (2009) found that the origin and evolution of Sirt Basin as a wide rift respond to the Hellenic subduction and lower mantle penetration, recording the development of slab pull forces in the basin's strain history. Capitanio, et al. (2009) believe that the Hellenic pull grew initially during the accumulation of slab material on the transition zones, inferring differential faulting in Sirt Basin between ~72 and 55Ma, then abruptly increased, at ~50Ma, inducing large extension in the Sirt Basin as well as in the Hellenic orogen, which accompany the rapid Hellenic slab penetration in the lower mantle. In addition Capitanio, et al. (2009), pointed out that the dynamics found here are compatible with those of lower mantle avalanche models, and show, for the first time, how deeply generated forces manifest at the surface and their control on the evolution of convergent margins.

2.1.3 Discussion and synthesis of published models

It may be concluded from the diversity of geological opinion that there is still a debate regarding the earliest tectonic evolution of the Sirt Basin. This is mainly for two reasons:-

- The absence of deep drilled well reaching to the basement in the deep troughs and
- The absence of deep seismic reflection and refraction data

Therefore, we can only hypothesize regarding the origin of the Sirt Basin. Several attempts have been made to define the tectonic phases based on the sedimentary fill of the basin (Fig. 2.9). These subdivisions were started by Harding (1984) who divided the sedimentary fill of the Sirt Basin into pre-graben, syn-graben and sag basin succession. There is no general agreement on what constitutes the pre-rift and syn-rift sequences and these disagreements are probably due to the multiple rifting stages that led to the formation of Sirt Basin (Tawadros, 2001). Fig. 2.9 shows these subdivisions according to various authors. For example, the Nubian sandstone (Late Jurassic-Early Cretaceous) were considered as pre-rift by Harding (1984), Baird et al. (1996) and Van der Meer & Cloetingh (1996) while it is considered as syn-rift by Grass (1996), Schroter (1996), Ahlbradt (2001), Abadi (2002) and Pawellek (2007) among many others. It is possible that the Sirt Basin area went through multiple stages of rifting since the Middle Triassic and that different parts of the basin acted differently at different times (Tawadros, 2001).

In general, the structural history of the Sirt Basin, taken from several published sources, can be summarised as follows:

1. The structurally complex period from the Precambrian to end of the Early Cretaceous (96Ma) represents the Tectonic Phase 1 of Baird et al., (1996). It consists of a pre-Hercynian sequence affected by:

    - NW-SE trending pull-apart basins (Fig. 2.10) developed during the Pan-African Orogeny (Tawadros, 2001 and Hallett, 2002).

    - Extension and formation of horst and graben system in the Cambrian (Klitzsch, 1971; Tawadros, 2001 and Hallett, 2002) indicated by the idea that structural highs consist mainly of granites and granodiorite, whereas the trough areas consist mainly of metamorphic rocks, (El Hawat and Pawellek, 2004) suggesting that rifting structures took place on reactivated basement faults originating in Late Precambrian time.

- Subsidence and deposition of shallow marine sediments and emplacement of acidic volcanics in the Late Cambrian (Tawadros, 2001).

- Continued extension into the Early Carboniferous

2. Followed by a Pre-rift continental regime post-Hercynian sequence associated with:

    - Thermal uplift and erosion during the Late Carboniferous and Permian due to the Hercynian Orogeny and subduction of the proto-Pacific oceanic plate beneath Gondwana (Hallett, 2002).

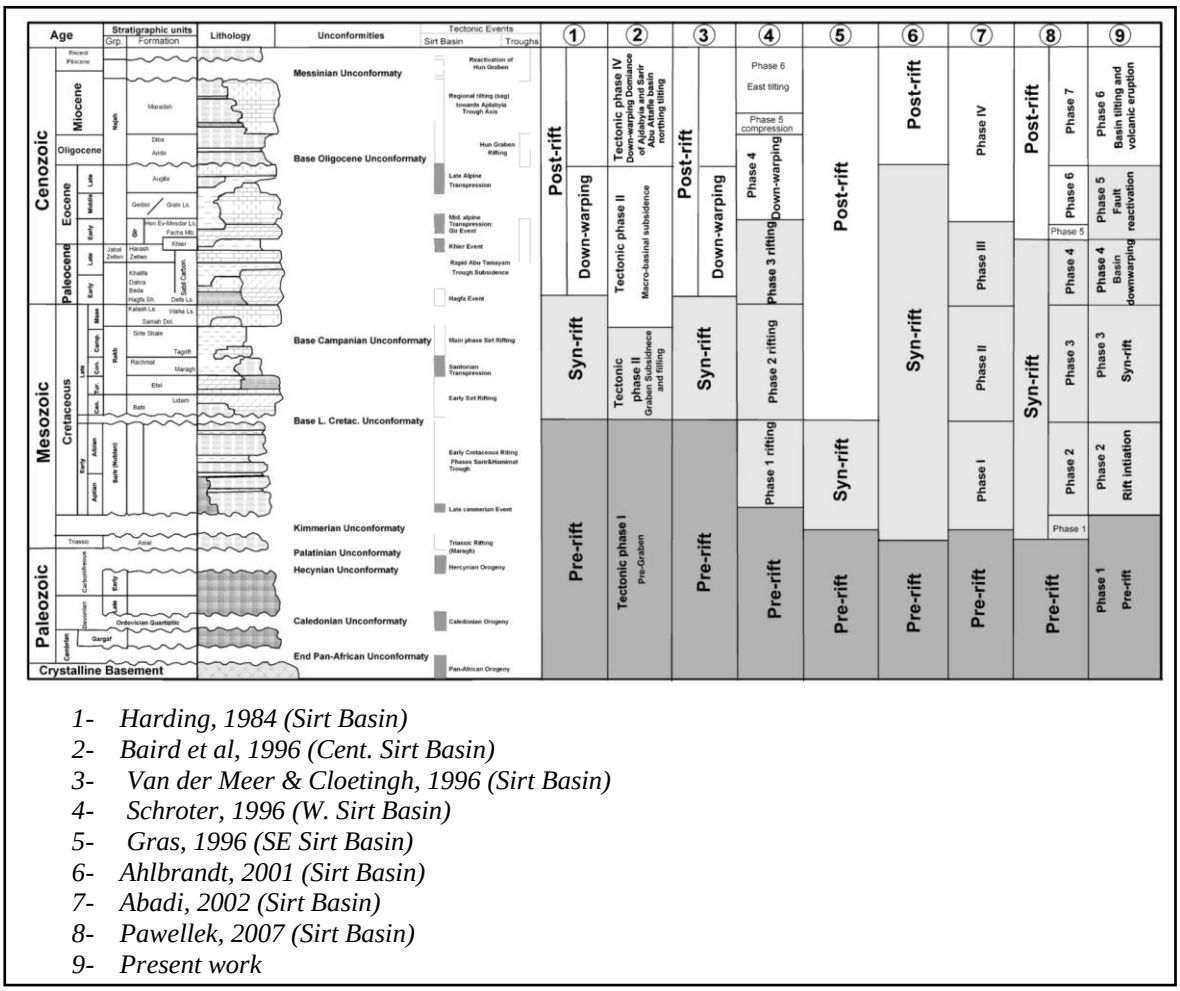
    - Central Libya developed as a positive region referred to as the Tibesti-Sirt Arch (Fig. 2.10) during the Hercynian Orogeny before it collapsed during the Early Cretaceous. At this stage the Sirt graben system was infilled predominantly by Nubian-type continental sandstones (Tawadros, 2001), and remained sub-aerially exposed until the Cenomanian.

3. Renewed extensional faulting and rapid subsidence occurred in the Cenomanian to Campanian (Gumati and Kanes, 1985; Gumati and Nairn, 1991) resulted from the Apulian plate separated from north Africa, during the Early Cretaceous creating a tensional regime on the plate margin

4. Deformation is associated with NW-SE compression and NE-SW extension (Burollet, 1963), and represents Phase 2 (97-74Ma) of Baird et al., (1996).

5. Following a period of quiescence and development of thermal sag basins over earlier rifts, northward convergence was resumed in the Early Eocene (Dewey et al., 1989). The area underwent thermal subsidence (Gumati and Nairn, 1991) and the earlier graben system became buried by platformal sediments (Burollet, 1963). Tectonic Phase 3 (74-36Ma) of Baird et al., (1996).

6. In the Late Eocene the motion of Africa relative to Europe changed from compressional to right lateral, and then into a NW-SE compressional regime in the Early Miocene (Van der Meer et al., 1993). This phase is equivalent of tectonic Phase 4 (Baird et al., 1996) and extends from the Oligocene to the Recent (36Ma – Present).



1- Harding, 1984 (Sirt Basin)
2- Baird et al, 1996 (Cent. Sirt Basin)
3- Van der Meer & Cloetingh, 1996 (Sirt Basin)
4- Schroter, 1996 (W. Sirt Basin)
5- Gras, 1996 (SE Sirt Basin)
6- Ahlbrandt, 2001 (Sirt Basin)
7- Abadi, 2002 (Sirt Basin)
8- Pawellek, 2007 (Sirt Basin)
9- Present work

Fig. 2.9 Rifting episodes of Sirt Basin according to different authors that have studied the basin during the last three decades (modified after Guiraud et al, 2005, Tawadros, 2001and the authors who mentioned in this figure).

This brief review of previous studies illustrates that the origin of the Sirt Basin has been related, not only to inter-plate motion between Africa and Europe but also, to intra-plate movements within the African Plate (Anketell, 1996). Those involved in tectonic analyses and modelling of inter and intra-plate relationships for the region generally pay scant attention to the Libyan margin. Studies on the closure of the Tethys tend to mention the Libyan margin only in passing, referring to major basins such as the Sirt as having developed in the Cretaceous but with little comment on how they formed (Hallatt, 2002 and Abadi. 2002).

Similarly, those involved in African intra- and epi-cratonic basin studies pay little

attention to the Tethyan cratonic margin other than to recognize the Sirt as the northernmost element of the sub-plate boundary stretching northeast wards from the Benue Trough.

The closely similar tectonic history of the Libyan epicratonic basins to that of other major cratonic basins in Africa and to those which led to the closure of the Tethys, supports a view that the Sirt Basin developed due to a combination of inter- and intra-plate movements resulting from the relative motions of the American, African and Eurasian plates during opening of the Atlantic Ocean and development of the Mediterranean.

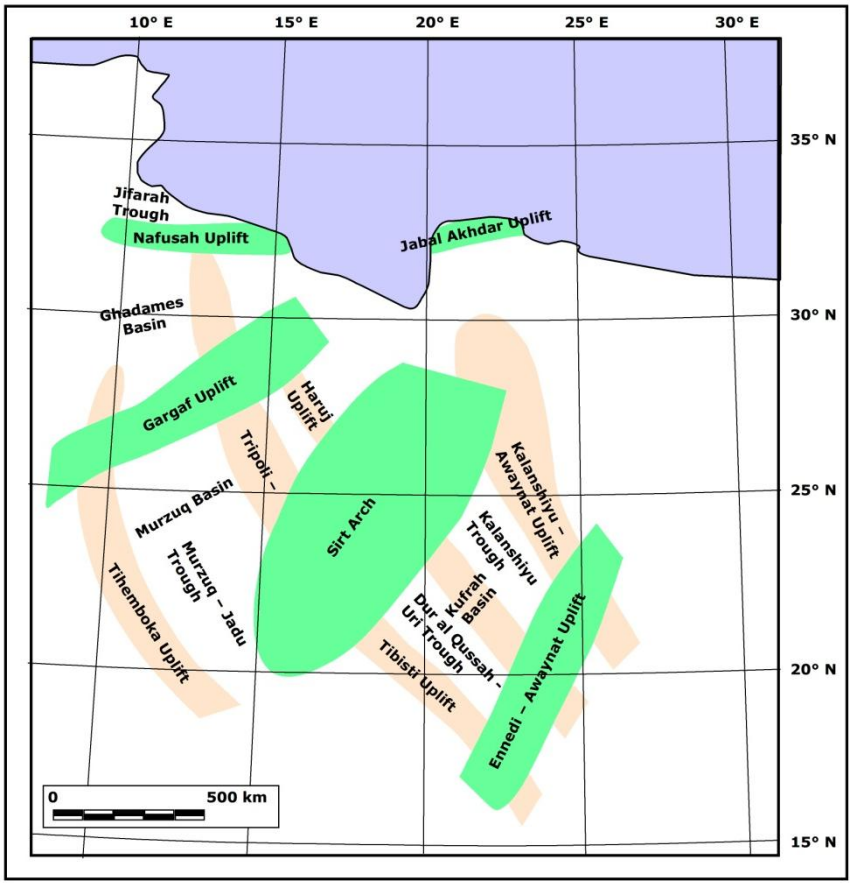


Fig. 2.10 Major structural elements of Libya. Light brown colours are Caledonian and green colours are Hercynian orogenies (after Klitzsch, 1970; Bellini and Massa, 1980).

2.2.0 Summary

Although Libya has relatively simple surface geology, it has a very complex subsurface geology and geological history.

The regional geology and the structural framework has been highly influenced by the Caledonian, Hercynian, and Alpine tectonic events which led the country to become a

site of deposition of large sheets of continental clastics, and several transgressions and regressions episodes with consequent accumulation of a wide variety of sedimentary rocks.

The surface geology of the study area is dominated by sedimentary rocks ranging in age from Late Cretaceous to Tertiary whilst the subsurface stratigraphic succession consists of a variety of lithologies ranging from Pre-Cambrian crystalline basement to Recent. Mesozoic and Tertiary lithologies are extremely variable, reflecting the tectonic and structural evolution of the Sirt Basin, which is closely related to the opening of the Atlantic Ocean and evolution of the Tethyan margin.

The tectonic evolution and stratigraphy of the Sirt Basin has been studied by many authors, most of whom believe that it represents an intracratonic basin constructed on the northern margin of the African Plate. The primary structural pattern in the Sirt Basin comprises NW trending horsts and grabens with NE-, ENE-, and E-W-trending clusters of faults and/or fault blocks present mainly in the SE part, around the southern edge of the Cyrenaica Platform

It may be concluded from the diversity of geological opinion that there is still a debate regarding the earliest tectonic evolution of the Sirt Basin. This is mainly for two reasons:- 1) The absence of deep drilled well reaching to the basement in the deep troughs and 2) the absence of deep seismic reflection and refraction data therefore, we can only hypothesize regarding the origin of the Sirt Basin.

CHAPTER 3: PETROLEUM GEOLOGY OVERVIEW

3.1 Introduction

Libya has been a favoured country for hydrocarbon exploration since 1956, when the first wildcat well was drilled. Very large volumes of oil and gas have been discovered in Libya, and the total original oil in place appears to be about 135 billion barrels, and total original recoverable reserves about 40.9 billion barrels (Hallett, 2002). This reserve has primarily resulted from the success rate of oil discovery in the Sirt Basin where 19 of the 21 giant fields, with an estimated 50 Bboe of resources discovered to date, are located (Le Heron, & Thusu, 2007).

Exploration has been extended into neighbouring basins (Fig 2.3) to the west (Ghadamis) and southwest (Murzuq) where the search for hydrocarbons continues. It is worth noting that several of the most important, recent discoveries were made between 1979 and 2000, in the absence of an aggressive drilling programme. New play concepts developed during this period have undoubtedly contributed to recent successes, through fruitful collaborations between oil companies and academia.

Libya can be divided into two discrete geological provinces based on the age of the hydrocarbon basins, and their sedimentary fill. The first province comprises a belt of tectonically active basins of Mesozoic-Cenozoic age that includes the complex, prolific and mature Sirt Basin in central northern Libya as well as the promising Libyan offshore areas (Fig 1.1).

The second province, shown on Fig. 1.1, is a regionally extensive Palaeozoic mega-province, comprising two intracratonic basins in western Libya (Ghadamis and Murzuq), and additionally the Al Kufrah Basin and the Cyrenaica Platform located in eastern Libya. During the Palaeozoic, all these basins appear to have been connected along a relatively stable platform area because they show similar sedimentological character and geological history and thus similar play concepts can be applied, such as a regionally developed source rock.

According to various literature sources (Boote, et al. 1998, Campbell, 1991, Thomas, 1995a, b, Baird, et al. 1996, Gurney, 1996, and Hallett, 2002), the oil reserves of Libya can be broken down by petroleum system (Table 3.1), by region (Table 3.2), or by age of reservoir (Table 3.3).

Table 3.1 shows the principal petroleum systems in Libya, although there are minor systems which are not shown. Also it can be noted that many systems have charged more than one reservoir and several systems contain a mix of oils from different source rocks and it should be noted that the reserve figures are approximations based on published data. However using the literature sources mentioned above, the figures are believed to represent a fair estimate of Libyan oil reserves (excluding gas).

Basin	Petroleum System	Core Area	Approx. orig. reserves (MMB)
Murzuq	Tanzuft - Mamuniyat	Elephant	1000
Ghadamis	Tanzuft - Mamuniyat	Al Hamra	20
	Tanzuft - Akakus/Tadrart	Cone. 66	350
	M/U Devonian - Awaynat Wanin	Al Hamra	550
Western Sirt Basin	Sirte Shale - Palaeocene/Eocene	Zailah, Ghani	750
Central Sirt Basin	Sirte Shale - Palaeocene	Az Zahrah-Al Hufrah	3850
Western Ajdabiya Trough	Sirte Shale - Upper Cretaceous	Wahah	4050
	Sirte Shale - Palaeocene	Nasser, Dayfah	4500
	Sirte Shale - Eocene/Oligocene	Zaitan Platform	100
Eastern Ajdabiya Trough	Sirte Shale-Nubian	Kalanshiyu High	500
	Sirte Shale - Palaeocene	Intisar	3350
	Sirt Shale - Eocene	Antlat	150
Eastern Sirt Embayment	Sirte Shale - Nubian	Sarir	8500
	Sirte Shale - Eocene/Oligocene	Jalu	4500
	Triassic - Amal/Maragh Fm.	Jakharrah	450
	Hybrid	Amal, Nafurah	6000
Offshore	Eocene - Farwah	Bouri	1500
	Other petroleum systems		1770
			40,890

Table 3.1 The principal petroleum systems in Libya from Boote, et al, 1998, Campbell 1991, Thomas, 1995a, b, and Baird, etal, 1996, cited in Hallett, 2002.

In contrast Table 3.2 shows the total dominance of the Sirt Basin which is partly attributable to the late generation of oil in this area. Almost certainly large volumes of early generated oil from the Murzuq and Ghadamis Basins have been lost as a result of trap destruction (Hallett, 2002). Whilst Table 3.3 shows the dominance of the Palaeocene carbonates and the Lower Cretaceous Nubian Sands which between them account for 55% of all the oil reserves in Libya.

The Sirt Basin (Fig 1.1) ranks 13th among the world's petroleum provinces and has the greatest reserves of all African basins containing approximately 80% of Libya's total proven oil reserves (41.5 billion barrels as of January 2007) as estimated by US Energy Information Administration (2007) which represent 29% of Africa's total. Over 23 large

oil fields and 16 giant oil fields occur in the province and 80% of the total recoverable oil and gas were discovered prior to 1970. It appears from these tables that the Sirt Basin represents the most productive area, mainly from two principal reservoirs, the Paleocene carbonates and the Nubian sands.

Region	Original oil in place MMB	Original recoverable reserves MMB	Number of discoveries	% of total reserves
Sirt Basin	117,000	36,700	345	89.8
Murzuq Basin	5,200	1,600	20	3.9
Offshore	8,200	1,500	25	3.7
Ghadamis Basin	3,850	950	90	2.3
Cyrenaica	520	140	8	0.3
Total	134,770	40,890	488	100

Table 3.2 Libya Total Oil Reserves by Region from Boote, et al, 1998, Campbell 1991, Thomas, 1995a, b, and Baird, etal, 1996, cited in Hallett, 2002.

Age	Original oil in place MMB	Original recoverable reserves MMB	Number of discoveries	% of total reserves
Eocene + Oligocene	15,390	5,770	72	14.2
Palaeocene	41,370	13,295	95	32.5
Upper Cretaceous + contiguous Precambrian	30,485	8,164	106	20.0
Lower Cretaceous	28,720	9,229	88	22.5
Palaeozoics + Quartzites	18,805	4,432	127	10.8
Total	134,770	40,890	488	100

Table 3.3 Libya, Total Oil Reserves, by Reservoir Age from Boote, et al, 1998, Campbell 1991, Thomas, 1995a, b, and Baird, etal, 1996, cited in Hallett, 2002.

The Paleocene carbonates, which include the Nasser (previously Zaltan), Dayfah, Intisar fields, and some western Sirt Basin oil fields contain one-third of all the oil in Libya, and the Nubian Sands, which are mainly located in the eastern part of the basin and include the As Sarir and Messiah fields, hosts a further quarter. Hallett (2002) has attributed the domination of the Sirt Basin to two main factors, the quality and thickness (up to 750m) of the effective Sirt Shale source rock (Fig. 3.1), and the late timing of oil generation and migration. It should also be noted that there are considerable areas of the Sirt Basin where the oil generating potential is poor, due to thinness of the source rock or an unsuitable kerogen type.

The Ghadamis Basin (Fig. 1.1) is considered a second basin for oil reserves and production. Many small accumulations in both structural and stratigraphic traps have been encountered in this basin. The basal radioactive Silurian hot shale (Tanzuft) represents the prolific source-rock in the basin, with thickness that rarely exceeds 100m.

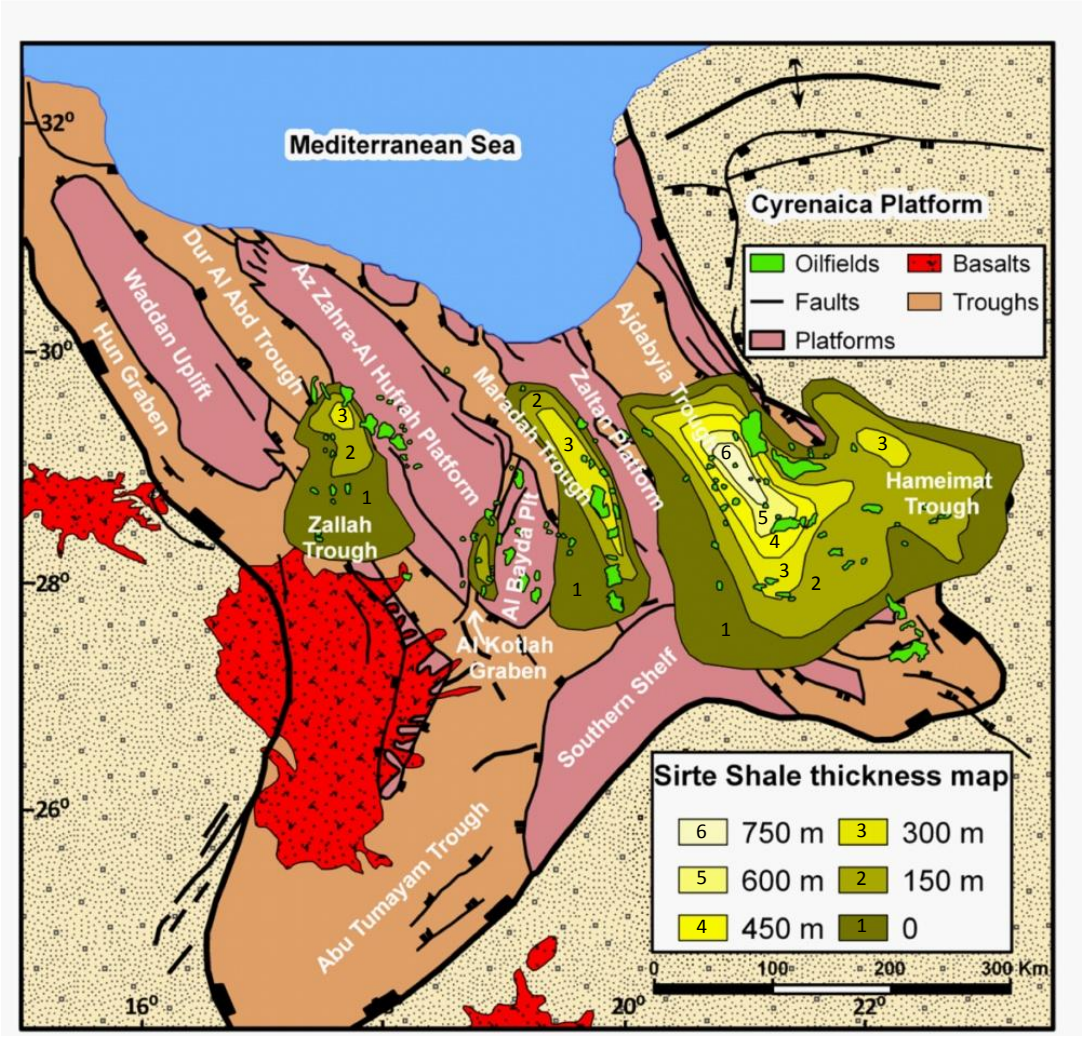


Fig. 3.1 Sirte Shale thickness map of Sirt Basin. Modified after El Alami at al, (1989); Rusk, (2001); Ahlbrandt, (2001); Hallett, (2002).

A proportion of the oil was generated before the Hercynian orogeny and has subsequently been lost as a result of trap destruction and leakage. Furthermore, a considerable proportion of Tanzuft source rock in the central Ghadamis Basin is now in the gas generating zone and its oil generating capacity is exhausted. In the Ghadamis Basin, approximately 260 exploration wells yielded 35 oil-field discoveries with an estimated 3 billion bbl of recoverable oil. The Ghadamis Basin petroleum systems involve Ordovician, Silurian, Devonian, and Triassic reservoirs charged by Lower Silurian and/or Middle to Upper Devonian source beds. Epeirogenic movements of the Caledonian Phase (c. 400 Myrs), represented as a regional unconformity at the top of

the Silurian creating the uplifts of the Al Qargaf and Tihemboka Arches and led to the beginning of the separation of the Ghadamis from the Murzuq Basins

Several major discoveries were made during the 1980s and 1990s in the Murzuq Basin where the Tanzuft shale is the only effective oil source of importance (Hamyouni, 1991) although the Silurian Tanzuft Formation is not present over considerable parts of the basin as the distribution is discontinuous and patchy, and its thickness does not exceed 45m. It is possible, however, that very minor amounts of early oil were expelled from Devonian Uennin organic-rich shale in the basin center (Meister et al., 1991). The expected structural trap types are low-relief, simple, and faulted anticlines; drape anticlines over paleotopographic relief or faulted structures (Rusk, 2001) basically the same as those in the Ghadamis Basin center. In comparison to the Sirt Basin, the Murzuq Basin potential is likely to be limited by the amount of oil generated from the Tanzuft hot shales in the Murzuq Basin and is probably not more than 5% of that generated by the Sirte Shale in the Sirt Basin.

The northwestern offshore (Fig. 1.1) Tripolitania Basin (Gabes-Sabratah Basin) is a deep, highly faulted, elongate trough which extends from the Gulf of Gabes to the northwestern margin of the Sirt Basin. The Bouri oil field discovered in this area is one of the largest in the Mediterranean. It is reservoired in Lower Eocene (El Garia Formation of the Metlaoui Group) nummulitic shoals that developed on a salt-supported ridge and represents the main pay in all Tripolitania Basin discoveries. The field is sourced by Ypresian shales deposited in basinal setting. Numerous other discoveries have been made in the area surrounding Bouri, but these discoveries are characterized by high amounts of gas and most of the fields contain gas-condensate or gas with a thin oil rim. In contrast, no hydrocarbons have yet been discovered in the northeastern offshore of Libya.

The Al Kufrah Basin (Fig 3.1) is separated from the Murzuq Basin by the Tibesti-Sirt arch whilst separated from Sirt Basin by the southern shelf. Till now no hydrocarbons have been discovered in the Al Kufrah Basin and however very few wells have yet been drilled. Indications from both well evidence and outcrop studies suggest that the Tanzuft Shale develops a more silty character in the Al Kufrah Basin and that the hot shale horizon is not present.

The Cyrenaica Platform which is located in the eastern part of Libya (Fig 1.1) underwent some oil exploration activities, where some 77 exploratory wells have been drilled, but unfortunately the results have been disappointing. In spite of several shows, the only significant success has been in the Ash Shulaydimah Trough where several

discoveries have been made in Paleocene and Eocene reservoirs at Antlat, and in wells A1, B1 and C1-NC129 (Hallett, 2002). These oils are hybrid oils derived from Cretaceous, Paleocene and Eocene source rocks. Excluding the Ash Shulaydimah Trough and the offshore area, no effective petroleum system has yet been established in Cyrenaica despite the presence of numerous shows. This is probably due to a combination of factors, including questionable source rocks and ineffective seals.

Different types of oil which vary greatly in character, from sweet, low-sulphur light oils to waxy, heavy, biodegraded and gassy crudes have been identified in Libya resulting from the nature of the source rock, and the subsequent maturation history. The Sirte Shale in Libya is one of the most valuable source rocks in the world with over 100 billion barrels of oil in place entrapped which represents only a small proportion of the amount generated (Hallett, 2002).

More than 90% of the world's discovered reserves have been sourced from six stratigraphic intervals, Silurian (9%), upper Devonian-Tournaisian (8%), Pennsylvanian lower Permian (8%), upper Jurassic (25%), Turonian (29%) and Oligo-Miocene (12.5%) as reviewed by Klemme and Ulmishek (1991). By contrast Libya is anomalous in that no more than 15% of its reserves were derived from these six intervals. Over 90% of Libyan oil was sourced from the Campanian Sirte Shale and the Silurian Tanzuft Shale.

The purpose of this chapter is to review hydrocarbon occurrences in the study area as a part of the Sirt Basin based on a review of the published literature and available oil company reports. Characteristic features of the oil fields previously discovered in the Sirt Basin (Fraser, 1967; Roberts, 1970; Sandford, 1970; Williams, 1972; Clifford et al, 1980; Brady et al., 1980) that are largely still producing, are referred to because they can provide analogs for further discoveries. It is with this purpose in mind that I also point out the oil discoveries in the Sirt Basin, even though they are located beyond the scope of the study area. Published models of the oil fields and plays and generalizations concerning petroleum systems of the Sirt Basin (Harding and Lowell, 1979; Parsons et al., 1980; Harding, 1983; Thomas, 1995a and b; Gumati et al., 1996; Wennekers, 1996; Hallett and Ghoul, 1996; Hallett, 2002) are also referred to, in order to give the reader necessary insight into the existing body of knowledge on the petroleum geology of the basin.

3.2. Petroleum Geology

The concept of petroleum systems is well established in geological literature (e.g. Hallett, 2002). It includes an identification of the factors that control the occurrence of oil and gas in a trap. Moreover in more detail, these types of studies play a key role in determining whether or not a prospect will be successful in harbouring a commercial deposit of oil and gas. Once a trapping situation has been identified from the interpretation of geological and geophysical data, it is necessary to understand how the hydrocarbons originated, where they came from and when they were produced. The process can be divided into four phases:

1. The quantity and composition (richness and thermal maturity) of the organic matter present in potential source rocks,
2. The temperature and pressure conditions necessary to convert organic matter into hydrocarbons (conditions necessary for hydrocarbon generation).
3. The timing of the generation and migration through carrier beds of hydrocarbons relative to time of trap formation (expulsion from the source rock)
4. Entrapment in a hydrocarbon trap (i.e., occurrence of reservoir rocks in structural and/or stratigraphic traps).

Knowledge of these factors is very important in assessing the degree of risk for a prospect. Although it was not a major objective of this study to conduct any new geochemical analysis, a review of the published literature and available oil company reports was undertaken to document the key information about the known hydrocarbon potential in the study area as a part of the Sirt Basin.

Compared with publications on stratigraphy and structure, relatively few studies have been published on petroleum geochemistry in the Sirt Basin. Geochemical studies have been done in the Sirt Basin by several different groups (e.g., Robertson Group). These studies, based on drill cuttings and/or core from numerous wells were mainly done for foreign oil companies operating in Libya. The information presented in this study is based primarily on a review of existing geochemical studies (data) undertaken by the Robertson Group (RG) for Mobil Oil Libya Limited, dated January 1989, entitled: “Petroleum Geochemical Evaluation of the West Sirt Basin“, report by El Alami at al. from Libyan Petroleum Institute (LPI), Libya (1989) reports by Geochem Laboratories, on a number of wells for various oil companies, including Oasis (Waha) and others. Another source of information is the Petroleum Geology of Libya by Hallett (2002), and

Libya; Petroleum potential of the underexplored basin by Rusk, (2001); and 'The Sirte Basin Province of Libya—Sirte-Zelten Total Petroleum System' by Ahlbrandt, (2001).

The first study prepared for the Libyan Petroleum Institute (LPI) was entitled "The study of the Upper Cretaceous Sirt Shale Sirt Basin, Libya" (El-Alami, et al, 1989). This study (approximate Latitudes 27^{o}-31^{o}N and Longtitudes 16^{o}-23^{o}E), investigated the source rock characteristics of 88 wells in the Sirt Basin. The main conclusion of the LPI study is that the Upper Cretaceous Sirte Shale unit is the main source rock in the Sirt Basin where it consists of calcareous shales and shaly limestones deposited in a semi-restricted environment. The distribution and geometry of the Sirte Shale appears to be influenced by the basin tectonics; namely, graben and horst features, with the thickest shales being present in the grabens or troughs (Fig. 3.1). The organic facies is mainly amorphous with a minor amount of algal herbaceous material in both the Zallah and Maradah Troughs. Total organic carbon (TOC) varies from about 1.9% to 3.8% in the Zallah Trough and reaches as high as 3.08% to 5.78% in the Maradah Trough. Thermal maturity (Fig. 3.2) is highest in the trough areas and oil generation started during the early Miocene. Migration distance is believed to be short, going from the graben area into traps associated with adjoining horst blocks.

The second study entitled "Petroleum Geochemical Evaluation of the Western Sirt Basin, Libya" was prepared by the Robertson Group for Mobil Oil Libya (Robertson Group, 1989). This study (approximate Latitude, 27^{0}-32^{0}N and Longtitude 16^{0}-20^{0}E), conducted on behalf of Mobil and National Oil Corporation (NOC), concluded that the Sirte (Rakb) shale and Rachmat Formations of Upper Cretaceous age are the principal source rocks in the Western Sirt Basin. Fifty-nine wells were selected for source rock analysis over the Sirt-Rachmat interval. These source rocks contain mixed kerogens comprising mainly marine, type II sapropelic kerogen and degraded humic material. Their occurrence is largely restricted to the grabens depocenters.

The average TOC values range between 2.0 and 3.0% and only rarely exceed 5%. Thermal maturity has been reached in both the Zallah and Hagfa Troughs with oil generation beginning in the mid-Eocene to end Eocene. Migration is from the troughs to traps located on the adjoining highs (i.e., horst blocks).

Some workers have also suggested that the Hagfa shales may be a potential source rock particularly in the deeper troughs (i.e., Ajdabyia Trough). Stratigraphic correlations indicate also that the Silurian Tanzuft shale, the main source rock in the Ghadamis and Murzuq Basins, is also present in the extreme northwestern part of the Sirt Basin.

3.3. Sirt Basin

The complex tectonic and sedimentary history of the Sirt Basin has resulted in multiple reservoirs and conditions that favoured hydrocarbon generation, migration, and accumulation. Most oil pools discovered are located on horst structures at relatively shallow depths. Production in the Sirt Basin comes from more than 20 intervals ranging in age from Precambrian to Oligocene, but the most important finds have been in the Lower Cretaceous Nubian sandstone, although Palaeocene reefs are also important reservoirs.

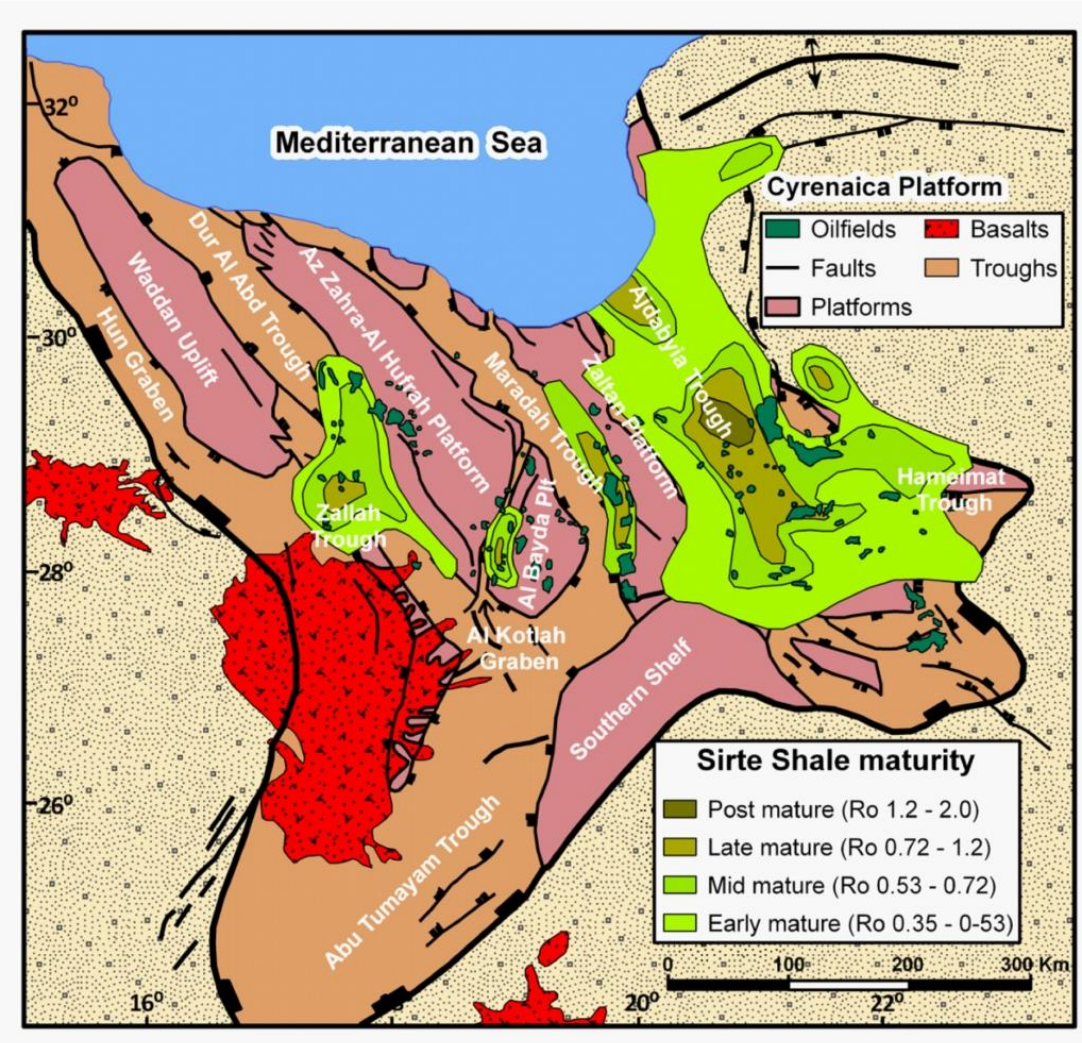


Fig. 3.2 Sirte Shale thermal maturity map of Sirt Basin. Modified after El Alami at al, (1989); Rusk, (2001); Ahlbrandt, (2001); Hallett, (2002).

Hallett (2002) reported that the oils are generally sweet, with sulphur content between 0.15 and 0.66%, and with relatively little gas. Sixteen of the twenty-one major oilfields are undersaturated. Oil gravity is usually within the range 44 to 32° API. Oil pools in the Lower Cretaceous are paraffinic with pour points around 38°C. Accumulations with a Paleocene top seal have pour points up to 13°C, and those with Oligocene and Eocene top seals have a pour point less than 9°C. Oil accumulations have been found from

depths of 700 m to as deep as 4000 m and within a temperature range of 52°C as high as 143°.

Published studies suggest that most of the oil in the Sirt Basin was derived from the Sirte Shale (Upper Cretaceous, Campanian/Turonian), (Parsons et al., 1980; Gumati and Schamel, 1988; Montgomery, 1994; El-Alami, 1996b; Ghori and Mohammed, 1996; Mansour and Magairhy, 1996; Macgregor and Moody, 1998; Ambrose, 2000) with an effective thickness of the Sirte Shale source rock is frequently over 250m, and in places reaches 700m with excellent characteristics (Fig. 3.1).

In addition to the Sirte Shale, several other potential source rocks have been identified, particularly in the eastern Sirt Basin. Mid-Triassic lacustrine shales with type II and III kerogen, derived from land and lake plants were encountered in wells in the Maragh Graben, and oils reservoired in the Amal, Jakharrah, the As Sarah fields, and the giant Awjila-Nafurah field, at least in part, were fed from this source. The isotopic signature of the latter group suggests land derived material deposited in a highly reducing environment. Mid-Cretaceous 'variegated shales' are under-investigated but viable source rocks, and may have considerable potential as the regional overview by Rusk (2001) revealed. They have a total organic carbon content of ~3%. These lacustrine to marginal marine shales, of Early Cretaceous (Barremian-Aptian) age, are recognized in the Maradah Trough and southern Hameimat Trough. In the Sarir area of the southern Hameimat Trough, this source rock yields a waxy crude with mostly type II and III kerogen. This source rock is probably locally developed, having fed adjacent structures.

The Sirte Shale is not an effective source rock in the Hun Graben area. To date no major oil shows have been found in the Sirt Basin west of the Zallah Trough. A significant source kitchen is present in the northern Zallah Trough and Dur al Abd Trough between the Mabruk and Az Zahrah fields, (Fig. 3.3) but peak maturity is only present in the Az Zahrah area and is only early mature to the north. This suggests that the Zallah Trough has only produced modest amounts of oil compared to other parts of the Sirt Basin and may explain why only a modest amount of hydrocarbons have been found on the Waddan Uplift.

The dominant hydrocarbon discoveries in Sirt Basin compared with other basins in Libya is due to three factors (Parsons et al., 1980; Baird et al., 1996; Hallett, 2002):

- the Mesozoic-Cenozoic age of the basin;
- the presence of the rich and prolific source rock in the Upper Cretaceous Sirte Shale;

- and the Cenozoic – Late Cenozoic age of oil generation and migration.

The most prolific reservoir is the Lower Cretaceous Nubian Sandstone followed by the Paleocene carbonates and then the Upper Cretaceous clastics. More than 80% of the fields are associated with structural traps and almost half the fields are found at depths of 2400-3200m.

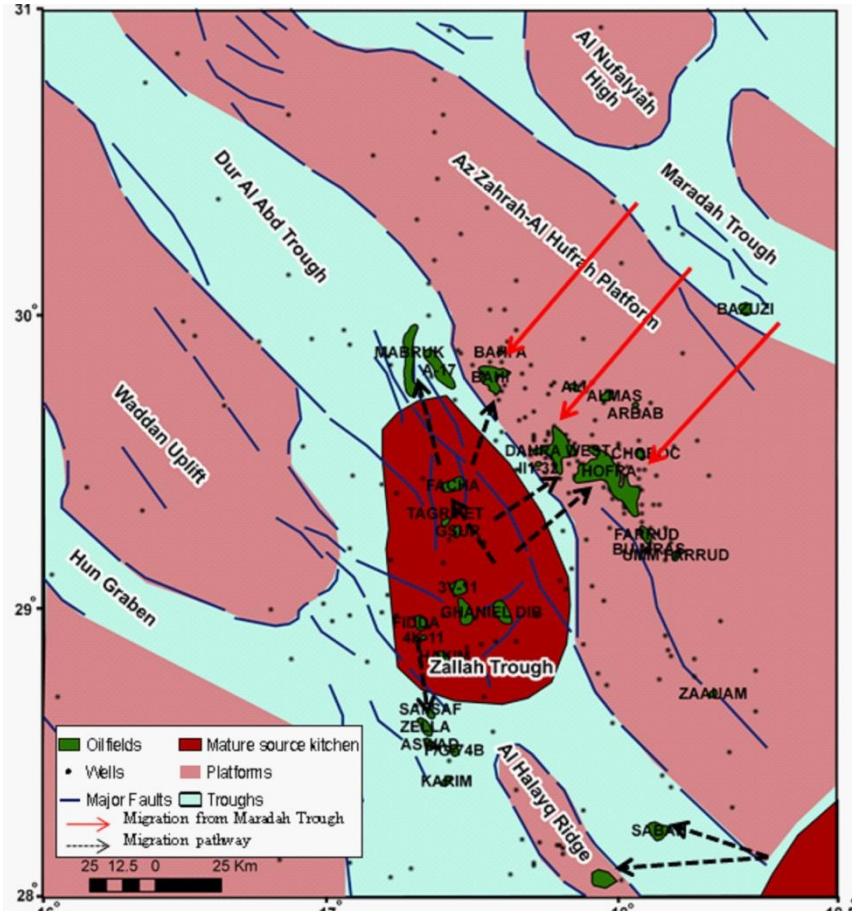


Fig. 3.3 Western Sirt Basin oil kitchen and migration directions map. Modified after Roohi, (1996a).

Peak oil generation is Late Eocene-Oligocene with migration during the Late Oligocene-Miocene. Due to major subsidence and eastward tilting of the basin from the mid-Eocene (Roohi, 1996b), oil migration from the source kitchen to the traps in the west Sirt Basin has been principally from northeast to southwest (Fig. 3.3) resulting in hydrocarbons migrating onto adjacent platforms via fault conduits on the eastern boundary faults of the platforms. Westward migration then occurred until a trapping configuration was encountered. Hydrocarbons frequently migrated as far as the western margin of platforms.

3.4. Study area (western Sirt Basin)

3.4.1 Geochemistry of the source rocks

The oil to source correlation scheme expressed in both reports by Robertson Group and El Alami et al. (1989), suggests that all oils within and around the Zallah Trough are from the same source rock – Sirte Shale and Rachmat, undifferentiated - and that various sub-groups correspond to slight differences in maturity. El Alami et al. (1989) provide an interpretation of the depositional environment of the Sirte Shale and a correlation scheme between oil and source rock, which is based on biomarker data from Geochem Laboratories. Given what is known of the petroleum systems in the eastern Sirt Basin, it is no surprise that the Sirte Shale must have been an important contributor to oils in all parts of the Sirt Basin of Libya and therefore also in the western part of the basin. That correlation between oil and source rock tends to eliminate the possibilities that other source rocks, such as Devonian and Silurian (Basal Tanzuft), would have contributed to the oil reserves of the western Sirt Basin.

A significant source kitchen is present in the northern Zallah Trough and Dur al Abd Trough extending from the Mabruk field to south of the Zallah Field (Fig.3.3).

3.4.2 Sirte Shale source rock characteristics

In this section the areal distribution, thickness and geochemical characteristics of the Sirte source rock is discussed.

- **Geometry and structure**

Fig. 3.4 is a gross thickness map of the Sirte Shale, the prime source rock in the study area. The greatest thickness is in the Zallah Trough where between 500 (152m) and 1000 feet (305m) of black shales are present over an area of approximately 8400 km². In the Zallah Trough and adjacent to the western edge of the Az Zahrah-Al Hufrah Platform thicknesses of over 1000 feet (305m) are present. Depth to the top of the Sirte Shale (Fig. 3.5) varies from about 5400 ft (1646m) below sea-level to 10,000 feet (3048m) below sea-level. In the Hun Graben, the Sirte Shale is just over 500 feet (152m) in thickness and the depth to top Sirte ranges from approximately 200 feet (61m) subsea in well A1-3 to some 700 feet (213m) above sea level in well B1-3. The Sirte Shale thickness map (Fig. 3.4) also shows an occurrence of Sirte Shale with greater than 500 feet (152m) in thickness in the most southern-eastern part of the Zallah Trough and in the northeastern part of the map area in the Maradah Trough.The Sirte Shale is absent (probably due to non-deposition) in the vicinity of the Az Zahrah-Al

Hufrah fields, structurally the highest part of the Az Zahrah-Al Hufrah Platform (Fig. 3.4).

- **Thermal maturity of organic matter**

Fig. 3.6 shows values of the thermal maturity for three wells based on the vitrinite reflectance (Ro) and on the spore colour index and the maturity summary for the Sirte and some Paleocene source rocks. In the area of greatest Sirte Shale thickness (i.e., Zallah Trough), the vitrinite reflectance (Ro) values range from 0.4 to just over 0.6. This places the Sirte Shales within the upper part of the 'oil window'. Higher Ro values, however, may be present in the most southern part of the Zallah Trough where very little data is available. Also in this area the proximity of Sirte Shale to the Late Tertiary volcanic rocks may have provided higher temperatures to "cook" the source rocks. Hence, depth of burial to the top and base of the Sirte Shale would not require increased depths in order to attain thermal maturity for oil generation in this area.

- **Source rock richness**

Fig. 3.7 shows source rock richness (TOC) of the Sirte Shale and some Paleocene source rocks from three wells. The Total Organic Carbon (TOC) values for the Sirte shale average between 1 to 2%, and in some places greater than 2%, in the Zallah Trough area. The Maradah (Hagfa) Trough (i.e., area within the study area) also shows TOC values between 1 and 2 %. These values indicate very good source rock quality. According to the Robertson study (1989), the organic facies range from amorphous (i.e., oil prone) to degraded, humic amorphous (i.e., gas prone).

Based on the Robertson study (1989), the estimated total hydrocarbon productivity from the Upper Cretaceous source rocks in the Zallah Trough is in the order of 10 billion barrels of oil–in-place. Moreover, sourcing of hydrocarbons from the Maradah Trough is estimated by Robertson (1989) to be 185 billion barrels of oil-in-place. As mentioned earlier, (Fig. 3.3) the postulated oil migration routes are upwards from the source areas of higher pressures such as the Zallah Trough (and also in the Maradah Trough) via carrier beds and/or faults into adjacent structural and stratigraphic traps. According to most workers, time of migration is estimated at post-Eocene. However, possible remigration of hydrocarbons may have also occurred at a later date (i.e., Miocene) with tilting of the various tectonic horst blocks, such as the Az Zahrah-Al Hufrah Platform, towards the east.

3.4.3 Reservoirs

Sirt reservoirs range in age from Lower/Upper Cretaceous to the Eocene (Fig 3.8). Sandstones predominate in the Cretaceous and carbonates are the main reservoirs in the

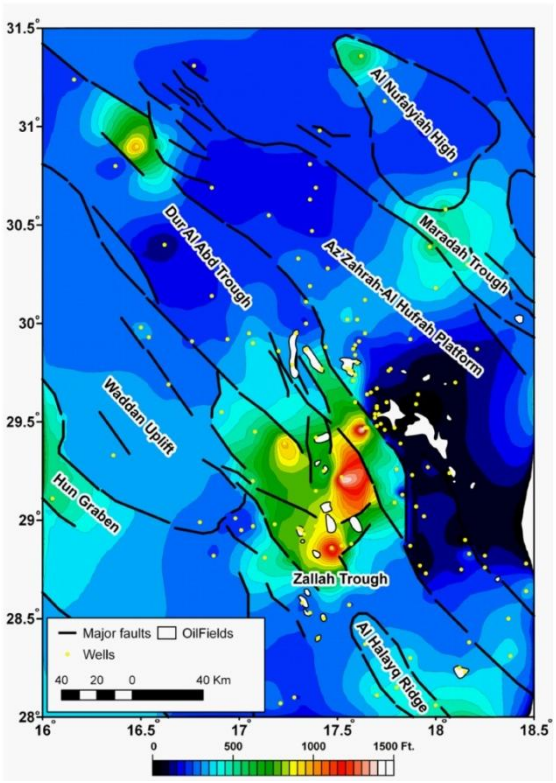


Fig. 3.4 Gross thickness map of the Sirte Shale of the study area. Modified after El Alami at al, (1989); Rusk, (2001); Ahlbrandt, (2001); Hallett, (2002).

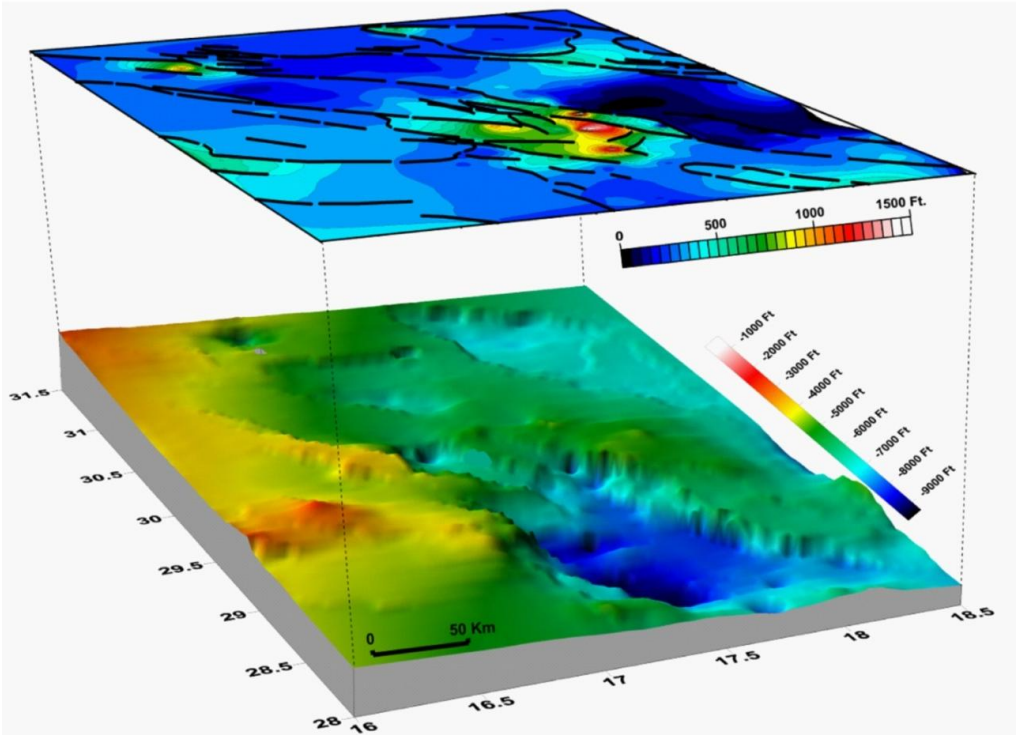


Fig. 3.5 Gross thickness map of the Sirte Shale in the study area supermposed on 3D prespictive image showing surface to depth of the Sirte Shale in the present time.

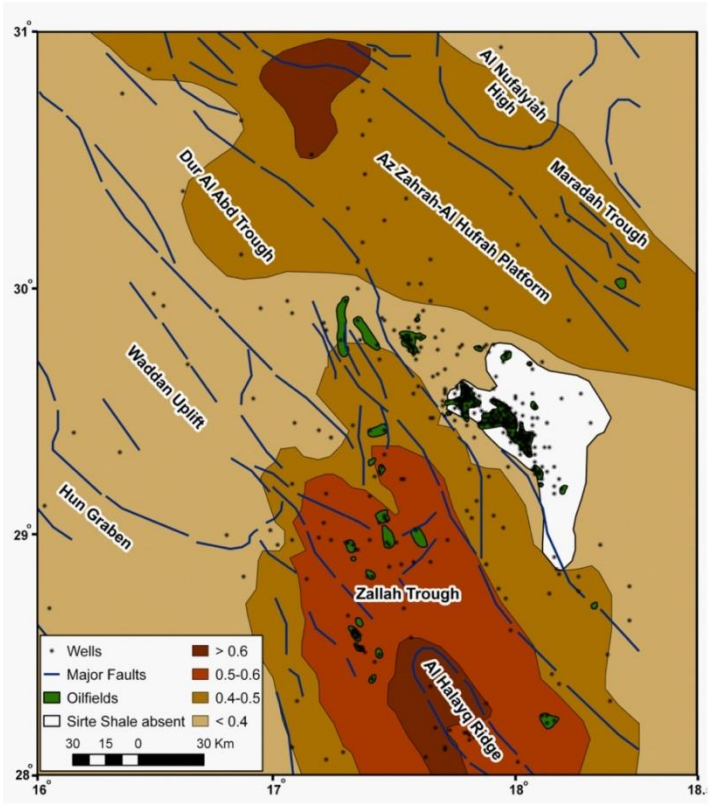


Fig. 3.6 Shows values of the thermal maturity for three wells in the study area based on the vitrinite reflectance (Ro), the spore colour index and the maturity summary for the Sirte and some Paleocene source rocks. Modified after El Alami at al, (1989); Rusk, (2001); Ahlbrandt, (2001); Hallett, (2002).

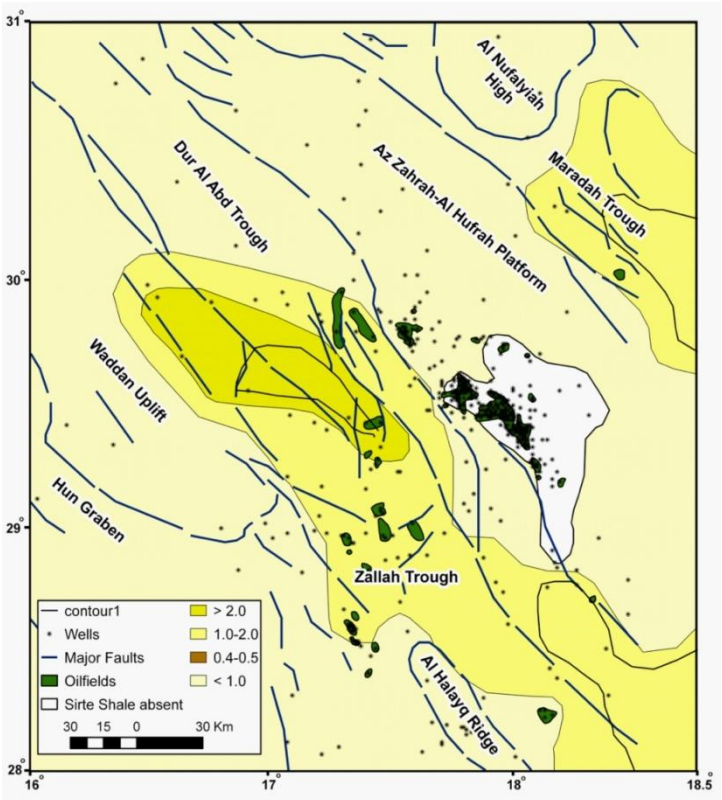


Fig. 3.7 Shows source rock richness (TOC) of the Sirte Shale and some Paleocene source rocks from three wells in the study area. Modified after El Alami at al, (1989); Rusk, (2001); Ahlbrandt, (2001); Hallett, (2002).

Tertiary. The following provides a summary of the more important reservoir units in the study area:

3.4.3.1 Pre-Upper Cretaceous reservoirs

Pre-Cretaceous clastic rocks form large but discontinuous bodies in many areas of Libya and might form significant reservoirs. It is worth noting that the exact stratigraphic position of these clastic rocks is often uncertain. In such cases it is a common practice to use the term 'basal sandstone' rather than specify formation or age of the pre-Cretaceous clastics. One of the biggest reserves of hydrocarbons has been discovered in basal sandstone referred to as the Sarir Sandstone at the Sarir oil Field in Concession 65 of SE Sirt Basin (Sandford, 1970).

3.4.3.2 Gargaf quartzitic sandstone

Although the Gargaf Formation is not known to contain any significant hydrocarbons within the present study area, minor oil shows have been recorded in drilling samples. The unit is characterized by matrix porosities averaging about 5 to 8 %. However, this hard sandstone is further characterized by numerous fractures, thus, contributing to additional pore volume as well as increased productivity. Its potentially large thickness in association with structural horst blocks that may be juxtaposed to the Sirte Shale source rock, make it a potential drilling target. However, there is an uncertainty concerning adequate top seal as the Bahi sandstone usually overlies it. The Gargaf is the main producing reservoir in the Wadi and Belhedan Fields located to the east of the study area.

3.4.3.3 Upper Cretaceous reservoirs

- **Bahi Sandstone**

Bahi Sandstone varies in thickness from 10s of feet (some metres) to over 100 feet (30.05m) in the study area. Porosities vary between 12 to 28 %. The Bahi Sandstone is a major oil producing unit in the Bahi Field where it displays an average porosity of 28 % and average permeability of 150 md. Oil shows have been recorded in many wells in the study area.

- **Lidam Formation**

The Lidam Formation, which usually overlies the Bahi Formation, is comprised of interbeds of limestone, dolostone and sandstone. Porosities can range from about 10 % up to 15 to 20 %. Its thickness is quite variable, ranging from about 10 (3.05m) to 30

feet (9.14m). To date, the only significant oil tests have been recorded in some wells from the Bahi Field.

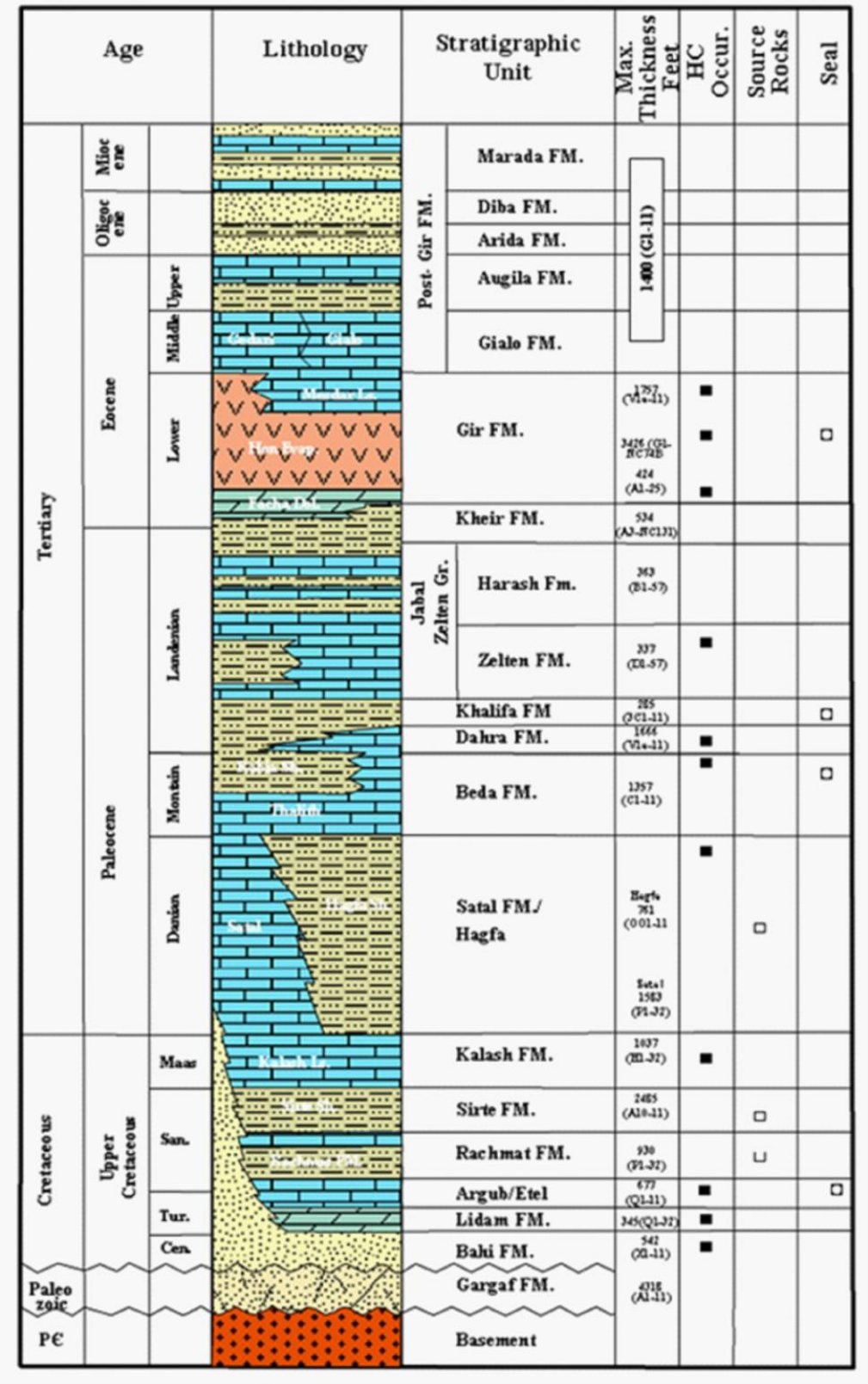


Fig. 3.8 Subsurface columnar stratigraphy for the study area (modified from Barr and Weegar, 1972). The compilation of source, reservoir,and seals mainly after El-Alami et al.(1989), Baird et al. (1996), Mansour and Magairyah (1996), Wennekers et al. (1996), and Ahlbrandt (2001).

❖ **Kalash Limestone**

Kalash Limestone is regionally widespread and ranges in thickness from about 100 (30.05m) to 200 feet (61m) and attains greater thicknesses in areas where the upper Satal 'buildup' is present. Porosities can range from about 15 to 25 %. Although oil shows have been described in many wells, to date the most significant test is from the KK1-32 well in the Bahi Field where over 1100 BOPD was recovered.

3.4.3.4 Paleocene reservoirs

■ **Satal Carbonates**

Satal Carbonates attain a gross thickness of up to 1800 feet (549m) just to the east of the Az Zahrah-Al Hufrah Platform in the vicinity of the Az Zahrah field. Its geometry and facies indicate a depositional body shaped like a carbonate reef or bank. Porosities range between 20 and 30 %. The Satal is oil productive in the Az Zahrah and Bahi Fields. Upper Satal (Danian) rocks up to 130m thick with excellent reservoir characteristics are associated with oil in the Mabruk, Bahi, Az Zahrah, Al Hufrah, Ali, Arbab and Almas Fields (**Fig 3.9**).

■ **Beda Formation (Rabia and Thalith Members)**

Over the study area, the Beda Formation ranges from about 100 (30.05m) to 125 feet (38.1m) in thickness. Porosities can range between 13 to 15 %. Trapping is mainly structural but mapping indicates a facies change from limestone to predominately shales such that local stratigraphic traps could be present. Within the study area, the Beda/Thalith is oil bearing in most of the fields, particularly in the areas south of the Waddan Uplift where the Beda is productive in structural traps.

■ **Dahra Formation**

In the study area, the Dahra Formation varies from 200 (61m) to 300 feet (91.4m) in thickness. Porosities range between 15 to 25 % in limestone. To date, the Dahra Formation is known to produce oil in most oil fields of the study area. These oil fields are all located along the western side of the major Az Zahrah-Al Hufrah Platform, a prominent tectonic feature of the area. These fields which are predominantly structural traps are:

- Mabruk – the main reservoir is the Upper Paleocene carbonate of the Dahra Formation which has fair reservoir quality; the regional seal is formed by Paleocene Khalifa Shale.

- Facha, Taqrifat, Qsur – is the main reservoir in the Upper Paleocene Dahra Formation with fair reservoir quality; the regional seal is formed by Paleocene Khalifa shale.

- Az Zahrah, Aswad, Safsaf – the main reservoir is the Upper Paleocene Dahra Formation that has fair reservoir quality and a regional seal formed by Paleocene Khalifah Shale.

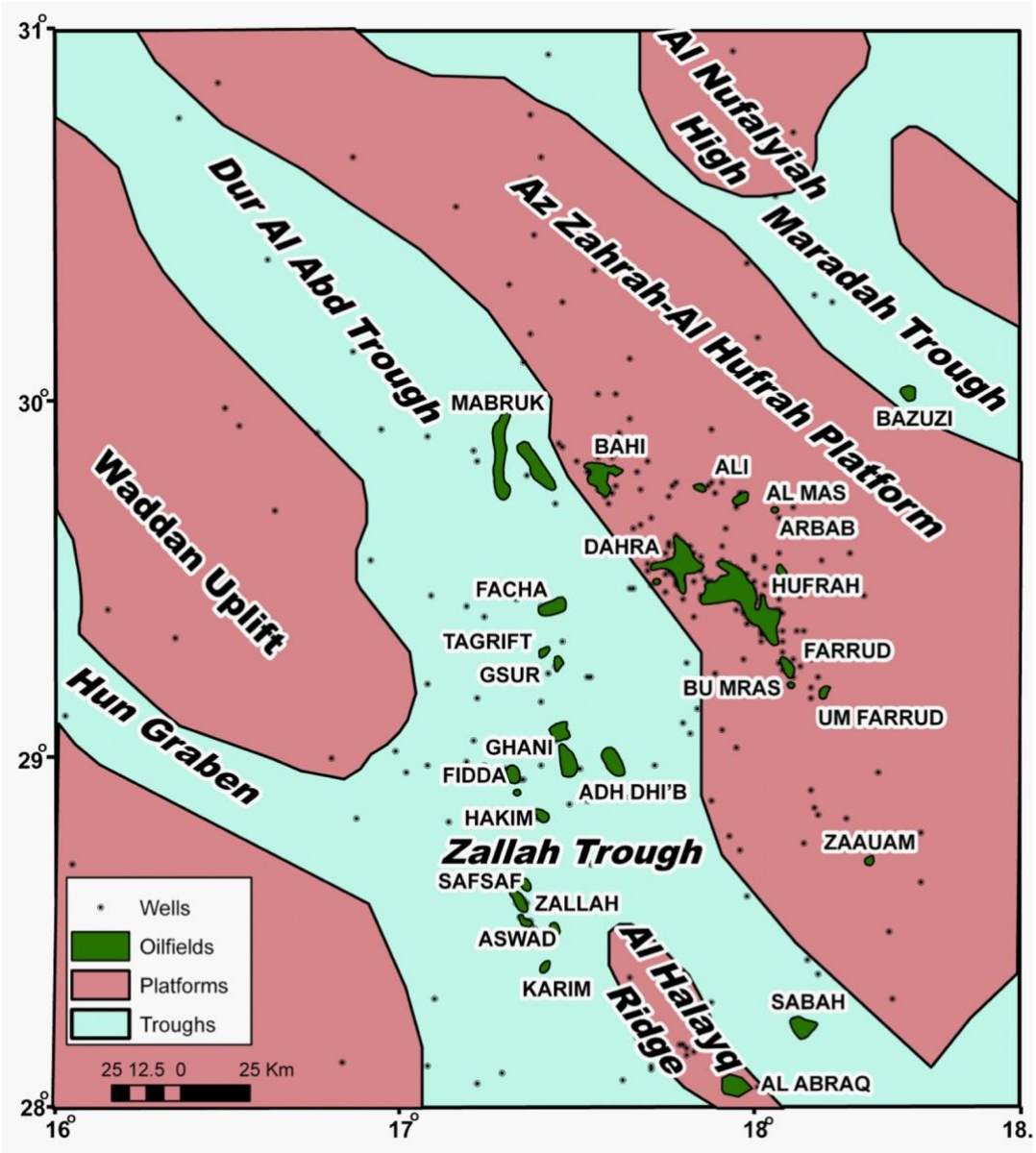


Fig. 3.9 Generalized tectonic map of the western Sirt Basin shows the location of the main oil and gas fields (Modified from Mouzughi and Taleb, 1981).

- **Zelten Formation**

Zelten Formation thickness varies between 150 (45.7m) to 200 feet (61m). To date, no commercial oil production has been found, although oil and gas have been tested in minor amounts in several wells in the Az Zahrah field. Relatively poor reservoir quality

and a possible lack of adequate top seal with the overlying Harash Formation, may be the reasons for the Zelten not being a significant reservoir in the study area.

- **Harash Formation**

Harash Formation thickness varies between 75 (22.9m) and 100 feet (30.05m). Reservoir quality is poor. Minor oil shows have been described from some wells in the Az Zahrah Field and gas was tested in the B10-32 well. The hydrocarbon shows are mainly in the wells that are in the highest structural position in the Az Zahrah Field.

3.4.3.5 Eocene reservoirs

- **Facha Dolomites (Gir Formation)**

It has excellent reservoir quality with a thickness of 100 (30.05m) to 150m (45.7m). Porosities range from about 20 to 25 %. To date, the Facha Dolomites have produced oil in the western group of oil fields in the study area and have been in production since 1979 (Fig. 3.9). Facha Dolomite is the main reservoir for the Ghani, Fidda, Adh Dhi'b, Hakim fields with excellent reservoir quality (enhanced by dolomitisation) and an Eocene Hon Evaporite Member provides the seal. The western closure of the Ghani field is dependent on fault seal.

- **Hon Evaporites (Gir Formation)**

Hon evaporites range from about 20 (6.1m) to up to 50 feet (15.2m) in thickness. Porosities are between 25 to 28 %. To date, oil has been found in several dolomite reservoirs from the base to about the middle of the Hon. It was noticed, based on previous information, that there is no significant hydrocarbons found in Cretaceous reservoirs in the Zallah Trough. This is probably due to the absence of good reservoirs above the Sirte Shale. The Kalash Formation constitutes a viable reservoir only on the adjacent platforms where nearshore facies were developed. In the Zallah Trough it is a tight chalky limestone with very poor reservoir characteristics. As far as the deeper reservoirs are concerned, the problem seems to be the lack of an effective conduit between the source rock and reservoirs beneath the Sirte Shale.

3.4.4 Traps

Several different play types have been described from the Sirt Basin (e.g., Fraser, 1967; Roberts, 1970; Sandford, 1970; Williams 1972; Clifford, et al, 1980; Brady, et al., 1980). Also, comprehensive field summaries have been published by Thomas (1985a) and Hallett (2002). It is well known that hydrocarbon traps can be classified either as structural, stratigraphic or combination of the two.

To summarise the above published work, structural traps**,** mainly fault-controlled, are a major cause for the trapping mechanism for many of the reservoirs in the Sirt Basin as shown in Fig. 1.1 which illustrates the main structural trends in the area. Typical structural traps in the area range from simple normal faults to more complex faults and fold structures associated with wrench faults. The Bahi and Az Zahrah and Al Hufrah Fields are much larger than other nearby Az Zahrah-Al Hufrah Platform oilfields as they have a rollover or fold component to them (Hallett, (2002).

Structural traps are dominant in the Zallah Trough and are mainly related to Eocene deformation on the heavily faulted western side of the basin:

- Mabruk, Facha and Taqrifat are situated on the up-dip side of the main depocentre of the basin and associated with NW trending faulted anticlines.

- The Ghani fields are located deeper in the trough in the Ar Ramlah syncline and are mostly fault-closures on the western margin of tilted fault blocks.

- Hakim and Fidda are located in the Ma'amir Graben which is the western and deepest part of the Zallah Trough.

- The Zallah fields are associated with larger anticlines, partially fault dependent on a terrace to the west of the Ma'amir Graben.

Fields of the Az Zahrah-Al Hufrah Platform were charged by long range migration (approximately 100km) up the western boundary fault of the Maradah Trough and into carrier beds of the Paleocene (Fig. 3.3). The platform was already tilted towards the northeast prior to peak oil generation in the Oligocene-Miocene directing oil towards the southwest.

Several types of stratigrapic traps are present in the study area and essentially they are characterized by facies changes from carbonates to argillaceous carbonates to shales in the Beda and Dahra Formations. In addition, the Lower Paleocene Satal Carbonate bank is a major reservoir with several oil fields. Additional potential exists along the Satal bank edge where localized areas of higher porosities as well as higher paleotopographic features can be expected. Generally most traps on the Az Zahrah-Al Hufrah Platform are structural i.e. NW-SE trending low relief anticlines related to mid-Eocene deformation. Complexity of Paleocene carbonates provides scope for stratigraphic traps,

for example, the Az Zahrah field is partly a stratigraphic trap due to the rapid shale out of the Dahra Formation to the west. The Bahi field may be fault bounded on its northern side.

3.4.5 Seals

In the Zallah Trough, the top seal for most of the Paleocene reservoirs consists of shale to shaly- carbonates (locally anhydrite is also present) with Paleocene shales forming the main seal Hallett (2002). In particular, the Khalifa Shale, which is present over the entire area, forms the seal to the underlying Dahra Formation. The Rabia Shale Member of Beda Formation provides the main seal to the Satal and Lower Beda Formation.

In the Eocene, the thick evaporites of the Hon Evaporite Member provide the top seal for the Eocene Facha and Hon dolomite reservoirs. The evaporites are over 600m thick in the Zallah Trough. The area is heavily faulted, particularly on western side of the Al Hulayq Ridge. Examples of sealing faults can be found, for example, the Facha reservoir is displaced against the Hon evaporites. The Ghani field is dependent on fault seal for closure on its western flank, but other faults appear to have leaked, and probably acted as conduits for hydrocarbon migration.

3.4.6 Migration

Migration in the study area has both vertical and lateral components while in general the Sirt Basin is considered as one of the best examples of a dominantly vertically migrated petroleum system as shown by Harding (1984), wherein Upper Cretaceous oil charges multiple reservoirs along fault zones adjacent to horsts and grabens (Price, 1980). Refinements of a dominantly vertical horst and graben model were provided by Baird, et al, (1996), who argued for normal listric extensional and growth faults in the Sirt Basin as opposed to the more nearly vertical faulting described by Harding (1984).

Guiraud and Bosworth (1997) demonstrated the importance of right-lateral wrench fault systems of Senonian age and pointed out the periodic rejuvenation of these systems in the Sirt Basin was particularly important to vertical migration of hydrocarbon. A contrasting view is offered by Pratsch (1991) who sugested that the Sirt Basin is an example of lateral migration and vertically stacked hydrocarbon systems isolated from each other.

In contrast, El-Alami et al (1989) suggested that all the oil in the western part had been sourced from northwest of Zallah Trough and Al Kotlah Graben (Fig. 3.3), based on the maturity and richness of source rock in the Zallah Trough. They further state that significant oil accumulations have migrated from kitchens in the east to the west, and

that oil has been trapped in the adjacent highs after vertical migration up-fault over relatively short distances along porous carrier beds.

Evidence that the reservoirs are vertically separated from the source rock, implies a vertical component of migration. Roohi, (1996a and b) has investigated the present structural configuration of the Sirt Basin and suggested that the hydrocarbon migration trends in the western Sirt Basin were mainly W-SW in direction, and that the Maradah (Hagfa) Trough (Fig. 3.3) is the principle site of major hydrocarbon generation for Az Zahrah-Al Hufrah and Al Bayda Platforms. The peak of the oil generation was mainly during the Oligocene-Miocene time when the burial depth of these source rocks was below a depth of 4000m (Zinati and Roohi, 2007). Therefore, generation, migration, and accumulations occurred mainly after the huge post Eocene subsidence, at a time when the present structural configuration of the basin had already been established and while source rocks in Zallah Trough were still marginally mature.

It seems that the Az Zahrah Field on the Az Zahrah-Al Hufrah Platform could have been fed from the adjacent western depression by vertical migration through the Gedari fault complex. The fields located to the west of the depression (Hakim, for instance) were fed with oil moving laterally and vertically to the reservoirs **(**Fig. 3.3**)**. In this case, the distance of migration for both lateral and vertical components, is relatively short. For Mabruk, on the other hand, there is a long lateral component from the Az Zahrah-Al Hufrah Platform adjacent western depression to the north. The vertical component is limited to the distance separating the source rock and the reservoir. Most of the oil discovered today surrounds the Az Zahrah-Al Hufrah Platform adjacent to the western depression.

The development of transfer or relay fault zones (transtensional and transpressional areas) were encountered in the study area has led to a more complex structural history. These type of structures produced additional migration routes to reservoirs occupying horst blocks (Knytl, et al., 1996; Van Dijk and Eabadi, 1996).

Refer to chapter 8 for the discussion of what is the significance of this work that will be presented.

3.5 Summary

The purpose of this chapter was to review hydrocarbon occurrences in the study area as a part of the Sirt Basin based on a review of the published literature and available oil company reports.

Libya can be divided into two discrete geological provinces based on the age of the hydrocarbon basins, and their sedimentary fill. The first province comprises a belt of tectonically active basins of Mesozoic-Cenozoic age that includes the complex, prolific and mature Sirt Basin in central northern Libya as well as the promising Libyan offshore areas.

The second province, is a regionally extensive Palaeozoic mega-province, comprising two intracratonic basins in western Libya (Ghadamis and Murzuq), and additionally the Al Kufrah Basin and the Cyrenaica Platform located in eastern Libya.

The Sirt Basin ranks 13th among the world's petroleum provinces and has the greatest reserves of all African basins containing approximately 80% of Libya's total proven oil reserves (41.5 billion barrels as of January 2007) as estimated by US Energy Information Administration (2007) and represents 29% of Africa's total. Over 23 large oil fields and 16 giant oil fields occur in the province and 80% of the total recoverable oil and gas were discovered prior to 1970.

Published studies suggest that most of the oil in the Sirt Basin was derived from the Sirte Shale (Upper Cretaceous, Campanian/Turonian), whilst the reservoirs are ranging in age from Lower/Upper Cretaceous to the Eocene. Sandstones predominate in the Cretaceous and carbonates are the main reservoirs in the Tertiary.

Several different play types have been described from the Sirt Basin dominated by the structural traps**,** mainly fault-controlled, are a major cause for the trapping mechanism for many of the reservoirs in the Sirt Basin. Typical structural traps in the area range from simple normal faults to more complex faults and fold structures associated with wrench faults. Structural traps are dominant in the Zallah Trough and are mainly related to Eocene deformation on the heavily faulted western side of the basin.

In addition several types of stratigrapic traps are present in the study area and essentially they are characterized by facies changes from carbonates to argillaceous carbonates to shales in the Beda and Dahra Formations.

The top seal for most of the Paleocene reservoirs consists of shale to shaly- carbonates (locally anhydrite is also present) with Paleocene shales forming the main seal.

Oil migration in the study area has both vertical and lateral components while in general the Sirt Basin is considered as one of the best examples of a dominantly vertically migrated petroleum system.

CHAPTER 4: REMOTE SENSING DATA INTERPRETATION

4.1 Introduction

Imagery data from Google Earth™ (Fig. 4.1) and MrSid (Fig. 4.2) covering the entire study area were used for the remote sensing component of this study. The main objective of conducting a remote sensing interpretation was to identify faults and fractures as well as major stratigraphic boundaries and use these mapped features along with geological and geophysical data to provide a more comprehensive analysis of the area.

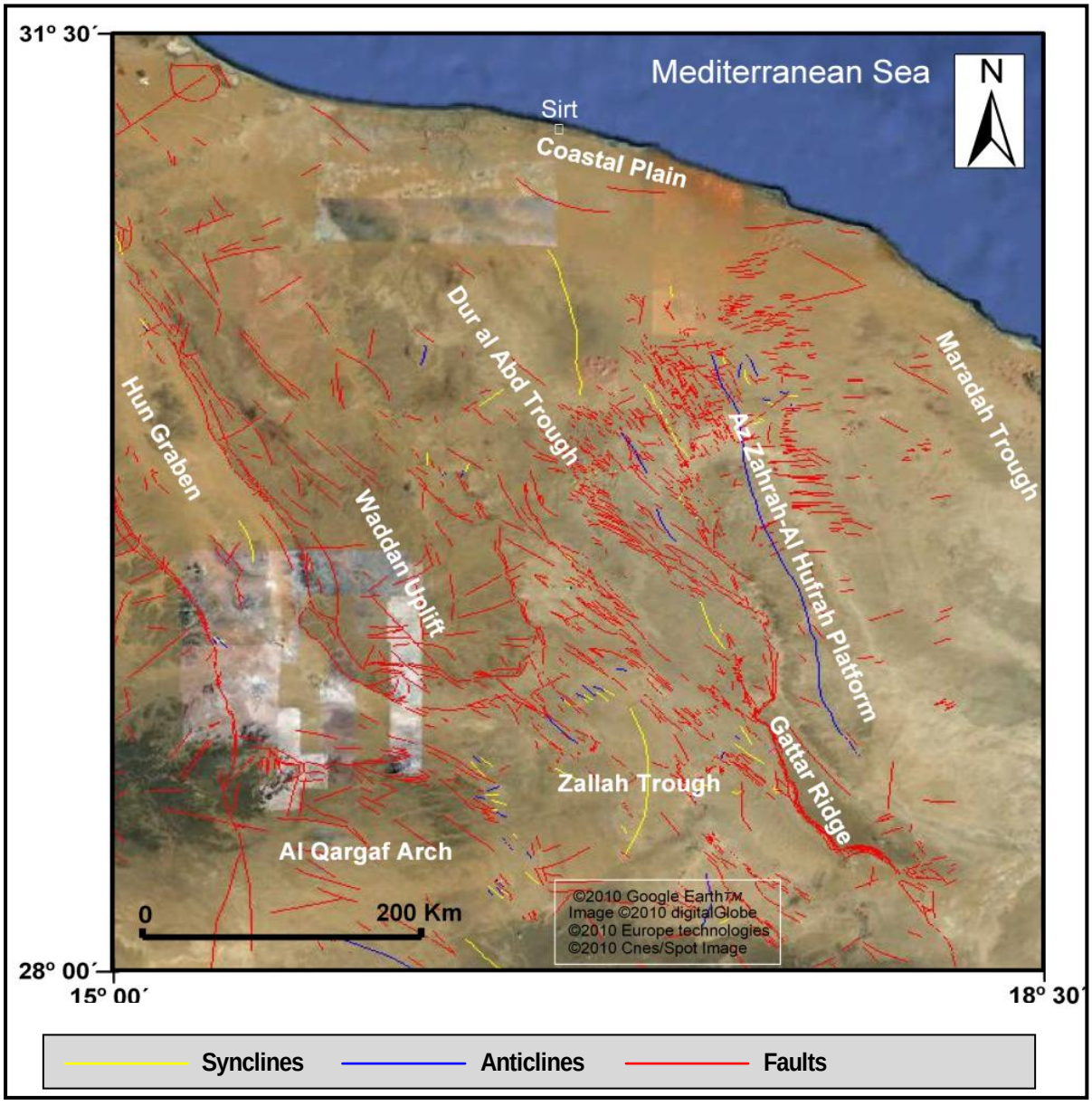


Fig. 4. 1 Data from Google Earth™ imagery that covers the study area showing the interpreted surface faults and folds, the location of the structural domains and other key structural features.

Most of the lineaments measured on remote sensing imagery were linear segments of stream valleys or other geomorphological alignments. These alignments are assumed to have formed as a result of differential erosion along lines of weakness (fracture zones) in the crust, produced by numerous episodes of tectonism.

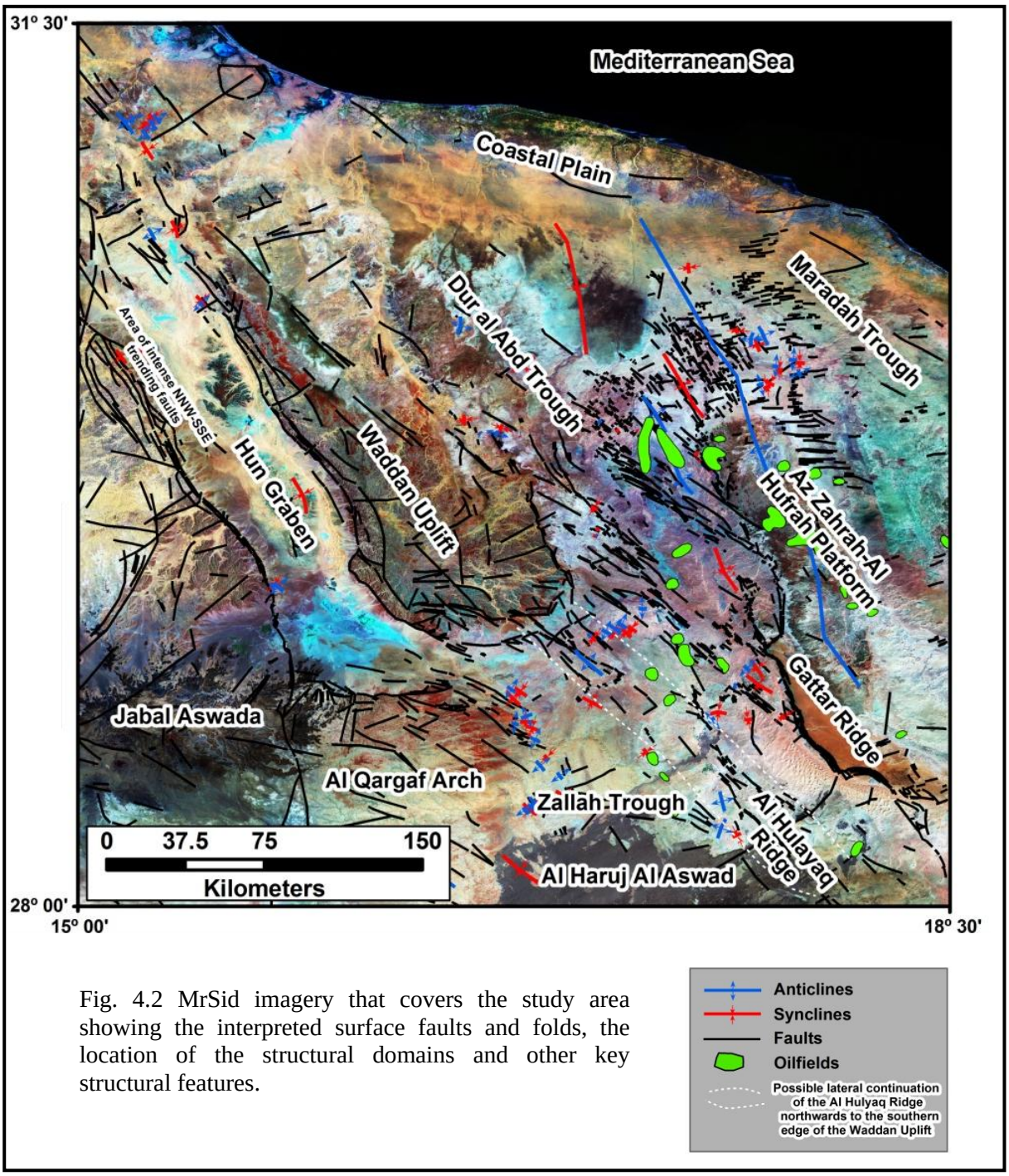


Fig. 4.2 MrSid imagery that covers the study area showing the interpreted surface faults and folds, the location of the structural domains and other key structural features.

A structural analysis has been made using Google Earth™ satellite imagery over the western Sirt Basin, Libya (Fig. 4.1) using the latest images available on Google Earth ™ (2010). In most of the area the satellite imagery has a resolution of about 15 m per pixel. This base imagery is 30m multispectral Landsat ™ which is sharpened with 15m

[panchromatic] Landsat imagery. However, Google ™ is actively replacing the base imagery in this region with 2.5m SPOT ™ data.

The other satellite date used was MrSid imagery (Fig. 4.2) with a Landsat TM band combination 7,4, and 2 as red, green and blue, which combines spectral information from the near- to mid-infrared part of the electromagnetic spectrum and therefore highlights features that would otherwise be invisible to the naked eye. This type of band combination enables interpretation of geological structure as well as spectral discrimination of surface lithologies (Drury, 2001, and Rajesh, 2004).

The interpretation was performed on-screen using ArcGIS software. Interpretation was carried out at different stages detailed as illustrated in Fig. 4.3 and summarized as major structures in Fig. 4.4. The interpretation has benefited from the integration of fault/fracture information derived from the SPOT satellite imagery with the selected windows of higher resolution (2.5m) Google Earth ™ program (Fig. 4.5). This helped to identify faults and fractures not visible on the Landsat TM optical imagery. The satellite imagery was an effective means by which to map the surface geological structure and geomorphology of the region and therefore enables the validation of existing geological mapping.

In addition to the satellite imagery, 1:250,000 scale published geological maps and accompanying reports were also used during the interpretation. The maps were scanned and geo-referenced to the satellite imagery.

The surface geology of this area (Fig. 1.3) is composed primarily of Late Upper Cretaceous, Tertiary and Quaternary surficial deposits. The study area is highly faulted, with a complex geological pattern, bounded to the west by a portion of the Hun Graben (Fig. 4.1-4.4 and 4.6) and containing prominent geological features of the Sirt Basin. The faulting style exhibited in this region is that of normal and strike-slip faulting with a general NW to NNW trend.

Figures 4.1-4.4 displays the interpreted segmented fault pattern composed of NW-SE and N-S to NNE-SSW striking fault systems that have formed at both the rift borders and within the basin. As a general rule, the NW-SE faults that are parallel to the major structural trend of the basin controlled the rate of rifting and subsidence whereas the NE-SW structure modifies the pattern formed by previous system to form the block structures.

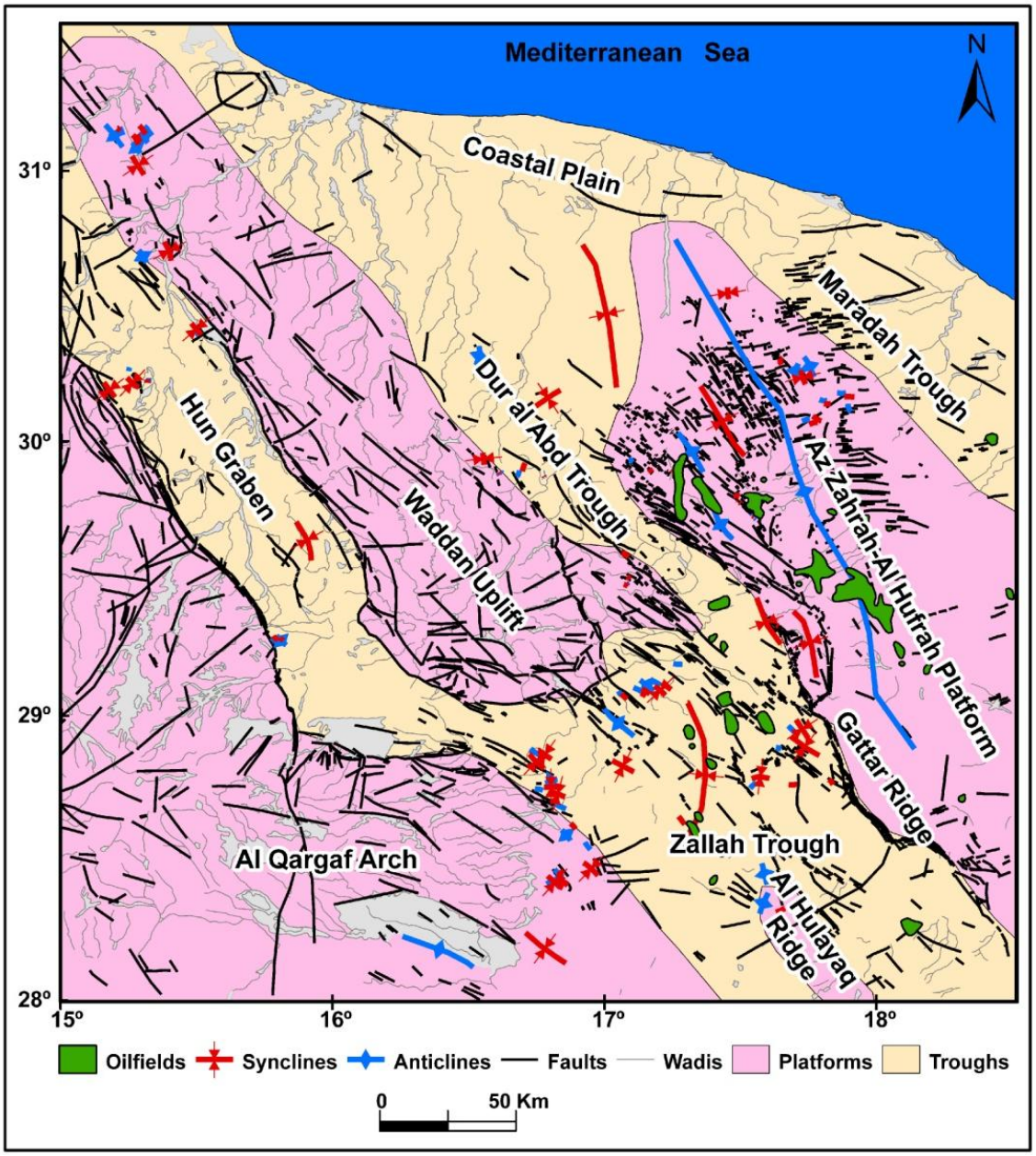


Fig. 4.3 Structural interpretation map showing the surface faults and folds interpreted form satellite imagery of the study area.

The NE-SW faults are limited in length and not continuous. Based on their characteristics, the NE-SW fault system can be classified as transfer faults.

Both sets of faults combine to control several structural and geotectonic elements; namely, the Zallah, Dur al Abd, Maradah Troughs, Hun Graben, the Waddan Uplift, Gattar Ridge, Az Zahrah-Al Hufrah Platforms, Al Qargaf Arch, and the intrabasinal Al Hulayq Ridge (Figs 4.1-4.4).

These blocks are bounded on one side by a major NW trending border fault system and a predominant stratal dip direction toward the border fault system. The Al Hulayq Ridge (Figs 4.1-4.4), projects into the area from the south, and forms a spur that divides the Ar

Ramlah Syncline, to the east and the Ma‘amir Graben to the west, and then passes beneath the Al Haruj Al Aswad volcanic centre to the south.

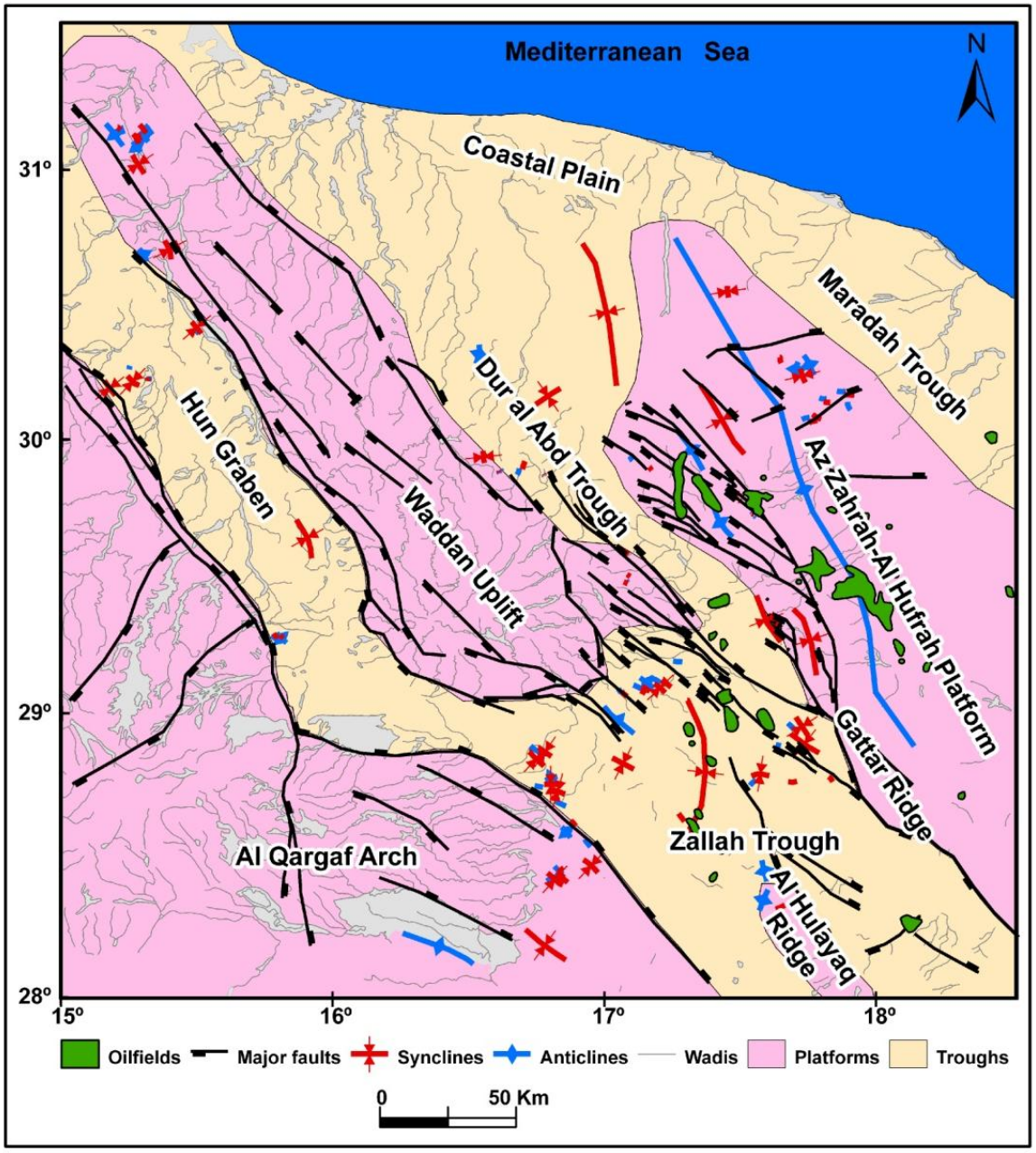


Fig. 4.4 Overview structural map showing the major faults with established sense of displacement and folds interpreted from satellite imagery of the study area.

4.2 Surface structures

On the basis of satellite image mapping and the published geological maps the major faults systems can be clearly defined (Figs 4.1-4.4). The main NW to NNW trending faults trend are up to tens of kilometers long. Viewed at different scales (Figs 4.1-4.4), the faults are offset by NNE trending 'hard-linked', oblique-slip transfer faults. The combined effect is a characteristic rhomboidal or zigzag fault pattern.

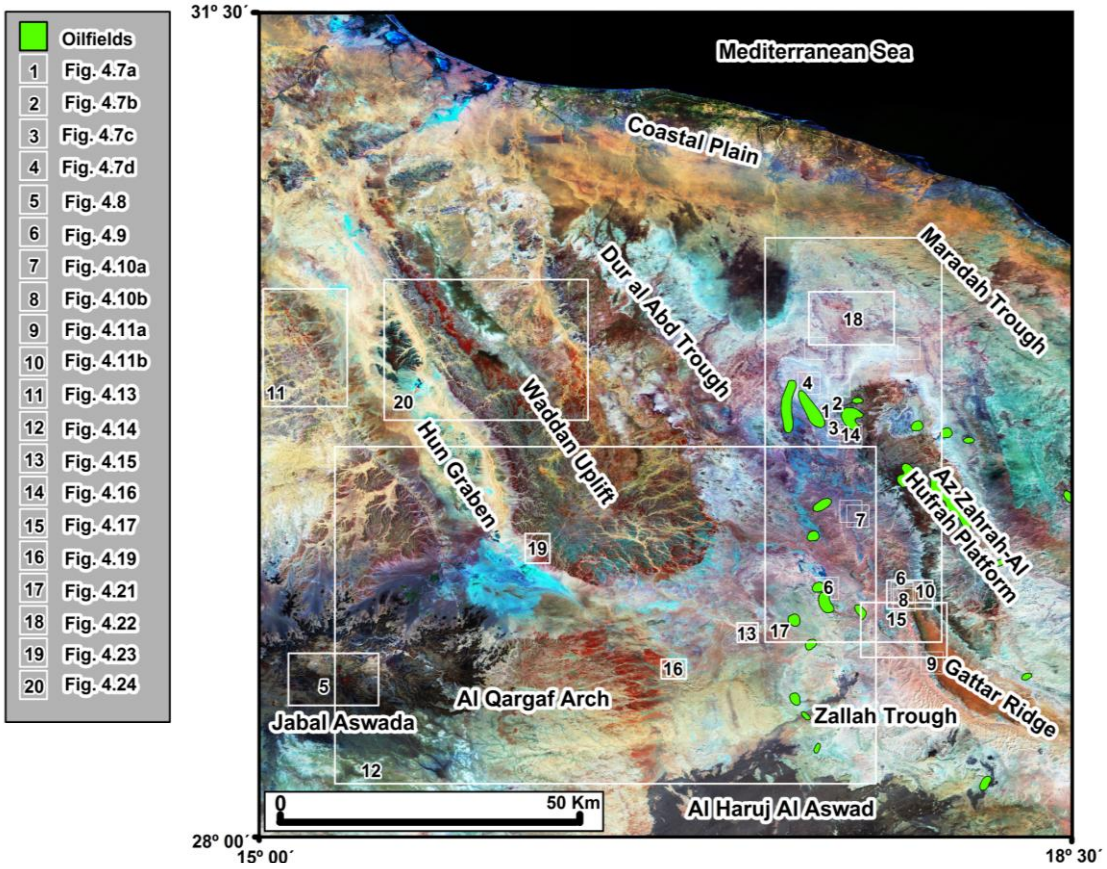


Fig. 4.5 Location map for images presented later.

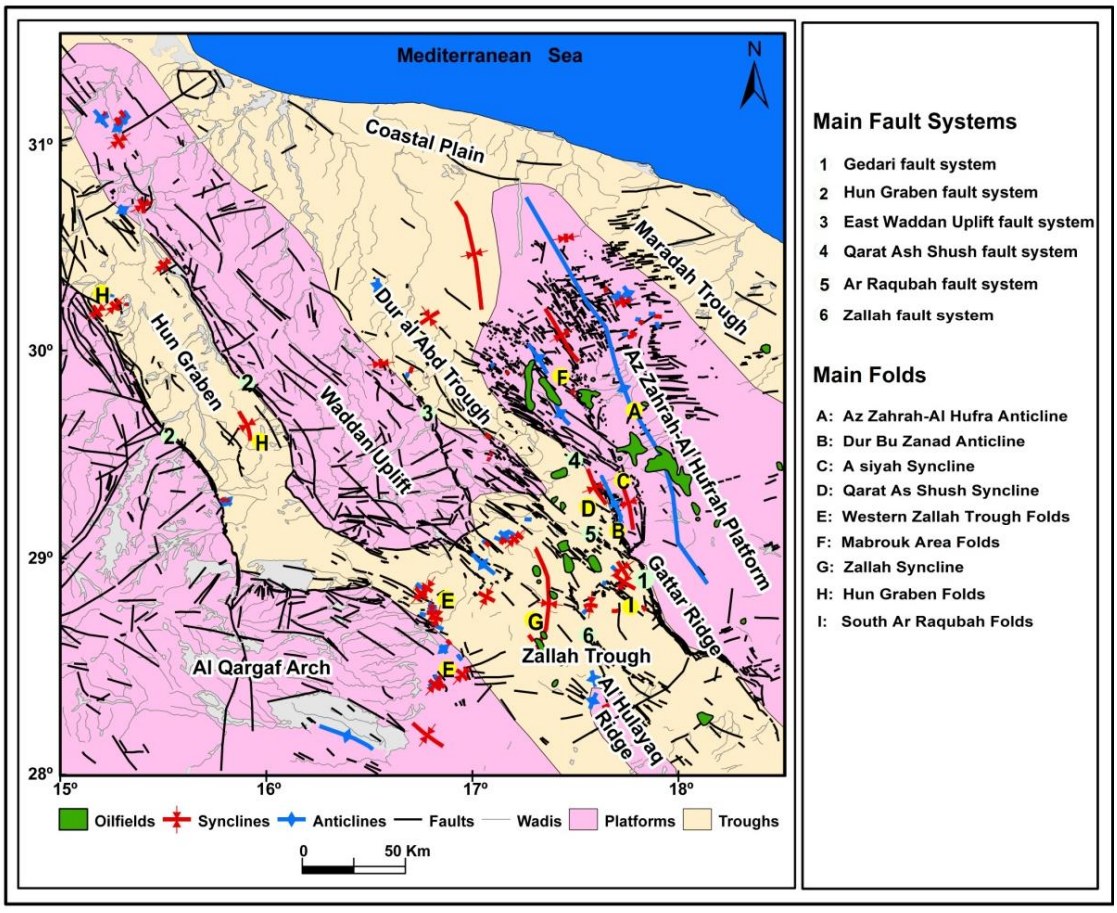


Fig. 4.6 The location of the main interpreted fault systems and folds overlaid on the structural map which has been interpreted from satellite imagery.

In the hangingwalls to the major faults, beds are gently inclined and warped forming synclines that trend parallel to sub-parallel to the main faults (Fig. 4.6 and 4.8a-d). Many folds within the study area are located sub-parallel to and bounded by the offset fault zones and occur as trains of hangingwall synclines and anticlines trending NNW to NW as well (Fig. 4.8). The beds are folded about NNE trending axes and limb dips rarely exceed 10° and the folds plunge both to the NW and to the SE (Fig. 4.8).

Many eruptions of basalt lavas are found in the southern part of the study area and some of them (Fig. 4.9) form linear trending NW-SE shapes consistent with the main fault systems of the study area. The distribution of these basalt lava eruptions may indicate the existence of faults that cannot be seen due to the younger sediments and the extensive lava flows (Fig. 1.3). These structures suggest that the area remained tectonically active even during post-Eocene times.

4.3 The major fault systems

The main basin (trough) boundaries of the study area (Fig. 4.6) are :- 1) the Gedari Fault system located along the eastern boundary separating the Az Zahrah-Al Hufrah Platform from the Gattar Ridge; 2) the Western boundary represented by Hun Graben Fault system; 3) the East Waddan Uplift fault system along the eastern margin of the Waddan Uplift; 4) the Qarat Ash Shush fault system; 5) the Ar Raquba fault system, and 6) the Zallah fault system, which together divide the main trough into a number of sub-blocks.

4.3.1 Gedari fault system

The Gedari fault system (Fig. 4.6) is well known to oil prospectors as it is the western boundary to the oil fields of Az Zahrah, Al Hufrah, Bahi, and Mabruk farther northwestwards (Klitzsch, 1970) and extends along the entire eastern boundary of the study area.

On satellite imagery at 17°50', 29°05' the southern Gedari fault system is consistent with what is believed to be a negative flower structure as the main fault branches towards the north into the Qarat Ash Shush fault system and Ar Raqubah fault system (Fig. 4.9).

The negative flower structures consists of Riedel-type splay faults, which merge in a major branch line to the south and there is a syncline as wedge-shaped left-lateral strike-slip depression bounded by the Gedari fault set in the east and the Qarat Ash shush fault set in the west exist in transtensional environments and these faults probably tend to join downwards onto a single strand in basement, with dominantly normal offsets.

The Gedari fault is marked by a series of major fault scarps which formed along a normal fault zone defining the western edge of the Gattar Ridge and the SW fringe of the Az Zahrah-Al Hufrah Platform (Fig. 4.6).

The fault zone is highly segmented and faults dip steeply towards the SW. The maximum downthrow of the SW block with respect to the NE block is more than 1000 m (Vesely, 1985 and Klitzsch, 1970).

These authors suggested that an original flexure was broken under continuing subsidence movements to explain the dip of the layers along the fault. Anketell and Kumati (1991b) suggested that the Gedari fault resulted from sinistral strike-slip movement and interpretations made in this study has confirmed these displacements (Fig. 4.10). The clear horizontal displacement of Eocene strata along the Gedari fault system and the Qarat Ash Shush fault system indicate sinistral strike-slip displacement (Fig. 4.10a and b) as explained by Anketell and Kumati (1991b).

Segmentation of the Gedari fault system has resulted in the development of relay ramps between overlapping fault tips at the southeast part of the study area (Fig. 4.11a and b). These relay ramps are arranged as right lateral stepping faults dipping to the NW in the extreme south and to NNW when they swing to ENE-WSW (Fig. 4.10a, b, and c).

The faults change from NNW-SSE trending to ENE-WSW trending, at 17°50', 29°05' (Fig. 4.6) before swinging directly north to follow the trend of an escarpment until 17°50' and 29°15'. Then the structure can be followed to 17°20', 29°45' where it branches to the northwest to link up with the northernmost faults of the Qarat Ash Shush fault system before continuing beyond the Mabruk oilfield. Here, the northern part of the Gedari fault system and the most northerly faults of the Qarat Ash Shush fault system (Fig. 4.6) cut the Early Upper Eocene and Lower Eocene sediments, and some of these faults display both NE and SW directed downthrows forming small horst-graben structures (Anketell and Kumati 1991b).

Numerous elongate asymmetric synclines associated with shallow west limbs and steeper dipping east limbs are developed in the hangingwall adjacent to west downthrowing normal faults predominantly along the eastern fault bounded margin of the Gedari fault system and the Gattar Ridge (Fig. 4.8). These hangingwall structures of the Gedari fault system are characterized by several large, doubly plunging, asymmetric hangingwall synclines, the largest of which, the Syiah syncline (Anketell and Kumati 1991b) is over 50 km long with westerly facing beds dipping up to 30° (Fig. 4.6, and 4.7). This syncline is flanked to the west by a broad gently dipping structure which

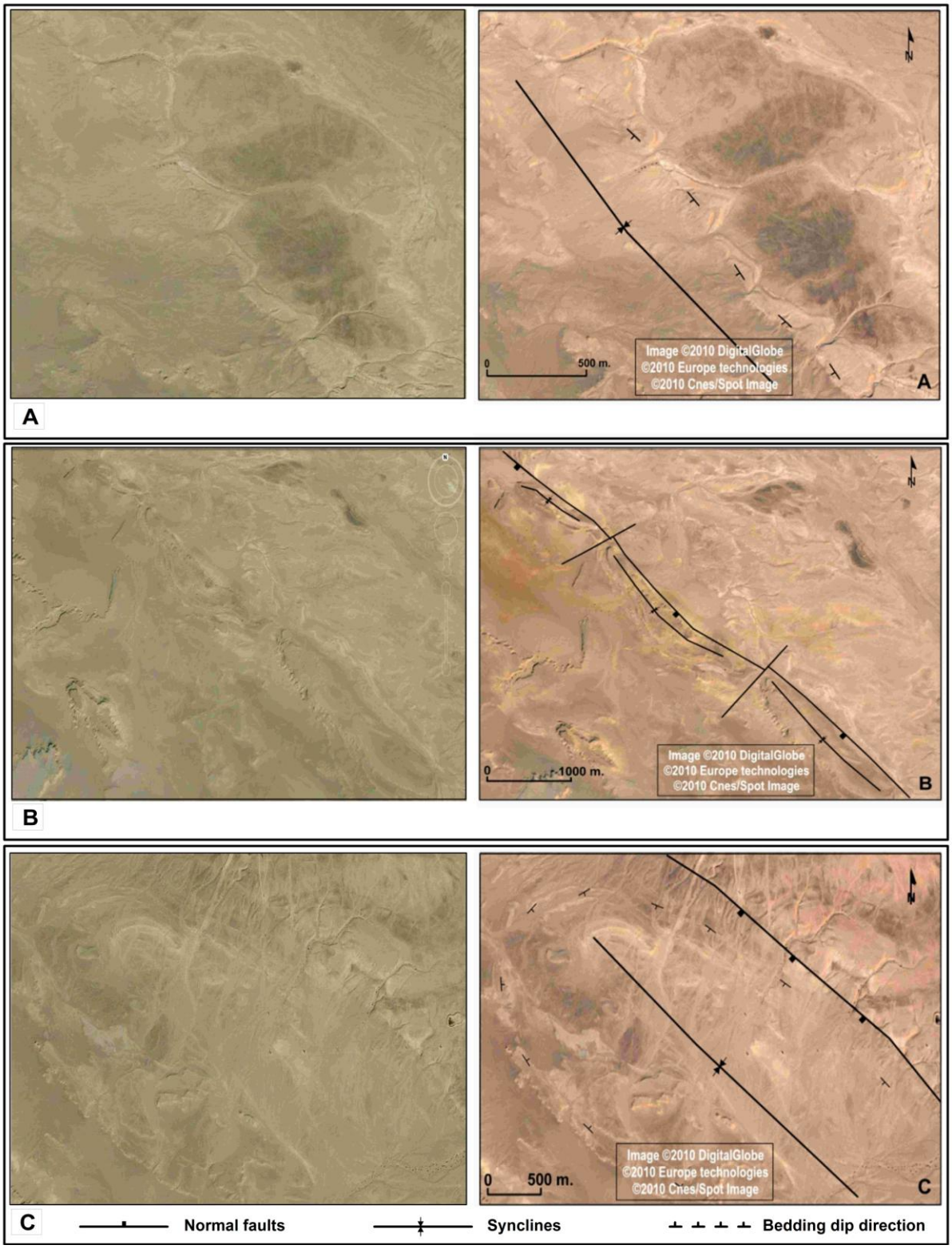
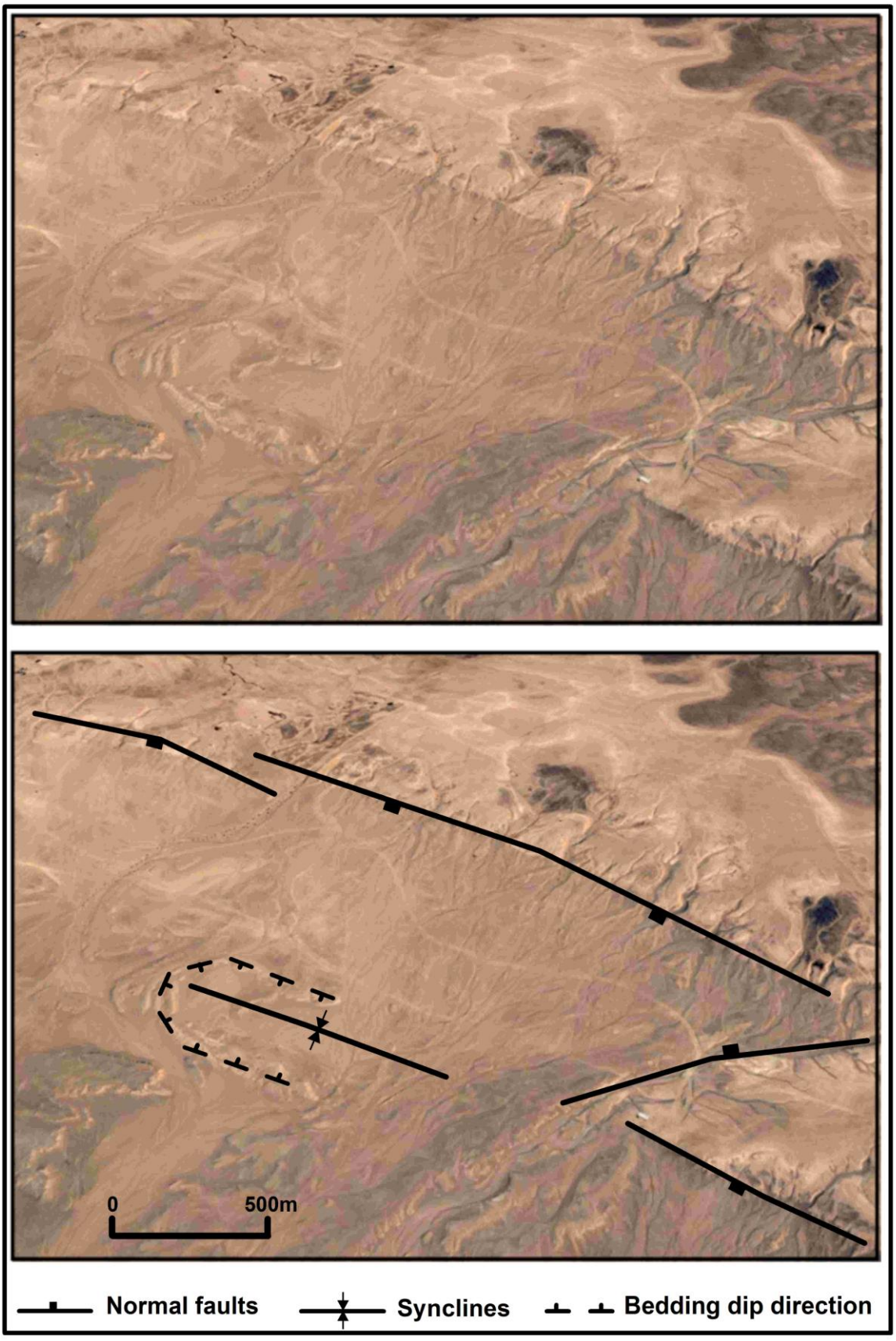


Fig. 4.7 Examples of fault related folds as they appear on satellite imagery, (adapted from Google Earth). (A): Fold (monocline) developed over normal (Gedari) fault with strata dipping into SW direction. (B): Syncline parallel or sub parallel to Gedari fault. (C) and (D): Folds are located sub-parallel to and bounded by the offset fault zones as well. For location see fig. 4.5. (adapted from Google Earth).



Continue Fig. 4.7D. For location see fig. 4.5.

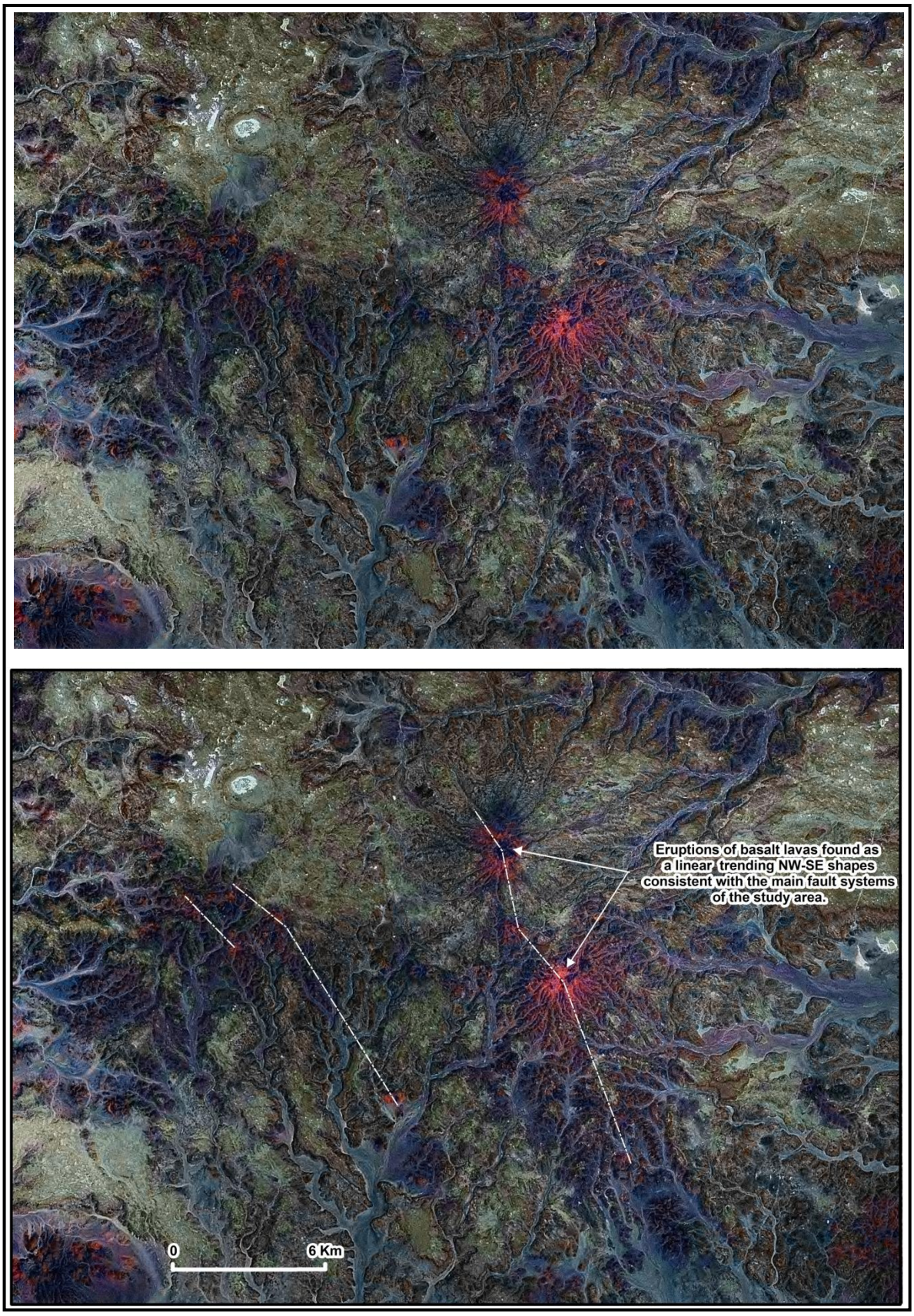


Fig. 4.8 Example of basalt lavas eruptions which found in the southern part of the study area form linear trending NW-SE shapes consistent with the main fault systems of the study area. For location see fig. 4.5.

4.3.2 Hun Graben fault system

The Hun Graben fault system is the westernmost tectonic element in the Sirt Basin (Fig. 4.1-4.4, 4.6, and 4.12) with major faulting occurring in post-Oligocene time (Abadi, 2002), and marked by escarpments and substantial fault displacement clearly visible at the surface. The faults are segmented and bound the Hun Graben on both the west and east sides (Fig. 4.12). To the west is the Ghadamis Basin and to the east the Waddan Uplift. The dominant structural grain, reflected by numerous sub-parallel faults along the graben margin, is NNW-SSE.

The western margin faults continue further to the north than those on the eastern margin changing from a NNW into a N-S trend whilst to the south they are deflected eastwards by the subsurface nose of the Al Qargaf Arch (Fig. 4.12). This caused the graben to swing SE and connects up with the northern end of the Zallah Trough. The connecting zone is complex and contains a major E-W fault, which demarcates the northern margin of an east-west trending ridge which runs parallel to the southern margin of the Waddan Uplift (Anketel, 1996).

Satellite imagery (Fig. 4.13) shows that the western margin at the northern end of the Hun Graben is bounded by irregular fault scarps associated with a series of overlapping en échelon normal faults downthrowing to the east. The zone probably coincides with diminishing offset along the western bounding fault of the Hun Graben.

In contrast, the eastern margin (fault system) of the graben is convex in plan and may be related to a small faulted terrace 8km wide and 35km long while the southern end of the Hun Graben appears to be cross-cut by an E-W trending fault zone with consistent downthrow to the north.

The satellite imagery emphasises the subtle topographic expression of the western boundary fault to the Hun Graben (Fig. 4.14a and b, for location see Fig. 4.5) and suggests that it extends beyond the E-W cross-cutting fault and may link to a major NNE-SSW trending fault system to the south that is covered by lava flows of Jabal Al Aswda.

The surface stratigraphy (Fig. 1.3) shows that along the western margin (fault system), the Late Cretaceous-Lower Paleocene Zimam Formation is juxtaposed against hangingwall strata including Upper Paleocene Shurfah Formation and Oligocene Ma'zul Ninah Formation. Graben infill is predominantly Oligocene Ma´zul Ninah Formation. The eastern bounding (fault system) fault juxtaposes Upper Paleocene Shurfah Formation and Eocene Bishimah Formation in the footwall against upper and lower members of the Oligocene Ma'zul Ninah Formation. Middle Eocene Al Jir Formation is

also exposed in the graben (Fig. 1.3). The basin bounding faults are associated with sub-recent to recent alluvial fans extending up to 5km into the basin.

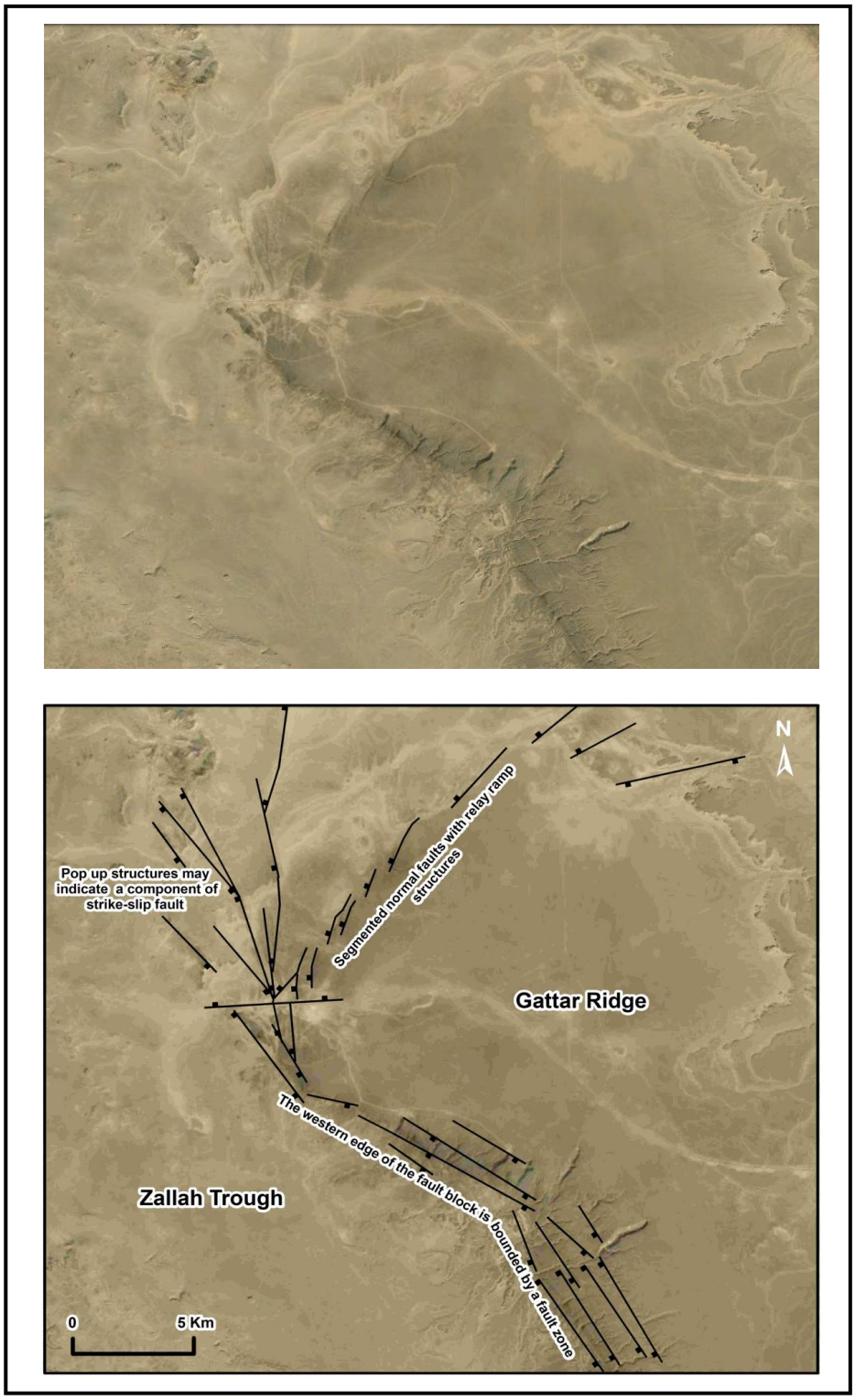


Fig. 4.9 Segmented normal faults with relay ramp structures associated with horsetail splay faults that may indicate a component of sinistral strike-slip as interpreted from satellite (Google Earth) imagery. For location see Fig. 4.5

An intense zone of close-spaced, NNW-SSE trending, minor faults is developed within the Paleocene Shurfah Formation and the upper member of the Zimam Formation on the northern tip of western Hun Graben fault system on the western margin of the basin (Fig. 4.12 and 13). ENE-WSW trending sets of faults are developed on both shoulders of the Hun graben, orthogonal to the main structural grain (north of Jabal Aswada and Al Qargaf Arch in Fig. 4.14). The faults clearly off-set NNW-SSE trending bounding faults and indicates a later set of faulting. Some of these faults may be associated with a minor component of strike-slip. An apparent orthogonal fracture system may be developed where there is no discernable off-set across the two fault trends.

4.3.3 East Waddan Uplift fault system

The Waddan Uplift (Fig. 4.1-4.4 and 4.6) forms a gently arched structural feature, generally elongated from NW to SE, (Jurak, 1985) and reaches a maximum altitude approximately at 16°30' E, 20°30' N.

The east Waddan Uplift fault system bounds the eastern part of Waddan Uplift which comprises several faults that show downthrows to the east, of the order of 300 to 500 m (Vesely, 1985). The sediments exposed along this fault system are gently tilted to the northeast at an angle of 2 to 3° which indicates less vertical displacement along this fault zone compared with the Gedari fault system to the east. This fault system is offset in the west central part by a north downthrowing, normal fault zone of the Al Qargaf Arch and is also separated by transverse faults striking E to ESE in the western part of the map, which belong to the periphery of the Hun Graben (Fig. 4.6 and 4.14).

In the south of the Waddan Uplift, and northern part of Zallah Trough, anticlines and synclines which may belong to the southern tip of the Waddan Uplift are common with hinges that strike NW-SE (Fig. 4.15). The dips of the fold limbs, however, attain as much as 10° to 20°, exceptionally 30°.

4.3.4 Qarat Ash Shush fault system

The Qarat Ash Shush fault (Fig. 4.6) is some 30 km west across the Gattar Ridge from the Gedari fault system and contains a series of left-stepping normal faults blocks. The Qarat Ash Shush fault system crops out in a NNW-SSE trending strip some 3 km wide along the western margins of the Qarat Ash Shush syncline parallel to the western margin of Gattar ridge. It shows opposing dip directions and changes in direction of throw along its length; however the net downthrow is westerly. In the northern part of

the zone, reactivation of faults has caused displacement of the Upper Eocene and Oligocene beds (Kumati, 1981; Anketell and Kumati, 1991b). It is obvious, particularly in the northern part of Qarat Ash Shush fault system, that the faults are arranged in an en echelon pattern trending NW to SE and some of them show a clear horizontal displacement of Eocene strata indicating sinistral strike-slip displacement along the



Fig. 4.10 (A): Example of sinistral strike-slip faults as appear on satellite imageries, (adapted from Google Earth). Left lateral horizontal displacement of strata A, B, and C.

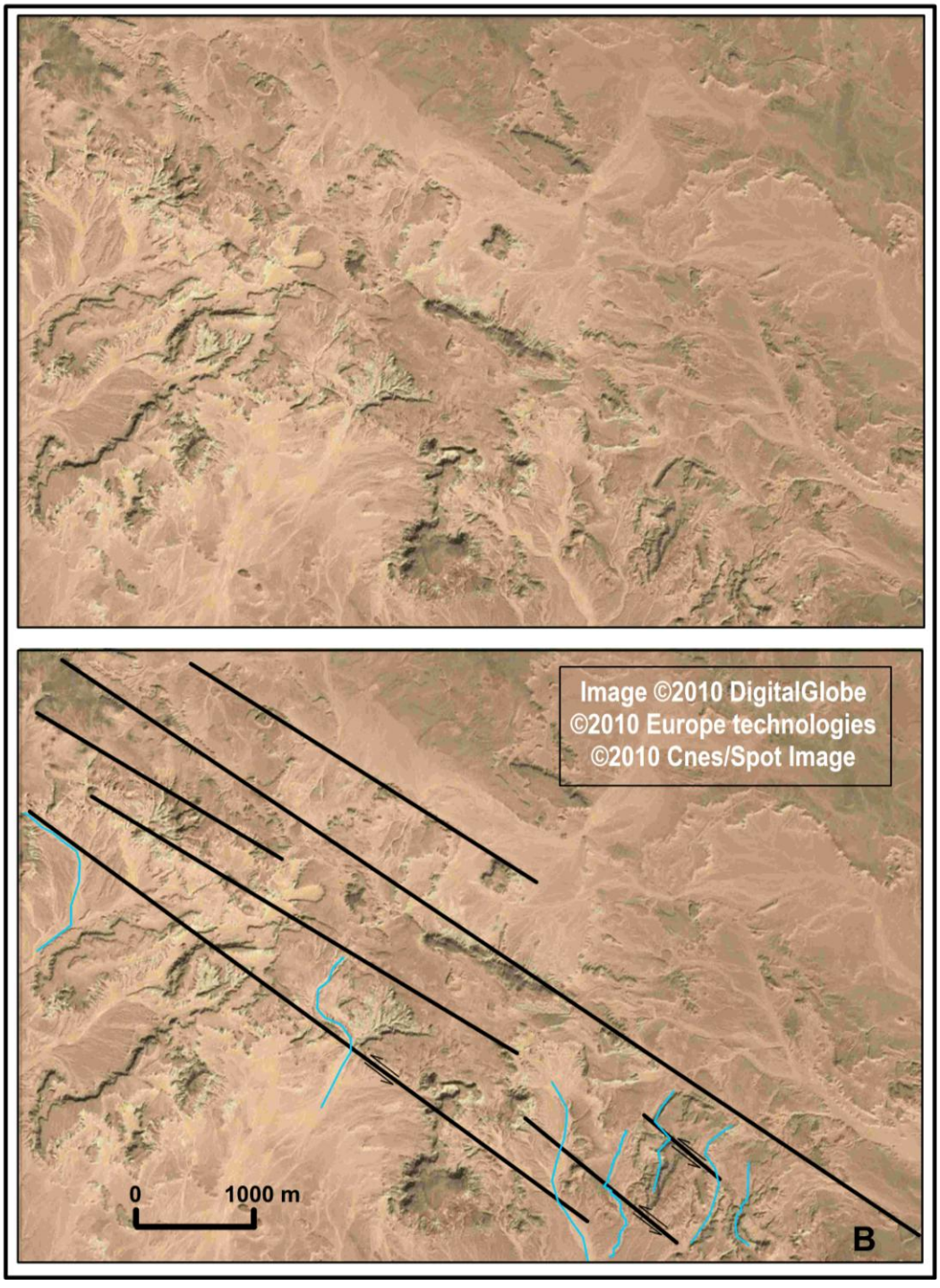


Fig. 4.10 (B): Example of sinistral strike-slip faults as appear on satellite imageries, (adapted from Google Earth). Wadis (valleys) horizontal displacement. (adapted from Google Earth).

eastern part of Qarat Ash Shush and to the west of the Gedari fault system (Fig. 4.6, and Fig. 4.10a and b). Some of these faults also are strongly segmented into en-echelon, right stepping fault arrays which produce horse-tail structures (Fig. 4.16).

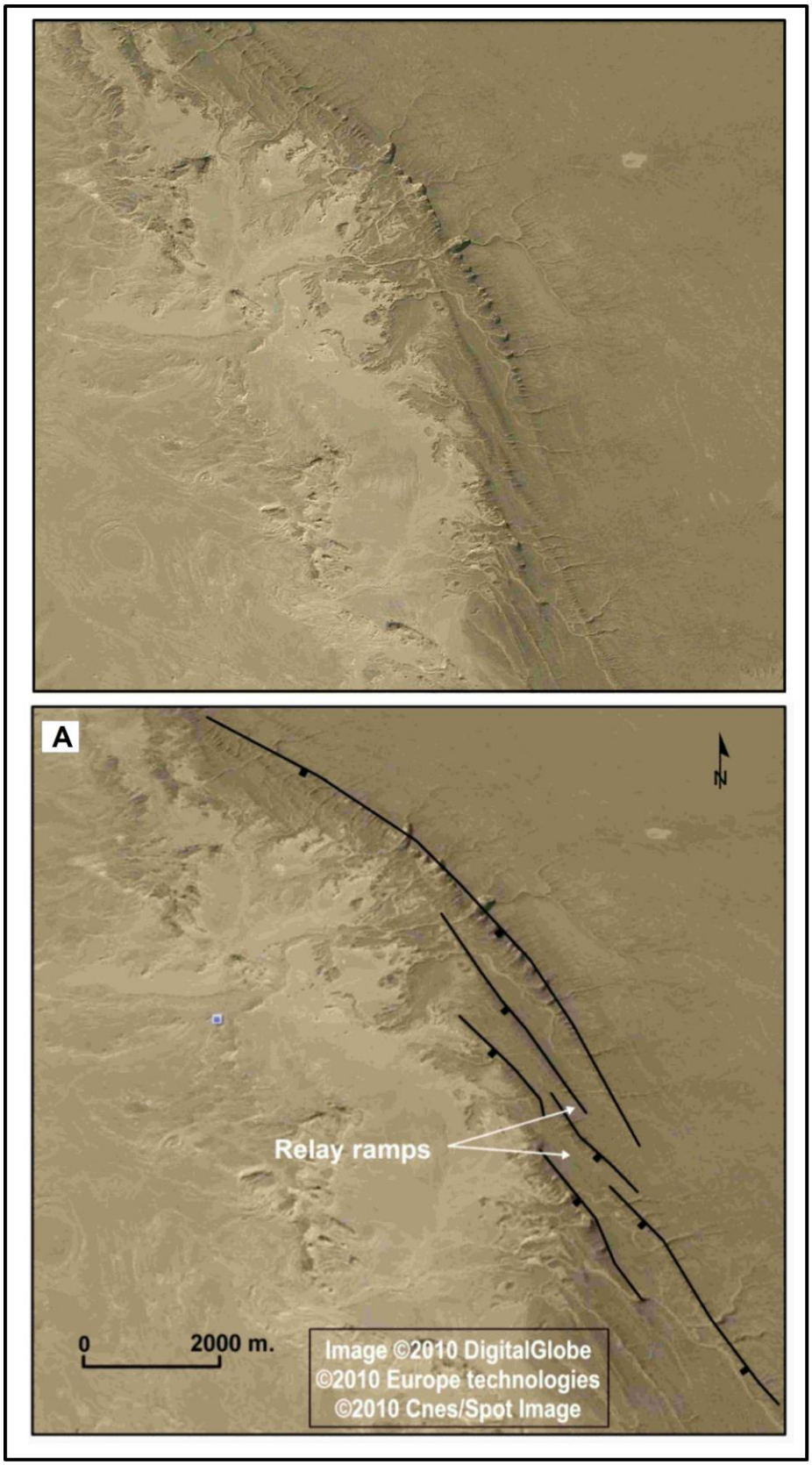


Fig. 4. 11a Example of relay ramp structures as appear on satellite imageries. The border faults (Gedari Fault) have a stepping geometry and similar dip direction, forming as asymmetric rift basin faulted margin and a hinged margin. (adapted from Google Earth).

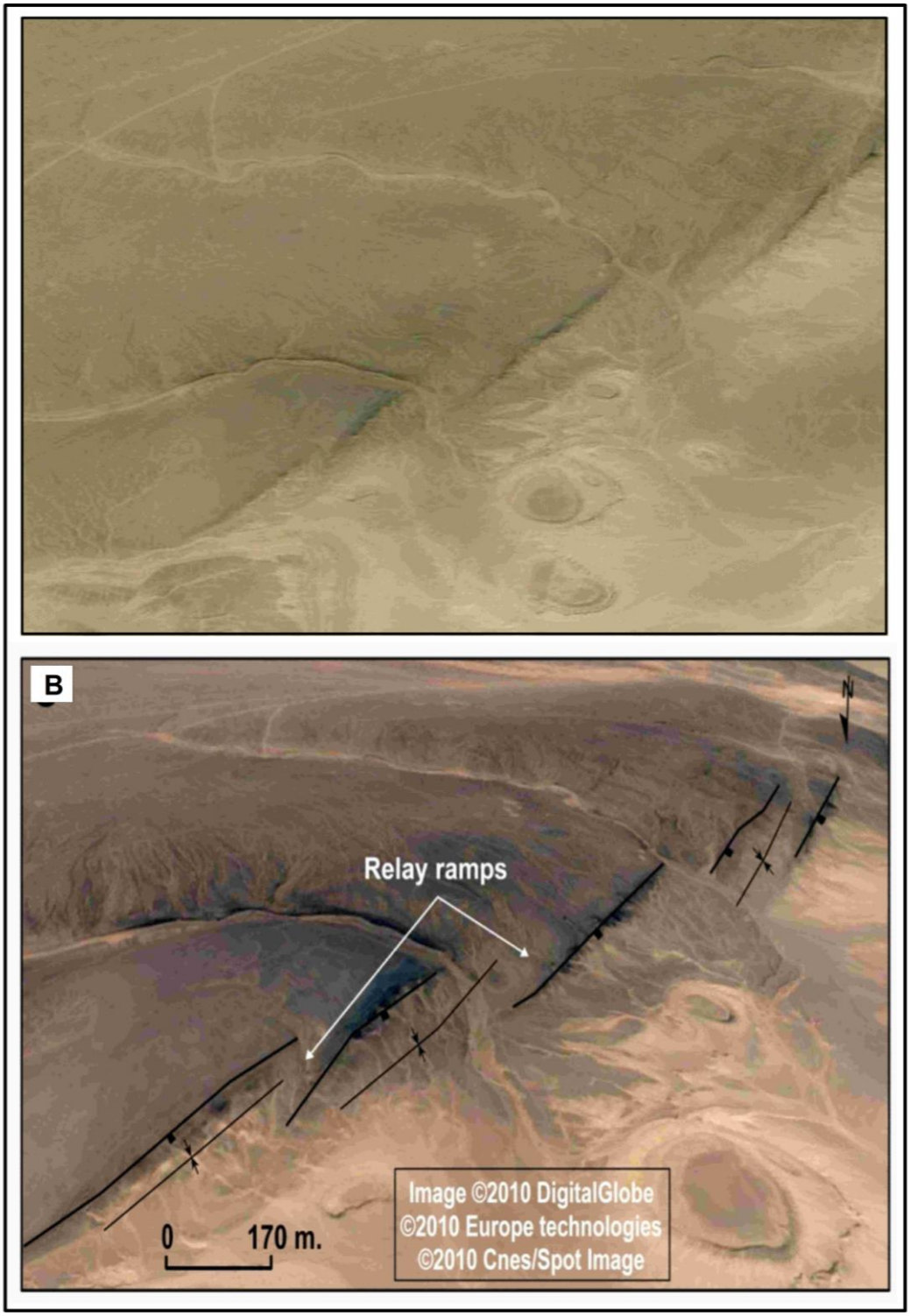


Fig. 4. 11b Example of relay ramp structures with adjacent elongated synclines as appear on satellite imageries. It shows a Fault displacement folds and relay ramp associated with stepping normal faults. (adapted from Google Earth).

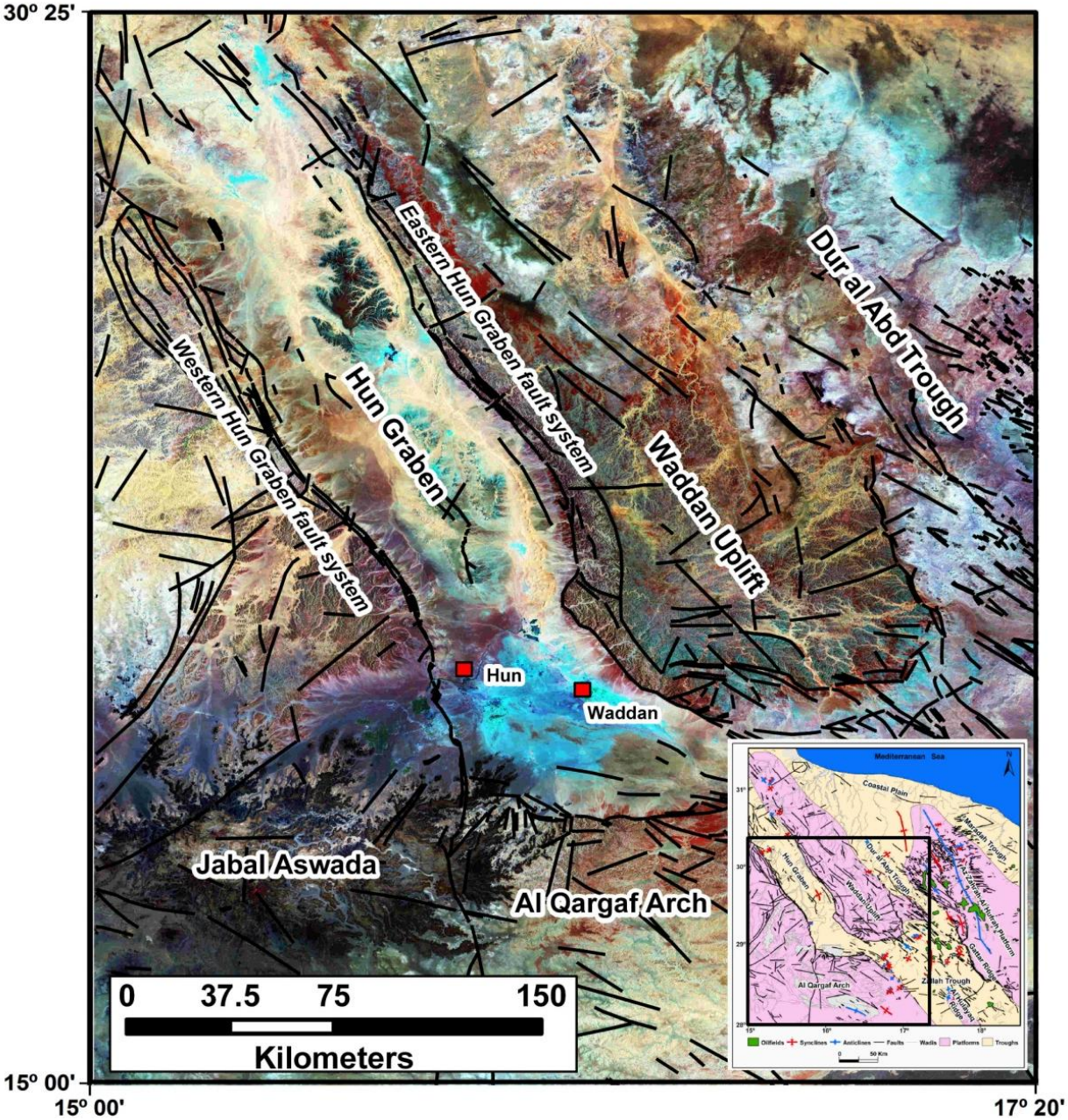


Fig. 4.12 The segmented faults which bound the Hun Graben on both the west and east sides as interpreted from satellite imagery of the study area. Inset box: Location in the study area.

The adjacent Qarat Ash Shush syncline changes direction of plunge along its length to define two small boat-shaped, gently dipping folds not seen at map scale (Fig. 4.3 and 4.4). Both synclinal zones are developed in close proximity to NNW-SSE fault zones to the southwest of the Asiyah syncline (Fig. 4.6).

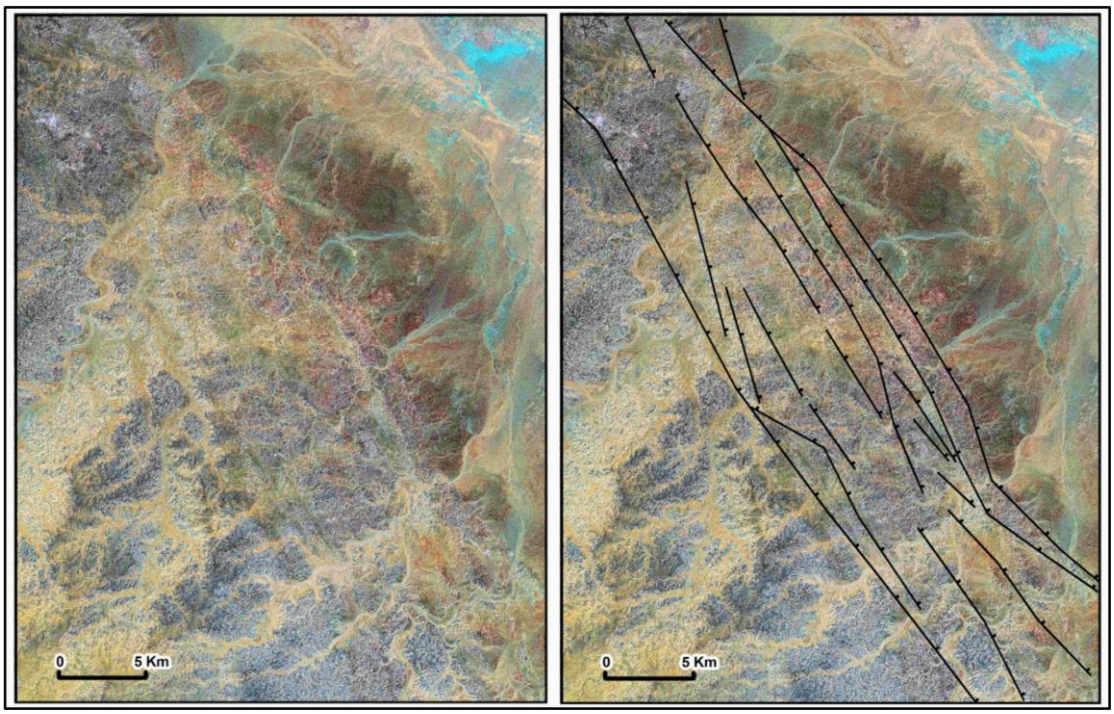


Fig. 4.13 Satellite imagery interpretation of the northern end of the western margin of the Hun Graben bounded by irregular fault scarps associated with a series of overlapping en échelon normal faults downthrowing to the east. For location see Fig. 4.5

4.3.5 Ar Raqubah fault system

At 17°50' 29°05', (Fig. 4.6) the Qarat Ash Shush fault system is flanked by two other zones which branch out to the NW and NE, respectively (Anketell and Kumati, 1991b). The NW trending fault system, to the west of the Qarat Ash Shush system can be traced for 25 km through the Qarat Ar Raqubah area and named by Anketell and Kumati, (1991b) as the Ar Raqubah fault system. Within this system the structure consists of a series of NW to NNW trending fault segments arranged as overlapping normal faults downthrowing to NW in a similar manner to some extent to the Qarat Ash Shush fault system. Some synclines and anticlines trending NW-SE (Fig. 4.6 and 4.17) in the south Ar Raqubah area display a gentle northwesterly plunge.

4.3.6 Zallah fault system

The Zallah fault system (Fig. 4.6) cuts through the central part of the study area from NW to SE and is divided into northern, middle and southern parts. The southern part of the fault bounds the Al Hulayq Ridge on both sides from the Ar Ramlah Syncline to the east and the Maʻamir Graben to the west (Fig. 4.18). Some small synclines and anticlines are located to the south of this fault system particularly in its central part (Fig.

4.18) where it bounds the Zallah sub-basin to the east. The northern section of the fault separates the Waddan Uplift to the west from the Facha Graben to the east (Fig. 4.7).

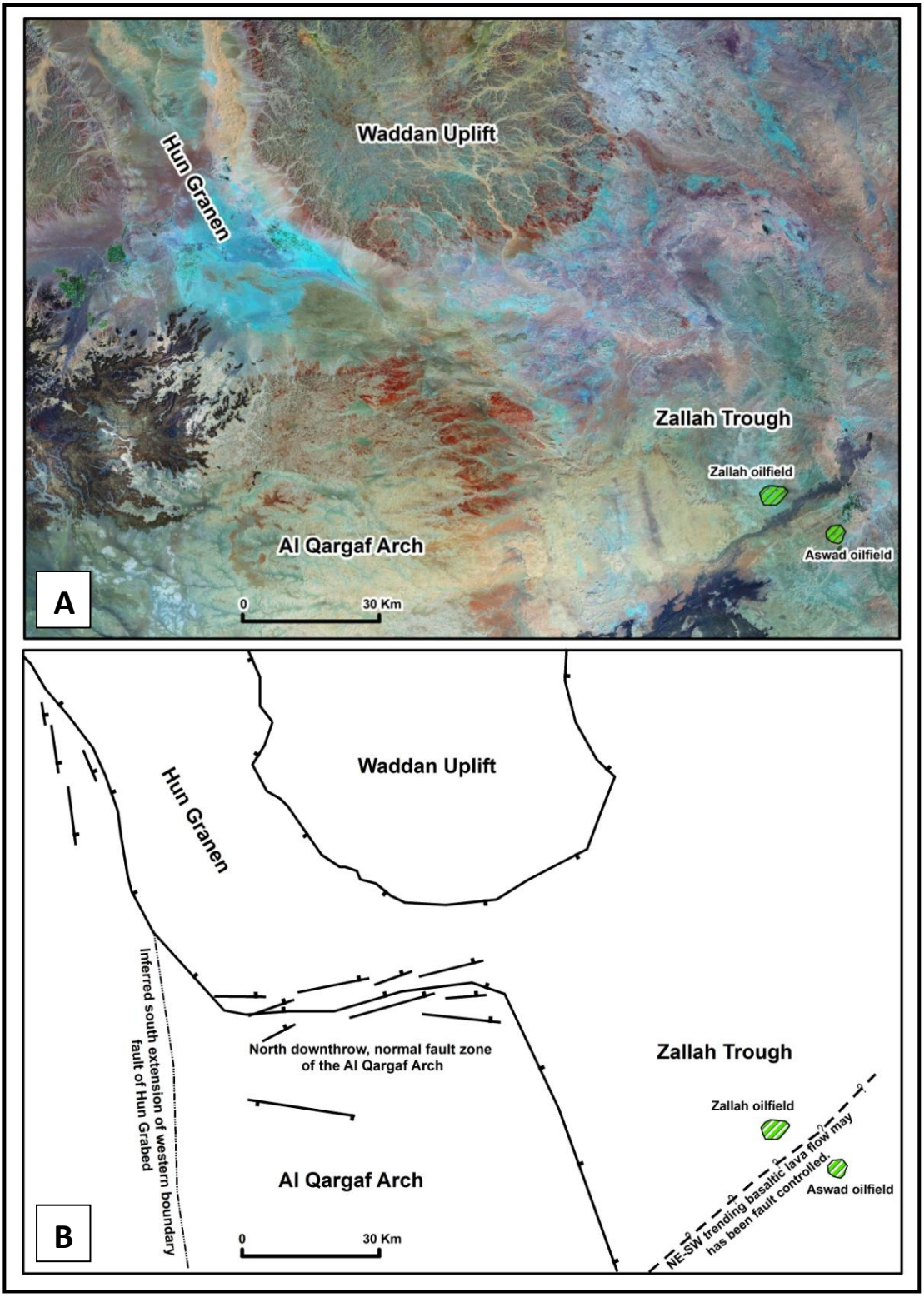


Fig. 4.14 (A) The southern portion of Hun Graben as appeara on satellite imagery. (B) Satellite imagery interpretation of the southern portion of the Hun Graben suggests that it extends beyond the E-W cross-cutting fault and may link to a major NNE-SSW trending

fault system to the south that is covered by lava flows of Jabal Al Aswda. For location see Fig. 4.5

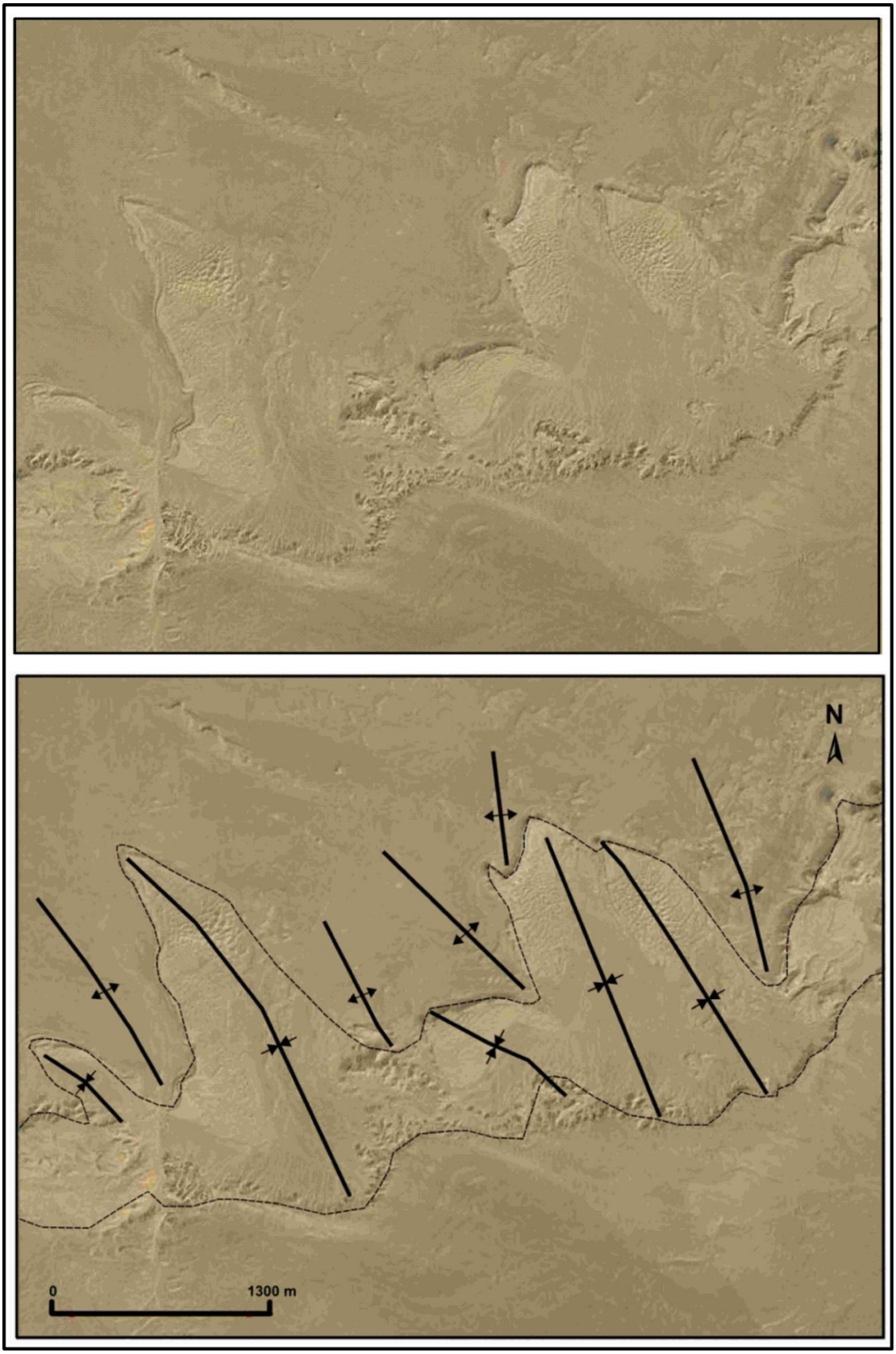


Fig. 4.15 Anticlines and synclines that may belong to the southern tip of the Waddan Uplift as interpretated from satellite imagery. (adapted from Google Earth and for location see Fig. 4.5).

The Zallah fault system forms a series of NNW trending fault segments arranged as overlapping normal faults dipping to the SW, changing to NE dip where the faults are arranged in a closely spaced en echelon pattern with NW-SE trend.

The faults cross-cut The Zallah fault system is characterized by the existence of major oil fields (Fig. 3.8) that are located parallel to this fault system such as the Hakim and Fidda oilfields (Fig. 4.7) which are associated with a narrow NNW-SSE trending surface anticlines expressed in the Maradah Formation and Late Tertiary-Quaternary sediments. The Hakim and Fidda structure is approximately 36.5 km long and approximately 4km wide with the Oligocene Ma'zul Ninah Formation exposed in the erosional core of the structure. The Ghani and Zenab fields are also located in the middle portion of this fault system in the vicinity of a NNW-SSE to NW-SE trending arcuate fault zone associated with normal downthrow to the west.

Late Eocene sediments (the Wadi Thamat Formation), Oligocene sediments (the Ma´zul Ninah Formation), and Late Tertiary-Quaternary deposits (Fig. 1.3).

The footwall to this system consists largely of Eocene Wadi Thamat Formation while the hangingwall sequence, to the west, consists of gently eastward dipping Wadi Thamat and Ma'zul Ninah Formations at surface (Fig. 4.6 and 1.3). Some of the faults are associated with normal displacement whilst others show no visible displacement at the resolution of the imagery and isolated NE-SE trending faults are also developed. The surface structure of Al Hulayq Ridge which represents the southern tip of this fault system appears to suggest that there is a lateral continuation of the Al Hulayq Ridge northwards to the southern edge of the Waddan Uplift.

4.4 Basin elements and Geotectonics of the Area

The satellite image interpretation integrated with the surface geological maps shows that the study area contains several basinal and geotectonic elements; namely, the Zallah, Dur al Abd, Maradah, Hun Graben, the Waddan Uplift, Gattar Ridge, the Az Zahrah-Al Hufrah Platforms, the Al Qargaf Arch, and the intrabasinal Al Hulayq Ridge (Fig. 4.1-4.4).

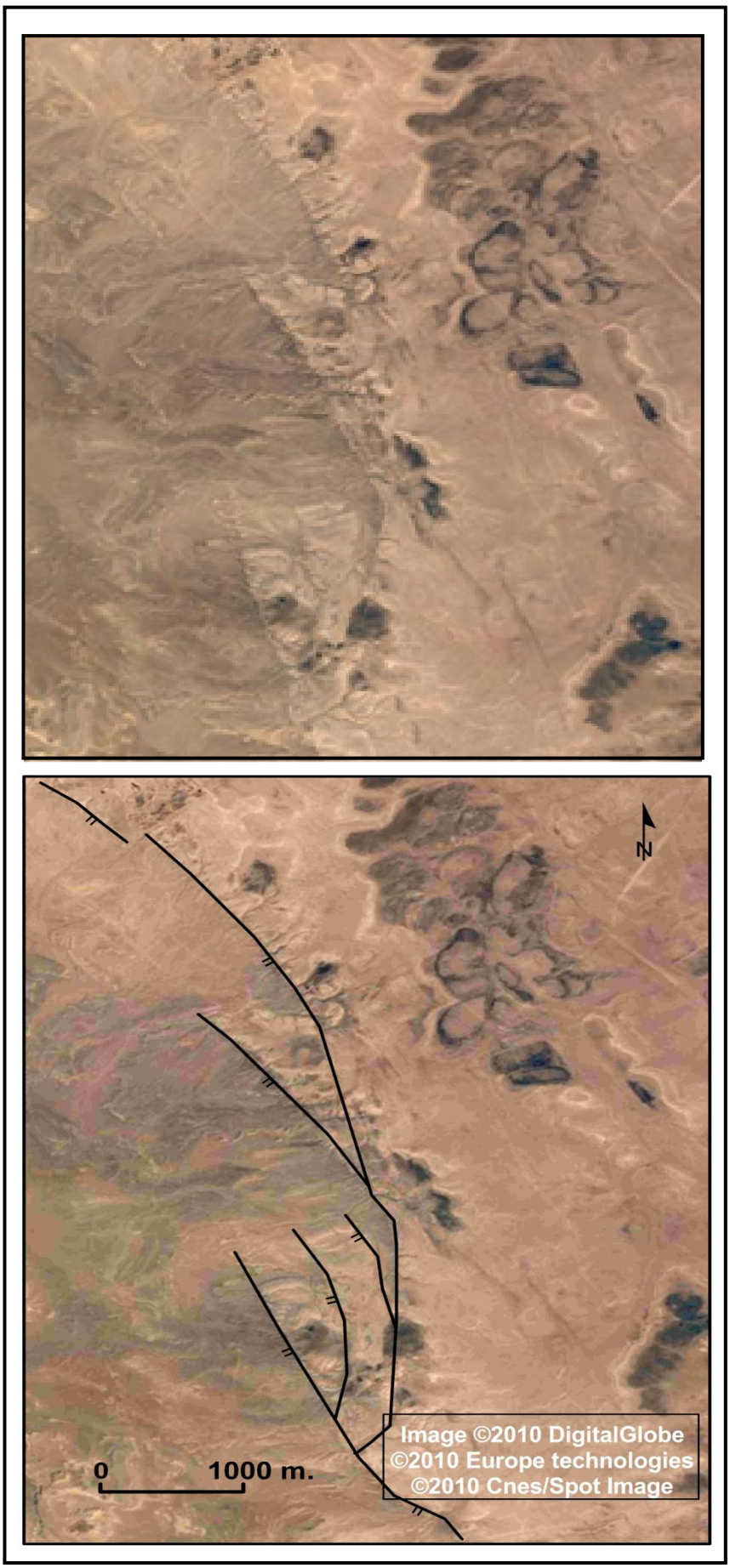


Fig. 4.16 Example of horse-tail structures as appears on satellite imageries, (adapted from Google Earth and for location see Fig. 4.5).

The study area can be divided into a number of tectonostratigraphic domains based on the following criteria:

- *Structural grain, i.e., the dominant trend of faults and associated folds.*
- *Homogeneity and orientation of bedding.*
- *Relative intensity of faults and fractures.*
- *Style of deformation.*
- *Surface stratigraphy.*
- *Structural geomorphology including drainage pattern and morphology.*

Using these criteria the following structural elements were identified from the data used. The structural domains generally show good internal correlation and are consistent with the known regional tectonic elements of the Sirt Basin.

4.4.1 Zallah Trough

The Zallah Trough (Fig. 4.6) is situated in the southern part of the study area (Fig. 4.1-4.4) and is an asymmetrical faulted graben which connects northwards with the Dur al Abd Trough and southwards with the Abu Tumayam Trough (Fig. 1.4) where they appear more or less as a continuous low NW-SE trending embayment. It is bounded by the Waddan Uplift to the northwest, the Al Qargaf Arch to the southwest and the Az Zahrah-Al Hufrah Platform to the east.

On the basis of satellite image mapping and the published geological maps (Vesely, 1985 and Jurak, 1985) the Zallah Trough is divided into a number of sub-basins (Fig. 4.17): the Facha Graben, Ar Ramlah Syncline, Zallah Sub-basin and Ma‘amir Graben (Schroter, 1996; Johnson and Nicaud, 1996). The Al Hulayq Ridge (Fig. 4.1-4.4), projects into the area from the south, and forms a spur that divides the Ar Ramlah Syncline, to the east and the Ma‘amir graben to the west, and then passes beneath the Al Haruj Al Aswad volcanic centre to the south. Due to down-faulting, the deepest part of the trough lies on the NE side of the axial Al Hulayq Ridge and the southwestern Az Zahrah-Al Hufrah Platform, with the Gattar Ridge recognized.

This interpretation reveals that the Zallah limits are reasonably well defined at surface and from satellite images (Fig. 1.3, and 4.1-4.4). The Zallah Trough is connected with the Hun Graben to the northwest by a complicated zone of wrench tectonics whose extension beneath the Al Haruj al Aswad volcanics remains uncertain. The Zallah Trough is an extremely complex area in terms of structural relationships in the western Sirt Basin.

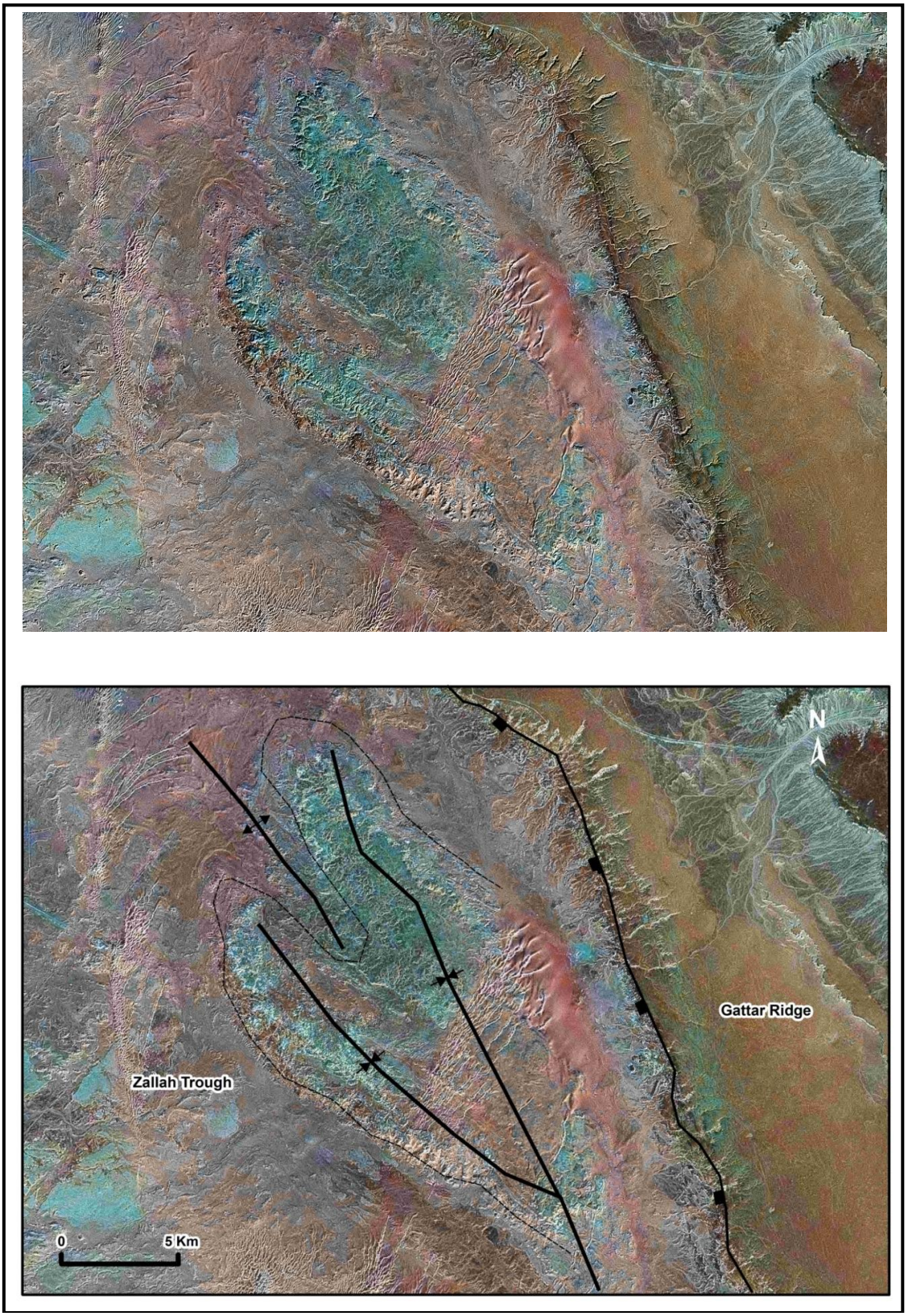


Fig. 4.17 Synclines and anticlines trending NW-SE located in the south Ar Raqubah area display a gentle northwesterly plunge (tenth of kilometres long) as interpretated from satellite imagery. (adapted from MrSid imagery and for location see Fig. 4.5).

Towards the northwest the Zallah Trough is bounded by several east trending, south downthrowing faults that are part of a normal fault zone that defines the southeastern margin of Waddan Uplift.

The southwestern margin is bounded by a north and east downthrowing, normal fault zone of the Al Qargaf Arch. Some large triangular bedding facets or ‘flat-irons’ of the exposed sediment along the western side of the trough indicate eastward dipping strata into the trough along the eastern end of the Al Qargaf Arch (Fig. 4.19).

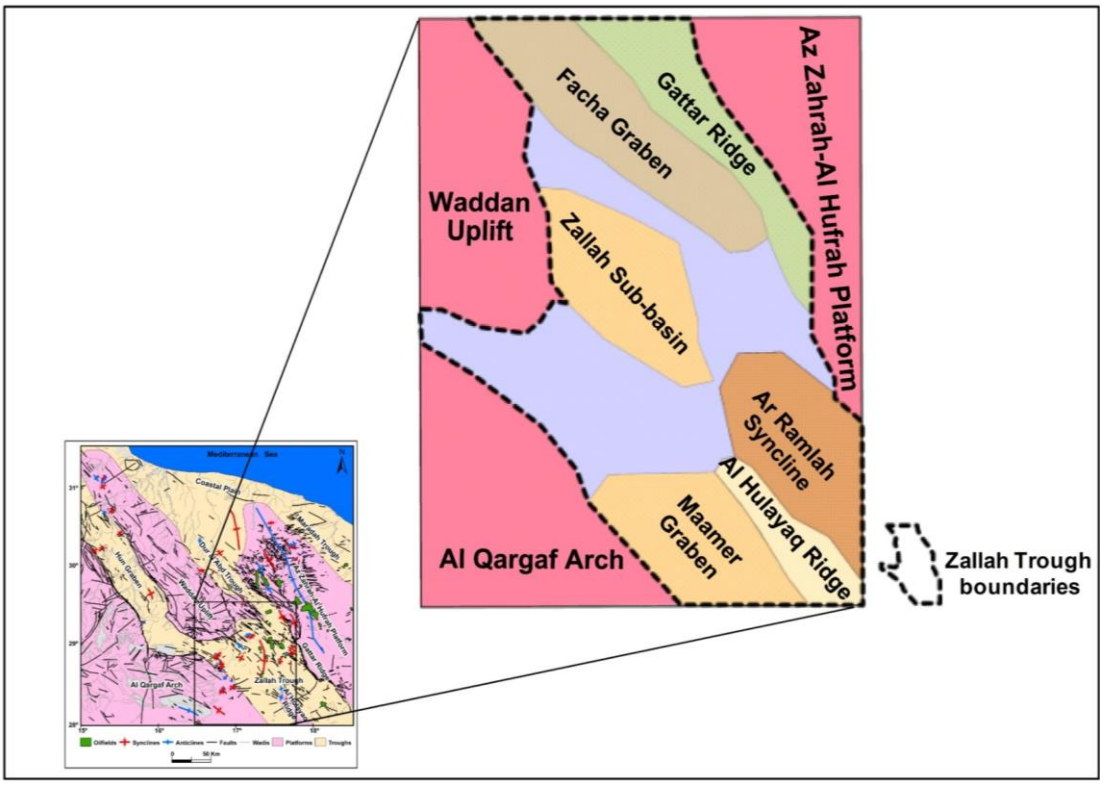


Fig. 4.18 Map shows Zallah Trough structural subdivisions. Inset: Location in the western Sirt Basin area.

A partial discontinuity is also represented by faults striking NW-SE in the southwestern corner of the study area, which belong to the periphery of the Hun Graben and are mostly covered with younger sediments and is manifest on the surface only by indications of a straight lineament (Fig. 4.14.a and b) indicated by a change of a series of wadis direction and a lithology (spectral reflectance) which seems to be differ from the pattern of adjacent features.

They are probably the southernmost spurs of this structure and the amplitude of the movement along the faults is clearly smaller than in the northerly continuation of the Hun Graben. Compared with the western margin, the eastern side of the Zallah Trough is more defined and marked by a series of major fault scarps which coincide with a normal fault zone defining the western edge of the Gattar Ridge as SW fringe of Az Zahrah-Al Hufrah Platform. The fault zone extends for approximately 180km along strike in the study area and has been described (see section 4.3.1) as the Gedari fault.

The interpretation also reveals that faults up to tens of kilometers long are the dominant structural element in the study area where the main NW-NNW structural trend coincides with the orientation of tectonic elements of the Sirt Basin. Most of these faults are associated with normal displacement whilst others show no visible displacement at the resolution of the imagery. NE-SW trending faults are also developed, and in most cases, appear to post-date and off-set the NNW-SSE trending faults.

Many fault-related folds (drag-folds) formed adjacent to the fault structures and are typically narrow asymmetric monoclinal structures with beds tilted generally less than 5°, although dips up to 20°-25° are estimated adjacent to faults.

Furthermore there are numerous elongate asymmetric synclines such as the Zallah syncline (Fig. 4.6) located in the central part of Zallah Trough associated with shallow west limbs and steeper dipping east limbs that are developed in the hangingwall and adjacent to west downthrowing normal faults on the eastern margin (Vesely, 1985). These hangingwall basins contain Oligocene Ma'zul Ninah, Miocene Al Khums and Late Tertiary-Quaternary sediments (Fig. 1.2).

The period of folding is connected with subsidence movements during the filling of the Sirt Basin (Vesely, 1985). Some of the fold structures may be due to compaction of sediments in troughs, which supplement the tectonic folding (Vesely, 1985) where the sedimentary sequences are mildly undulated into synclines and anticlines, the axes of which are parallel to the principal tectonic direction, i.e. NW-SE.

According to satellite interpretation most of the subtle low amplitude periclinal structures which are exposed at surface coincide with producing oil fields. The Zallah Trough is a well-known oil-producing area with over 20 significant oil discoveries, (Fig. 4.6) and production from various oil fields (Hallett and El-Ghoul, 1996). The Zallah Trough oil fields (Fig. 3.8, and 4.6) are situated mainly on the updip edges of interpreted folds.

4.4.2 Dur al Abd Trough

The Dur al Abd Trough (Fig. 4.6) represents a more or less continuous elongated low of three troughs, including Dur al Abd, Zallah and Abu Tumayam Troughs from north to south respectively which runs from the Sirt embayment coast in the north to the southern (shelf) boundary of the Sirt Basin (Fig. 1.4). Some authors believe that the Zallah Trough narrows northwards and becomes shallower to form the Dur al Abd Trough (Hallett 2002).

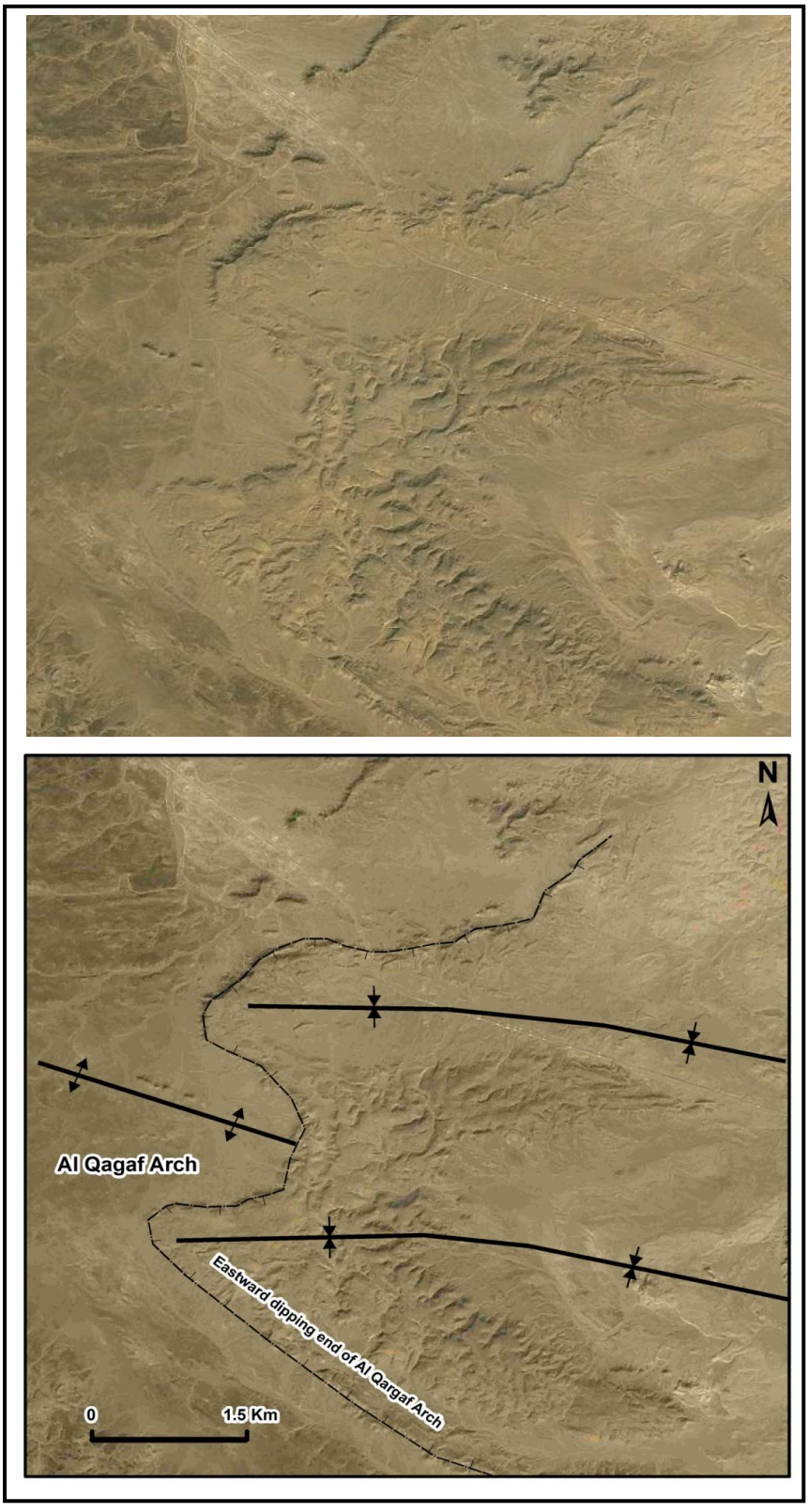


Fig. 4.19 Some large triangular bedding facets or 'flat-irons' in exposed sediment along the western side of the Zallah Trough indicate eastward dipping strata into the trough along the eastern end of the Al Qargaf Arch. (For location see Fig. 4.5).

The Dur al Abd Trough separates the Az Zahrah-Al Hufrah Platform from the Waddan Uplift in the area of the Mabruk field and it is difficult to follow north of the Mabruk

field where it loses its identity in the faulted northeast flank of the Waddan Uplift. The Dur al Abd Trough is a 50km wide NW-SE trending, fault bounded graben in the Mabruk area but broadens out further south and has greatest fault displacement in the east. It extends approximately 175km northwards from the Facha field. The Dur al Abd, and Zallah Troughs seem to be in the first instance a continuous trough that follows the NNW-SSE trending structural grain of the region, however the data reveal a structure that acts as a bridge that separates them from each other possibly extending from northern Gattar Ridge to the southeastern part of the Waddan Uplift (Ar Raqubah fault system, (Fig. 4.6).

The Dur al Abd Trough is extensively faulted and characterized mainly by two fault trends, one that is parallel to the NNW-SSE dominant fault trend of the Sirt Basin and has an associated subsidiary later ENE-WSW transverse fault set and a second N-S trending fault set that are evident on the northeastern dipping flank of the Waddan Uplift and extend into the Dur al Abd Trough. Displacement across the graben bounding faults is approximately 250m (Roohi, 1996b, and Hallett, 2002).

Based on this surface interpretation it is difficult to split the northern extension of Dur al Abd Trough from the adjacent Az Zahrah-Al Hufrah Platform to the east. The Mabruk field is the only field that lies within the Dur al Abd Trough with the Facha field on its faulted western flank on the Az Zahrah-A Hufrah Platform.

4.4.3 Az Zahrah-Al Hufrah Platform

The Az Zahrah-Al Hufrah Platform (Fig. 4.6) is located in the eastern part of the study area between the Dur al Abd and Zallah Troughs to the west and the Maradah Trough to the east and is bounded on the south by the NNE-SSW trending Kotlath Graben which separates it from Al Bayda Platform (Fig. 2.4). On its southwest margin, the Gattar Ridge is formed by downfaulting to the WSW. The platform occupies a 40,000km² area and dips towards the northeast with a northern boundary that is poorly defined and may be affected by wrench-faulting close to the present coastline (Anketell, 1996). The western platform boundary fault in the SW region is characterised by a complex series of en echelon faults indicating a sinistral strike-slip movement, with associated riedel shears forming small-scale horst and graben structures during the Eocene (Anketell and Kumati, 1991b).

The western platform boundary fault (Gedari fault) lies close to the assumed junction between the basement west and east African plates, which were active during the

Cretaceous and reactivated as sinistral wrench faults in the Eocene time (Anketell, 1996 and Jerzykiewicz, et al. 2002) as shown in Fig. 4.20.

This western boundary fault zone of the Az Zahrah-Al Hufrah Platform is defined by: NNE-SSW trending monoclinal flexures in the bedding (Fig. 4.7) which provide a sense of relative downthrow across the fault zone. The northeasterly tilt of the platform occurred during the post-Eocene and is associated with extensive faulting and fracturing with identification of the main faults trending NNE-SSW being considered as a reactivation of pre-rift faults, NW-SE Cretaceous syn-sedimentary faults and NNW-SSE Late Eocene (post-rift) faults (Roohi, 1996a and b; Schroter, 1996).

Faults within the platform have generally less than 60m displacement whereas the platform bounding faults have 800-1000m displacement (Wennekers et al., 1996; Roohi, 1996a and b; Schroter, 1996; Hallett, 2002). From a surface perspective, the northern end of the platform is expressed at surface by a homoclinal shallow northeast dipping panel predominantly of U. Eocene Wadi Thamat Formation. An elongate erosional window occurs along the western margin of the platform exposing the M. Eocene Al Gatta Member.

Large SW dipping triangular bedding facets of the lower member of the Oligocene sediments help to define the limits of the platform at surface forming elongated synclines parallel to the western platform boundary faults (Fig. 4.7a-d). The Az Zahrah-Al Hufrah Platform at the northern end (Fig. 4.21) is marked by a two north-northwest plunging nose of a large low-amplitude gentle flexures anticlines which are expressed by erosional features and surface geomorphology. An anticlinal monoclinal fold (Fig. 4.6) defines the western margin of the dominant fault trend within the platform is NNW-SSE with subsidiary E-W to ENE-WSW trending faults (Fig. 4.7) consistent with the Sirt Basin structures. Combination of the NNW-SSE and ENE-WSW trending faults impart a grid-like pattern that resembles crosscut fault structures (Fig. 4.22). The Az Zahrah Al Hufrah Platform comprises carbonates of the Lutetian to Priabonian (Eocene) Wadi Thamat Formation (Fig. 1.3) and are outcrop equivalents to major deeper hydrocarbon reservoirs specifically in the eastern portion of Sirt Basin.

These beds are cut by a NW-trending system of fractures, characterized by swarms of vertical extension joints accompanied by crosscut sets (Fig. 4.22) of hybrid and shear joints, and normal faults. Many of the NE to E-W interpreted lineaments exhibit fractures, and are particularly conspicuous in the north of the platform where they are possibly due to the influence of additional fracture systems related to major flexures trending obliquely to the NW-SE direction. As any crosscutting feature must be younger

than the rock or sediment it cuts across, these major E-W trending flexures and associated fracture systems were formed during the post-Eocene phase of deformation, and are cross-cut obliquely by fractures of the NW-trending system.

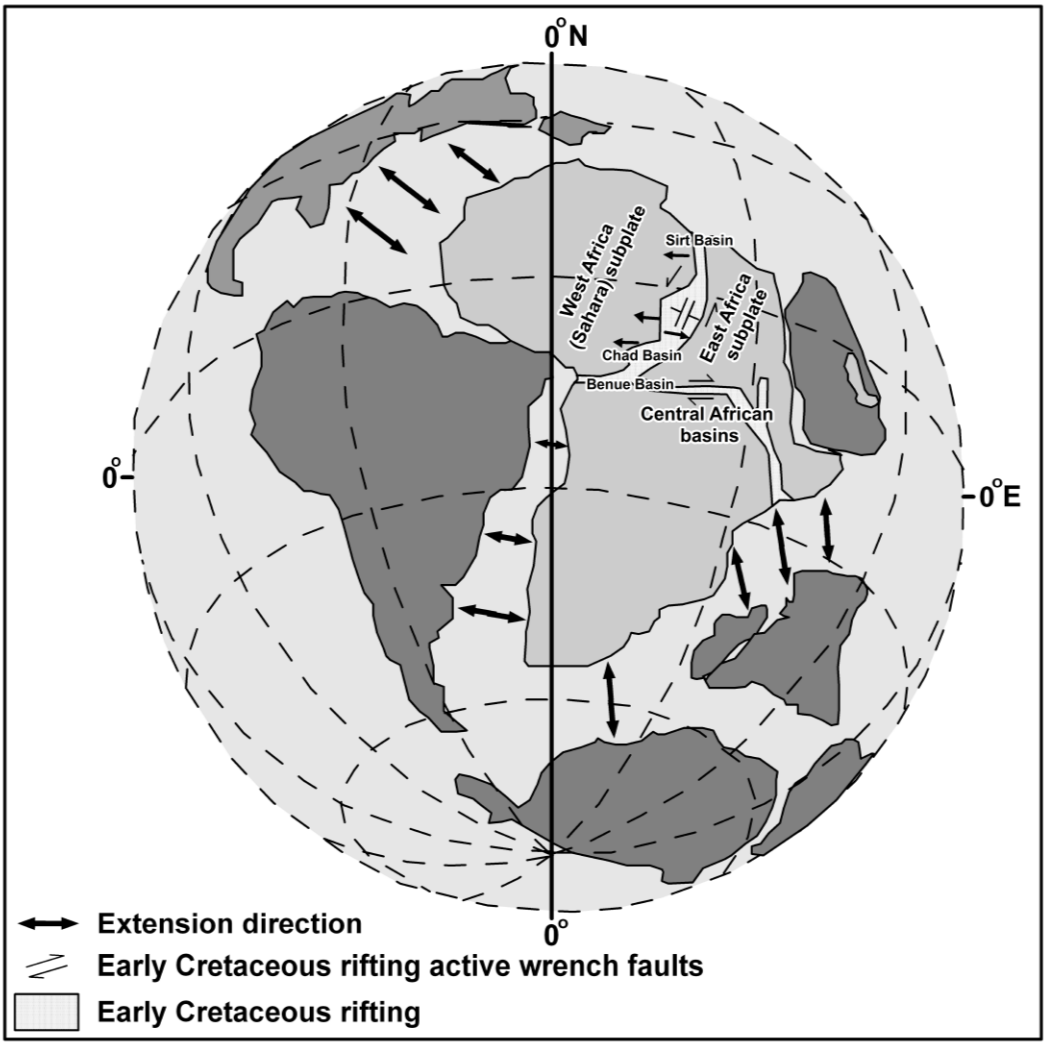


Fig. 4.20 The early opening phase of the South Atlantic (Arrows show relative motion of the continents away from Africa plate) and the geometry of the Early Cretaceous rift systems in Africa. The Sirt Basin is located at the northern end of the Sirt-Benue fracture zone which extends south through the Chad depression into the Benue Trough that opened in response to a northeast extension on the East African subplate (modified after Fairhead and Green 1989, Fairhead. and Binks. 1991, Guiraud, and Maurin, 1992, and Anketell, 1996).

4.4.4 Hun Graben

The Hun Graben (Fig. 4.1-4.4, and 4.6) is an elongated structure feature measuring 300 km long and averaging 40 km in width, has a distinct surface expression and forms a present day fault bounded depression indicating that it is one of the youngest tectonic elements in the region. The development of the Hun Graben, however, is controversial. Klitzsch (1970) indicated that the graben was downthrown 500-800m relative to the Tripoli-Tibesti Uplift (Fig. 1.4) and also suggested that the graben was initiated prior to the Late Cretaceous and that the western margin was Paleocene in age. Cepek (1979)

estimated a vertical throw of 100-120m and an Oligocene age for the development of the graben whilst Abadi (2002), suggested the major faulting occurring in post-Oligocene time.

The graben narrows at the southeast near the town of Hun (Fig. 4.1-4.4, 4.12 and 4.14) and its connection with Zallah Trough is complicated by strike-slip faulting. The structure underlying the Al Haruj al Aswad volcanics is uncertain, but Klitzsch, (1970) inferred the presence of a remnant of the Palaeozoic Kalanshiyu Trough below the volcanics. Based on the drainage pattern analysis (Fig. 1.3) the Hun Graben appears to cross-cut existing southwest draining wadi channels. Along the eastern margin of the basin, (Fig. 4.23) wadis are generally narrow and become incised as they approach the margin of the graben indicating that they have been rejuvenated by a relative drop in the surface elevation within the graben.

This is evidenced by a relatively linear major northeast draining channel present on both flanks of the Hun Graben. The drainage channel is deflected as it enters the Hun Graben due to normal faults and related gentle folding of strata adjacent to the faults. These relationships imply that the palaeo-drainage (at least pre-Oligocene age) was to the northeast and was subsequently modified by development of the Hun Graben in the Oligocene.

Drainage within the graben is characterized by large arcuate drainage channels or Wadis (dry valleys) in the Hun Graben. The shape of these wadis reflects the deflection of the drainage channels along the bedding contact between relatively hard and soft lithological units, which have been deformed into a subtle synclinal warp (Fig. 4.23 and 4.24). A northward draining NNW-SSE trending axial drainage system is located mainly along the eastern margin of the graben. Most drainage channels entering the western side of the graben converge towards a common point or drainage sink towards the northern end of the Hun Graben.

A number of NNW-SSE open folds (Fig. 4.6) have been interpreted within Ma´zul Ninah Formation strata along the margins of the graben. The folds have probably formed in response to drag in the hangingwall to the basin bounding faults or possibly due to roll-over on non-planar faults in the sub-surface.

4.4.5 Waddan Uplift

The Waddan Uplift (Fig. 4.6) is a gentle north-northeast tilted block, approximately 250km long with a width of 105km in the south, narrowing to 75km in the north before it disappears below the coastal plain. The uplift terminates in the south against the

northeastern extension of the Al Qargaf Arch (Fig. 4.12, and 4.14). The dominant fault trend is NNW-SSE with a subsidiary orthogonal set trending ENE-WSW (Fig. 4.1-4.4). The northeastern margin of the Waddan Uplift is extensively faulted due to dextral shear along a WSW-ESE basement fault (Anketell, 1996).

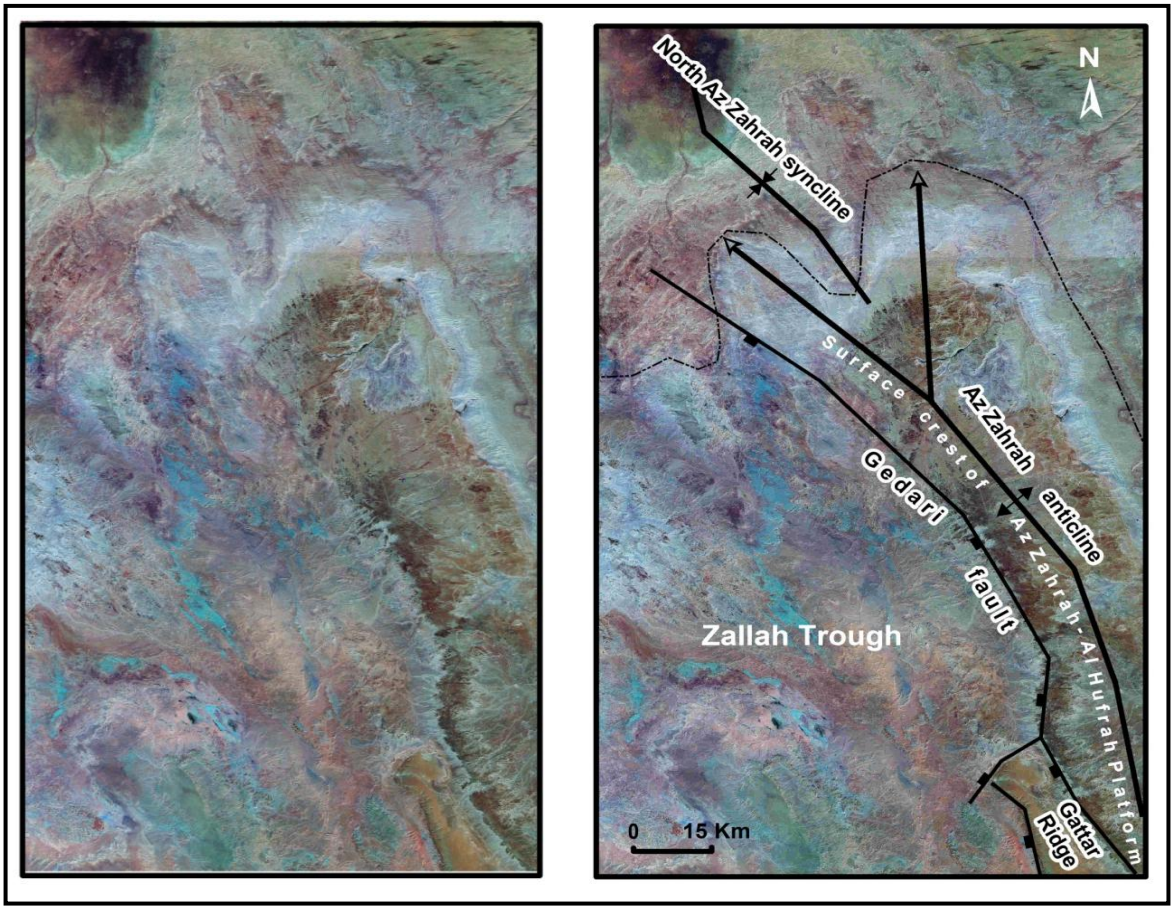


Fig. 4.21 Satellite (MrSid) imagery showing the northern end of Az Zahrah-Al Hufrah Platform which is marked by a two north-northwest plunging nose of large low-amplitude gentle flexures anticlines which are expressed by erosional features and surface geomorphology. For location see Fig. 4.5.

The southern end of the uplift has a convex morphology to the south and is characterised by a discrete fault bounded margin with downthrow to the southwest, south and southeast. The western boundary is marked by the eastern boundary fault of the Hun Graben (Fig. 4.12, and 4.14). The topographically highest point of the Waddan Uplift is located towards the southern end. This area characterised is by radial drainage although the crest of the structure is marked by NNW-SSE trending drainage divide, located some 20km east of the western faulted margin of the Waddan Uplift.

The internal structure of the Waddan Uplift is comparatively simple with a NNW-SSE trending trellised drainage pattern controlled by NNW-SSE trending, south-southwest

downthrowing normal faults (antithetic to the northeast to north-northeast drainage direction).

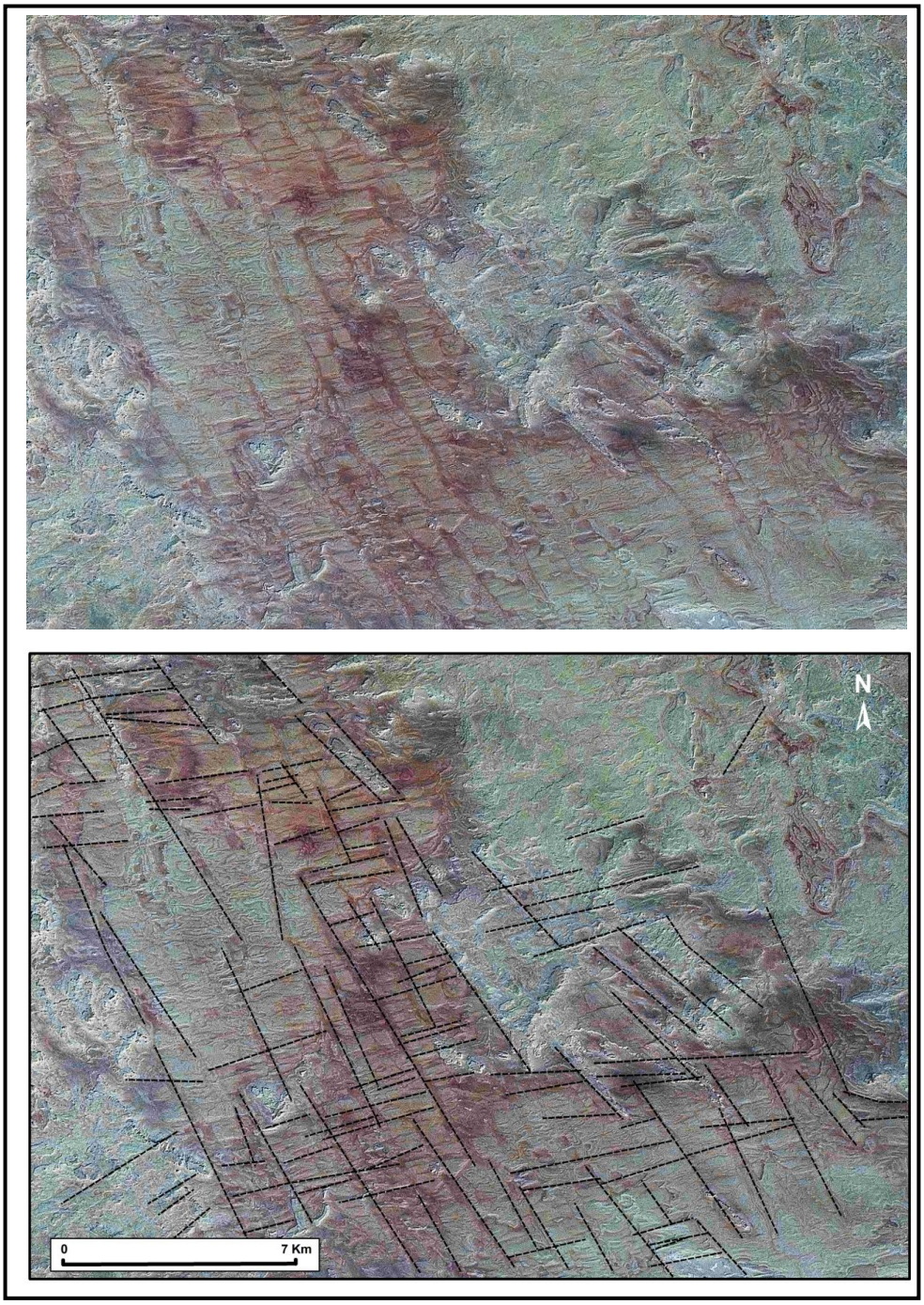


Fig. 4.22 Satellite (MrSid) imagery showing a combination of the NNW-SSE and ENE-WSW trending faults that impart a grid-like pattern that resembles crosscut fault structures at the northern end of Az Zahrah-Al Hufrah Platform. For location see Fig. 4.5.

The northern half of the platform (Fig. 4.6) is characterised by a north and north-northeast-trending dendritic drainage pattern down the sub-horizontal dip slope of the structure. A more organized trellis drainage pattern is developed towards the northern end of the structure parallel to the NNW-SSE and ENE-WSW trending fracture system.

Elongate erosional escarpments of more resistant lithologies and/or fault scarps (Fig. 4.24) may also control linear NNW-SSE trending Wadi channels. The southeastern part of the Waddan Uplift appears to be associated with a downthrown fault block which is defined by a broad low amplitude anticlinal structure developed in Wadi Thamat Formation.

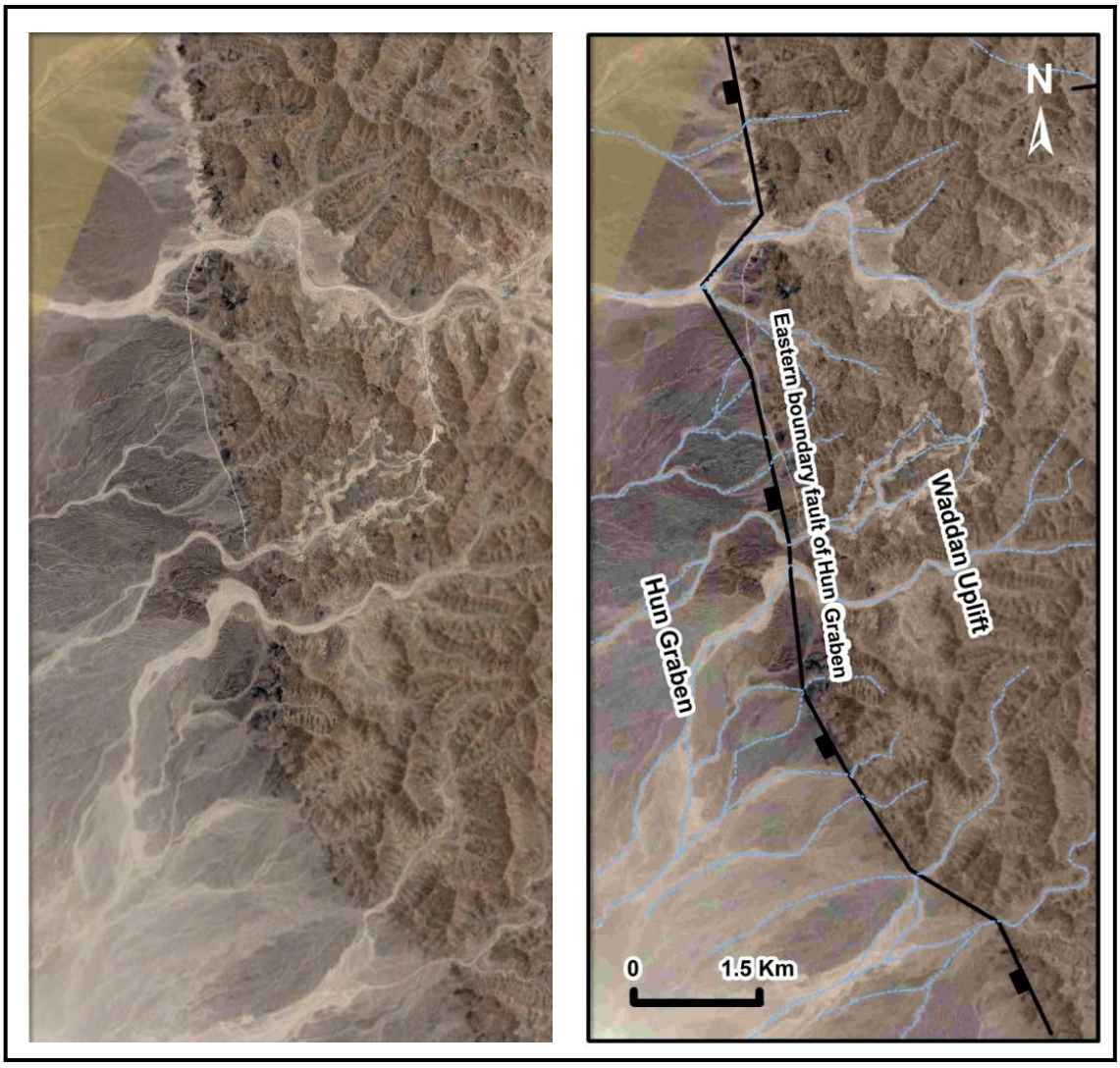


Fig. 4.23 Satellite (Google Earth) imagery showing wadis along the eastern margin of the Hun Graben are generally narrow and become incised as they approach the margin of the graben indicating that they have been rejuvenated by a relative drop in the surface elevation within the graben.

4.4.6 Gattar Ridge

The Gattar Ridge (Fig. 4.6) is coincident with a 15km wide, 120km long NNW-SSE trending northeast tilted panel of Al Jir Formation at surface. It appears as a terrace adjacent to the south western boundary fault of Az Zahrah-Al Hufrah Platform which projects into the eastern side of the Zallah Trough.

The western edge of the fault block is bounded by a fault zone up to 1km wide, consisting of overlapping parallel normal faults consistently downthrowing to the west. It is also characterized by segmented normal faults with relay ramp structures associated with horsetail splay faults that may indicate a component of sinistral strike-slip (Fig. 4.9).

The panel is bounded to the north-northwest by an ENE-WSW trending transverse fault. To the north-northwest the Gattar Ridge dies out into an area of close spaced faults with a NW-SE trend. The faults cross-cut Eocene-aged Wadi Thamat Formation, Oligocene-aged Ma´zul Ninah Formation and Late Tertiary-Quaternary deposits. The dominant fault trend is NNW-SSE and subsidiary E-W and NE-SW faults sets are also developed.

4.4.7 Maradah Trough

The Maradah Trough (Fig. 4.6) is located in the northeastern portion of the study area and is a deep, narrow, NW-SE-trending basin bounding the Az Zahrah-Al Hufrah Platform to the west and swings to a NNE trend around the southern termination of the Al Baydah Platform and then shallows rapidly to the southeast onto the Southern Shelf. In the north, the Maradah Trough narrows and shallows rapidly between the Az Zahrah-Al Hufrah Platform and the Shammar and An Nawfalfyah Highs. North of this it widens and deepens again towards the Sirt Gulf (Anketel 1996).

The dominant fault trend bounding the trough is NNW-SSE with subsidiary NNE-SSW trending consistent with the Kotlath Graben and the basin southern shelf towards the south (Fig. 2.4).

4.4.8 Al Hulayq Ridge

The Al Hulayq Ridge is a NNW-SSE trending narrow basement ridge or horst block which protrudes into the southern part of the Zallah Troughh (Fig. 4.1-4.4). The western margin of the high is structurally complex and associated with a series of drag folds developed within Paleocene-Eocene strata. The folds create hydrocarbon traps and may represent part of a flower structure which formed in response to dextral shear during the Oligocene (Knytl et al., 1996).

The surface structure appears to suggest that there is a lateral continuation of this feature northwards to the southern edge of the Waddan Uplift (Fig. 4.2). The Hakim and Fidda oil fields are on strike with the Al Hulayq Ridge, while two broad, low amplitude periclines at surface may be related to the reactivation of faults bounding the Al Hulayq Ridge. The fields are expessed at surface by periclines developed mainly in Eocene

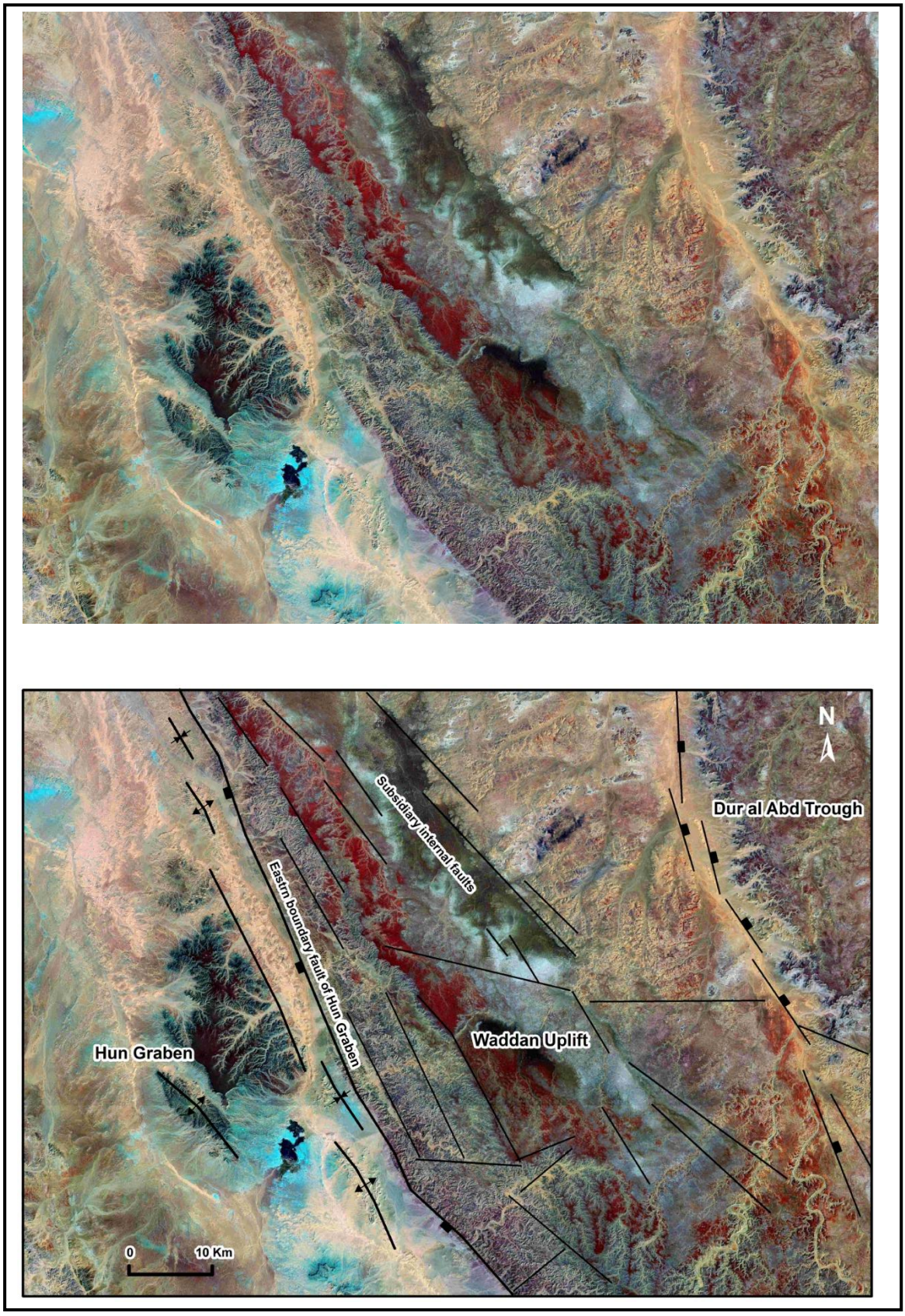


Fig. 4.24 Satellite (MrSid) imagery showing the shape of wadis (valleys) reflect the deflection of the drainage channels along the bedding contact between relatively hard and soft lithological units, at the central part of Waddan Uplift (For location see Fig. 4.5).

Wadi Thamat Formation. The Zallah fault system (See section 4.3.6) bounds the Al Hulayq Ridge on both sides from the Ar Ramlah Syncline to the east and the Maʻamir Graben to the west (Fig. 4.18). This fault system forms a series of NNW trending fault segments arranged as overlapping normal faults downthrowing to the SW, changing to NE throw when the fault bounds the Al Hulayq Ridge on the east side.

4.4.9 Al Qargaf Arch

The Al Qargaf Arch (Fig. 4.6) is an E-W trending Hercynian structure located on the southwestern edge of the study area and exposes Palaeozoic strata (outside of study area) onlapped by Oligocene cover rocks. Regionally the structure forms a WSW-ENE topographic high which separates the Murzuq and Ghadames Basins (Fig. 2.3).

The core of the structure is formed by Jabal Hasawnah which is elevated 800m a.s.l. The structural grain of the Al Qargaf Arch is dominated by ENE-WSW trending faults and resistant ridges (possibly silicified relict fault planes and/or igneous dykes). Subsidiary WNW-ESE to NW-SE and N-S trending faults possibly also occur.

4.5 Orientation analysis of the structural features

Orientation is considered to be one of the most revealing characteristics of linear features such as surface lineaments, fracture zones, surface fracture traces, and basement faults. Rose diagrams provide one of the most informative ways of representing orientation data (Drury, 2001, and Rajesh, 2004).

Direction statistics for all the interpreted linear features acquired in the study area were calculated and given as a total distribution and then the totals are broken down by the major basin elements of the area. Hundreds of lineaments were recognized. Their lengths, range between a hundred meters up to hundreds of kilometers long and the dominant trends are between N25W and N55W (Fig. 4.25) which coincides with Sirt Basin structures. The lengths were ignored in these rose diagrams where the longest lineaments are bounding the Hun Graben.

The rose diagrams were generated based mainly on total frequency. A majority of the surface linear features in the region from these rose diagrams have five preferred orientations: N25-35W in the Hun Graben, N40-50W in the Zallah Trough, N45-55W in the Dur al Abd Trough, N35-55W in the Az Zahrah-Al Hufrah Platform, and in contrast in the Waddan Uplift a N55-65E trend. In general the NW to NNW trends form a series of an elongate fault segments arranged as overlapping normal faults dipping to the SW, changing to NE dip where the faults are arranged in a closely spaced en

echelon pattern with NW-SE trend. These can measure up to 300 km long in the Hun Graben. This trend forms the dominant structural grain in the region and may reflect the regional structural styles of the study area and is in good agreement with the orientation of major tectonic elements of the Sirt Basin structures.

On the contrary, those surface linear features oriented northeast-southwest appear to be related to local geological structures which are less prevalent than those oriented northwest to southeast. In addition, ENE-WSW trending sets of faults are developed on both shoulders of the Hun Graben, orthogonal to the main structural grain. The faults clearly off-set NNW-SSE trending bounding faults and appears to post-date and off-set the NNW-SSE trending faults.

The Gedari fault system is one of which composed of two different trends where it changes from NNW-SSE trending to ENE-WSW trending, at 17°50', 29°05' (Fig. 4.6) before swinging directly north to follow the trend of an escarpment until 17°50' and 29°15'. Then it can be followed to 17°20', 29°45' where it branches to the northwest to link up with the northernmost faults of the Qarat Ash Shush fault system and then continuing beyond the Mabruk oilfield.

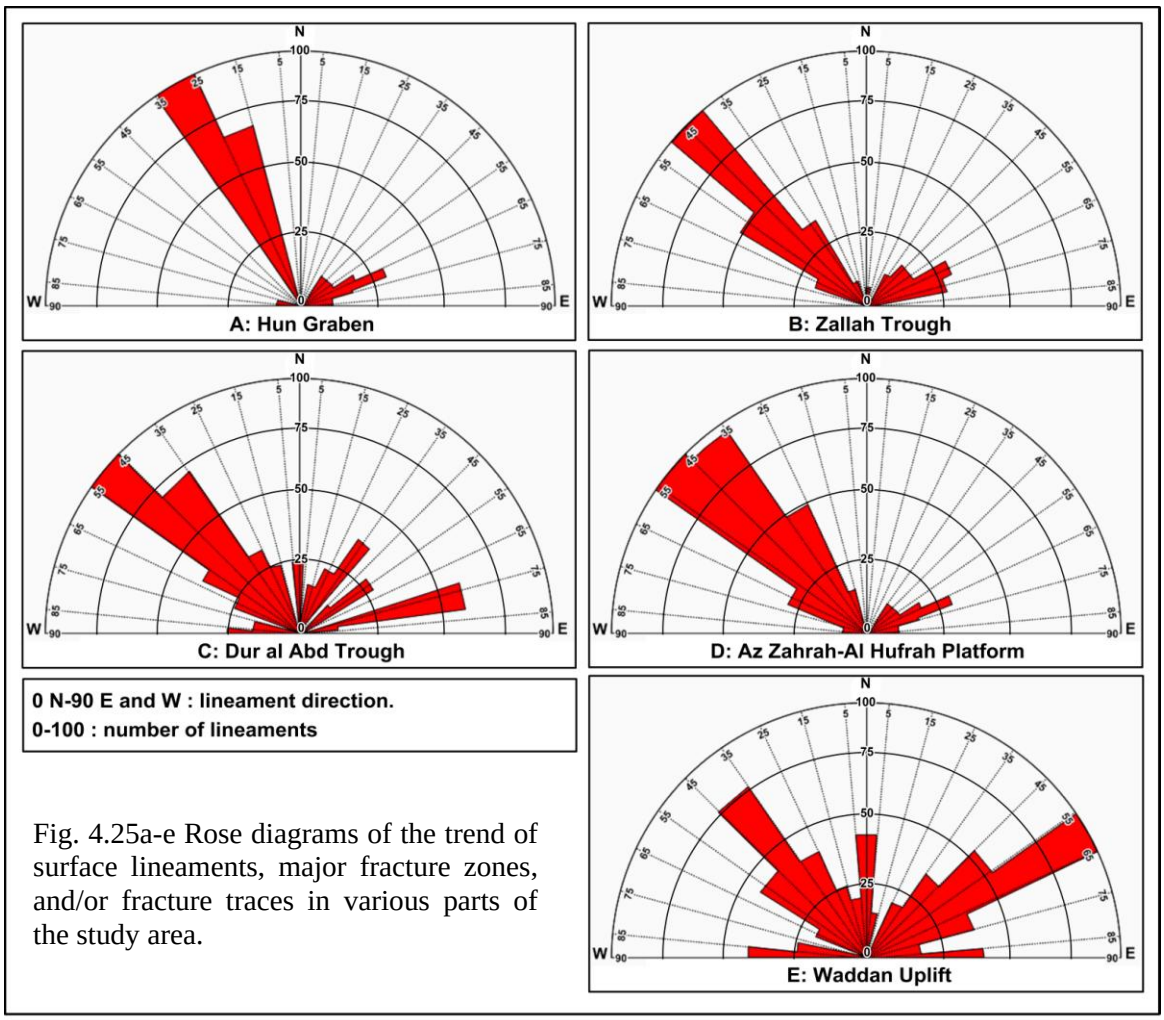


Fig. 4.25a-e Rose diagrams of the trend of surface lineaments, major fracture zones, and/or fracture traces in various parts of the study area.

A similar combination of NNW-SSE and ENE-WSW trending faults particularly in the northern part of Az Zahrah-Al Hufrah Platform imparts a grid-like pattern and may reflect conjugate fault structures.

It should be mentioned that some lineaments, mapped from the remote sensing data were not present in the geologic maps, which suggest that this image lineament interpretation provides new geologic perspectives even in an area which has been well mapped because of petroleum exploration. Some of the newly recognized lineament may be faults that were not previously mapped. It seems to be that the longest linear features in the study area were found on the western and eastern margins of the Hun Graben (Fig. 4.6, and 4.12).

4.6 Relative timing and age of the structures within the study area

The dominant structural features in the study area are:

- NNW-SSE trending extensional faults and associated monoclinal folds which form the dominant structural grain of the area. These structures are related to pre-Upper Cretaceous NE-SW extension possibly associated with local reactivation of existing Pan-African structures.

- ENE-WSW trending normal fault zones and associated monoclinal flexures clearly offset all Cretaceous age structures and may be related to Alpine deformation. They could also be influenced by reactivation of deeper Hercynian structures.

- NNW-SSE to NW-SE trending broad, low amplitude, periclinal folds and intervening anastomosing synclines are likely to be related to differential compaction above and adjacent to Cretaceous age structures.

- E-W trending normal faults were probably formed by Miocene deformation and reactivation of older Hercynian structures especially around the Al Qargaf Arch.

- NNW-SSE trending extensional faults of the Hun Graben associated with present day topographic and geomorphological expressions are at least Oligocene in age. The western boundary fault of the Hun Graben appears to cross-cut the E-W northern boundary fault of the Al Qargaf

Arch. Some ENE-WSW trending faults appear to off-set the bounding faults to the Hun Graben suggesting they developed during the Oligocene or during Alpine deformation.

All of these trends are associated with similar trending minor faults with no apparent sense of offset. All faults appear to be steep dipping and generally associated with normal displacement. Most normal faults show soft-domino linkage and hard linkage is not common. The western boundary fault of the Gattar Ridge may be associated with transtensional sinistral strike-slip, possibly related to reactivation of an originally Cretaceous age fault (Anketell and Kumati, 1991b).

4.7 Significance of surface structure features for petroleum exploration in the study area

It has been observed in this study on the basis of remote sensing interpretation that at least in some parts of the study area, oil and gas traps line up well with the trends of surface major structural features such as folds, lineaments, fracture zones, and/or fracture traces. As a result, surface structural features have been used to examine any relationship with the existence of explored oilfields in the study area.

Some of the existing oil and gas fields in the central part of Zallah Trough apparently are structures oriented in a northwest-southeast direction consistent with the trends of the Zallah fault system (Fig. 4.6) which is characterized by the existence of major oil fields (Fig. 3.8) that are located parallel to this fault system, e.g., the Hakim and Fidda oilfields, which are associated with a narrow NNW-SSE trending surface anticline expressed in Maradah Formation and Late Tertiary-Quaternary sediments (Fig. 1.3). The Hakim and Fidda structure is approximately 36.5 km long and approximately 4km wide exposed in the erosional core of the structure along strike with the Al Hulayq Ridge, while two broad, low amplitude periclines at surface may be related to the reactivation of faults bounding the Al Hulayq Ridge. The Ghani and Zenab fields are also located in the middle portion of this fault system in the vicinity of a NNW-SSE to NW-SE trending arcuate fault zone associated with normal downthrow to the west.

The Karim field is one of the largest in the study area. It is a NNW-SSE trending periclinal structure expressed at surface in Oligocene Ma´zul Ninah and Miocene Maradah Formations (Fig. 1.3). The structure has gentle plunge to the SSE and may be structurally closed at its northern end by NE-SW trending transverse faults associated with normal displacement. NW-SE trending normal faults cross the structure with downthrow dominantly to the southwest. The main axis of the structure is 38km long and its width is 24.5km at surface. A narrow NE-SW trending basaltic lava flow (Fig.

4.14) separates Aswad from the Zallah oilfields to the north and appears to occupy a palaeo-valley which is now topographically inverted. The NE-SW linear trend of the preserved flow may have been fault controlled.

The Aswad and Zallah fields (Fig. 3.9, and 4.6) are associated with a large subtle domal structure, 27km long by 22.5km wide expressed at surface within Ma´zul Ninah and Maradah Formations. The Ma´zul Ninah Formation is exposed in the eroded core of the structure (Fig. 1.3, and 4.6). The fold structure is bounded by a NNW-SSE trending fault on its eastern side with downthrow to the west. Similar trending normal faults occur near the crest of the structure.

The Mellugh, Ghani and Zenab fields (Fig. 3.9, and 4.6) are located in the vicinity of a NNW-SSE to NW-SE trending arcuate fault zone associated with normal downthrow to the west. The Daba, Gsur, Tagrifet and Facha fields are situated towards the northern end of the Zallah Trough on a NNW-SSE trend on the hangingwall side of the boundary fault of the Gattar Ridge. The area is also situated to the north of a synclinal area. Faults in the vicinity of the oil fields are downthrow to the northeast along the strike continuation of the eastern boundary faults of the Waddan Uplift.

The Mabruk field is considered to be the only field that lies within the Dur al Abd Trough with the Facha field on its faulted western flank on the Az Zahrah-A Hufrah Platform.

Additionally many major oil fields (Fig. 3.9) are located along the western crest of the Az Zahrah-Al Hufrah Platform such as the Bahi field which is situated in an erosional window developed above the structural crest of the Az Zahrah-Al Hufrah Platform, 4.5km east of the fault bounded western margin of the platform. The Az Zahrah oil field is situated within a NNW-SSE trending open syncline east of the monoclinal margin of the Az Zahrah-Al Hufrah Platform.

A number of NE-SW trending transverse faults occur in the area separating the Az Zahrah oil field from the Bahi field. The Al Hufrah oilfield is located to the east of the monoclinal margin of the Az Zahrah-Al Hufrah Platform in a similar structural position to the Az Zahrah field. A significant NE-SW trending, possibly fracture controlled, erosional window is present to the north of the field, and the Ali and Almas fields are located on the eastern edge of the study area. They are located on the gentle northeast dipping limb of the Az Zahrah-Al Hufrah Platform.

Fig. 3.9 and 4.6 show the distribution of the oil and gas fields in the study area and one can see from this interpreted satellite data that both the geometry of individual oilfields and the relative locations of most oilfields clearly follow the trends of the surface

lineaments in the area. The consistency in orientation and the association in position between the surface structural features and the oilfields make it very attractive to use surface structural features as a guide for delineating new oil and gas traps in the study area.

Based on the above observations, it is reasonable to conclude that any potential new oil and gas reservoirs in the remaining parts of the study area, if they exist, will be likely associated with the surface structural features and fracture traces in the region. Therefore, surface structural features and fracture analysis should be employed as a cost effective tool for delineating preliminary locations for more sophisticated and more expensive geophysical and/or geochemical surveys in the study area.

4.8 Summary

The main objective of conducting a remote sensing interpretation was to identify faults and fractures as well as major stratigraphic boundaries and use these mapped features along with geological and geophysical data to provide a more comprehensive analysis of the area.

The study area is highly faulted, with a complex geological pattern, bounded to the west by a portion of the Hun Graben and containing prominent geological features of the Sirt Basin. The faulting style exhibited in this region is that of normal and strike-slip faulting with a general NW to NNW trend. It is also characterized by segmented normal faults with relay ramp structures associated with horsetail splay faults that may ALSO indicate a component of sinistral strike-slip deformation has occurred. In general the NW to NNW trending faults form a series of an elongate segments arranged as overlapping normal faults dipping to the SW, changing to NW dip where the faults are arranged in a closely spaced en echelon pattern with a NW-SE trend.

In the hangingwalls to the major faults, beds are gently inclined and warped forming synclines that trend parallel to sub-parallel to the main faults. These numerous elongate asymmetric synclines associated with shallow west limbs and steeper dipping east limbs are predominantldeveloped in the hangingwall adjacent to west downthrowing normal faults along the eastern fault bounded margin of the Gedari fault system and the Gattar Ridge.

The main basin (trough) boundaries of the study area are :- 1) the Gedari Fault system located along the eastern boundary separating the Az Zahrah-Al Hufrah Platform from the Gattar Ridge; 2) the Western boundary represented by Hun Graben Fault system; 3)

the East Waddan Uplift fault system along the eastern margin of the Waddan Uplift; 4) the Qarat Ash Shush fault system; 5) the Ar Raquba fault system, and 6) the Zallah fault system, which together divide the main trough into a number of sub-blocks.

Segmentation of the Gedari fault system has resulted in the development of relay ramps between overlapping fault tips at the southeast part of the study area. These relay ramps are arranged as right lateral stepping faults dipping to the NW in the extreme south and to NNW when they swing to ENE-WSW.

The satellite image interpretation integrated with the surface geological maps shows that the study area contains several basinal and geotectonic elements; namely, the Zallah, Dur al Abd, Maradah, Hun Graben, the Waddan Uplift, Gattar Ridge, the Az Zahrah-Al Hufrah Platforms, the Al Qargaf Arch, and the intrabasinal Al Hulayq Ridge. Moreover the Zallah Trough is divided into a number of sub-basins: the Facha Graben, Ar Ramlah Syncline, Zallah Sub-basin and Ma‘amir Graben.

Rose diagrams reveal that the majority of the surface linear features in the region have five preferred orientations: N25-35W in the Hun Graben, N40-50W in the Zallah Trough, N45-55W in the Dur al Abd Trough, N35-55W in the Az Zahrah-Al Hufrah Platform, and in contrast in the Waddan Uplift a N55-65E trend.

According to satellite interpretation most of the subtle low amplitude periclinal structures which are exposed at surface coincide with producing oil fields. It has been observed in this study on the basis of remote sensing interpretation that at least in some parts of the study area, oil and gas traps line up well with the trends of surface major structural features such as folds, lineaments, fracture zones, and/or fracture traces.

It should be mentioned that some lineaments, mapped from the remote sensing data were not present in the geologic maps, which suggest that this interpretation provides new geologic perspectives even in an area which has been well mapped during the ongoing petroleum exploration.

CHAPTER 5: SUBSURFACE (BOREHOLE DATA) ANALYSIS

5.1 Introduction

In this chapter, an analysis of borehole data from the numerous wells that have been drilled in the study area (Libyan Petroleum Institute database) is presented. The aim is to supplement the surface interpretations (presented in Chapter 4) with constraints from the subsurface.

This subsurface information is presented in the form of geological cross sections and maps that show the distribution of stratigraphic layers, their thickness variations, and their attitudes (structure). Thickness ("isopach") maps were considered as horizontal stratigraphic layers although one of the common sources of errors in subsurface isopach maps is the too great apparent stratigraphic interval caused by steeply dipping strata at the point where the well is drilled. These maps were constructed by subtracting the depth in a hole of the top of a rock layer from the depth of the base of the layer. The value is again plotted on a map along with thickness calculations of the particular layer from all other wells in the area, and the data are contoured. An isopach map is very important in the determination of the tectonic framework or the structural relationship that is responsible for a particular type of sediment accumulation. This implies that the shape of a basin, the position of the shoreline, areas of uplift, and under some circumstances the amount of vertical uplift and erosion can be recognized by mapping the variations in thickness of a given stratigraphic interval (Bishop, 1960).

Geographical Information Software (GIS) was used to co-locate thematic layers and form the basis for construction of geological structure maps for detailed analysis of the structural features. This has enabled a coherent view of the relationship between the surface structural features, seen mainly in the horizontal plane (satellite imagery), and subsurface features seen mainly in the vertical plane (well data).

The subsurface stratigraphy of the Sirt Basin (Fig. 2.8) has been the subject of many publications and summary volumes (e.g., Barr and Weegar, 1972; Megerisi and Mamgain, 1980; Banerjee, 1980; Anketell and Kumati, 1991a; Gumati and Kanes, 1985 and Bezan, 1996). The Barr and Weegar (1972) stratigraphic nomenclature has essentially been adopted in the present study with minor modifications by Gumati and Kanes (1985) and Schroter (1996).

On the basis of the borehole data, the subsurface stratigraphic succession comprises a

variety of lithologies ranging from Pre-Cambrian crystalline basement to recent sedimentary rocks. Total sedimentary thickness exceeds 3000 m (9843') and is mostly beds of Cretaceous and Cenozoic age in the deepest parts of the troughs, diminishing to 1200 m (3937') on the regional highs (Fig. 5.1). The sedimentary lithologies are extremely variable, reflecting the complex tectonic and structural evolution of the Sirt Basin.

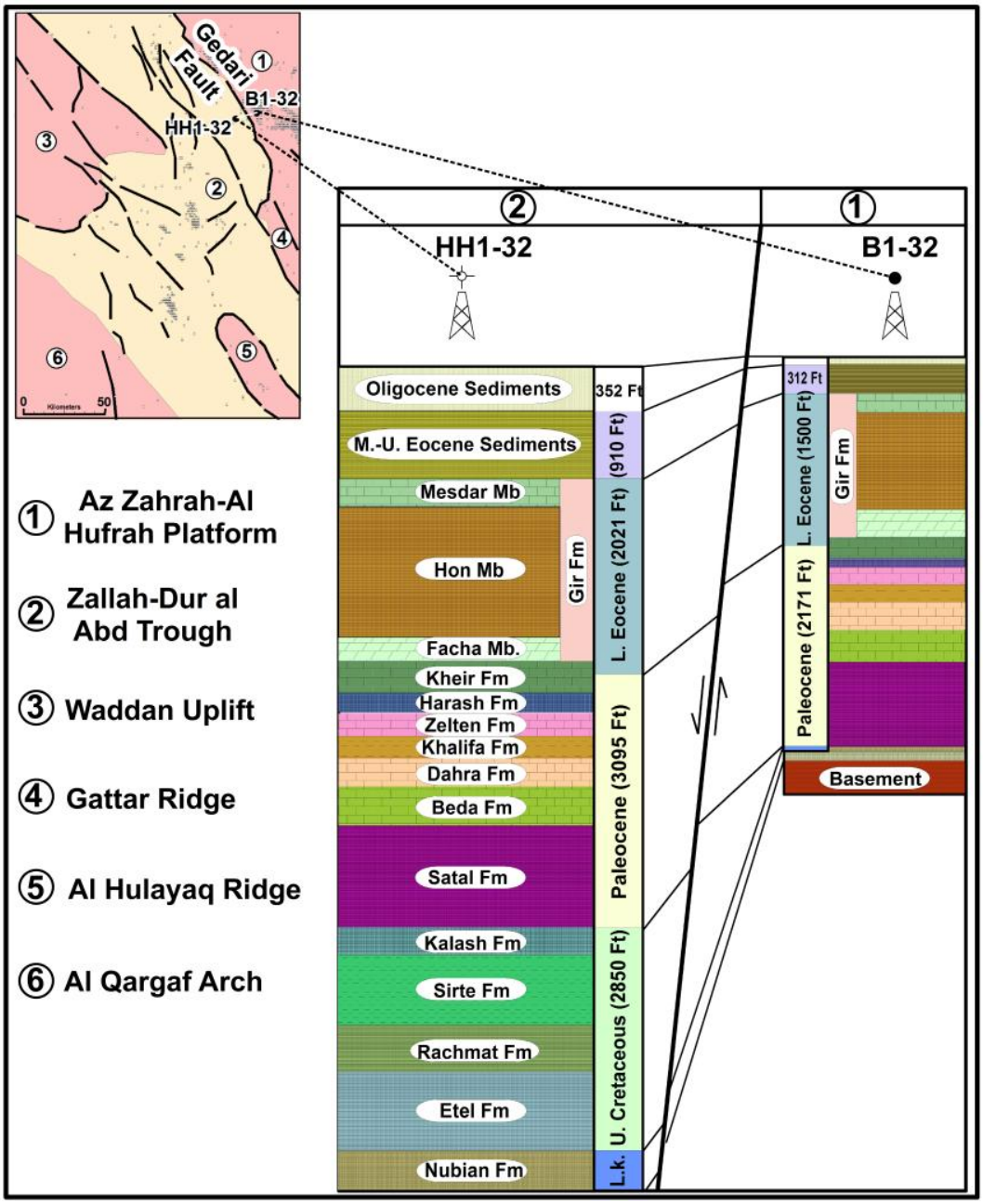


Fig. 5.1 A stratigraphic comparison between two wells drilled on both sides of the Gedari fault showing significant differences in the stratigraphic record correspond to differences in subsidence on the opposite sides of the fault. Inset shows location of the two wells with respect to Gedari fault.

Several important breaks in sedimentation, related to episodes of tilting and faulting with subsequent erosion and deposition, occur within the succession (Kumati, 1981) as

shown in the stratigraphic succession of Fig. 2.8 and 5.1.

5.2 Contour maps interpretation

5.2.1 Basement map

A contour map of the top of the basement in the study area (Fig. 5.2) constructed from drillhole data (variations in elevation on the basement relative to sea level) shows the general present day basement surface configuration as well as several major and minor structural features. Understanding the spatial distribution of present day basement surface configuration helps to delineate basin depth and shape and is one of the important tools for petroleum exploration.

Fig. (5.2) shows that the study area basement is steepening rapidly from about 584 m (1916') b.s,l. in the south eastern part on Al Qargaf Arch to more than 2914 m (9559') in well H1-32 in Central Zallah Trough. For rocks forming the basement age see chapter 2, section 2.4.2.

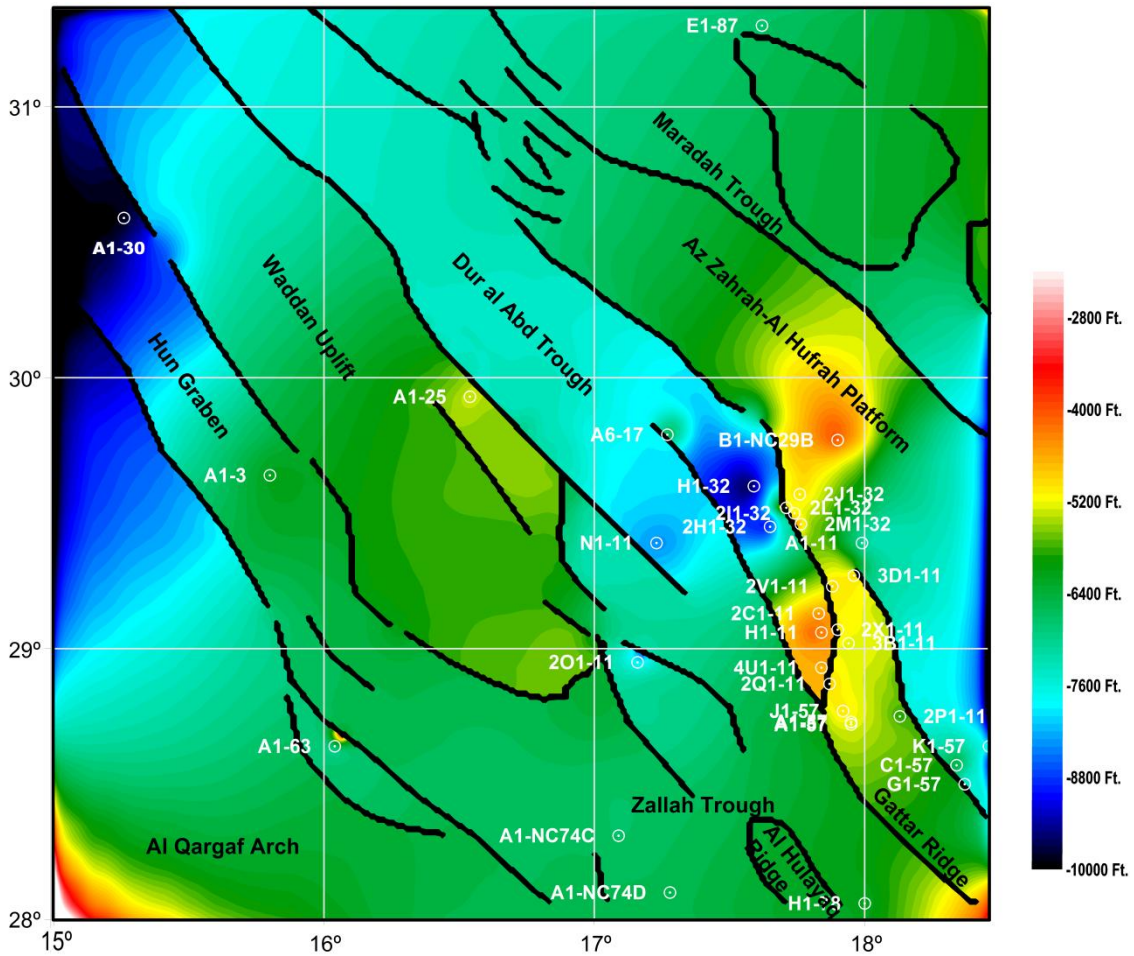


Fig. 5.2 Contour map of top basement for the study area (constructed from drill hole data (variations in elevation on the basement relative to sea level).

Hun Graben contains about 1463 m (4800') of sediment, where the depth to basement varies from -1886 m (-6189') (well A1-3) to -3010 m (-9876') (well A1-30) with its surface dipping towards the northeast (Fig. 5.2), a feature that may partly be inherited from the northeastern flank of the Ghadamis Basin. Hallet and El-Ghoul, 1996 pointed out that the maximum downthrow on the western faults is in the order of 500 m (1640') whereas on the eastern flank faults downthrow on the order of 2000 m (6561').

Basement underlies the Waddan Uplift at a depth of only -1402 m (-4600') west of the Zallah Trough, (Fig. 5.2) however the platform is tilted towards the northeast, which means that the depth to basement adjacent to the Dur al Abd Trough is -2250 m (-8367') in well N1-11. As in the Hun Graben, the depth to basement in the northeastern portion of the Zallah Trough adjacent to the Az Zahrah-Al Hufrah Platform along to the Gedari fault is -2914 m (-9559') in well H1-32 suggesting the deepest of the rifted area in the present day. The shallowest depth to basement occurs mainly over Az Zahrah-Al Hufrah Platform ranging in depth between -1317 m. (-4320') (well A1-11) in Al Hufrah oil field located in the centre of the area to about -1510 m (-4953') (well 2X1-11) towards the south and southeast where the most produced oil fields are located.

5.2.2 Lower Cretaceous thickness map

Based on the well data, isopach and structural contour maps have been constructed for the study area (Figs 5.3 A & B to 5.6 A & B). The oldest basin-fill comprises (Fig. 2.8 and 5.4 A & B) very thin pre-Cretaceous (Triassic?) sandstones, overlain by unsilicified Lower Cretaceous sandstones with varying in thickness from troughs to the platforms (see Chapter 2).

The isopach map (Fig. 5.3A & B) shows the thickness distribution of the Lower Cretaceous sediments, which ranges from 0 to 1152' (351m). This map is based on a limited number of data because most of the studied wells did not drill complete sections. Nevertheless, the map reflects the effect of the underlying palaeotopography. Over the Zallah Trough, the Lower Cretaceous sediments are thicker and attain a maximum thickness at N1-11, G1-44, and A1-NC74D wells (see Fig. 5.3 A for well location). This is indicated by a narrow band of isopach contours trending northeast-southwest, from the central part of the map to the southwest reflecting the presence of a regional syn-sedimentary fault affecting the Lower Cretaceous and older sediments with down to the basin throw. This shows the area most likely to contain the optimum thickness of Lower Cretaceous sediments thickness.

The thickness of the Lower Cretaceous sediments decreases rapidly over the most of the

area in some portions to nil whilst reaching a minimum thickness of 4.9' (1.5m) in the east at V1a-11, on the western Az Zahrah Platform. In the SE of the Dur al Abd Trough, where the Mabruk field is located, the thickness of the Lower Cretaceous Nubian Sandstone (Fig. 5.3A & B) does not exceed 30.5 m (100') (wells A6-17 and G1-17). Lower Cretaceous sediments (Fig. 5.3A & B) are mainly deposited in the structural lows of the Waddan Uplift and attain a maximum thickness at well A1-44 (43 m [140']) on the highest elevation to the south.

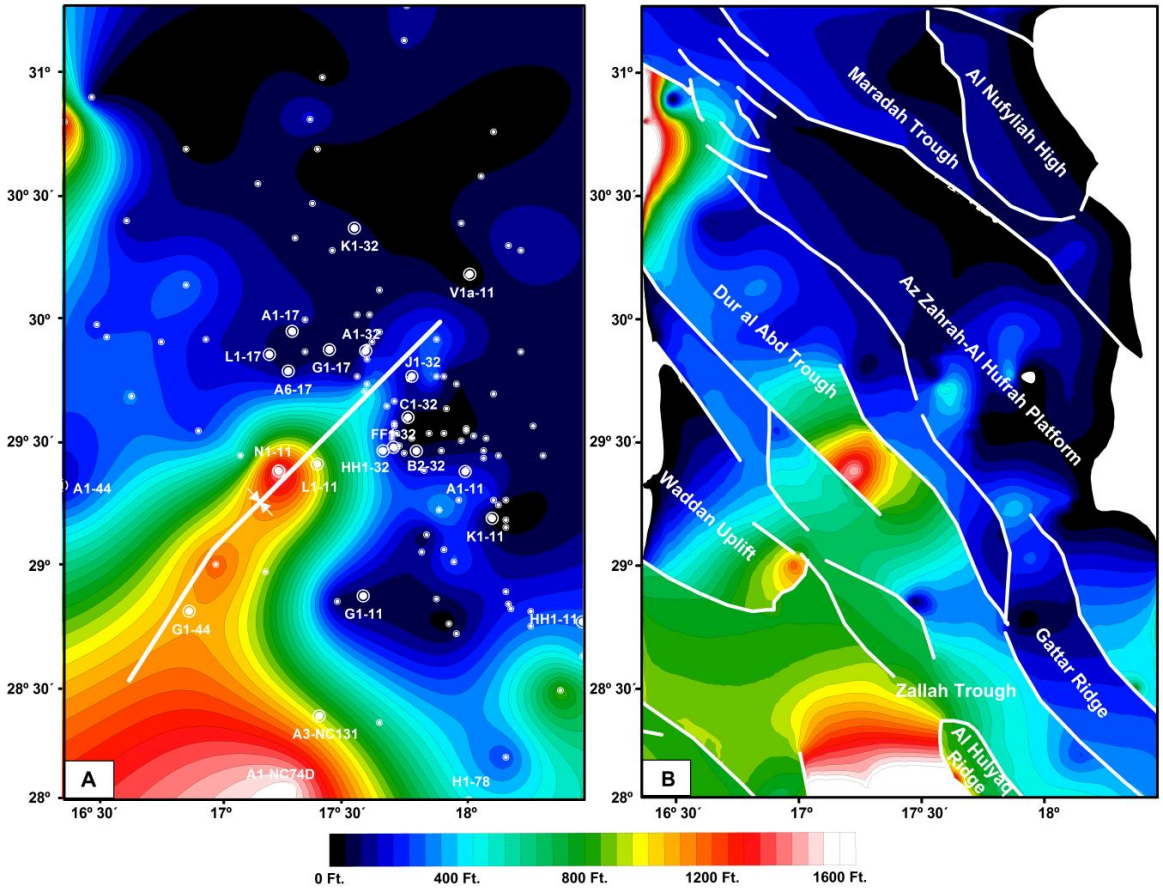


Fig. 5.3 Isopach and structural thickness map of Lower Cretaceous time for the study area. Left hand images represent the thickness maps and white bold line appears as synclines represent the thickest trend in the area during that time. Right hand images represent the thickness maps integrated with main tectonic elements of the Sirt Basin and the white bold lines represent the major faults (after Mouzughi, and Taleb1981).

5.2.3 Upper Cretaceous thickness map

In contrast to the Lower Cretaceous sediments, the isopach distribution map of the Upper Cretaceous sediments shows a well developed Upper Cretaceous section (Fig. 5.4A & B) overlying the Lower Cretaceous sediments reaching 1263 m (4143') (Well A3-NC131) thickness at the Karim oil field in the centre of the basin compared with less than 91 m (300') (wells J1-32, K1-32, B2-32 and C1-32) on the adjacent Az Zahrah-Al Hufrah Platform. The sequence includes Bahi clastics, Lidam and Argub carbonates, Sirt shales and Kalash carbonates (See Chapter 2).

Upper Cretaceous sediments (Fig. 5.4A & B) in Dur al Abd Trough range in thickness from 488 m (1601') at well A6-17, and less than 411 m (1348') at well A1-17 to the central portion of the trough. Upper Cretaceous sediments over the Waddan Uplift (Fig. 5.4A & B) ranging between 373 m (1225') thick (well C1-39) towards the northwest and 299 m (980') (well A1-44) on the highest elevation to the south.

Over the Az Zahrah-Al Hufrah Platform, the thickness of the Upper Cretaceous (Fig. 5.4A & B) is about 331 m (1087') (well A1-32) with a depth to the top-Cretaceous about -1144 m (-3753') north of the platform and about 353 m (1158') (well HH1-11) at a depth of about -1928 m (-6324') further south. In contrast the Upper Cretaceous does not exceed 61 m (200') at a depth of about -1144 m (-3753') on the central western margin near the Az Zahrah field. The major oil fields of the area are located here at the highest and updipping part of the crest towards the western margin of the platform.

The Upper Cretaceous thickness map also shows evidence for emergent areas in the central portion of the platform from west to east including the Gattar Ridge and the Az Zahrah-Al Hufrah Platform indicating a palaetopographic high, when the U. Cretaceous sediments have either been eroded or not deposited at the G1-11, K1-11, and A1-11 wells. These were identified by Roohi (1991b) and he suggested that they formed a large irregular-shaped island, surrounded by marine conditions to both the north and south (Fig. 5.4A & B) and since Danian times the palaaotopographic high has been tilted ENE indicated by its subsidence about 610 m (2000') lower than the Az Zahrah field.

It is evident that most of this tilt was imposed during the Late Eocene-Oligocene tectonic disturbance, and was accompanied by extensive faulting and fracturing (Roohi 1996b). This late movement has had a controlling effect on the migration of hydrocarbons on the platform.

5.2.4 Paleocene thickness map

The Paleocene was a period of thermal subsidence with minor reactivation or rejuvenation of tectonic activity on faults formed during the post Cretaceous. The rift topography was gradually infilled and covered by sedimentation. A thick Paleocene section (Fig. 5.5A & B) is present in the Zallah Trough reaching a thickness of 943 m (3095') in Well HH1-32 located in the east of the basin on the boundary with Az Zahrah-Al Hufrah Platform. The sequence comprises mainly carbonates and evaporates (see Chapter 2).

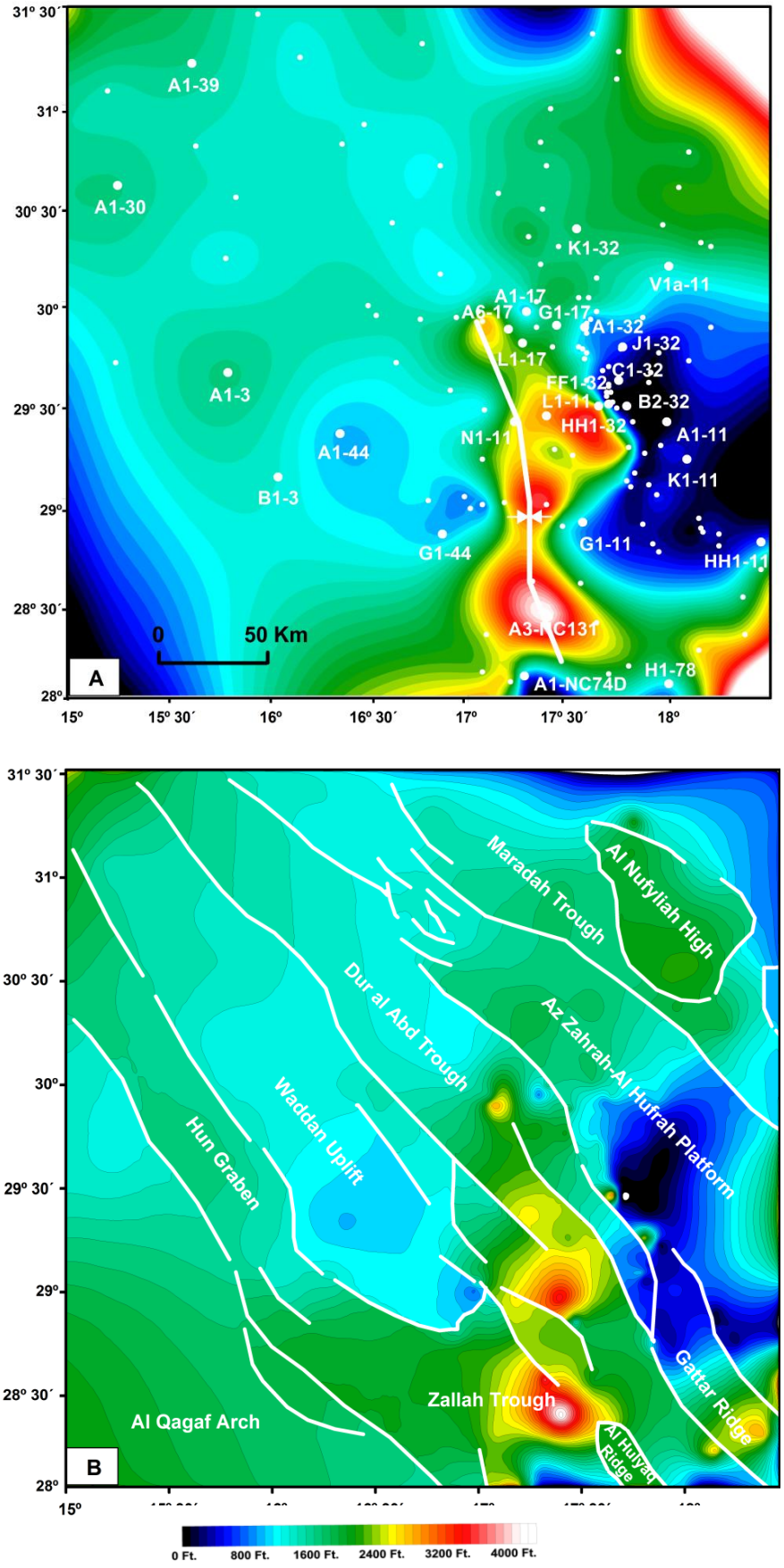


Fig. 5.4 Isopach and structural thickness map of Upper Cretaceous time for the study area. Left hand images represent the thickness maps and white bold line appears as synclines represent the thickest trend in the area during that time. Right hand images represent the thickness maps integrated with main tectonic elements of the Sirt Basin and the white bold lines represent the major faults (after Mouzughi, and Taleb1981).

In the southeastern Dur al Abd Trough in the Mabruk field, the thickness of Paleocene sediments (Fig. 5.5A & B) ranges between 823-869 m (2700-2850') (wells L1-17 and A1-17) and the depth to top Paleocene is -457 to -610 m (-1500 to -2000'). The Paleocene section in the Hun Graben (Fig. 5.5A & B) includes 67.5 m (251') carbonates (well A1-3) and 89 m (293') (well B1-3) to the south which is overlain by almost 610 m (2000') of Eocene and Oligocene dolomites, gypsum, anhydrites and shale. Over the Waddan Uplift, Paleocene sediments (Fig. 5.5A & B) range in thickness between 334 m (767') (well C1-39) and 404 m (1327') (well A1-44) indicating the area during Pre-Paleocene was tilted to the SE.

The whole Az Zahrah-Al Hufrah Platform was submerged during the Late Maas-trichtian and sedimentation continued through the Paleocene stage (Fig. 5.5A & B) and thick sequences of more shallow marine carbonates, shales and evaporites were deposited in this region. The total thickness of the Paleocene sediments appear to be homogeneous and ranging between 646 m (2121'), at well K1-32 north, 669 m (2196') at well B2-32 central and 764 m (2508') at well HH1-11to the south of the platform.

5.2.5 Eocene thickness map

During the Late Paleocene, basin architecture was modified by a renewed period of rifting indicated by formation of an extensive evaporite basin over 1432 m (4697') thick at well G1-NC74B developed in the southern part of the Zallah Trough during the Eocene (Fig. 5.6A & B). The sequence is dominated by the Hon Member of the Gir Formation in several wells. The evaporites form a seal for the underlying Facha Dolomite Member, which is the principal reservoir of the Zallah, Aswad, Fiddah, Hakim, and Adh Dhi'b fields and is also productive at the Al Ghani field (Hallet and Ghoul, 1996).

The Eocene sediments in Hun Graben range in thickness (Fig. 5.6A & B) between approximately 580 m (1904') to the north (well A1-30), and 636 m (2085') in the centre (well A1-3) and about 658 m (2159') (well B1-3) to the south. In the Dur al Abd Trough the Eocene evaporites (Fig. 5.6A & B) are reduced to a few stringers of anhydrite and are thus unlikely to form an effective seal for the underlying reservoirs with a sediment thickness ranging between 366-427 m (1200-1400') (wells L1-17 and A1-17). The tilting appears to have mostly applicable to the Eocene section in Waddan Uplift (Fig. 5.6A & B) which is thin or absent to the north but reaches a thickness of about 319 m (1048') (well A1-44) on the highest elevation to the south.

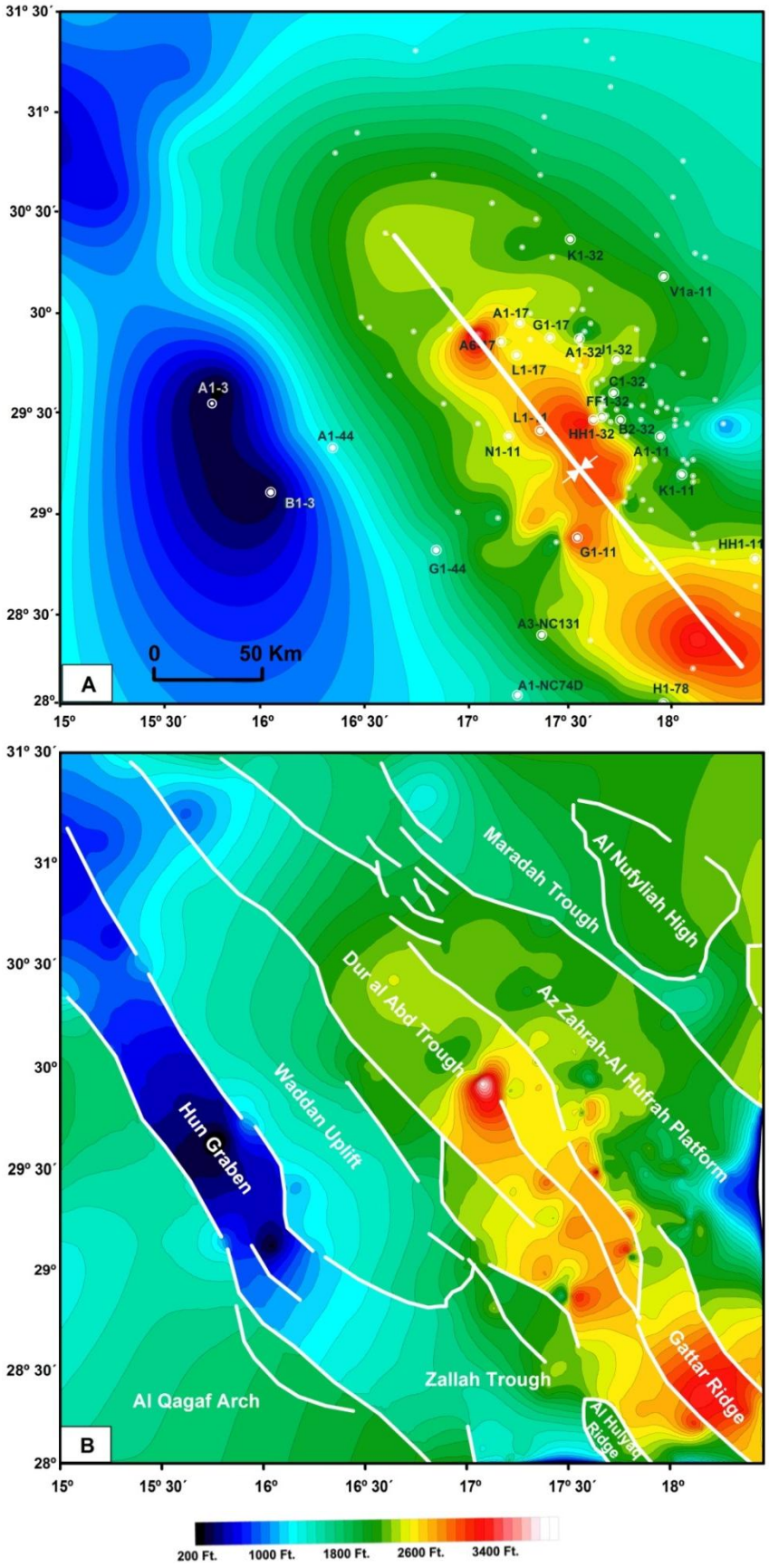


Fig. 5.5 Isopach and structural thickness map of Paleocene time for the study area. Left hand images represent the thickness maps and white bold line appears as synclines represent the thickest trend in the area during that time. Right hand images represent the thickness maps integrated with main tectonic elements of the Sirt Basin and the white bold lines represent the major faults (after Mouzughi, and Taleb1981).

The submerging of Az Zahrah-Al Hufrah Platform during the Eocene led to the deposition of thick sequences of evaporites, more shallow marine carbonates, and shales (Fig. 5.6A & B). The total thickness of the Eocene sediments appear to gradually increase in thickness from north to south as shown at well K1-32 north, approximately 563 m (1846'), well B2-32 approximately 584 m (1917') and HH1-11 approximately 642 m (2107') to the south of the platform.

5.2.6 Oligocene-Miocene sediments

The Oligocene and Miocene rocks are too shallow to be of interest in this area, compared with the older rock units and not considered in the well data available in this study.

5.2.7 Cross section constructed from well data

Fig. 5.7 shows a geological cross section (shown here in depth per foot) made from borehole data across the study area in the trend of the NE–SW in dip direction in order to image the structures clearly and provide an understanding of the geological history of this part of the Sirt Basin. It comprised from 13 wells from well A1-40 at the Tripoli-Tibesti Uplift to the southwest to well A1a-NC29A on the Maradah Trough to the east. Probable major faults (block boundary faults) that separate the regional structural elements of the study area such as the Waddan Uplift, Dur al Abd Trough, Zallah Trough and Az Zahrah-Al Hufrah Platform have been identified.

The section is dominated by thick sediments (U. Cretaceous, Paleocene, and L. Eocene) that are almost present in the graben and trough area but have been broken and moved up and down by many near-vertical faults which seem to be extended into the basement.

The structural interpretation of this section indicates extensional tectonic events affecting the Upper Cretaceous sediments as outlined by grabens and tilted troughs, controlling thickness variations of these sediments. One can note that many major faults bounding the major structural elements shown on this show successive movements expressed by thickness variations with a slip movements affecting the all the stragraphic section from basement to surface as a vertical slip normal faults.

The thickness and subsidence variations suggest several important pulses in tectonic activity resulted in fault movements and basin rifting. During the Pre-Cretaceous time, and being structurally controlled from the east by the hinge fault zone west of Az Zahrah-Al Hufrah Platform (Gedari fault) which seems to be the master fault in the study area where the stratigraphic layers are thicken adjacent this to fault.

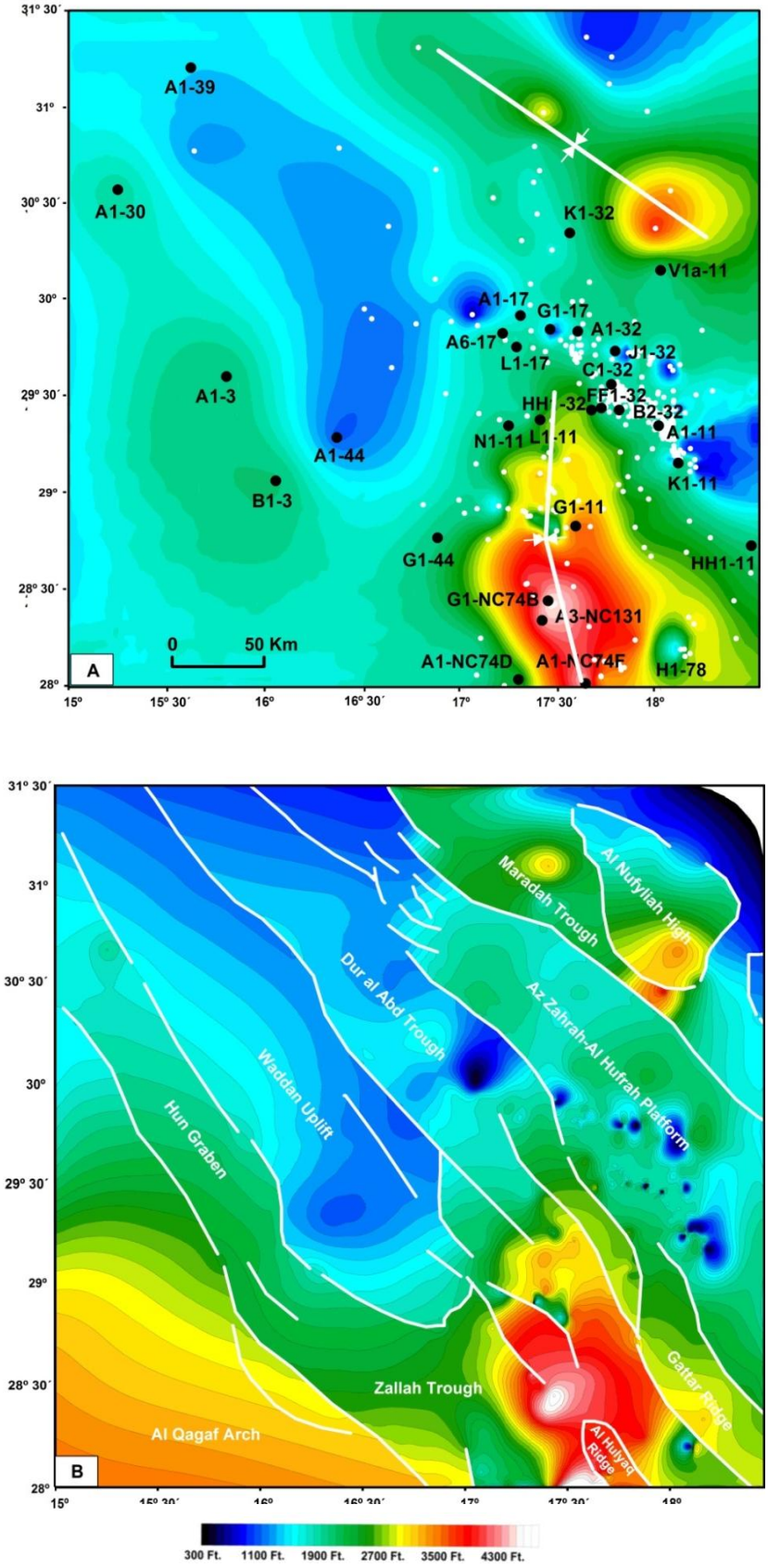


Fig. 5.6 Isopach and structural thickness map of Eocene time for the study area. Left hand images represent the thickness maps and white bold line appears as synclines represent the thickest trend in the area during that time. Right hand images represent the thickness maps integrated with main tectonic elements of the Sirt Basin and the white bold lines represent the major faults (after Mouzughi, and Taleb1981).

Due to down-faulting, the deepest part of the Zallah Trough lies on the NE side of the axial towards the southwestern Az Zahrah-Al Hufrah Platform, with the Gattar Ridge recognized. It is more defined and marked by a two major fault scarps which coincide with a normal fault zone defining the western edge of the Gattar Ridge as SW fringe of Az Zahrah-Al Hufrah Platform.

The Gedari fault which downfaulting to the WSW is vertically displace extends along the whole sedimentary sequence of the study area since Upper Cretaceous till Eocene. The maximum downthrow of the SW block with respect to the NE block is more than 1000 m (Vesely, 1985). Whilst the fault which separates Zallah Trough from Waddan Uplift to the dominated by a major NNW-SSE trending normal western fault system which comprises several faults that show downthrows to the east, of the order of 300 to 500 m (Vesely, 1985).

The sedimentary section overlying Cambro-Ordovician and occasionally the Precambrian basement complex which considered as the first syn-rift sediment in the area is unsilicified Nubian Sandstones of Lower Cretaceous age (Fig. 5.7) varies considerably both in thickness and lithology in the Western Sirt Basin. The Waddan Uplift has a convex morphology and is characterised by a discrete fault bounded margin with downthrow to the east, represent the highest topographical point in this section (610 m [2000'] a.s.l). To the west of this cross section the Hun Graben forms a present day fault bounded depression indicating that it is one of the youngest tectonic elements in the region although the development of the Hun Graben, however, is controversial.

5.3 Rifting phases

In total, we recognize six lithostratigraphic sequences (phases) in the area's stratigraphic framework. The thickness ("isopach") maps (Figs 5.3A&B to 5.6 A&B) display trends of thickening and thinning of each layer and, thus, indicates the locations of possible major structural and stratigraphic trap trends.

5.3.1 Pre-rift (Pre-Cretaceous) phase

The study area pre-graben (pre-rift) initiation stage and its sedimentary products are of a varied character since this is a category of convenience to include all tectonic and sedimentary activity preceding the Cretaceous time (well B1-32, Fig. 5.1). Sediments of this pre-rift phase actually include many phases that are quite unrelated to Sirt Basin rifting. These include the earliest sequence that contains mainly localized Gargaf Formation sediments of Cambro-Ordovician Quartzite as well as younger Palaeozoic

sandstones and Early Mesozoic sandstones deposited prior to the formation of the Sir Arch (El-Hawat et al, 1996). The timing of this uplift that created the Sirt Arch is debatable; historically it is considered to be a mid-Paleozoic event, but it could have formed in the Mesozoic preceding an Early Cretaceous rifting event Bellini and Massa, 1980; Van Houten, 1980; Anketell, 1996).

5.3.2 Graben-fill phases

The graben-fill stage has been divided into four structurally active and structurally inactive periods to better reflect local structural history. These four cycles are shown in section view in Fig. 5.8 and map view in Fig. 5.3A & B to 5.6A & B. Syn-rift faulting commenced in the Early Cretaceous followed by Late Cretaceous marine siliciclastics, shales, and carbonate rocks, overlain by Paleocene-Eocene carbonate and evaporite strata and then terminal continental siliciclastics strata representing the post-rift stage of the development of the area assigned to post-Eocene time.

5.3.3 Rift initiation (Early Cretaceous) phase

The thickness of the Lower Cretaceous sediments (Fig. 5.3A & B) increased abruptly in the central and southwest part of the Zallah Trough, the northwestern part of Dur al Abd Trough, and southeastern part of the Waddan Uplift which suggests rapid subsidence caused by the initial activation of the faults at the time of deposition. In the other words the thickness of the Lower Cretaceous sediments decreases rapidly over the rest of the area, reaching its minimum thickness of 1.7 m (5') in the east at V1a-11 well. Generally the pre-Upper Cretaceous isopach map demonstrates the presence of three depocentres developed in the hanging wall of major extensional faults (Fig. 5.3A & B). In the Zallah and Dur al Abd Troughs two of the depocentres are dissected by the overlap of the normal faults. The third of these depocentres is now inverted and corresponds to the southern portion of the Waddan Uplift shown on thickness map. Further to the east, the Gedari fault seems to have been inactive during this period as indicated by little change in the thickness of pre-Upper Cretaceous sediments.

The thin or absent Lower Cretaceous sediments which are preserved in the present day topographic lows resulted from a non-tectonic origin on the present Az Zahrah-Al Hufrah Platform, and Gattar Ridge suggesting that the area was uplifted during the Early Cretaceous.

These sediments over the area of NW trending positive elements have been either eroded or were not deposited. These variations reflect the pattern of the future horst and graben structure, which apparently did not fully develop until later during the

Cretaceous. During this period, a sequence of non-marine 'Nubian' Sandstones represents the earliest synrift continental siliciclastic infill of the subsiding grabens and is generally missing or very thin on the platforms and highs either overlying the Precambrian basement rocks or conformably underlying the marine sequence of Upper Cretaceous variegated shale.

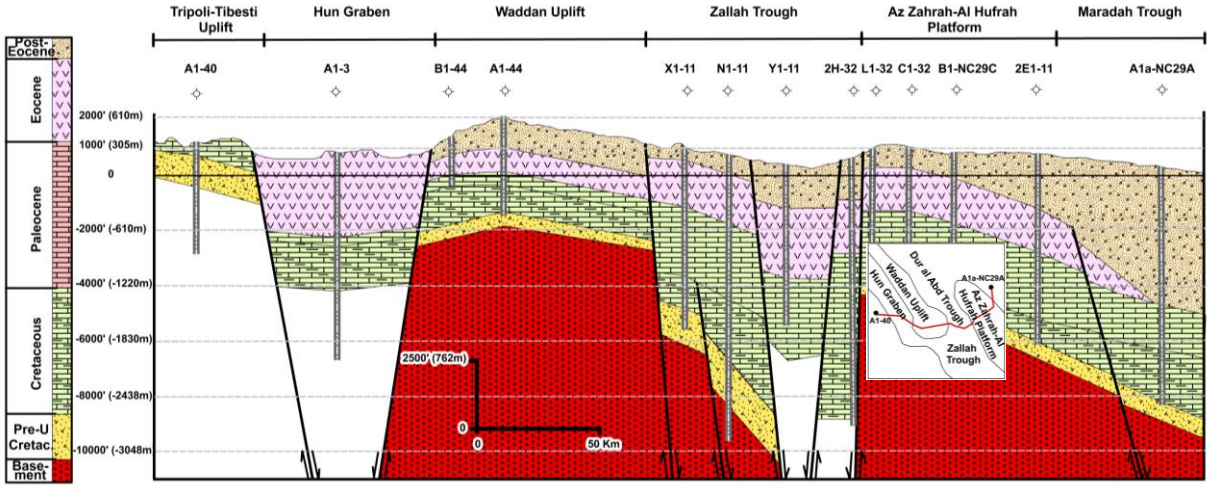


Fig. 5.7 Geological cross section (See the inset for location) constrained by well data showing the tectonic evolution of the study area. Note the numerous faults, with only the larger ones shown here, demonstrating the distributed nature of deformation in the study area.

The Lower Cretaceous sediments have been penetrated by only a few wells, therefore to substantiate the interpretation made in this study, further deep drilling, combined with high resolution seismic is needed particularly in deep trough area. Borehole data used in this study (Fig. 5.3A) suggest that the Early Cretaceous rift initiation sequence was deposited in a NNE-SSW-trending depression in a local downwarped area with a weak fault control. This is indicated by a narrow band of isopach contours trending NNE-SSW, reflecting the presence of a regional syn-sedimentary fault affecting the Lower Cretaceous sediments and older formations (Fig. 5.3A).

This trend seems to be consistent with the NNE-SSW and WNW-ESE trends of Pan-African and older fold axes (Assaf, 1991) and it is possible that the rejuvenation of many of these structural trends might have occurred. The Early Cretaceous trend follows that of the Sirt Arch which itself is interpreted to be coincide with the NE-trending basement structural grain of the Hercynian Orogeny resulting in the older Paleozoic section being folded, uplifted, and eroded (Aliev et al., 1971; Burollet et al., 1978; Boote et al., 1998).

During the Early Cretaceous, stress fields in North and Central Africa began a clockwise rotation, under the influence of new forces related to the opening of the South

Atlantic (Guiraud and Maurin, 1992), followed by a left lateral wrenching between southern European microplates and North Africa (Pawellek, 2009). In section 2.2 (see Figure 2.6) the rifting episodes of the Sirt Basin according to different authors over the last three decades were discussed. It is clear that our rift initiation (Early Cretaceous) phase is in agreement with Early Cretaceous rifting phase of Schroter, (1996) for the W. Sirt Basin.

5.3.4 Main syn-rift (Late Cretaceous) phase

In the Sirt Basin, an unconformity marks the most prominent change in the basin history from continental (Nubian) to marine infill. The Upper Cretaceous sediments are preserved in a thick section in the troughs suggesting high rift-type subsidence rates occurred in the Late Cretaceous. The sediments also transgressed with reduced thickness across all the highs, including the pre-Late Cretaceous topography of the Az Zahrah-A Hufrah Platform. Thus the subsidence rates vary greatly between grabens and neighbouring platforms. This resulted in strong lateral differentiation between basin, platform and nearshore lithofacies (Fig. 5.1). All the formations of this Late Cretaceous transgressive cycle exhibit similar lithofacies in the basins and platforms (Schroter, 1996) and a characteristic usually dolomitic/sandy/anhydritic nearshore equivalent toward the pinch-out edge.

During the main phase of rifting, the Upper Cretaceous graben-fill sequence was deposited mainly in two depocentres trending N-S and NNW-SSE separated by a local E-W trending high (Fig. 5.4A). This potentially means that the extension during this time was E-W to ENE-WSW-directed instead of NW-SE-directed as it was in the Early Cretaceous. This rift climax phase is expressed by a total of thickness of 1263 m (4143') in well A3-NC131 in the Zallah Trough compared to very thin occurrences or an absence of these sediments approximately 8.5 m (28') in well FF1-32 on the Az Zahrah-Al Hufrah Platform (Fig. 5.4A & B). The considerable growth of this sequence across the main fault systems shows that they were active throughout this time.

5.3.5 Basin downwarping (Paleocene) phase

Graben-fill was completed by the end of the Cretaceous but subsidence continued during the Paleocene forming a structural sag (Hallet, 2002) characterized by the highest regional subsidence rates in the study area. This is attributed to a uniformly high subsidence rate for the troughs and platforms with greater subsidence and deposition occurred within the Zallah sub-basin than around its margins indicating that high post-

rift subsidence rates are clearly restricted to the trough while platform areas show less subsidence.

In the Paleocene, deposition occurred during a relatively inactive structural period during basin down-warping (Parsons et al., 1980) (Fig. 5.8 and 5.5A & B). The Paleocene was a time of warm oceans and generally high sea levels. In North Africa, vast epicontinental seas extended far inside the African continent (Guasti & Lüning, 2009) and Paleocene seas overflowed the sub-basinal margins and extended further than the Late Cretaceous seas after infilling large-scale topographic relief. Sediments were deposited across a broad and generally stable shelf. The study area at this time was a NW-SE-trending feature suggesting a NE-SW extension direction. The Hun Graben (Fig. 5.5B) seems to have been an area of high topographic relief during this time indicated by the thin or absent Paleocene sediments. This confirms that this graben formed during post-Paleocene time. In contrast to the Hun Graben, the Gattar Ridge was a part of trough area as indicated by its high thickness of Paleocene sediments during this time (Fig. 5.5B). The stratigraphic sequence deposited across the study area during this period includes the Hagfa, Satal, Beda, Dahra, Khalifa, Zelten, and Harash Formations (Fig. 2.8) which are entirely marine and include limestones, dolomites, anhydrites, shales and a small number of sandstones. This downwarping phase created stratigraphic aquifers, carbonate reservoirs and seals.

5.3.6 Fault reactivation (Eocene) phase

Within the Sirt Basin a period of intense rifting resulted in an abrupt deepening of the basin and finally deposition of Late Eocene evaporites and dolomite (Abadi 2002). Fault controlled deposition in the study area resumed during the Eocene when a thick stratigraphic interval of sediments were deposited in the main depocentre trending NW-SE. This can be considered as the fifth sequence that accumulated in the study area (Fig. 5.8 and 5.6A & B). It seems that a weak reactivation of faulting is recorded during Paleocene but became stronger during Eocene times recorded by differences in thickness of the Hon evaporites that formed and under extensional faulting combined with strike-slip movements in the central part of the study area (Anketell and Kumati, 1991b). The Eocene isopach map (Fig**.** 5.6A & B) shows the thickness distribution of the Eocene sediments, which rapidly thicken from 91 m (300') over the footwall to 1433 m (4700') in the basin shows evidence for the presence of two depocentres developed in the hanging wall of major extensional faults (Fig**.** 5.6A & B) trending NNW-SSE in the

Zallah and Dur al Abd Troughs and the Maradah Trough/Al Nufyliah High which is now inverted in the northeastern part of the study area.

A marine sequence that includes evaporites, limestones, and dolomites comprising the Kheir, Gir, Gialo and Gedir Formations (Fig. 2.8) were deposited across the study area during this period.

5.3.7 Basin tilting and volcanic eruption (Post-Eocene) phase

The final phases of rift evolution include formation of anticlines which exhibit a NNW-SSE strike, and show of Oligocene (Ma'zul Ninah Formation) cores flanked by Miocene (Maradah Formation) outcrop indicating a pre-Middle Miocene gentle compression leading to a slight inversion of the central study area (Fig. 1.3). It can be speculated that this was due to a compressive stress normal to it, i.e. approximately in a NNE-SSW direction (Schafer et al, 1980) that was probably induced by the Miocene Eurasian/Afro-Arabian collision (Schafer et al, 1980; Anketell and Kumati, 1991b; Anketell and Ghellali, 1991). A final phase of post-rift tilting in the study area is coincident with extrusion of the Al Harug Al Aswad basalts from 8 to 2 Ma. This NE tilting effect is seen across the whole Sirt Basin and may be caused by Alpine-related tectonic pulses in the post-Eocene resulting in northward tilting of the basin.

5.4 Discussion of Sirt Basin sub-surface structure and rifting

The Sirt Basin is characterized by several rifts, separated by large horsts or platforms, (Fig. 2.4) each with its own distinct tectonic and sedimentary history (Ibrahim, 1991; Baird et al., 1996; Ambrose, 2000; Hallett, 2002).It evolved to its final configuration through tectonic events that were closely linked to the North African continental margin (Jongsma, et al., 1985; Guiraud and Maurin, 1992; Anketell, 1996; Anketell and Kumati, 1991a and b). Harding (1984) first recognized that the Sirt Basin had developed through three stages (Fig. 2.6). The pre-graben initiation stage has the regional character to its tectonic, structural and stratigraphic development. This was followed by a syn-rift stage that was characterized by normal faulting which resulted in the formation of horsts and grabens, and geographically variable structural histories and stratigraphic successions. The post-rifting stage is characterized by basinal-centric subsidence and sediment thicknesses that are greater in the central parts of the basin than at its margins.

Several attempts have been made to define the rift phases within the Sirt Basin based on the sedimentary fill. Broadly speaking, the main phases of extension and subsidence

where; 1) the Jurassic-Early Cretaceous, 2) Late Cretaceous, and 3) Paleogene (Anketell, 1996; Van der Meer and Cloetingh, 1996; Ambrose, 2000; Hallet, 2002; Bosworth et al., 2005) although Thusu, (1996) believes that there was some local rifting that commenced in the Triassic, and perhaps continued also into the Permian, that was related to the initial opening of Neotethys (Stampfli, et al., 2001). Extension may be still active in the present-day Hun Graben and locally offshore (Boote, 2008).

To date there is no general agreement on what constitutes the pre-rift and syn-rift sequences and these disagreements are probably due to the multiple rifting stages that led to the formation of Sirt Basin (Tawadros, 2001). Fig. 2.6 shows these subdivisions according to various authors. For example, the Nubian sandstone (Late Jurassic-Early Cretaceous) were considered as pre-rift by Harding (1984), Baird et al. (1996) and van der Meer& Cloetingh (1996) while it considered as syn-rift by Gras (1996), Schroter (1996), Ahlbradt (2001), Abadi (2002) and Pawellek (2007) among many others. The diversity of geological opinion regarding the tectonic evolution of the Sirt Basin can be explained by two reasons, firstly an absence of deep wells reaching to the basement in the troughs and, secondly by an absence of better quality deep seismic reflection and refraction data. For more details refer to section 2.2.0 and Fig. 2.6 in chapter 2 which shows these subdivisions according to various authors.

5.5 Summary

The aim of this chapter was to supplement the surface interpretations presented in Chapter 4 with constraints from the subsurface. This subsurface information is presented in the form of geological cross sections and maps that show the distribution of stratigraphic layers, their thickness variations, and their attitudes (structure).

On the basis of the borehole data, the subsurface stratigraphic succession comprises a variety of lithologies ranging from Pre-Cambrian crystalline basement to recent sedimentary rocks. Total sedimentary thickness exceeds 3000 m (9843') and is mostly beds of Cretaceous and Cenozoic age in the deepest parts of the troughs, diminishing to 1200 m (3937') on the regional highs

The structural interpretation indicates extensional tectonic events affecting the Upper Cretaceous sediments as outlined by grabens and tilted troughs, controlling thickness variations of these sediments.

In total, six lithostratigraphic sequences (phases) in the area's stratigraphic framework were recognized. The thickness ("isopach") maps display trends of thickening and

thinning of each layer and thus, indicate trends and locations of possible major structural and stratigraphic traps.

The study area pre-graben (pre-rift) initiation stage and its sedimentary products are of a varied character since this is a category of convenience that includes all tectonic and sedimentary activity that preceded the Cretaceous time. The graben-fill stage has been divided into four structurally active and structurally inactive periods to better reflect local structural history. Syn-rift faulting commenced in the Early Cretaceous followed by Late Cretaceous marine siliciclastics, shales, and carbonate rocks, overlain by Paleocene-Eocene carbonate and evaporite strata and then terminal continental siliciclastics strata representing the post-rift stage of the development of the area assigned to post-Eocene time.

The Lower Cretaceous thickness trend is NNE-SSW and WNW-ESE aligned whilst the Upper Cretaceous graben-fill sequence was deposited mainly in two depocentres trending N-S and NNW-SSE separated by a local E-W trending high. This potentially means that the extension during this time was E-W to ENE-WSW-directed instead of NW-SE-directed as it was in the Early Cretaceous. Graben-fill was completed by the end of the Cretaceous but subsidence continued during the Paleocene forming a structural sag characterized by the highest regional subsidence rates in the study area. The study area at this time was a NW-SE-trending feature suggesting a NE-SW extension direction. Fault controlled deposition in the study area resumed during the Eocene when a thick stratigraphic interval of sediments deposited in the main depocentre trending NW-SE.

A final phase of post-rift tilting in the study area is coincident with extrusion of the Al Harug Al Aswad basalts from 8 to 2 Ma. This NE tilting effect is seen across the whole Sirt Basin and may be caused by Alpine-related tectonic pulses in the post-Eocene resulting in northward tilting of the basin.

CHAPTER 6: SEISMIC DATA INTERPRETATION AND RESULTS

6.1 Introduction

The seismic reflection method has played an important role in the exploration of oil and gas since the first seismic surveys were performed at the beginning of last century. This method is considered to be one of the powerful remote sensing techniques that can image the subsurface over depths from several meters to several kilometers. The basic idea is to generate an acoustic wave field from a localized source which travels down through the subsurface and partly reflects at locations where the acoustic rock properties change. The reflected wave field is measured by an array of localized receivers on the surface.

The volume of seismic datasets has increased tremendously particularly over the last three decades, the area covered by the surveys has grown and the sample density has increased. Analysis of this increasing amount of data requires an increase in the efficiency of the interpretation process and one way forward is to improve the visualization of the data.

This chapter addresses the interpretation and summarizes results of a study of the seismic data made accessible to the project. The objective of this part of the multi-disciplinary study was to gain a better understanding of regional structural and stratigraphic relationships.

This chapter is based on the interpretation of approximately 5000 km of 2D seismic data with various spacings available mainly in the eastern half of the study area (Fig. 6.1) provided by the Libyan oil companies and owned by Teknica Oil Company which has reprocessed the seismic data that were used in this study (Appendix 1). Teknica received some of this seismic data as paper copies, which were then scanned to obtain digital SGY files necessary for interpretation. Post-stack processes such as deconvolution and migration were investigated by Teknica to determine their usefulness in improving the interpretability of seismic data. After converting the seismic data into digital files they were imported into the study area database.

Seismic base maps were also digitized in order to locate some of the seismic lines loaded in the database. Teknica has recognized that much of the seismic was recorded from a Vibroseis source. However, several paper seismic sections were recorded by a Thumper source while a few seismic sections were recorded with dynamite over a broad time interval (1968 to 1998) and covered the western part of Sirt Basin-Libya (Fig. 6.1).

The 2D seismic over the basin reveals a complete picture of a series of the Late Cretaceous to Late Eocene tectono-stratgraphic sequences along the western portion of the Sirt Basin.

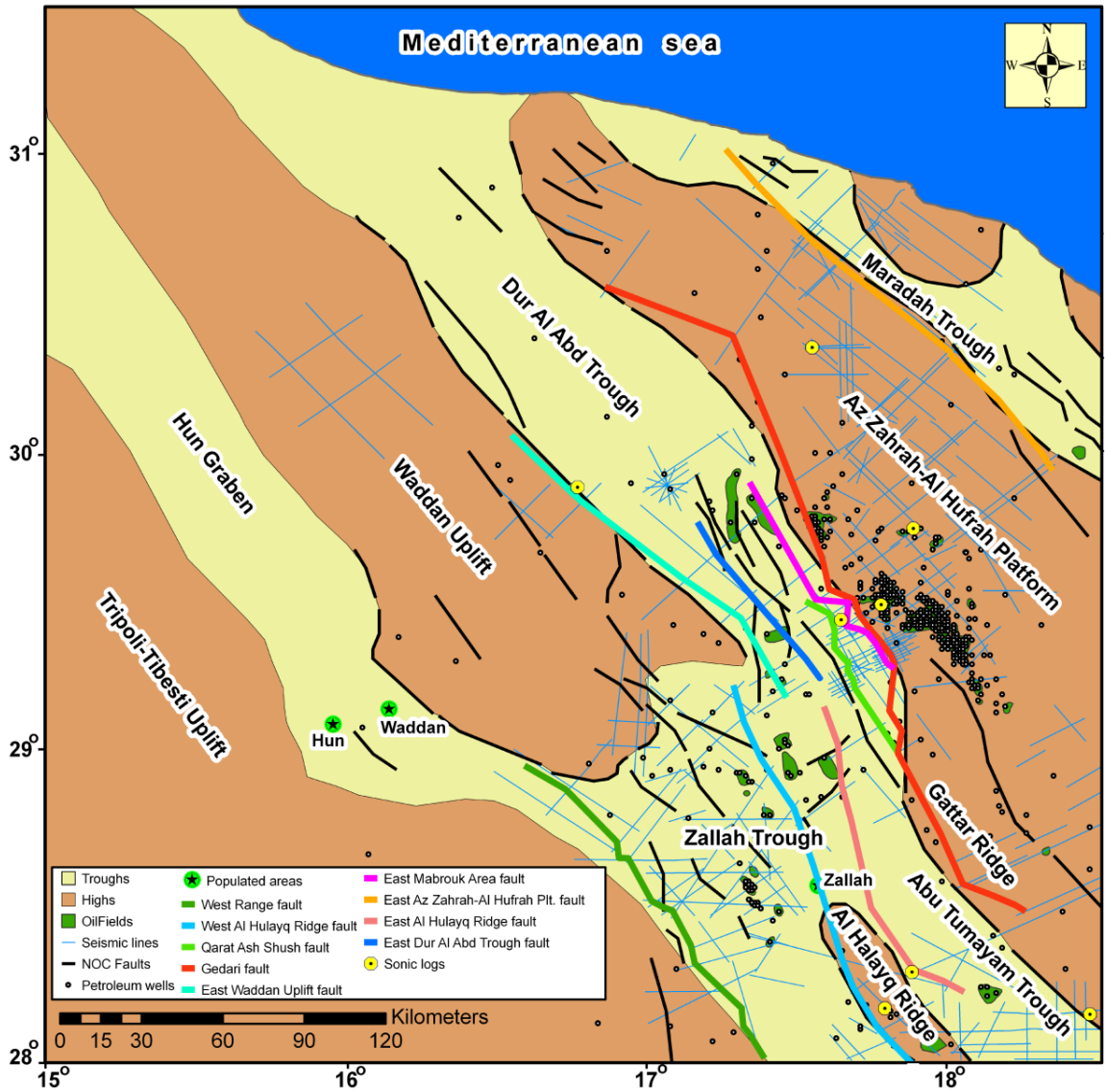


Fig.6.1 Illustrates the major faults interpreted from seismic data overlaid on a simplified tectonic elements map of the study area. It also showing location of oil fields, wells, and seismic profiles used in this study.

The data used in this study have been loaded and interpreted by Seisworks/2D Landmark software in Durham University (See section 6.4). The SeisWorks 2D technology is part of the SeisWorks family of products, the oil and gas industry's leading integrated seismic interpretation and analysis software package. SeisWorks software provides an extensive set of functional capabilities for the management, access, display, and interpretation of large-survey data sets and offers comprehensive geological, geophysical and petrophysical data integration. Support for integrated multi-

survey project interpretation (through 2D/2D merge and 2D/3D merge capability), in time or depth is available.

The interpretation of 2D seismic data with various spacing; combined with borehole data, has been used to give a clearer definition of the location and nature of the boundaries of the major tectonic features, and to provide support for the interpretation and understanding of the geological history of the NW Sirt Basin (See chapter 4 and 5). The data have generally been shot in a NE–SW dip direction and a NW –SE strike direction in order to image the structures clearly. Interpretation and mapping of several seismic horizons of regional extent along with identified faults has allowed the construction of regional structure maps that would be a good source to show potentially prospective trends for oil accumulations.

The interpretation of available seismic coverage has enabled the construction of integrated geological cross sections, permitting the construction of 4 regional seismic traverses (different in length). The interpreted seismic traverse profiles have been composed from individual seismic lines of different vintages and different field acquisition and processing parameters and has been incorporated into the combined traverse sections Three representative seismic cross sections, oriented perpendicular to the strike of the study area fault array, illustrate the key seismic reflectors and faults mapped in the footwalls and hangingwalls to the principal fault systems. The fourth section was created parallel to these trends along strike to show the tilting of the structural blocks.

6.2 Dataset

The 2D seismic data is good in quality, especially on the shallow areas but gets difficult to interpret beyond 2500 milliseconds. In the highly faulted areas, because of the various vintages of data, there are differences in acquisition parameters, processing stream and, most importantly, several seismic datum's which resulted in significant mis-ties between the different surveys. As a result, the mis-tie problem was addressed (and solved) by Teknica (Appendix 1) to ensure reliable correlations for mapping purposes. This section also has suffered from an interpretation delay because of the use of several different coordinates systems that had to be converted to UTM Zone 33N in order to achieve a comprehensive GIS database for the study area. The principal aim here was to correlate the seismic dataset with the well data and use the combined dataset for seismic analysis and interpretation in the Landmark Seisworks/2D software. Realistic correlation between the two datasets was then, in turn, used to define the structural

configuration of the study area. In addition, the georeferencing of geophysical and geological data proved to be valuable for determining the structural setting and evaluating the hydrocarbon potentialities of the sub-surface rocks (Shaaban, and Ghoneim, 2001).

6.3 Well Correlations

About 300 wells with some sonic logs have been collected by Teknica and imported into the study area database. About 110 of the sonic logs are located mainly in the eastern portion of the area especially in the Az Zahrah and Al Hufrah field areas, and other smaller hydrocarbon field areas. Of the remaining wells with sonic logs, eight (Fig. 6.1) were converted to synthetic seismograms that were tied to the nearest seismic lines. Synthetic seismograms are artificial seismic traces used to establish correlations between local stratigraphy and seismic reflections (to match the seismic extracted in wells) using well log data to create synthetic seismograms is a common practice in geophysical studies. Some wells contained a full sonic log from near surface to T.D. Many wells contained a partial sonic log, some more complete than others.

Synthetic seismogram correlations from the 8 wells and their corresponding nearest seismic traces created by Teknica have been used to produce well to seismic correlations (Fig. 6.2). Examinination of all of the correlations indicates that this approach is adequate to derive information about the subsurface region from calculations utilizing the travel times of the observed seismic waves and also the challenge of choosing credible regional and localized correlations.

6.4 Interpretation workflow and products

The set of 252 seismic lines were imported into Landmark in the SEG-Y format. A new seismic survey folder was created in Landmark to store the lines. The original number of the seismic data was assigned to each line and they were sorted and organized. The well data were added and analyzed together with the seismic profiles for interpreting seismic stratigraphic horizons. Correlation of seismic time horizons on seismic sections obtained for the study area, required implementation of a specialized sequence of steps in order to successfully obtain meaningful time and depth structure maps, and fault patterns.

The interpretation was carried out using the Seisworks/2D (Landmark), using a general, and very simplified, workflow as shown in (Fig. 6.3) along with Surfer 8 software as

well for contouring surfaces. The interpretation of horizons was dependent on the structure control tied to the 8 wells distributed somewhat randomly in the area.

Thirteen horizons (with only four or five having widespread correlation over the study area) (Table 6.1) were picked according to the seismo-stratigraphic features such as onlap and truncation. This helped in defining the unit surfaces and the change in amplitudes defined the changes in lithology and facies extents.

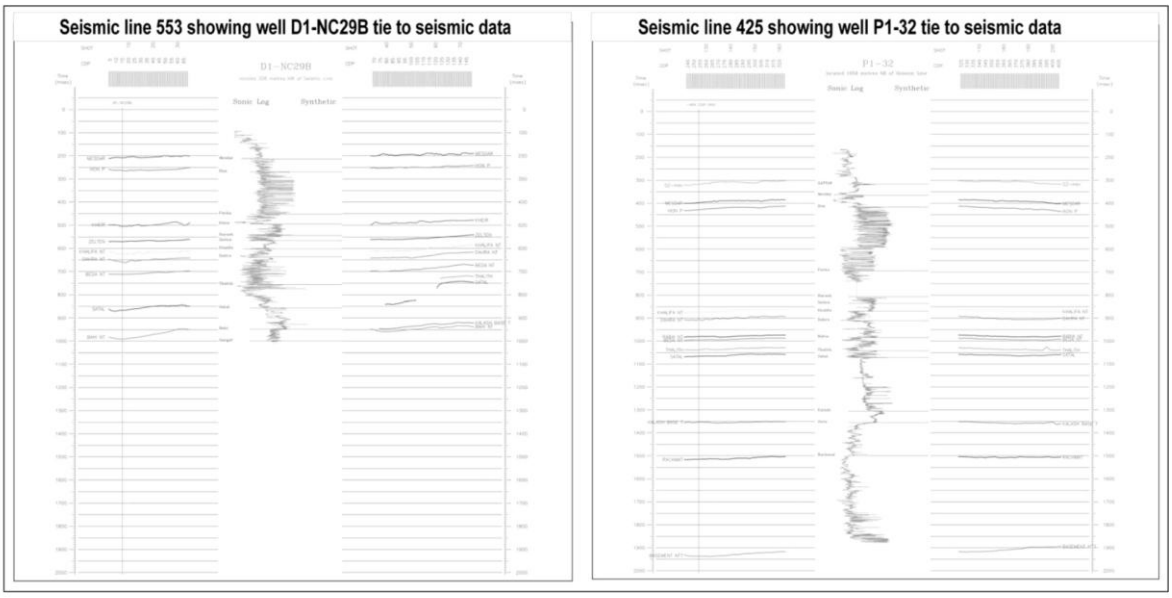


Fig.6.2 Selected sonic wells that were used for well to seismic correlation (synthetic seismogram correlation).

Evaluation of the seismic data showed that the near top Hon and near top Sirte (near base Kalash) seismic markers held the most promise as regional markers. Several seismic markers carried from the synthetic to seismic tie points proved to be local in nature. Consequently the seismic interpretation was started by interpreting the near base Kalash, (Late Cretaceous) which is one of the clearer horizons to build up an understanding of the regional trends of the structures of the area. This horizon is represented by a consistent trough near the top of Sirte (described below), characterized by a strong reflector. It was easy to follow because of its clear and coherent seismic character except in the areas of intense faults. The horizon was initially interpreted around the tied wells in the clearer areas and was then extended throughout the rest of the area with special care given in the highly faulted areas. The creation of this surface showed the main structural features in the area and their trends, and also helped in understanding the structure below and above each age period between the Late Cretaceous to Late Eocene. The same process of interpretation was applied to the Eocene near top Hon horizon

Seismic Time (Horizons)	Colors	Wavelet Picked	Horizon Age	Time structure maps	Isochrons maps	Average velocity maps
Top Gattar	Grass Green	PEAK	Middle Eocene			
Top Mesdar	Bright Green	PEAK	Lower Eocene			
Top Hon	Blue	PEAK	Lower Eocene	Top Hon	Top Hon to Top Facha	Top Hon
Top Facha	Light Magenta	PEAK	Lower Eocene			
Top Kheir	Dark Green	PEAK	Early Eocene-Late. Paleocene			
Top Harash	Haze Blue	PEAK	Late Paleocene		Top Harash to Top Zelten	
Top Zelten	Yallow	PEAK	Middle Paleocene	Top Zelten		
Top Khalifa	Pale Green	PEAK	Middle Paleocene			
Top Dahra	Green	PEAK	Middle Paleocene	Top Dahra		
Top Beda	Glden Yellow	PEAK	Middle Paleocene			
Top Satal	Blue Violet	PEAK	Early Paleocene		Top Satal to Base Kalash	
Base Kalash	Light Blue	TROUGH	Late Cretaceous	Base Kalash		Base Kalash
Top Bahi	Grey	PEAK	Early Upper Cretaceous			

Table 6. 1 A summary of the interpreted horizons.

This was followed, from the bottom to the top by picking the top of Early Upper Cretaceous Bahi Formation horizon and ending in the Gattar Formation of Late Eocene age. The Late Cretaceous was followed by a number of Paleocene horizons, (Satal, Beda, Dahra, Khalifa, Zelten, and Harash Formations) and then the Eocene age horizons, comprising, Kheir Formation, Gir Formation (Facha, Hon, and Mesdar Mbs), and Gattar Formation. The gridded time surface maps were used to produce isochronal maps by subtracting the deeper horizon from the shallower horizons.

As the interpretation progressed on some seismic lines, it was recognized that very few of the seismic markers recognized on the synthetic seismogram to seismic correlations were regional in their extent. Several seismic markers carried from the synthetic to seismic tie points proved to be local in nature. These markers, however, proved to be valuable benchmarks (i.e. reference markers) to help in the location of other seismic markers that would have been difficult to interpret without these frames of reference.

A process of depth conversion was applied to the seismic dataset. An average velocity was estimated by dividing the TVD value of a well top formation by the corresponding one way travel time. This has been done to get depth maps of the study area. The near top Hon, near top Dahra, and near top Sirte (near base Kalash) were found to be the most clear seismic markers that were correlated. Many localized time markers above the Mesdar and from the Mesdar to near base Kalash were also correlated to benchmark the

geological section. The seismic sections and sonic logs clarified some of the differences that appeared irresolvable between the Zallah Trough, the Gattar Ridge, Dur al Abd Trough, and the Az Zahrah-Al Hufrah Platform. The result is that the correlation between the tectonic elements is possible and confidence in reflector correlation was good. As this phase of work progressed, several more localized time markers were identified particularly within the Zallah Sub Basin.

6.4.2 Fault identification and analysis

An extensive evaluation of the major fault intersections on the regional time markers and the ground surface was undertaken. Once completed, time structure maps were constructed on the main regionally extensive time markers. (i.e. Hon, Zelten, Dahra, and base Kalash).

The previously identified major faults zones (structural hinge zones) separate the regional structural elements of the study area such as the Waddan Uplift, Dur al Abd Trough, Zallah Trough and Az Zahrah-Al Hufrah Platform. Geologic cross sections and surface geology maps were also used to assist in the interpretation process.

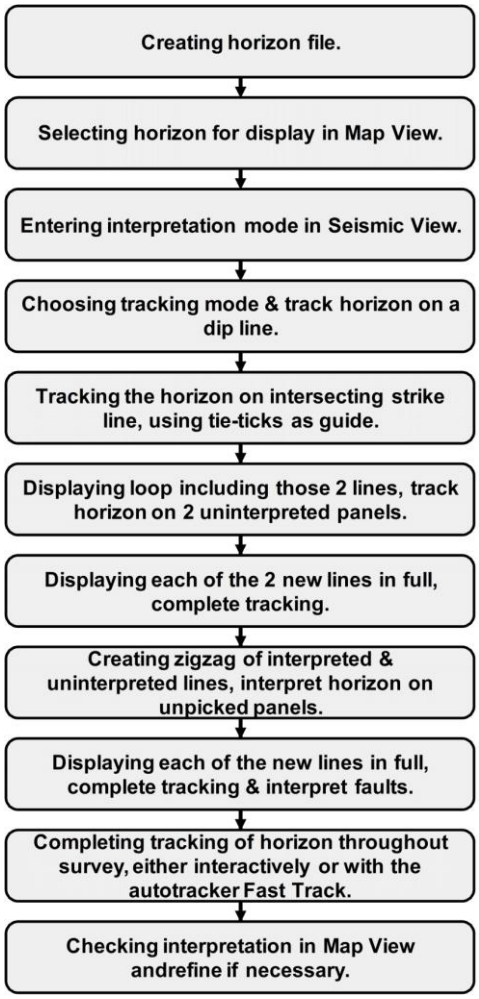


Fig. 6.3 Typical workflow for interpreting horizons

The workflow (Fig. 6.4) for interpreting faults has been developed as a systematic approach to fault interpretation recommended by Seisworks/2D staff. Generally, it was best to interpret major faults first, which are recognized on the basis of discontinuities in reflections falling along an essentially linear pattern; then work with secondary faults. Otherwise, the interpreted map and perspective views may become so cluttered with unassigned fault segments which will be difficult to discern trends. At any point in the fault interpretation a correlation of all the picked fault segments are assigned to a specified fault name. The primary criterion for recognizing a fault on a seismic reflection profile is as a break in the lateral continuity of a reflector or a group of reflectors falling along an essentially linear pattern. Picking faults can be difficult because sometimes the reflectors hang over the actual fault. Fault identification was generally easier than horizon picking although there were some difficulties when comparing seismic lines one by one, in assigning the fault picks to a specified fault name to complete the plan view analysis. It is possible to map the extent of the fault estimated by using the lateral and vertical displacement gradients (Walsh and Watterson, 1987) in 2D seismic data. Figure (6.5) shows that isolated faults picks may show complex patterns, however a fault correlation can be made on the basis that a series of fault cuts lie along the same trend.

The fault analysis was completed on all seismic time marker horizons up to the ground surface. Deformation is distributed over a wide area across many closely spaced faults and the focus here was mainly on the larger or more continuous faults. Faults generally trend north-northwest to northwest, with only minor branches and transfer zones of differing orientations. This trend generally coincides with the axis of the Sirt Basin.

In general faults are spaced irregularly, and are mostly depicted here as single faults with occasional synthetic or antithetic faults; however, only the larger or more continuous faults are shown. The observed disruption of seismic data suggests numerous additional minor faults are present and any many structures extend upward into the Tertiary section. Analysis of the plan view orientation of basement-rooted faults was made by identifying all faults with a clear throw at the near base Kalash seismic time marker. Fault intersects of the near base Kalash seismic time marker, with throws between 20-30 ms were considered to most likely be basement rooted. On a line-by-line basis, the lines were compared to determine the best match of fault intersects.

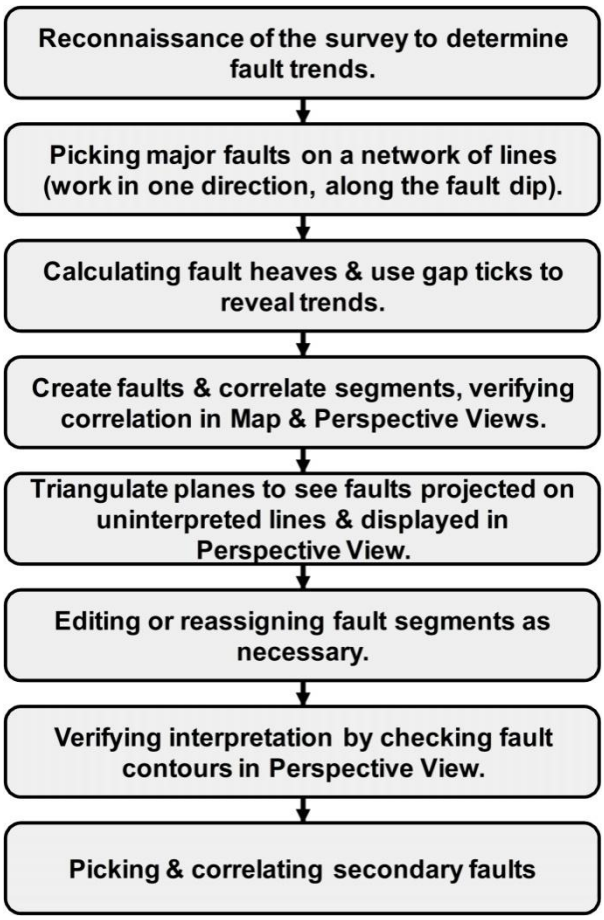


Fig.6.4 Workflow for interpreting faults

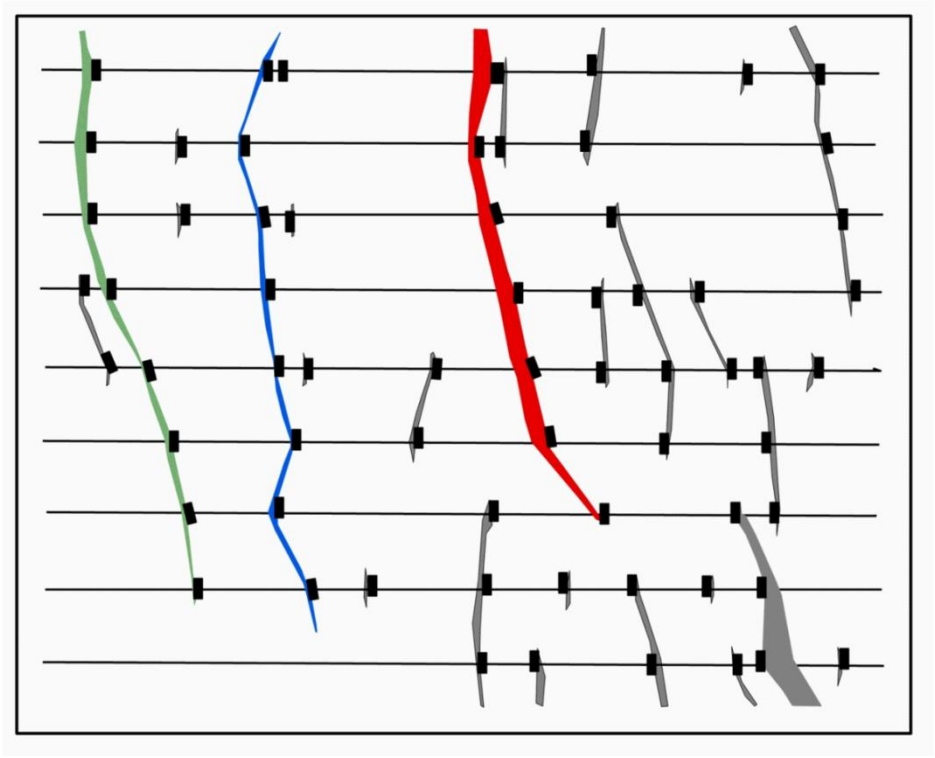


Fig.6.5 Map of fault cuts on a series of 2D-seismic lines. A set of fault cuts have been correlated to form a single, continuous structure (highlighted in different colours).

The fault intersects most likely to correlate on trend were first analysed with respect to the Tectonic Elements of Sirt Basin (Mouzughi, and Taleb1981) published by NOC (National Oil Corporation of Libya) and then entered into the database.

This was an extremely comprehensive analysis and seemingly rewarding in that a very believable pattern of faults emerged. Many of the fault patterns had a very good agreement with the Tectonic Elements of the NOC map while some of the fault patterns did not agree. The fault intersects and resulting patterns identified at the near base Kalash were used as a template for identifying the fault patterns on the overlying seismic time markers. The same comprehensive line by line interpretation procedure was used again and the overlying Time Structure Maps were then contoured with the plan-view fault pattern identified from seismic data.

6.4.2.1 Major seismic fault population

Nine sub-populations of major normal faults (Fig. 6.1) have been identified in the study area, distinguished by the size of the faults and the period of time during the rift phase, when they were active.

1- Gedari fault
2- Qarat Ash Shush fault
3- East Dur al Abd Trough fault
4- East Az Zahrah-Al Hufrah Platform fault
5- East Waddan Uplift fault
6- East Mabrouk Area fault
7- West Al Hulayq Ridge fault
8- East Al Hulayq Ridge fault
9- West Range fault

6.5 Seismic and geological cross sections correlation

The 2D seismic data are ambiguous deeper than the Late Cretaceous base Kalash age. Based on Teknica report (Appendix 1), it was because of the vintage of the data acquisition and also the seismic data scanned from paper sections identified some limitations. Scanned data did not record the seismic troughs faithfully enough to rely entirely on them for interpretation. The poor recording of the seismic troughs during the scanning process was partly due to the quality of the paper print, the scale of the paper print, and sometimes due to the trace display selected by the original processor. Some of the paper data was recorded in variable area mode where no trough was available during the scanning phase.

Subsurface mapping and hence the understanding of the structural evolution of the study area was enhanced by integrating the geological cross sections (shown here in depth per foot) made from borehole data. These were constructed and used in a parallel and followed the same geometric rules as seismic cross sections (see Fig. 1.4 for location).

This integrated approach allowed extra accurate and consistent information on rock unit depths to be obtained and improved visualization of the spatial and temporal relationships of units occurring in the area. Supplemental seismic data can be helpful in interpreting the horizontal variations between the borehole data used in the geological cross sections (see Chapter 5). It is generally desirable to have data points relatively evenly spaced along the line of section, wherever this is permitted by well control.

Four cross sections were constructed from seismic and borehole data (Table 6.2) for the purpose of structural interpretation; the three sections oriented perpendicular to the main structural trends, give the most representative view of the folds and faults geometry and the section parallel to these trends along the strike shows the tilting of the structural blocks.

The borehole cross sections (see chapter 5) were used to inform the direction that the seismic cross sections were drawn in order to provide an optimum view of the present day basin structure and/or structural trends. The sections also allowed interpretation of the rock unit thickness variations and facies changes, the position of depo-centers, depositional trends and/or paleo-structures (e.g. paleo highs). Both seismic and geological cross sections aid recognition of the structural and stratigraphic controls on petroleum accumulation in the area.

The area mapped shows a regional dip to the northeast and is intersected by many faults, folds, ridges and platforms (Fig. 6.1). Hydrocarbons appear to have accumulated on the crest of some of these structures in multiple horizons where each horizon has the characteristics that enable them to hold hydrocarbons.

6.5.1 Cross-section A-A’

This cross section is, comprised of four seismic lines (25-103 (TD-7), 17VR141-83, BPL-SSL-4BR28-75 and ELAQ-SSL-ES-105-83) with a combined (straight line) length of approximately 180 km (Fig. 6.6). The section crosses the northern part of the study area, trends southwest to northeast, and represent dip lines, perpendicular to the main structural trends of the area (Fig. 1.4). Based on the seismic lines, a geological cross section taking the same trend constrained by 8 wells from well D1-17 on the Waddan

Uplift to the southwest to well B1-24 on the Az Zahrah-Al Hufrah Platform to the east (Fig. 6.7) was drawn.

CROSS SECTION		SEISMIC DATA			GEOLOGICAL (BOREHOLE) DATA							
Name	Direction	Seg #	Line Segment	CDP(Trace)	Well Name	Feet_KB	Feet_Depth	Lat.	Long.	Reached_FM	Age	Status
			Name	Interval	D1-17	1387	5096	29.69	16.64	Gargaf Fm.	Cambro-Ordovic.	Dry
		1	25-103 (TD-7)	50	B1-25	940	5679	29.91	16.76	Gargaf Fm.	Cambro-Ordovic.	Dry
		2	17VR141-83	25	F1-17	889	6819	29.92	16.94	Gargaf Fm.	Cambro-Ordovic.	Dry
A-A'	NE-SW	3	BPL-SSL-4BR28-75	50	K1-17	926	7731	29.95	17.05	Bahi Fm.	E. U. Cretaceous	Dry
		4	ELAQ-SSL-ES-105-83	50	D1-NC57	628	8118	30.33	17.30	Gargaf Fm.	Cambro-Ordovic.	Dry
					C1-NC57	557	7140	30.47	17.37	Lidam Fm.	E. U. Cretaceous	Dry
					E1-24	542	7186	30.63	17.36	Lidam Fm.	E. U. Cretaceous	Dry
					B1-24	510	7915	30.69	17.39	Gargaf Fm.	Cambro-Ordovic.	Dry
		1	OMV78-06	40	F1-44	846	6834	28.95	17.01	Gargaf Fm.	Cambro-Ordovic.	Dry
		2	OMV78-12	40	U1-11	676	7365	29.16	17.21	Hagfa Fm	Lower Paleocene	Dry
		3	OMV80-15-09	50	3L3-11	700	5600	29.25	17.44	Gargaf Fm.	Cambro-Ordovic.	Oil
		4	TDX12-M328	62.5	3Q4-11	658	5500	29.23	17.41	Beda Fm	Middle Paleocene	Dry
		5	379	25	Y1-11	631	5811	29.32	17.45	Beda Fm	Middle Paleocene	Dry
B-B'	NE-SW	6	453	20	P1-32	722	10464	29.47	17.64	Etel Fm	E. U. Cretaceous	Dry
		7	V-2170	25	2H1-32	773	9720	29.47	17.65	Gargaf Fm.	Cambro-Ordovic.	Dry
					Q1-32	1150	5064	29.54	17.69	Gargaf Fm.	Cambro-Ordovic.	Dry
					2J1-11	1005	4432	29.25	18.08	Gargaf Fm.	Cambro-Ordovic.	Dry
					A1-NC29C	938	5017	29.74	17.95	Satal Fm.	Lower Paleocene	Oil
					2E1-11	943	6895	29.87	18.21	Bahi Fm.	E. U. Cretaceous	Dry
		1	NC131-90-43	20	A1-NC74C	1202	9099	28.31	17.09	Gargaf Fm.	Cambro-Ordovic.	Dry
		2	NC131-82-10	50	A3-NC131	949	13436	28.40	17.40	Lidam Fm.	E. U. Cretaceous	Oil
C-C'	E-W	3	NC131-82-10E	50	F1-57	1078	10591	28.37	17.64	Gargaf Fm.	Cambro-Ordovic.	Dry
		4	NC131-82-29	50	B1-57	1108	10390	28.30	17.87	Gargaf Fm.	Cambro-Ordovic.	Dry
		5	57-83-85	20	I1-57	653	10060	28.42	18.14	Gargaf Fm.	Cambro-Ordovic.	Dry
					G1-57	625	8531	28.50	18.37		Basement	Dry
		1	32-302TD-7	50	L1-32	682	7648	30.12	17.64	Gargaf Fm.	Cambro-Ordovic.	Dry
		2	T-29X	50	D1-32	811	8348	30.02	17.55	Gargaf Fm.	Cambro-Ordovic.	Dry
		3	T-29X-1	50	CC1-32	608	6830	30.02	17.60	Gargaf Fm.	Cambro-Ordovic.	Dry
		4	555	20	A2-32	723	7092	29.95	17.64	Gargaf Fm.	Cambro-Ordovic.	Dry
		5	467	20	B1-NC29B	996	5129	29.77	17.90	Gargaf Fm.	Cambro-Ordovic.	Dry
		6	516	20	D1-NC29B	838	5654	29.77	17.87	Gargaf Fm.	Cambro-Ordovic.	Dry
D-D'	NW-SE	7	393	20	U1-32	847	4200	29.74	17.88	Satal Fm.	Lower Paleocene	Dry
		8	407	20	V1-32	953	4840	29.64	17.91	Gargaf Fm.	Cambro-Ordovic.	Dry
		9	11-90-11	12.5	2N1-32	923	4420	29.55	17.99	Bahi Fm.	E. U. Cretaceous	Dry
					F6-32	984	4882	29.51	17.97	Gargaf Fm.	Cambro-Ordovic.	Oil
					A24-11	948	3200	29.45	18.01	Dahra	Upper Paleocene	Oil
					A82-11	884	3251	29.41	18.06	Dahra	Upper Paleocene	Dry
					A38-11	897	3250	29.40	18.07	Dahra	Upper Paleocene	Dry
					A56-11	851	3800	29.35	18.13	Satal Fm.	Lower Paleocene	Dry

Table 6.2 The seismic and geological data used to construct cross sections.

The seismic cross-section A-A' on the Waddan Uplift (columns A and B Fig. 6.6) is crossed by ≈ 60% of Line 25-103 (TD-7)), then moves across the Dur al Abd Trough (part of 25-103 (TD-7) and all of 17VR141-83), onto the Az Zahrah-Al Hufrah Platform (BPL-SSL-4BR28-75) and across part of the Maradah Trough (ELAQ-SSL-ES-105-83). There is a large gap of ≈ 18 km (at columns B and C Fig. 6.6) between Line 25-103 (TD-7) and 17VR141-83 that is constrained by wells B1-25 and F1-17 over the fault hinge zone between the Waddan Uplift and the Dur al Abd Trough. Another gap of about 25 km (at columns G and H Fig. 6.6) between 17VR141-83 and BPL-SSL-4BR28-75 can be seen and is filled by well D1-NC57 located at the eastern fault hinge zone of the Az Zahrah-Al Hufrah Platform.

It is clear from this seismic profile that the faults show a normal geometry and are shown schematically on the geological cross section (Fig. 6.7). Some faults extend from the base of the interpretable section (base Kalash) into the Lower Tertiary, while others

faults only cut the Lower Tertiary. Most of the horizons above the near base Kalash are more easily interpretable and a thicker stratigraphic section was observed in the troughs compared to the adjoining highs as confirmed by the geological cross section.

At the southeastern end of the Waddan Uplift there are at least five, large down-to-basin (i.e. to the NE) faults with apparent normal throws of 10 to 200 ms (the displacement can not be seen clearly on this seismic line due to resolution). This fractured area probably includes the eastern fringe of the Waddan Uplift as well as the entire hinge zone between this horst and the Dur al Abd Trough to the east. Horizons in this part of the section are clearly dipping to the east. Most of the sequence is present from the Gargaf sediments of Cambro-Ordovician age to the Gir Formation (Hon Mb) of Lower Eocene age, with the Satal Formation being the thickest in this megasequence indicating that Waddan Uplift was low during Lower Paleocene compared with the rest of the neighboring areas. It is unclear whether the absence of the Middle Eocene strata in this area was due to continued emergence and non-deposition, or post-Middle Eocene erosion. In any event, uplift of the Middle Eocene strata on parts of the current Waddan Uplift indicates that most of the uplift has occurred since the Middle Eocene.

Within the Dur al Abd Trough (columns C, D, E, F, G, and part of H Fig. 6.6) the reflecting horizons are for the most part horizontal with some secondary faulting (throws ≈5 to 40 ms) concentrated at about the middle to shallow depths (down to 1.0 s), above the Base Kalash / Top Sirte (light blue) reflector, and below Dahra (green) reflector.

There are at least 3 major faults that extend below the seismic section and these major faults branch out into smaller faults reminiscent of “flower structures” suggesting that the Dur al Abd Trough has been the focus of some large-scale wrench tectonics. Also the displacement is distributed among several fault strands that are seen to coalesce at depth. This image is comparable with other examples of continental transform faults (e.g. Ben-Avraham, 1992), and is typical of a flower structure such has often been shown to be associated with strike-slip faulting (Harding, 1985).

The F1-17 and K1-17 wells constrain the geological cross section (Fig. 6.7) and intersect the Dur al Abd Trough. This area seems to be suffered from at least three stages of tectonic events, it commencing with possible rifting during the Upper Cretaceous (not penetrated by any boreholes in the central part of the trough) and was followed by a large amount of subsidence during the Paleocene and Eocene.

Final rifting occurred during the post-Eocene as evidenced by a very thick sediments of this age.

The eastern portion of line 17VR141-83 and the next seismic line of the cross section, BPL-SSL-4BR28-75, (columns G, and part of H Fig. 6.7) spans a large data gap (of ≈25 km). Within this gap there is possibly a major, down-to-the northeast fault zone with throws of ≈700 m as suggested on the geological cross section A-A' (Fig. 6.7).

The line BPL-SSL-4BR28-75 (columns I, Fig. 6.6) represents the starting point of the hinge zone between the Dur al Abd Trough and the Az Zahrah-Al Hufrah Platform which is disrupted by 4 or more basement-rooted faults with predominantly down-to-basin (i.e. to the southwest) throws of between 10 and 80 ms. This hinge zone probably corresponds to part of the Gedari fault system that is located east of well D1-NC57. The reflecting horizons in this part of the section are for the most part dipping towards the southwest.

Between the Gedari fault hinge zone and the Az Zahrah-Al Hufrah Platform-Maradah Trough hinge zone to the northeast, the cross section shows the Az Zahrah-Al Hufrah Platform to have a basic anticlinorium form. The clear crest of this "anticline" is located at about the middle point between columns I and J (Fig. 6.6) and was most likely formed at some time since the Late Eocene because of the absence of any Late Eocene strata on or around the Az Zahrah-Al Hufrah Platform. The crest of the anticlinorium forms the current ridge of the Az Zahrah-Al Hufrah Platform. The updoming clearly narrows towards the north, and all evidence of its existence is lost near the Mediterranean coast line. This anticlinorium is characterized by a number of faults extending upwards to the surface with small throws. Several seismic reflections on Az Zahrah-Al Hufrah Platform between correlated seismic time markers near top Dahra and near base Kalash, indicate apparent down-lap to the northeast that may be interpreted as stratigraphic example of lateral accretion where possible Early – Middle Paleocene platform edge carbonates (Satal Formation) grade to off-platform limey shale's (Hagfa Formation). The observed relationship could also be explained by localized inversion on this platform giving a local unconformity.

The NE end of the section (column K Fig. 6.6) is considered to be the Az Zahrah-Al Hufrah Platform-Maradah Trough hinge zone, a region which is heavily fractured by five or more large, down-to-basin faults with apparent normal throws.

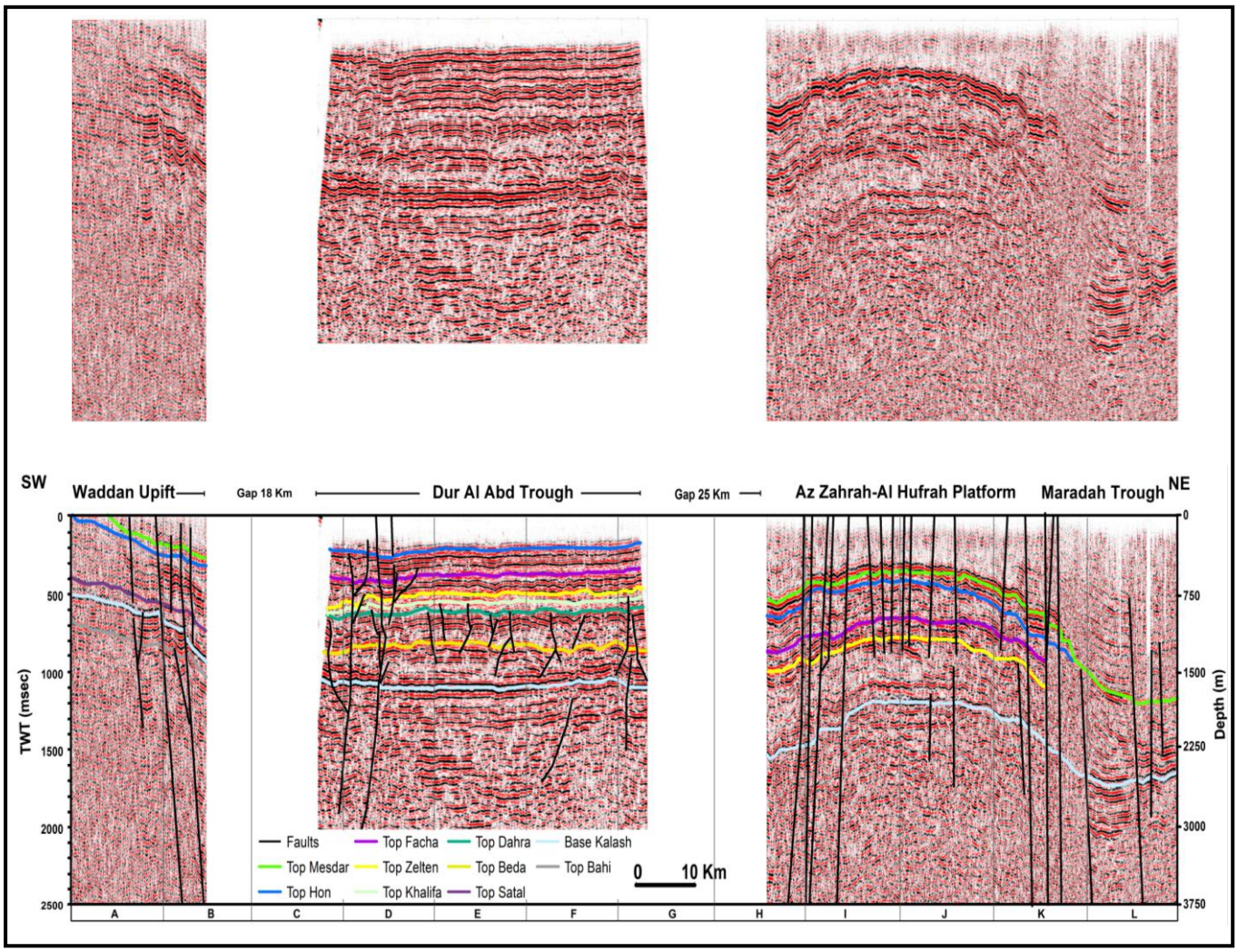


Fig.6.6 Seismic cross section A-A' view of present day structure across the study area from the southwest to the northeast (See figure 1.4 for location).

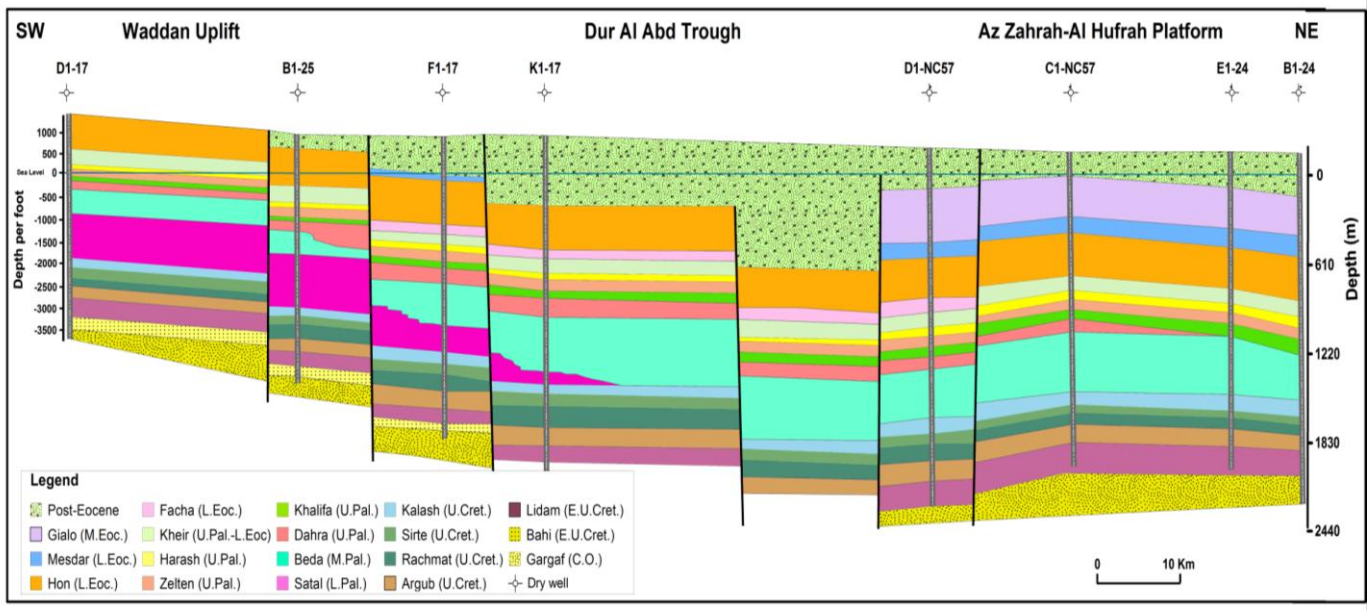


Fig. 6.7 Geological cross section A-A' view of present day structure across the study area from the southwest to the northeast (See figure 1.4 for location).

These probably also have significant wrench movement and the area between is expected to be shattered by numerous smaller faults that cannot be easily seismically resolved. To the NE of this hinge zone, the section intersects the Maradah Trough, which is characterized by the existence of a mini–depocentre (column L Fig. 6.6) of cross section A-A'.

6.5.2 Cross-section B-B'

This cross section is also a dip section approximately parallel to and 88 km southeast of A-A' and is composed of seven seismic lines (from southwest to northeast respectively; OMV78-06, OMV78-12, OMV80-15-09, TDX12-M328, 379, 453 and V-2170) for about 175 km long (Table 6.2). Two small gaps exist; one between lines OMV-15-09 and TDX12-M328 (≈ 3 km) (last portion of column D Fig. 6.8) and the second between lines TDX12-M328 and 379 (≈ 7 km) (column E Fig. 6.8).

The corresponding geological cross-section follows the same trend and has been constructed using12 wells from F1-44 at Waddan Uplift to the southwest to well 2E1-11 on the Az Zahrah-Al Hufrah Platform to the east (Fig. 6.9).

The southwest end of the seismic section just intersects the southern tip of the Waddan Uplift (OMV78-06), (column A Fig. 6.8) and then crosses into the Zallah Trough (OMV78-06, OMV78-12 and OMV80-15-09) (columns B, C and the first quarter of column D Fig.6.8), then over part of the Al Halayq Ridge (OMV80-15-09, TDX12-M328 and 379) (the middle point between columns D and E-Fig 6.9) and runs into the Dur al Abd Trough (Line 379) (columns E and F - Fig.6.8). To the east, the Az Zahrah-Al Hufrah Platform is crossed by Lines 379, 453 and V-2170 (columns G, H, I, J and the first quarter of column K Fig.6.8) and the section ends over the fault hinge zone between the Az Zahrah-Al Hufrah Platform and the Maradah Trough (Line V-2170) (last quarter of column K and L Fig.6.8).

The eastern part of Waddan Uplift (column A Fig 6.9) shows steep northeast and northwest dipping normal faults that extends to the surface and separates this part of uplift from the western flank of the Zallah Trough. This is followed by a series of NE and SW dipping normal faults, that step the reflections in the basin down to the synclinal axis of the Zallah Trough at about column C Fig. 6.8 (Line OMV78-06). Based on the geological cross section (Fig. 6.9) about 305m (1000 feet) of post-Eocene sediments accumulated in the section drilled by well F1-44 on the eastern part of Waddan Uplift.

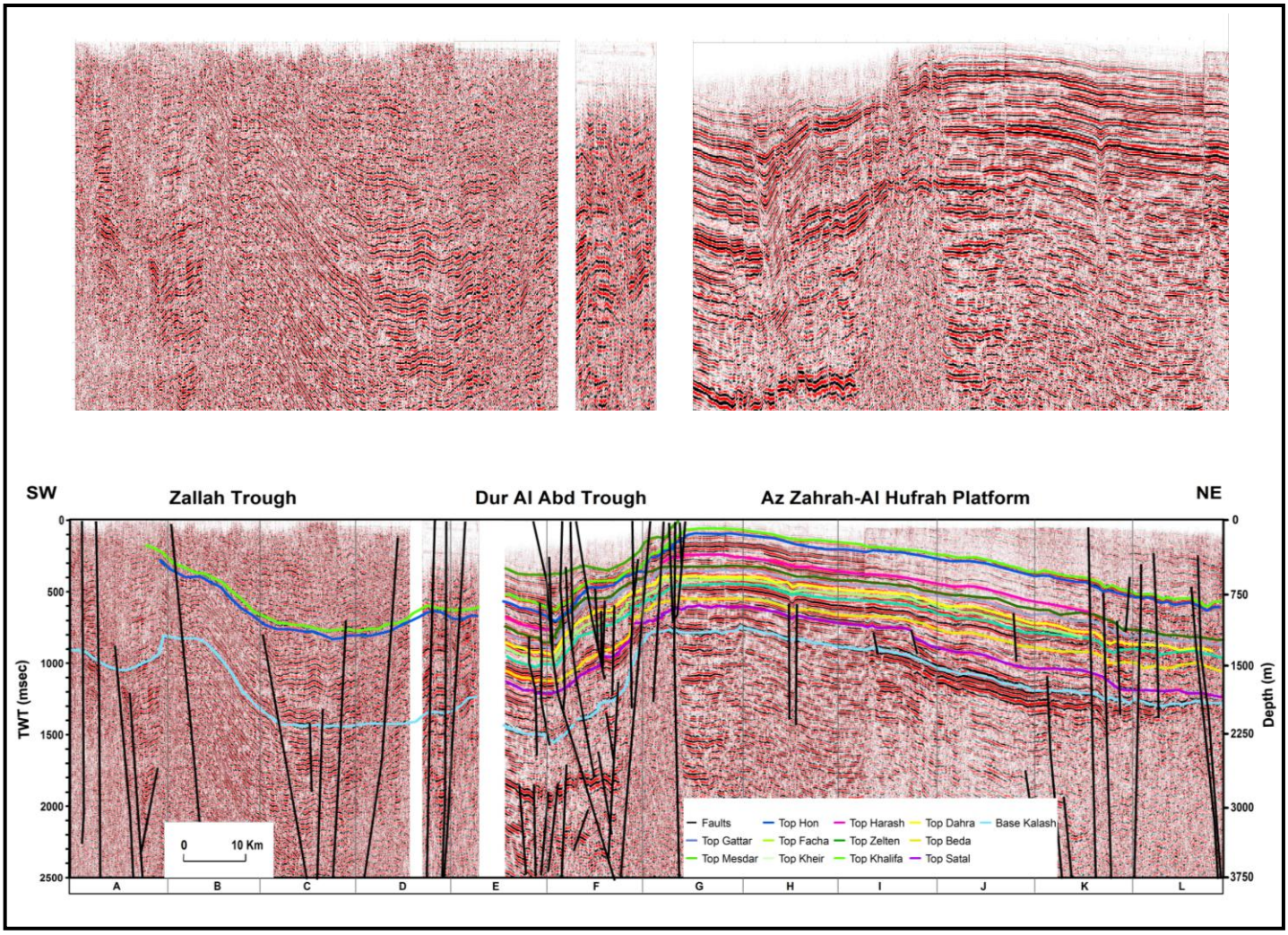


Fig. 6.8 Seismic cross section B-B' view of present day structure across the study area from the southwest to the northeast (See figure 1.4 for location).

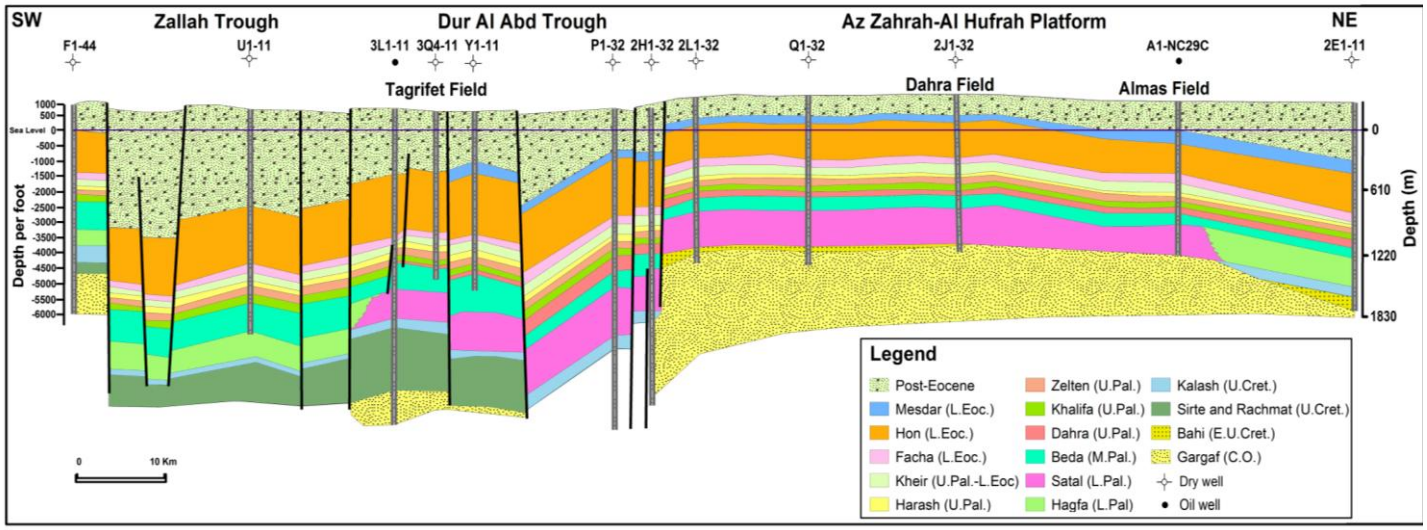


Fig. 6.9 Geological cross section B-B' view of present day structure across the study area from the southwest to the northeast (See figure 1.4 for location).

Based on the geological cross section (Fig. 6.9) about 305m (1000 feet) of post-Eocene sediments accumulated in the section drilled by well F1-44 on the eastern part of Waddan Uplift. This indicates that this part of Waddan Uplift was deeper during post-Eocene compared to further north (geological cross section A-A') where no post-Eocene sediments have been recognized. The Zallah Trough is now the adjoining structural block instead of the Dur al Abd Trough that appears further east across the Al Halayq Ridge. This part of the Zallah Trough most likely represents the deepest part of the trough with more than 1067m (3500 feet) accumulation of post-Eocene sediments. An absence of the Mesdar Member of the Gir Formation compared with Dur al abd Trough and Az Zahrah-Al Hufrah Platform, suggests that this part of the Zallah Trough was high during Late Lower Eocene. The last portion of seismic line OMV78-06 to the middle of line OMV80-15-09 (column D Fig.6.8) represents the north eastern side of the Zallah Trough in which the beds dip to the southwest and appear to exhibit only minor deformation although in this area the data quality is poor. Some of the normal faults have throws that increase with depth indicating repeated displacement.

To the east of the Zallah Trough, a high structure has been identified which possibly corresponds to the northern tip of Al Halayq Ridge (including its flanking hinge zones). Its crestal zone is located between columns D and E (Fig.6.8). Both sides of crestal zone are flanked by large, SW- and NE-dipping, normal faults and towards the north-east these flanking faults (in an area of good seismic data quality), a synclinal axis forms the western edge of the Dur al Abd Trough within which the horizons are interpreted to have been downthrown by a total of ≈ 400 ms from the Al Halayq Ridge at the deepest horizon level ("Gargaf"). This synclinal axis migrates north-eastward, up section to the middle point between columns F and G (Fig.6.8) at Mesdar and Hon reflector depths.

A heavily fractured area in the Dur al Abd Trough (centred on column F) displaying a number of NE- and SW-dipping faults, without a clear change of throw at all depths is likely to be another zone of wrench tectonics. To the east of this area, the hinge zone between the Dur al Abd Trough and the Az Zahrah-Al Hufrah Platform (the first quarter of column G Fig. 6.8) is characterized by a large fracture zone in which the majority of the faults appearing to be down to basin normal faults and smaller antithetic faults are also present. This hinge zone fault boundary corresponds to the Gedari fault and the largest vertical displacement of a reflector is the deepest interpreted seismic horizon with about 750 ms throw.

A significant monoclinal flexure (at the middle point between column F and G Fig. 6.8) forms the hanging wall to the Gedari fault. The monocline involves all interpreted

reflectors that are located above the fault. The structure dips to the SW, away from the fault and is bounded on its SW by synclinal and anticlinal fold axes. This monoclinal structure is characterized by steep dips of more than 60° that are greater on deeper horizons (base Kalash Reflector). These hangingwall folds of the Gedari fault system are characterized by several large, doubly plunging, asymmetric hangingwall synclines, the largest of which, the Syiah syncline bound the monocline from the west is known to be over 50 km long with westerly facing beds dipping up to 30° measured from the outcrop (Anketell and Kumati 1991b). The synclines are parallel to the principal tectonic direction, i.e. NW-SE. The doubly plunging synclines, where the plunge is toward this centre are widely recognized in the deepest part of the Gedari fault. The fault displacement varies within the fault surface where the displacement is zero at the fault tips and usually increases to a maximum near the centre of the fault surface led the fold plunging to that centre.

Many of the major faults in this Gedari hinge zone extend below the seismic section and these major faults branch out into smaller faults reminiscent of "flower structures" suggesting that the edge of the Dur al Abd Trough has been is the same large scale wrench tectonic zone that was discussed in relation to seismic cross section A-A'. It is thought to be that much of this deformation originated in the post-Oligocene period of the Sirt Basin. This accompanied inversion and compression that reactivated the area's horst and graben system and added a complex of strike-slip wrench faulting generated anticlines and synclines (Jerzykiewicz. et. al. 2002).

The geological cross section (Fig. 6.9) shows that in this area and there are significant differences in the stratigraphic record between the downthrown and upthrown side of the Gedari Fault Zone. Comparison of the wells drilled on both sides of the Gedari Fault Zone and seismic reflection section show that the total thickness of the Cretaceous and Tertiary strata on the downthrown side of the fault is two to three times greater than on the upthrown side (e.g. approx. 4145m (13,600') in well P1-32 vs. 1439m (4,720') in well HH1-32) (see Fig. 5.1). These thickness differences correspond to differences in accommodation space (or subsidence) on the opposite sides of the fault.

The Az Zahrah-Al Hufrah Platform is located east of the previous Gedari fault (columns G, H, I, J and the first quarter of column K Fig.6.8. It is crossed by the last two thirds of seismic line of 379 to about the first quarter of line V-2170. The platform is characterized by relatively unbroken post-Cretaceous sediments that generally dip gently and uniformly toward the northeast. There is some evidence for very sparse

deformation, that is mainly limited to deep faults with small throws rooted in the basement, but disappear upwards in the Paleocene and Eocene strata. The Satal Formation which is composed of carbonate "reef" build up seems to dominant part of the cross section that has been affected by the relatively low throw faults with normal displacements of 10-20 ms.

The hinge zone between the Az Zahrah-Al Hufrah Platform and the Maradah Trough (last quarter of column K and L Fig. 6.8) corresponds to the last portion of V-2170 and is characterized by typical down-to-basin faults that appear to have a normal throw, but which may also have a wrench component into the plane of section. It appears that the younger horizons in this area are cut by a more dense network of faults than on the Az Zahrah-Al Hufrah Platform, The majority of the faults show down-to-basin normal throws and seem to start in the basement and decrease in throw upwards, usually disappearing before the surface is reached.

6.5.3 Cross-section C-C'

This dip cross section is again a composite section, however in this case there are no gaps between the individual lines. The line trends WSW to ESE and is approximately 150 km long and crosses most of the structural domains that exist in the southern part of the study area (Fig. 1.4). It is composed from the west to east by five individual seismic lines of good data quality (NC131-90-43, NC131-82-10, NC131-82-10E, NC131-82-29 and 57-83-85) as shown in Figure 6.10. The section seems to be a more complicated part of the study area compared with cross section A-A' to the north and cross section B-B' crossing the central part of the study area.

The western end of this section intersects the Gargaf-Al Harug Al Aswad Uplift (first quarter of column A Fig. 6.10) (part of NC131-90-43) and then crosses the hinge zone between this and the Zallah Trough (last quarter of column A Fig. 6.10). The section then crosses the Zallah Trough (NC131-90-43, NC131-82-10 and part of NC131-82-10E) (columns B, C, D, and E Fig. 6.10). The last portion of seismic lines NC131-82-10E, all of line NC131-82-29 and part of line 57-83-85 cross the Al Halayq Ridge portion (columns F, G, H, and I Fig. 6.10) followed by Abu Tumayam Trough (column J Fig. 6.10) before terminating on the western part of Az Zahrah-Al Hufrah Platform or the Gattar Ridge (columns K and L Fig. 6.10) as it is mapped in this region. A parallel geological cross section was constructed from 6 wells started with well A1-NC74C at Gargaf-Al Harug Al Aswad Uplift (Al Qargaf Arch) to well G1-57 at the southwestern periphery of Az Zahrah-Al Hufrah Platform to the east (Fig. 6.11).

The seismic data quality is only fair to poor on line NC131-90-43 at the western end of this cross section where it intersects the Gargaf / Al Harug Al Aswad Uplift (Al Qargaf Arch). In this region, the reflector sequence appears to be an eastward dipping (and thickening) sequence of undulating sediments that are intermittently broken by down-to-basin (and a few down-to-margin) faults. Most of these faults appear to extend from the basement to the surface and have an approximately constant throw along their entire length. Displacement is distributed among several fault strands that are seen to coalesce at depth suggesting a typical 'flower structure' located at the middle point of column A (Fig. 6.10). There is an apparent fault (at the middle of column C Fig. 6.10) located unfortunately in a poor part of this section shows potentially a very big offset (c. 1000ms) of the blue and pink horizons and it can not to be recognized clearly on the geological cross section (Fig. 11) due to lack of wells surrounding to it. This fault seems to be bounding the deepest part of the Zallah Trough which spans columns C to E (Fig. 6.10).

Moving to the east, the individual sequence packages in the Zallah Trough have almost constant thickness and dip towards two synclinal axes, confined to columns D and E (Fig. 6.10). The lines NC131-82-10 and NC131-82-10E (column E Fig. 6.10) are characterized by a deeper synclinal axial zone that is heavily tilted and fractured by several large basement-to-surface normal faults. It is flanked on the western side by a small horst block that formed between N-S striking, basement rooted faults.

The bottom of the asymmetric syncline increases with depth towards to its western flank. This syncline is a graben feature that was formed on a horst block that cut the near top Zelten and near base Kalash seismic time markers prior to Eocene to Recent faulting.

In this area based on the geological cross section (Fig. 6.11) this asymmetrical syncline (in the middle point between column D and E shown in Fig. 6.10 and eastern side of Zallah Trough shown in Fig. 6.11) is the deepest in the study area where the total depth exceeds 3040m (10000 feet) in well A3-NC131. Oil produced wells (such as A1-NC131, A2-NC131 and A3-NC131) of the Karim Oil Field were located on the small horsts (last quarter of column D Fig. 6.10) These attractive exploration targets in the Eocene Gir (Facha Member) carbonates are flanked on either side by the mini-depocentres of the Zallah Trough. The hydrocarbons probably migrated into the horst from the two Zallah Trough "kitchens" that flank it to the east and west (see chapter 3).

East of the fault bounded NC131-82-10 synclinal depocentre, the strata rise steeply eastwards (last quarter of column E Fig. 6.10) crossing at least three down-to-the-Zallah

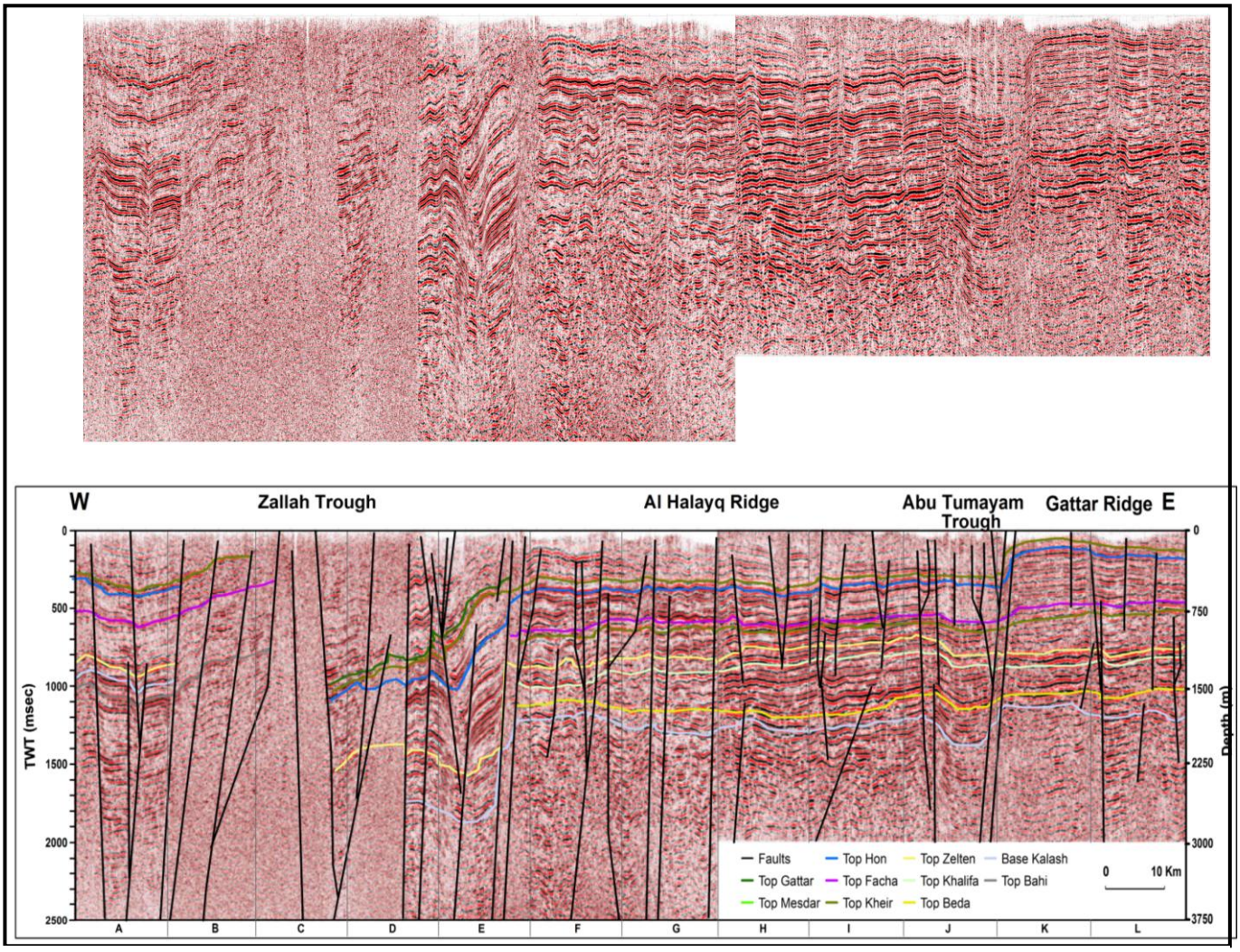


Fig. 6.10 Seismic cross section C-C' view of present day structure across the study area from the southwest to the northeast (See figure 1.4 for location).

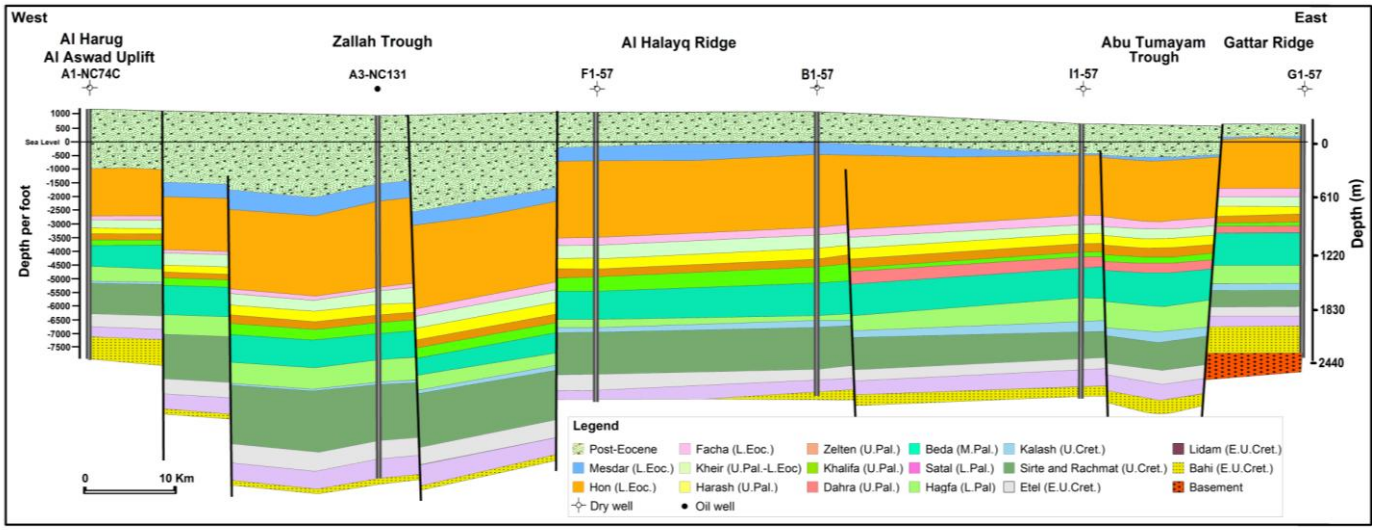


Fig. 6.11 Geological cross section C-C' view of present day structure across the study area from the southwest to the northeast (See figure 1.4 for location).

Trough normal faults) with about 600 ms total throw to a narrow hinge zone along the western flank of the Al Halayq Ridge. This hinge zone (Column G) consists of two or more tilted fault block "steps" separated from the Al Halayq Ridge by three or more large, basement-to-surface normal faults with down-to-basin variable throws of up to 150 ms.

The Al Halayq Ridge is located on a part of line NC131-82-10E, across NC131-82-29 and a part of line 57-83-85 (columns F, G, H, and I Fig. 6.10) and in general the reflectors / beds on this ridge are flat lying and the entire rock sequence appears to thin. It is clear that the bedding at the western part of this ridge has been more intensely deformed by basement driven faulting, than the eastern half although the number of faults seems to be the same. Most of the basement faults do not reach the surface, but at least two of them at column I (Fig. 6.10) appear to crop out.

North eastwards of this hinge zone, cross section C-C' enters the downwarped (graben?) Abu Tumaym, which (at column J Fig. 6.10) is the southern extension of Dur al Abd Trough across an E-W trending barrier. The deepest point of this trough is at the middle point of column J (Fig. 6.10) and within it the sediments are gently bowed downwards, with no apparent thickening, towards the trough's centre.

East of the trough, a faulted zone belongs to the Gattar Ridge, located on columns K and L (Fig. 6.10). This zone is bounded to the west by at least two large faults that evidently extend from the basement to the surface. This hinge zone is bounded to the west by at least two large faults that evidently extend from the basement to the surface. Within this area the sediments dip gently to the west, are undeformed and have constant thickness which indicates it subjected to less tectonic activities than western side of this hinge zone. Gattar Ridge is most likely to be a part of Az Zahrah-Al Hufrah Platform with a similar stratigraphic sequence down to the basement evident in well G1-57 (Fig. 6.11).

6.5.4 Cross-section D-D'

Cross-section D-D' is a strike direction traverse trending NW-SE for about 115 km (Fig. 1.4). It is located in the northeast part of the study area and is composed of 9 individual seismic lines respectively; 32-302TD-7, T-29X, T-29X-1, 555, 467, 516, 393, 407 and 11-90-11) as shown on table (6.2). With the exception of one, small (≈ 1 km) offset gap between lines 32-302TD-7 and T-29X, cross-section D-D' is continuous, however it contains some bends and steps.

The section is located near the centre of the Az Zahrah-Al Hufrah Platform and crosses most of the oil fields that have been discovered on this platform (Fig. 1.4). This strike cross section clearly shows that this part of the platform has mostly uniform horizontal bedding, except in the region of the first two columns (A and B) of Fig. 6.12. The sections confirm that the strike direction (NW-SE) shows less structural complexity with most of the faults located below the base Kalash reflector.

The seismic cross section is accompanied by a geological cross section along the similar trend and location. The geological cross-section is constructed from 14 wells from well L1-32 in the northwest to well A56-11 in the central part of Az Zahrah-Al Hufrah Platform to the southeast (Fig. 6.13).

In the northwest, on the central part of the Az Zahrah-Al Hufrah Platform, (seismic line 32-302TD-7, columns A and B Fig. 6.12) the reflectors drop off to the north. This is due to a combination of shallow horizon dip and the combined throws of ten or more large faults that mostly dip to the north. These extend from the basement to the surface and may be down-to-north transverse (accommodation) faults trending NE-SW thought to be bounding the platform from the north. They seem to affect the whole of the stratigraphic sequence of this region, but given there is no change in the thickness of the layers throughout the whole stratigraphic sequence as shown in Fig. 6.13 it must mean these faults are post-Eocene in age. In general, through the rest of the section, most of the reflectors are generally flat lying and approximately constant thickness and faults mainly occur below the base Kalash horizon with exception of columns E and F (Fig. 6.12) where some faults are located above this horizon.

The highest structural point of the line is located in the middle point between columns E and F of Fig (6.12) and this zone appears to be the “crest block” of this portion of the Az Zahrah-Al Hufrah Platform. Within this “core block” the beds rise gently upwards in location close to the Almas Oil Field and the Arbab Oil Field. Also both the Az Zahrah and the Al Hufrah Oil Fields are mostly located in this core area of the Az Zahrah-Al Hufrah Platform.

Within the Az Zahrah-Al Hufrah Platform, and especially to the south of the “core block” (columns G to L Fig. 6.12) below base Kalash horizon (Upper Cretaceous) sediments show indications of small highs (horsts?) and lows (grabens?) generally bounded by normal faults with upward diminishing throws. The axis of the first syncline is located at column G (Fig. 6.12) and the amplitude of its “low” decreases upwards with basin fill and is best expressed at the Base Kalash/top Sirt (light blue) reflector level. Examples of these troughs can be seen on columns J, K, and L (Fig.

6.12). Each of these troughs (and their separating grabens), appear to be bounded by normal faults that are rooted deep in the basement and diminish in throw upwards to end in Late Cretaceous at the base Kalash/top Sirte (light blue reflector).

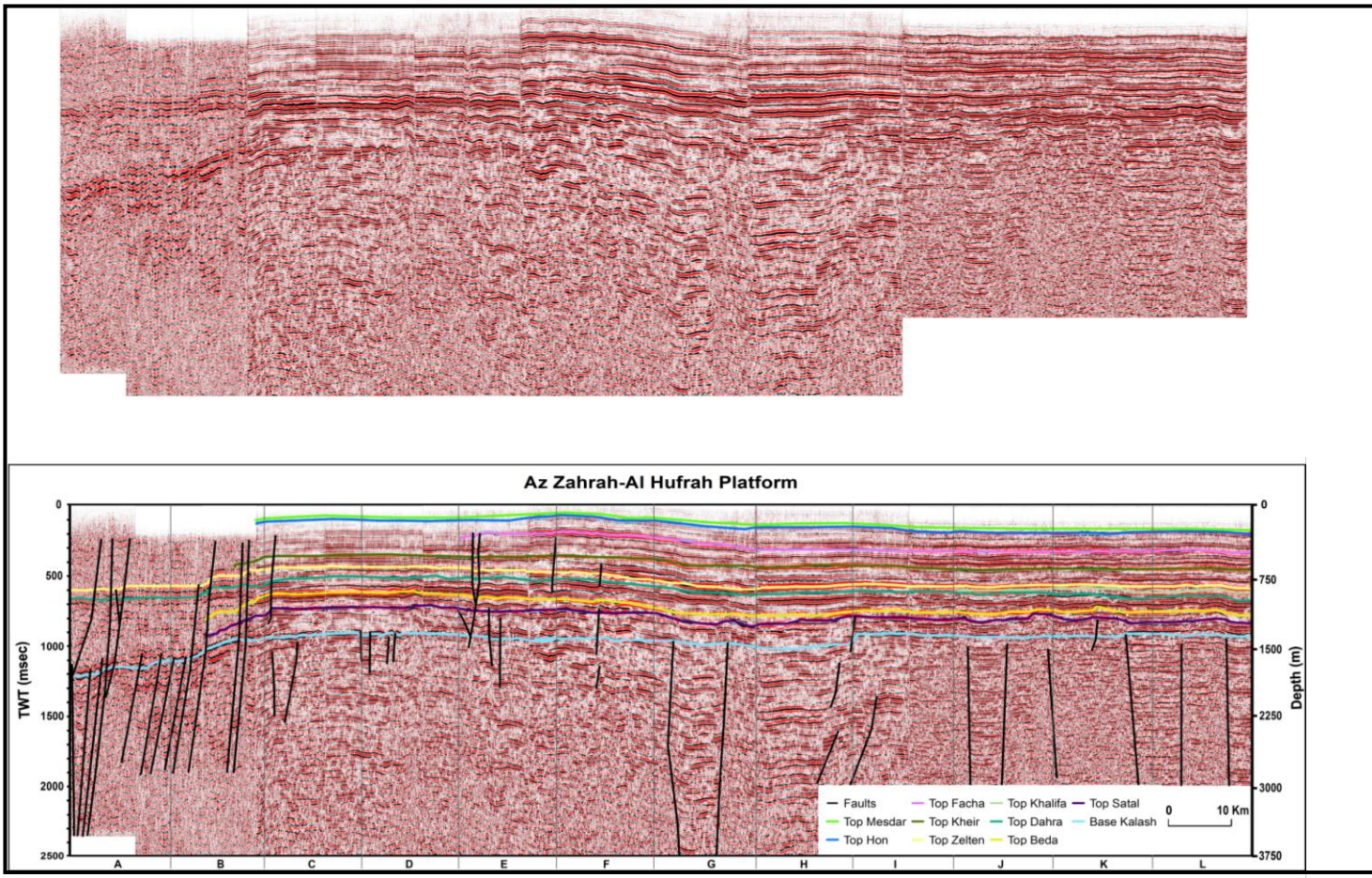


Fig. 6.12 Seismic cross section D-D' view of present day structure across the study area from the southwest to the northeast (See figure 1.4 for location).

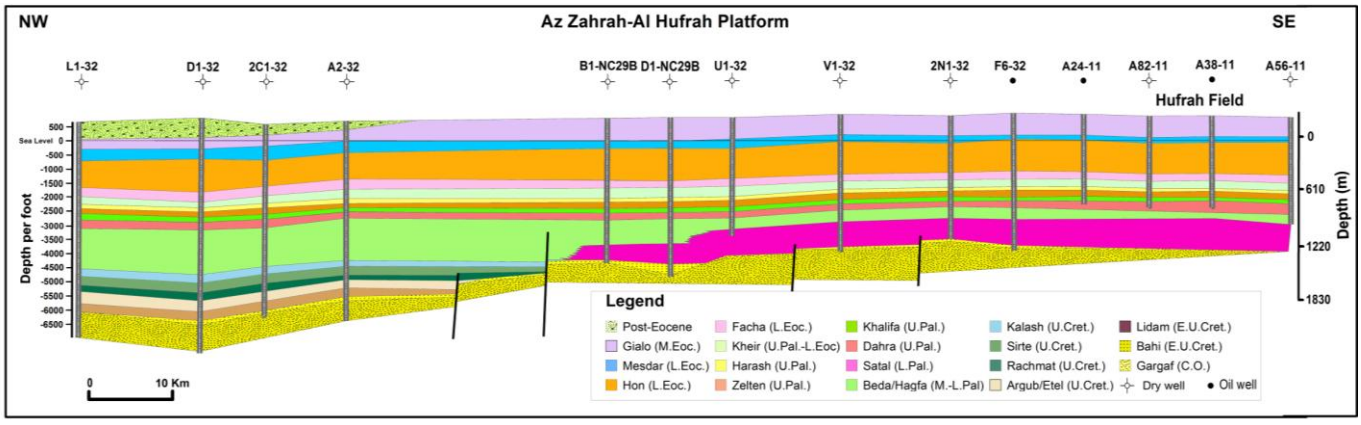


Fig. 6.13 Geological cross section D-D' view of present day structure across the study area from the southwest to the northeast (See figure 1.4 for location).

In general as illustrated, display of the seismic and well data together strengthens the interpretation of both. Subtle, uninterpreted faults indicated by the well data can be interpreted on the seismic data, and changes in the patterns in the seismic data can influence the stratigraphic interpretation of the well data. Based on all the interpreted seismic and well-based geological cross sections the study area seems to be more tectonically and structurally complicated to the south. The resulting increasing number of the faults has led to more tectonic blocks being defined in the south. The Waddan Uplift, Dur al abd Trough, and Az Zahrah-Al Hufrah Platform are intersected on cross section A-A' on the northern part of the area to Waddan Uplift, Zallah Trough, the Dur al Abd Trough, and Az Zahrah-Al Hufrah Platform on cross section B-B' in the central part of the area.

The Al Harug Al Aswad Uplift (Al Qargaf Arch), Zallah Trough, Al Halayq Ridge, Abu Tumayam Trough and Gattar Ridge or southwestern fringe of Az Zahrah-Al Hufrah Platform is intersected on cross section C-C' to the south of the area. Conversely, the strike-parallel cross section D-D' shows that the most of the reflectors are generally flat lying and approximately constant thickness and faults are mainly occur below base Kalash horizon indicating that the strike direction cross section (NW-SE) is less structurally complicated compared to the NE-SW trending cross sections. Also the general structure of the study area is illustrated by normal faults which are approximately symmetrically distributed around the main structural elements extend up to the surface and by inference the main phase of active extension must be Late Cretaceous. Some of these faults below base Kalash might be related to the Early Cretaceous extension that might be NW-SE orientated as shown by the isopach maps in Chapter 4.

Many of these normal faults which trend NW-SE and NE-SW are clearly offset or disrupt most of the sedimentary sequence particularly the near base Kalash marker indicating that they penetrate deep into the section, probably into the Precambrian basement that directly underlies this horizon on the footwalls blocks. Some folds have been identified in the study area parallel to the major faults are interpreted to have been either generated by compaction in the troughs or they may have connected with subsidence movements during the filling of the Sirt Basin.

6.6 Seismic subsurface maps

The 2D seismic data was used to define principal horizons based on key seismostratigraphic features. This study can be considered a regional study and for this

reason these key horizons, that were regionally or semi regionally correlatable, served as time markers and contribute to understanding of the structural configuration of the area. They are also chosen to obtain regional thickness, structural contour, and time maps of the area.

Generally the created seismic horizon time structure maps were generated by griding the correlated time points in order to highlight the main depocentres across the area and be able to constrain the amount of extension across the faults within each age. In some areas, especially in extensional terrains, (Groshong, 2006) folds with steep limb dips are rare or do not occur at all and so the closely spaced contours could be replaced by a fault on the basis of consistency with the local structural style.

Also the high and low areas on a structure contour either isochron or isopach maps of a marker horizon should be explained as blocks most likely separated faults and also faults cause characteristic thickness variations on isopach maps (Hintze 1971).

6.6.1 Time structure maps

Many time structural maps were generated to define the main structural trends across the study area between the Late Cretaceous, the start of main rift phase and the Late Eocene, post rift phase. The created seismic horizon time structure maps (Figs. 6.14 – 6.18) were made by gridding the correlated time picks and the intersections of the identified major faults in plan view. Editing of contour points was, sometimes necessary where the contours were near faults. Since the seismic time markers are very close together, the fault intersects from these seismic time markers were considered acceptable to include in the construction of all of the time structure maps, as the shift in fault pattern would be very small.

The dominant faults picked on the seismic data are normal faults trending north-northwest to south-southeast and northwest to southeast, dipping mainly southwest or northeast towards the basin. The central part of the area is characterized by a major north-northwest to south-southeast-trending elongate low representing the Zallah Sub Basin (Trough). It is cut in places by an important set of northeast trending faults that segment the trough into more depocenters (see Chapter 4). The interpreted major faults also show an en-echelon style that might reflect oblique extension.

6.6.1.1 Near base Kalash

The near-Base Kalash is the deepest regional horizon that was generated in this study and ranges from 337 ms (TWT) at its shallowest on the Waddan Uplift to 2100 ms

(TWT) in the Zallah sub-basin at its deepest. This horizon map (Fig. 6.14) shows two sets of elongated structural closure domains. An elongate NW-SE-trending structural low occurs in the central and eastern portion of the area, deepens and contains several large normal faults typical of a classical graben (Fig. 6.15). The extent of this graben is indicated by the closely spaced contours at approximately 1200 ms. In the west and southwest, the closure trends NE-SW, where as in the north it changes to a more NNE-SSW direction.

A fault bounded structural high is apparent on the Az Zahrah-Al Hufrah Platform (Fig. 6.14), continues into the Dur al Abd Trough northwest of the Az Zahrah and Al Hufrah fields and also apparent on the Al Halayaq Ridge to the south and east of the study area. Potential fault bounded closures (high or low) also exists to the east of the Waddan Uplift near the western extent of the Dur al Abd Trough.

In the northeast portion of the study area from the Az Zahrah-Al Hufrah Platform north-east onto the Maradah (Hagfa) Trough, the time structure falls off into a structurally lower area with values down to 1500 ms.

A structurally lower area is also shown on the Zallah Sub Basin. At 17.8° E and 29° N (Fig. 6.15) the Gedari fault branches to the northwest to link up with the southernmost the Qarat Ash Shush fault and then at 17.75° E and 29.5° N links with the south Mabrouk fault (For fault names see Figure 6.1) forming what might be a near-vertical flower type structures suggesting strike-slip motion (e.g., Harding, 1985). Deformation is transferred in a step-wise fashion toward the southwest.

6.6.1.2 Near top Dahra

The near Top Dahra horizon is shallower and it's contours range from 250 ms on the Az Zahrah-Al Hufrah Platform to 1500 ms on the eastern part Zallah sub-basin (Fig. 6.16). It is characterized by a low area in the central part of study area from the south Zallah Trough up to the Dur al Abd Trough shown by TWT intervals between 1000 to 1500 ms (Fig. 6.15). Another low is present in the northeast portion of the study area from the Az Zahrah-Al Hufrah Platform north-east into the Maradah (Hagfa) Trough, the time structure contours falls off into this structurally lower area to 1500 ms. The fault intersects determined at most of the seismic time horizons were used to create the near Top Dahra time structure map, and it shows the major faults of the study area.

A simple fault-bounded structural high (Fig. 6.17) is evident northwest to southeast along the Az Zahrah-Al Hufrah Platform and through the Az Zahrah Field. One small fault-bounded closure exists in the Dur al Abd Trough to the northwest of the Az

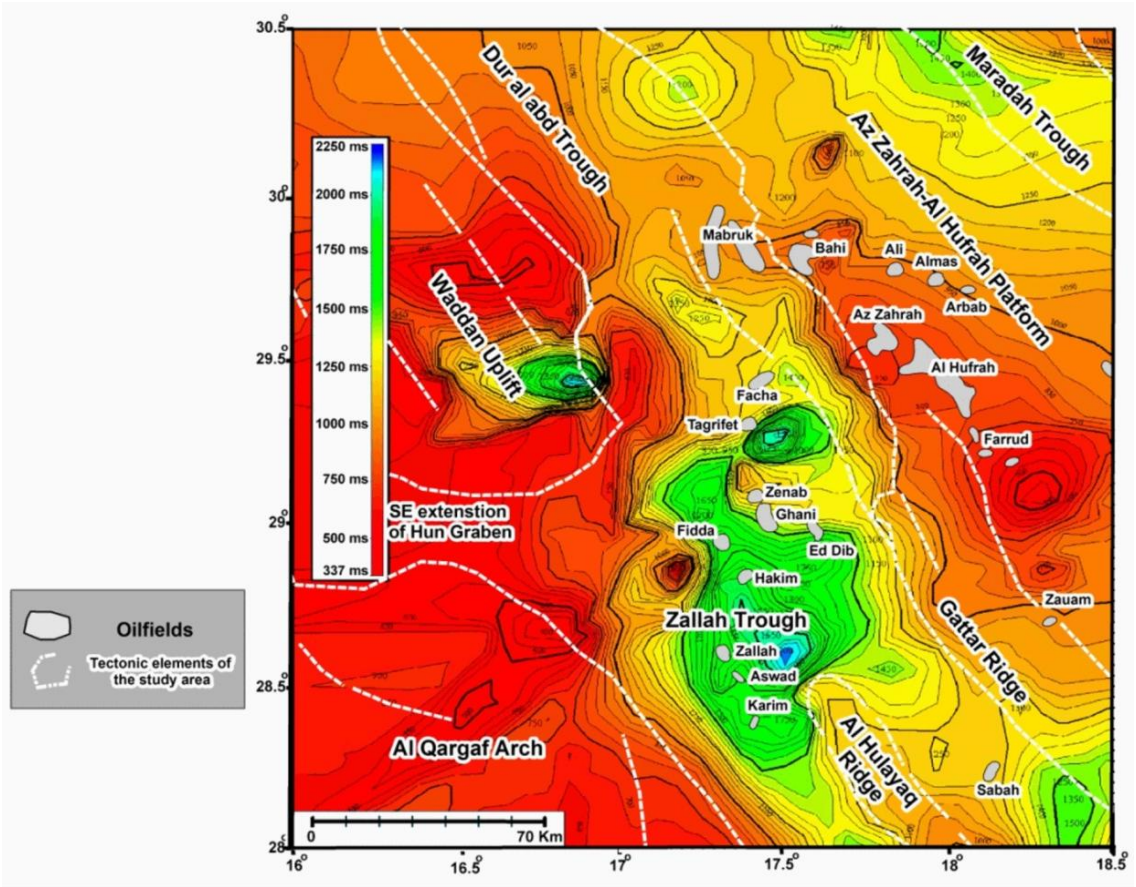


Fig. 6.14 The time contour map of near base Kalash

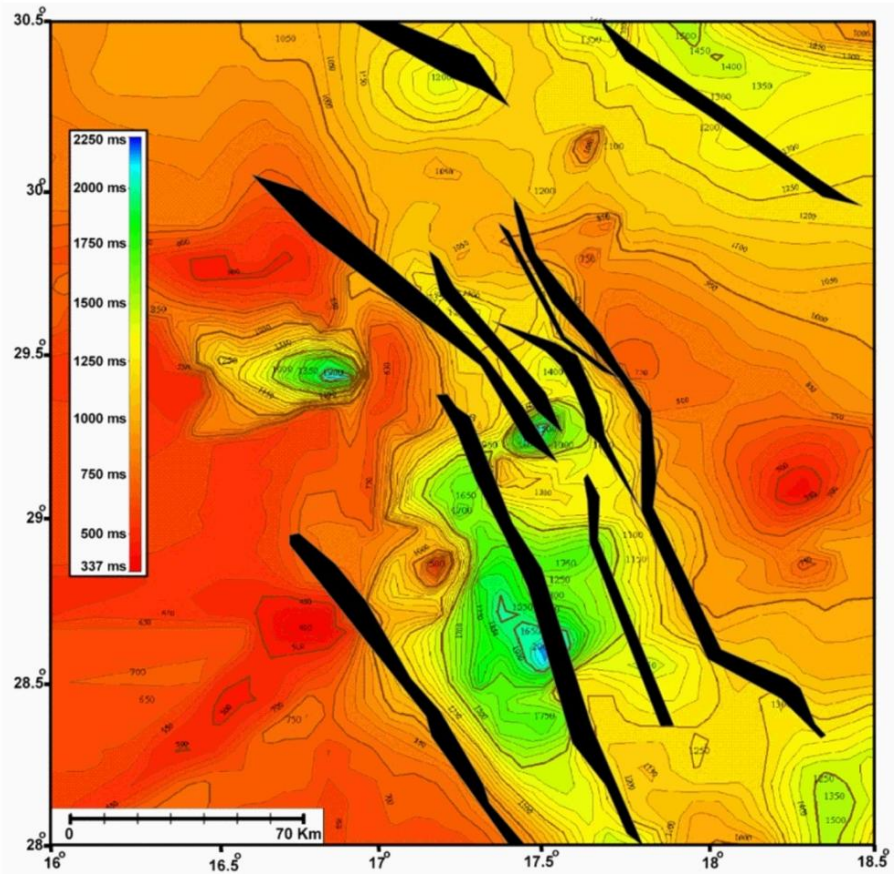


Fig. 6.15 The time structure contour map of near base Kalash

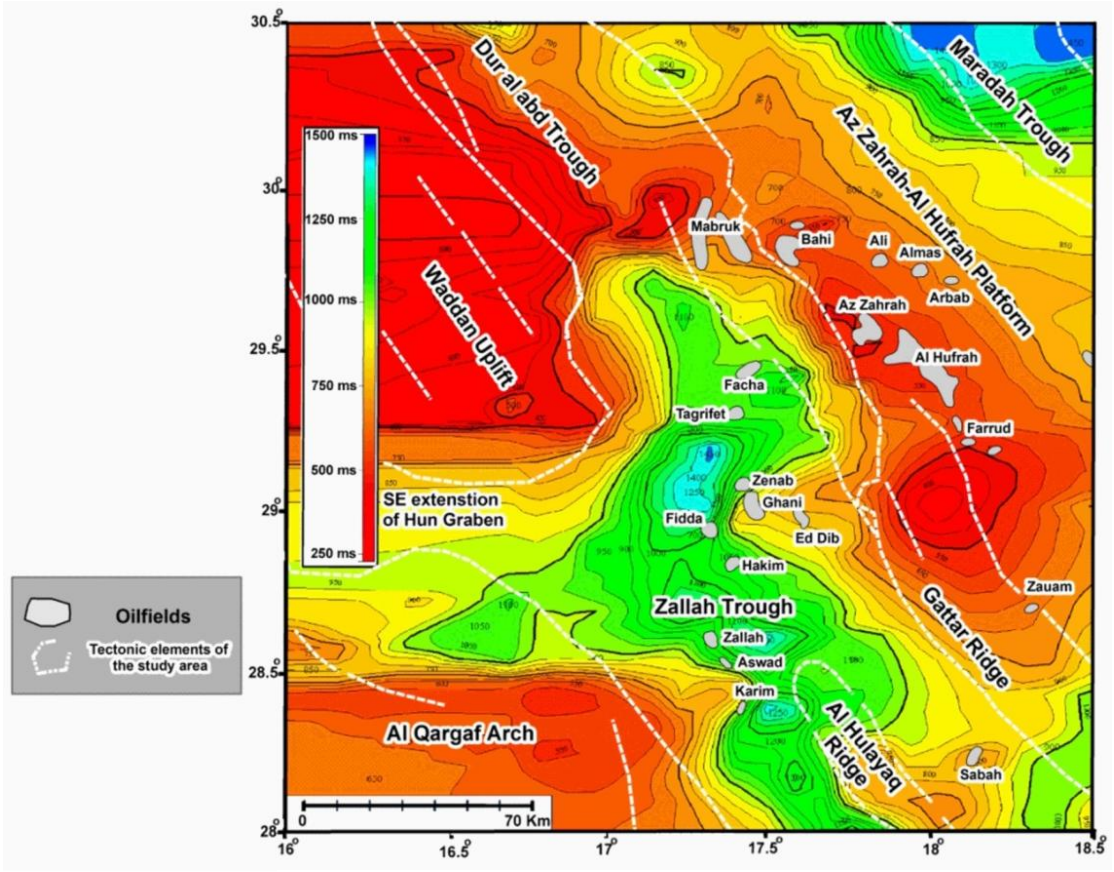


Fig. 6.16 The time contour map of near top Dahra

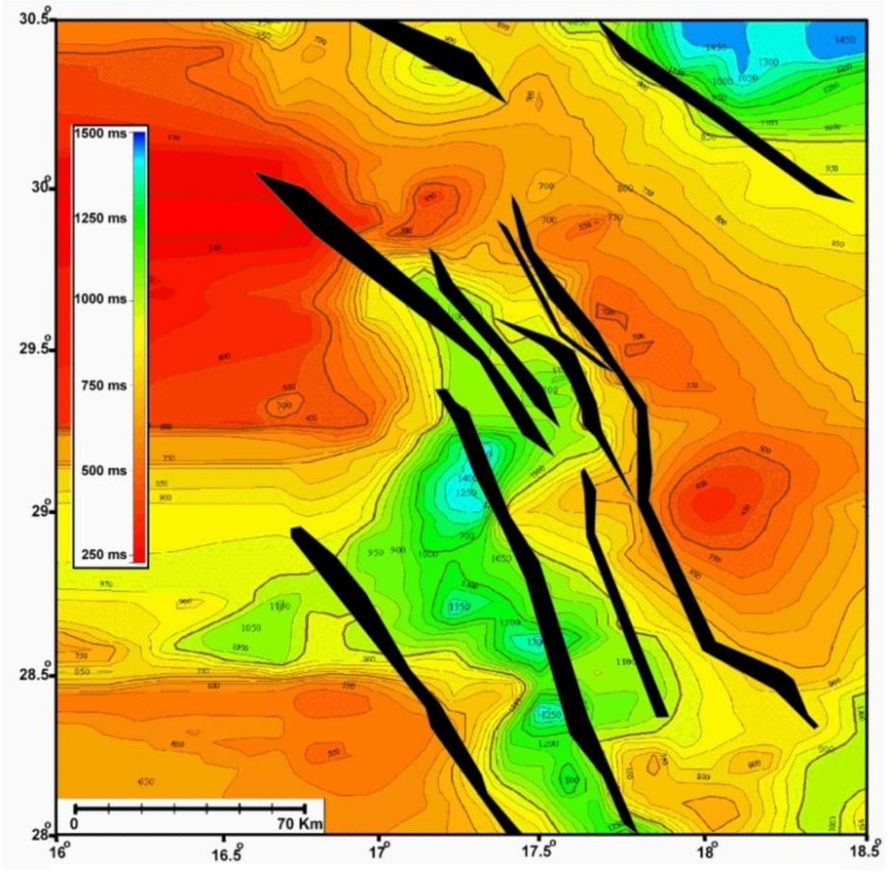


Fig. 6.17 The time structure contour map of Near Top Dahra

Zahrah hydrocarbon field. Another fault-bounded closure is evident in the southern portion of the study area occupied by the Al Halayaq Ridge.

6.6.1.3 Near top Hon

Contours on the near Top Hon range from 0 ms on the Waddan Uplift and 130 ms on the Az Zahrah-Al Hufrah Platform to 1200ms on the southern part of the Zallah Sub Basin (Trough). At outcrop, the Hon Equivalent Al Jir Formation (see Fig 1.3) on the Waddan Uplift is the equivalent to the near Top Hon 0 to 100 ms seismic time contours on the western portion of the study area (Fig. 6.18).

The deepest part of this horizon defines a smaller basin than the Near Top Dahra in the Zallah Trough) with small depocentres in the north and south. Northeast of the study Az Zahrah-Al Hufrah Platform north, the time structure falls off into into the Maradah (Hagfa) Trough.

A fault bounded structural high (Fig. 6.19) is apparent on and around the Az Zahrah-Al Hufrah Platform. Fault-bounded closures are also apparent on the Al Halayq Ridge to the south and east of the study area. Simple fault-bounded closures are also visible in the northern portion of the Dur al Abd Trough on and to the north of the study area.

6.6.2 Isochron maps

It has been recognized in this study that the resolution of the seismic reflection data is satisfactory only in the stratigraphic range between Late Cretaceous and Early Eocene times. As a result, the analysis of the seismic sections provides more precise definition of the Paleocene basin architecture than in the other stratigraphic intervals. The Paleocene basin fill is very important because it contains most of the oil fields of the study area. Based on the time structure maps and the cross section interpretations (See section 6.5 and 6.6.1), faulting is noticeable, however, the quality of seismic in some parts of the study area appear to be low which may create an impression that the tectonic deformation of the basin fill is not very extensive. Unfortunately, the resolution of the seismic sections within these time intervals is not adequate and detailed interpretation of the basin architecture of the pre-Late Cretaceous and post-Early Eocene intervals is not possible on the basis of seismic sections to hand.

An isochron represents the time interval between two events. Isochron maps are created in SeisWorks/2D by flattening the shallower horizon, which is then treated as a datum with a time value of 0. The distance (in milliseconds) from it to a deeper horizon is computed on a trace-by-trace basis. These data can then be displayed in map views,

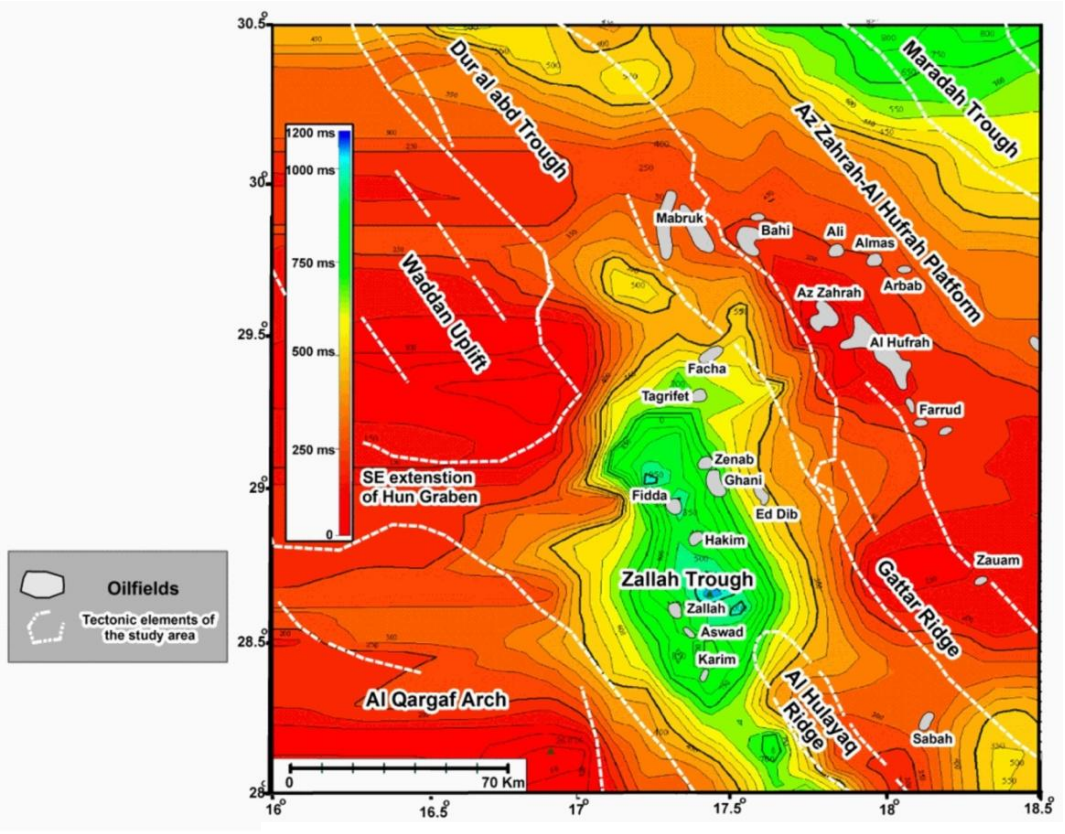


Fig. 6.18 The time contour map of near top Hon

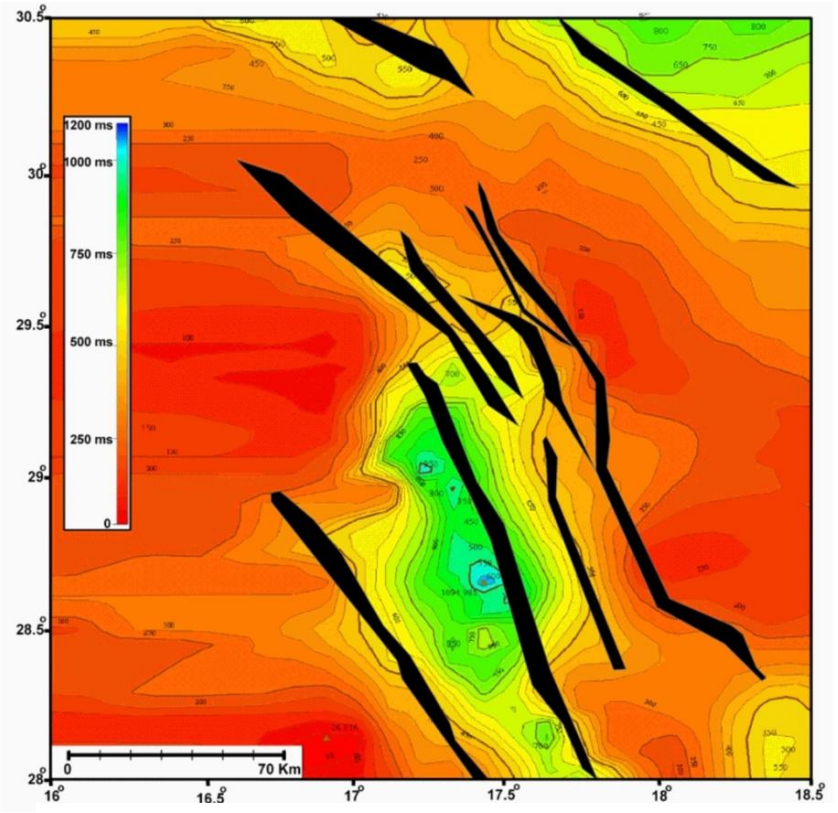


Fig. 6.19 The time structure contour map of near top Hon

where the minimum and maximum values represent the minimum interval and maximum interval between the two horizons. An isochron of two seismic time markers indicates the time structure of the deeper horizon at the time the shallower horizon was deposited.

A linear trend of closely spaced structure contours that form a monoclinal fold on the marker surface may provide a clue to the presence of a fault but not necessarily give an accurate location. For example, the traces of most faults in the study area are in regions of closely spaced contours and follow the contours of the block boundaries.

The contours are colour coded with blues showing the structurally high time areas (isochron thins) and reds indicating the structurally low time areas (isochron thicks). Of the many isochron maps that were created during the seismic data interpretation of the study area, only 3 isochron maps were selected to represent different periods of tectono-stratigraphy to define the main structural trends across the area between the Late Cretaceous, and Upper Eocene times.

6.6.2.1 Near top Satal to near base Kalash (Late Cretaceous to Early Paleocene)

At Top Satal time, about 5 closures (thick regions) are present in the area (Fig. 6.20). A major northwest to southeast trend is strongly reflected in this map as a large closure over the Gattar Ridge on the southeast portion of the Az Zahrah-Al Hufrah Platform.

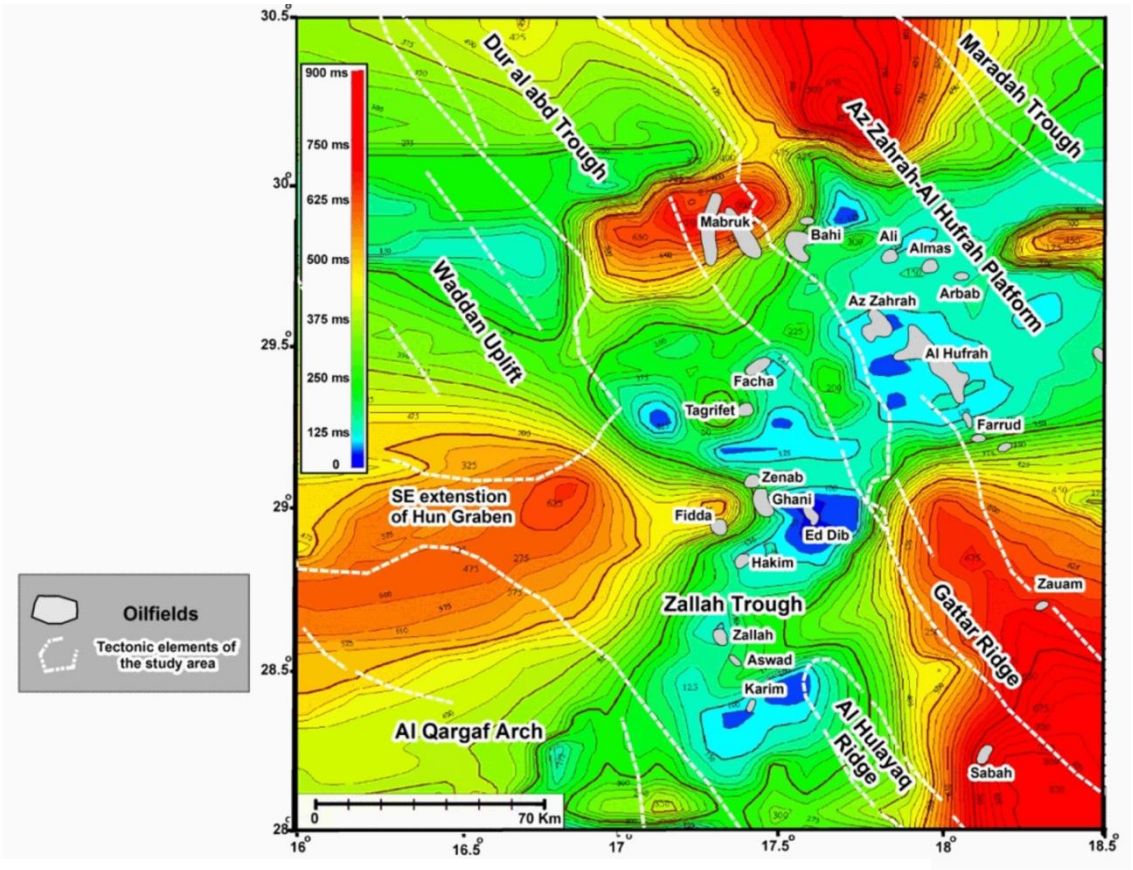


Fig. 6.20 The near top Satal to near base Kalash isochron contour map.

In the northern portion of the area, two other smaller simple closures are apparent which trend northeast and northwest appear to be separated at that time by an anticlinal ridge trending northeast-southwest from the Gattar Ridge. A fourth closure is apparent over the extension of Hun Graben separated by ridges from surrounding closures.

The fifth thick region is a smaller simple closure that may be identified on the northeastern part of Az Zahrah-Al Hufrah Platform trending mainly in an east-west direction. This section of the stratigraphy of the area represents the combination of the Kalash and Satal Formations and attains a thickness of 900 ms while it is 30 ms (TWT) at its thinnest. The Kalash Formation is regionally widespread and based on borehole data, it ranges in thickness from about 30.5m (100') to 61m (200') and attains greatest thicknesses in areas where the upper Satal carbonate? 'buildup' is present.

The Satal attains a gross thickness of up to 549m (1800') in the southern portion of the Az Zahrah-Al Hufrah Platform over the Gattar Ridge. In contrast, this horizon is thinner in the trough areas which has led to the formation of an apparently elongate linear thin trending northeast-southwest (0 – 250 ms) starting from Zallah Trough, passing across the Dur al Abd Trough, extending to Az Zahrah-Al Hufrah Platform where it separated the platform into two depocentres as shown in figure (6.20). Based on borehole data the thinning of Satal Formation in the troughs is related to a facies change to the Hagfa Shale.

6.6.2.2 Near top Harash to near top Zelten (Middle Paleocene to Late Paleocene).

Four major depocentres appear between these horizons (Fig. 6.21). The main depocentre of the area is slightly migrated toward the south central part of the study area and is shows the formation of the Zallah sub-basin. This area appeared thin on the previous isochron map. Another active zone is observed in the northen part of the Az Zahrah-Al Hufrah Platform surrounding the Mabruk oilfield. It is semi-circular in shape trending northeast-southwest direction with a thickness is varies ranging from 60 to 250 ms.

At Top Harash time, a simple closure in thickness contours is apparent on the southern portion of the Az Zahrah-Al Hufrah Platform surrounding the Farrud oilfield. This simple closure may be shown to extend to the Gattar Ridge in the southeasten portion of the study area. A fourth closure is located towards Maradah Trough where it sits on the boundary with Az Zahrah-Al Hufrah Platform with an east-west trend.

Overall, the Middle to Late Paleocene thickness varies from 10 to 320 ms however the dominant thickness is between 10 and 180 ms. According to borehole data, its thickness varies between 23m (75') and 30.49m (100').

6.6.2.3 Near top Hon to near top Facha (Late Lower Eocene to Early Upper Eocene).

This map (Fig. 6.22) shows clearly a big closure in thickness contours with a ENE-WNW trend exists in the south central part of the study area ranging in thickness from 200 to 500 ms extending from the northeast corner of the Zallah Sub Basin (over Zallah, Aswad, and Karim oilfields) to the southern portion of Az Zahrah-Al Hufrah Platform surrounding the Zauam oilfield (Fig. 6.22) which suggests an elongated NE-SW rift initiated during that age in this portion of the study area.

It is separated from another simple closure trending NW-SE in the central part of the study area that appears to be controlled by northeast-southwest trending lineaments. The thickness varies from 0 to 530 ms with a dominant thickness between 0 and 200 ms.

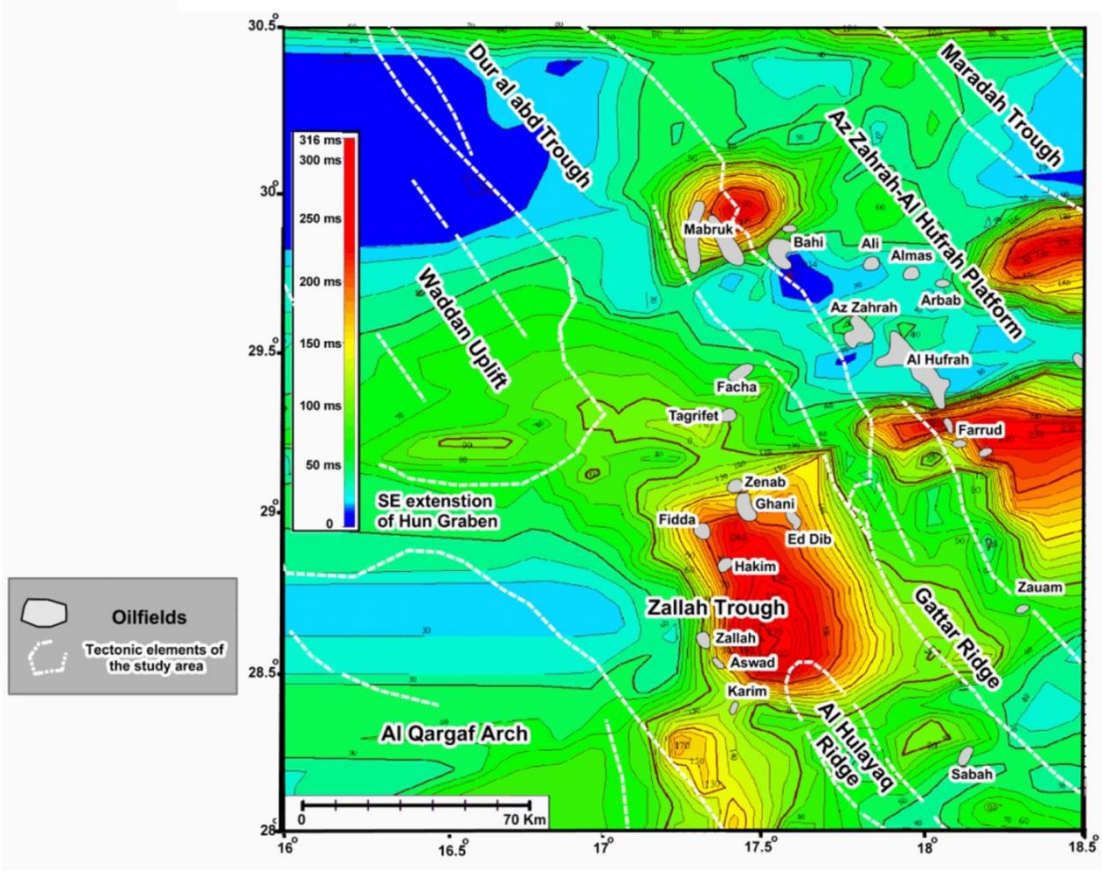


Fig. 6.21 The near top Harash to near top Zelten isochron contour

6.6.3 Velocity analysis and isopach (Thickness) maps

Landmark SeisWorks software which was used in this study produces maps in two-way time (TWT) whilst a meaningful interpretation needs to be displayed in depth. The main

task of seismic data interpretation is to construct contour seismic maps showing the two way time to a reflector as picked on the seismic sections. The isochron maps are the most important products that are created using two-way time (TWT), but to generate depth (isopachs or isodepth) maps requires a seismic time-depth conversion process. The depth conversion process is usually carried out using formation average velocity information derived from well data. So, it is necessary to convert from time(s) to depth (ft or m), and in this regard we should know the seismic velocity of the material derived from subsurface borehole logs data.

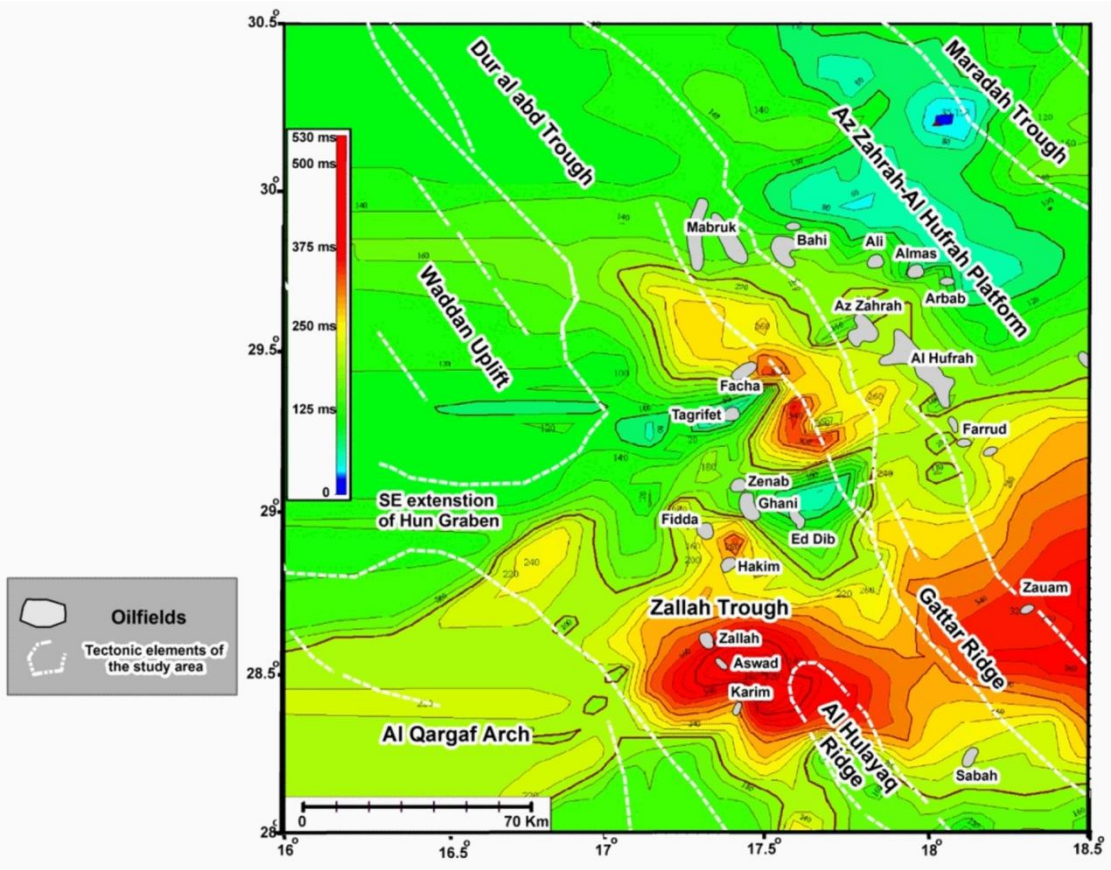


Fig. 6.22 The near top Hon to near top Facha isochron contour map.

Velocity is widely used in various areas in seismic data processing (such as multifold seismic data stacking and migration) and seismic stratigraphic interpretation, as well as determination of information regarding structural geology and lithology. Seismic velocity is also used to obtain information about anisotropy and heterogeneity of the elastic medium. Many considerable researches in this regard have been published during the last three decades (Ivansson, 1985; Chiu and Stewart, 1987; Iverson, 1988; Zhu and McMechan, 1988; Abdalla and Stewart, 1990; Stewart, 1990).

Average seismic velocity is affected by rock properties such as:

1. Porosity
2. Lithification
3. Pore pressure
4. Fluid saturation

The average velocity V is simply defined as the velocity over a certain reflecting surface below the seismic reference datum (Dobrin, 1976).

$V = Z/T$

Where: Z: is the depth to the reflecting surface from the wells, and T: is the one way transit time to the reflector from the same reference. Tables 6.3, and 6.4 show the sonic wells used to calculate velocity and depth to near base Kalash and top Hon Surfaces. The resultant average velocity maps were used to convert the produced isochron maps to isopach (Thickness) maps in this study.

6.6.3.1 Velocity analysis

6.6.3.1.1 Average velocity to the near base Kalash surface

The near base Kalash surface is approximately equivalent to the top of the Sirt Shale and is a widespread unit that is predominantly shale (calcareous mudstone) with siltstone and limestone intrabeds between the Rachmat and Kalash formations. It is the main source rock in the Sirt Basin.

Well	East_Z33N	North_Z33N	KB	TD	Base Kalash		
					TWT_ms	Depth_ft	Velocity_ft/s
B1-25	670052	3309839	941	*5679*	558	4091	14664
B1-32	768306	3268610	1275	*4940*			
B1-57	781571	3133810	1109	*10396*	1186	7907	13334
D1-NC29B	777955	3296856	844	*5660*			
H1-NC74F	839755	3119679	794	*13142*	1406	7771	11054
J1-NC74B	705872	3159018	1214	*7850*	1328	7135	10745
K1-32	744019	3362548	605	*7720*	1170	5546	9480
P1-32	755583	3262703	723	*10470*	1328	7834	11798
Average velocity							**11846**

Table 6.3 The sonic wells used to calculate velocity and depth to near base Kalash surface.

Well	East_Z33N	North_Z33N	KB	TD	Hon		
					TWT_ms	Depth_ft	Velocity_ft/s
B1-25	670052	3309839	941	*5679*	-	307	
B1-32	768306	3268610	1275	*4940*	115	877	15245
B1-57	781571	3133810	1109	*10396*	320	1571	9822
D1-NC29B	777955	3296856	844	*5660*	225	1115	9910
H1-NC74F	839755	3119679	794	*13142*	494	1907	7722
J1-NC74B	705872	3159018	1214	*7850*	573	2515	8778
K1-32	744019	3362548	605	*7720*	436	1726	7917
P1-32	755583	3262703	723	*10470*	412	1601	7770
Average velocity							**9595**

Table 6.4 The sonic wells used to calculate velocity and depth to near top Hon surface.

The near base Kalash horizon and the near top Hon horizon are widely geographically distributed in the study area and have been chosen for the average velocity analysis. The area with sufficient seismic and well data that was of good enough quality to use for velocity mapping of the near base Kalash Surface (Top Sirte Shale) is shown by figure (6.23). The average velocity to the near Base Kalash Surface values that were used are clearly shown along with the contours where the average velocities were between 5500-17000 f/s (Fig. 6.23). The average velocity is highest over and about the southern Waddan Uplift to the northern part of Zallah Sub Basin (Trough). Here the average velocities vary between 11000 f/s and 17000 f/s whereas over and about Az Zahrah and Al Hufrah oilfields they vary between 9000 f/s and 13500 f/s.

The average velocity map (Fig. 6.23) displays a general northwest to southeast trending higher velocity zone (anomalous average velocities to the near Base Kalash of more geologic structure (faults). The map shows that the average velocity along this trend than 11000 f/s) in the central part of the study area that follows the trend of major increases from the southeast to northwest directions as observed in Figure (6.23). The map also showed that flanking this high (and often interfingering with it) on its northeastern and southwestern sides are northwest-southeast trending low velocity values (troughs). In these "troughs" the average velocities are less than 9000 f/s. The minimum average velocity values are found on both the northeastern and southwestern sides of the study area.

It appears that the average velocity values for the near Base Kalash horizon are sometimes high in the structurally high areas of the study area and low in the structurally deeper parts. This may be due to changes in the lithology, where low velocities probably indicate more shaley sediments in the deeper parts and high velocities probably indicate carbonates although the main lithology of this horizon is

shale sediments. This thought were not observed or confirmed by any cores or well logs which was not available in this study.

6.6.3.1.2 Average velocity to the near top Hon surface

The lithology of what consists mainly of interbedded dolomite and anhydrite where halite is an important constituent in the southwest part of the Zallah Trough. Indeed, the approximate lateral extent of the halite facies is often referred to as the Zallah sub-basin. The near top Hon (Fig. 6.24) has its lowest average velocities (0 f/s) in the southwestern part of the study area (at about 16^{o}15'E and 28^{o}45'N) as the top of the Hon either outcrops at the surface, no data available, or is located above the Seismic Datum Plane. Therefore, the area of precisely useable data is extends eastwards from 16^{o}50'E to 18^{o}30'E. In contrast, the study area is characterized in the northern and northeastern sides of the velocity mapped area by a crescent-shaped region of higher velocities (8000 f/s to 11000 f/s).

From the southeastern half of the map to the central part, the area is dominated by three low velocity zones (6000 f/s to 2000 f/s) along a northwest-southeast trough. The lowest velocities occur in the northern zone (3000 f/s to 2000 f/s). These three low velocity zones are separated by two higher velocity "ridges" trending northeast-southwest characterized by velocities above 7000 f/s. This generalization that low velocity values are found where the time values are greatest for this interval (Fig. 6.24) suggests that structural highs have maximum velocities and structural lows have minimum velocities. This may indicate evaporates, fine clastics and shale-rich sediments were deposited in the lows and deeper parts of the area, and the higher velocity reflects platform carbonates formed on the shallower northern and northeastern sides of the mapped area. This also coincides with the halite, which is considered an important constituent in the southwest part of the Zallah Trough.

6.6.3.2 Isopach (Thickness) maps

Subsequent to performing a well synthetic to seismic line tie analysis and then the integrated seismic line interpretation, average velocity maps to the Top Satal (Base Kalash to Top Satal) Surface, and the Top Hon Surface were generated. These were then used through a cross-multiplication of grids process with the respective time structure maps, to produce integrated thickness contour maps for both surfaces in the limited area of the seismic coverage. These data were then gridded and contoured to produce; 1) the final thickness contour map of Top Satal (Base Kalash to Top Satal),

(Fig. 6.25) and 2) The thickness contour map of Top Hon to Top Satal interval herein shown in Figure (6.26).

The isochronous map and average velocity are used to convert the reflection time to depths, in order to construct the thickness contour map. An isopach is a measure of the distance (feet or meters) between two horizons. To calculate the isopach, the isochron were converted from time to depth and was carried out by dividing the isochron maps by 2000 in order to change the time units to one-way time in seconds and then multiplying the result by the appropriate average velocity horizon at depths in the wells that correspond to the age of the seismic horizon. This process is necessary to show the structural elements in the depth contour maps in terms of depth rather than time.

6.6.3.2.1 Near top Satal (base Kalash to top Satal) (Late Cretaceous to Early Paleocene)

An isopach contour map of the Near Top Satal (Base Kalash to Top Satal) represents the Late Upper Cretaceous and Lower Paleocene sediments distributed in the study area (Fig 6.25). These range in thickness from 91m (300')-610m (2000'0 with the thickest part appearing as a major NW-SE trending contour part-closure in the southeast portion of the Az Zahrah-Al Hufrah Platform and Zallah Trough.

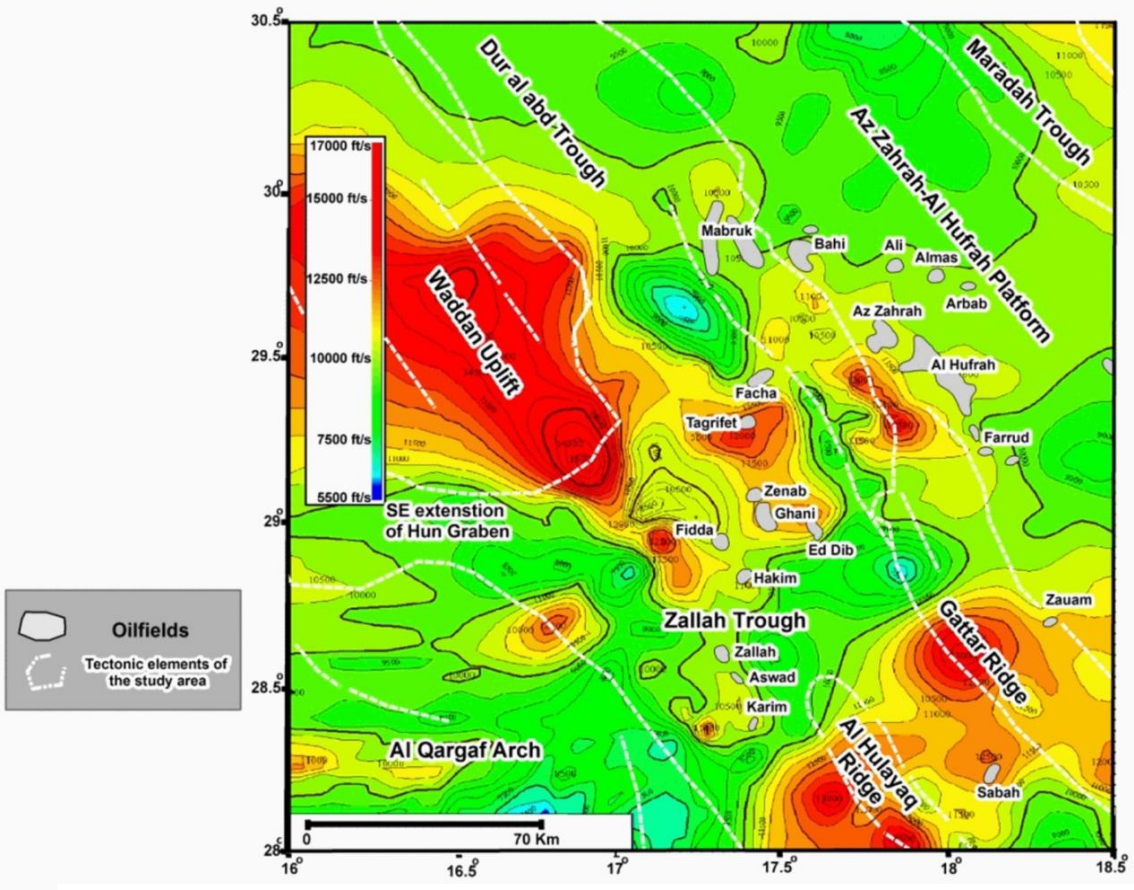


Fig. 6.23 The average velocity to the near base Kalash surface contour map.

In this part of study area, the near top Satal (Base Kalash to Top Satal) depth contour map attains a gross thickness of up to 549m (1800'). The second thickest part is found in the northwestern side of this map, where thicknesses of more than 427m (1400') are connected to the southeast by a series of narrow elongated thickness closures up to 457m (1500').

The elongate closure seems to be a graben bounded by two faults on both sides. This indicated by the closely spaced contours. These sediments thin in the central part of the study area and toward the eastern, northeastern and southwestern sides of the map ranging with thickness between 91m (300')-244m (800').

The reduction in thickness of these sediments is probably due to local uplift and erosion during the Late Upper Cretaceous to Lower Paleocene age as appeared on the map of fig.6.25.

In contrast, thinning of this unit occurs in the trough area as shown by an elongate linear low trending northeast-southwest (91m [300'] – 213m [700'] thicknesses) starting from

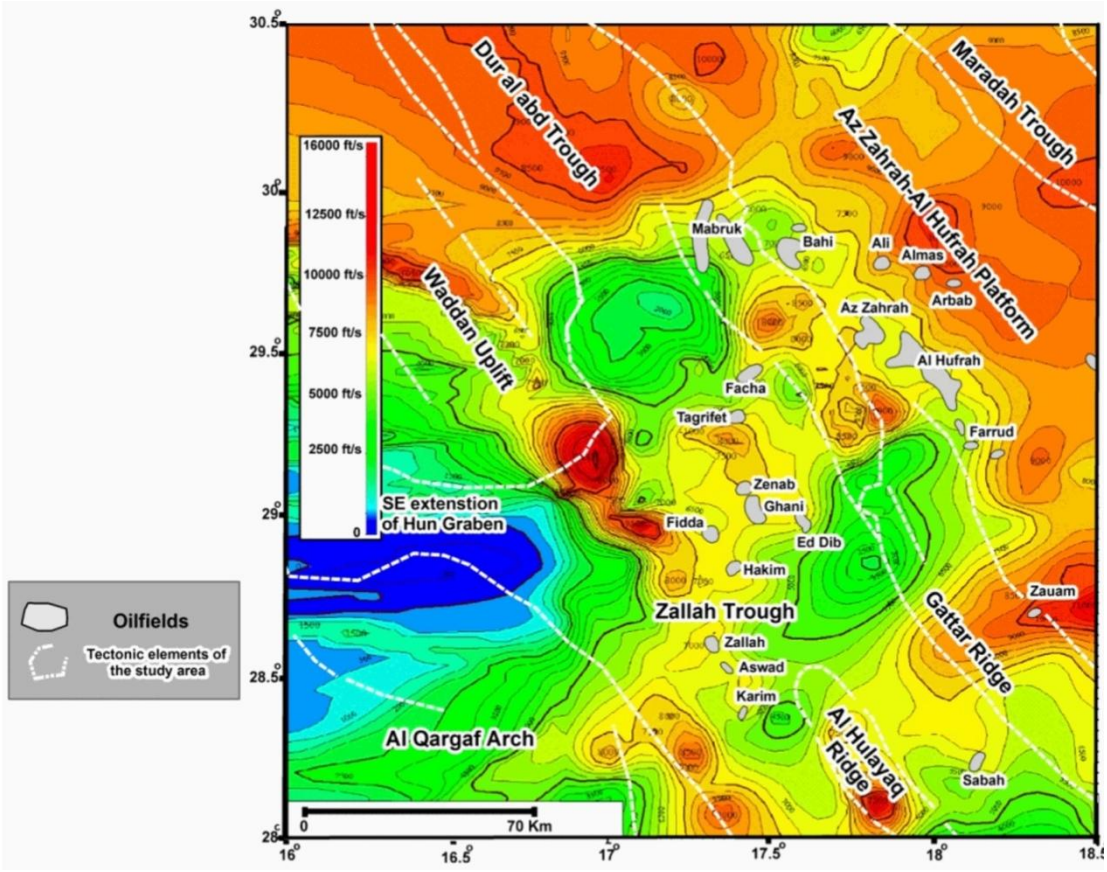


Fig. 6.24 The average velocity to the near top Hon surface contour map.

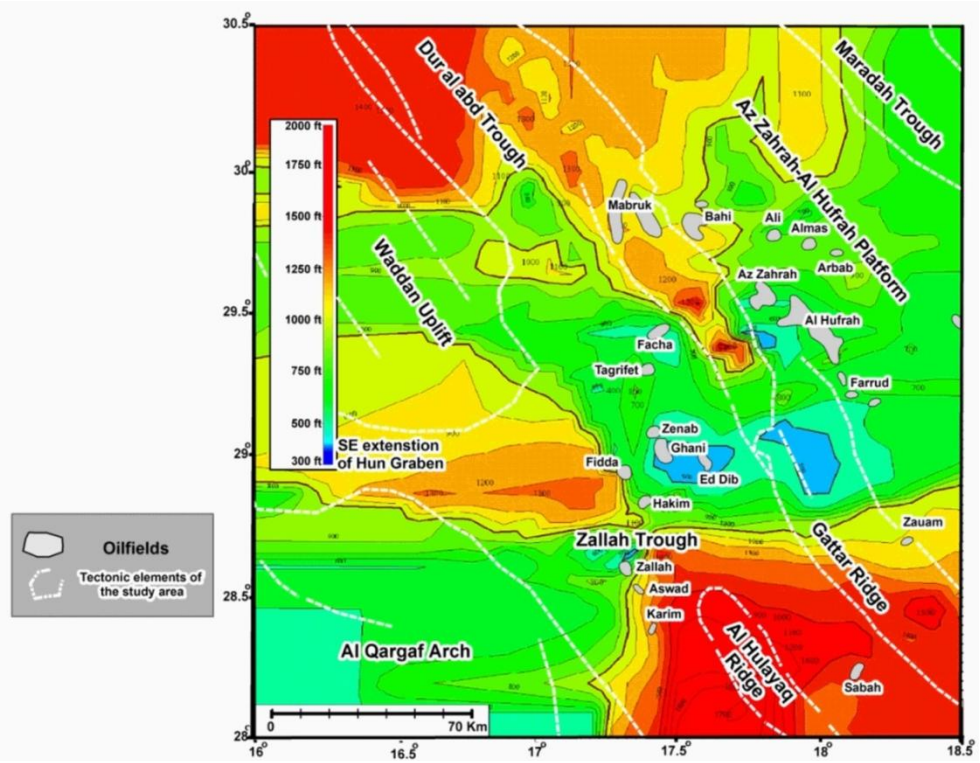


Fig. 6.25 The near base Kalash to near top Satal thickness contour map.

the Zallah Trough, passing through the Dur al Abd Trough and extending to Az Zahrah-Al Hufrah Platform where it separates into two depocentres as shown in figure (6.25).

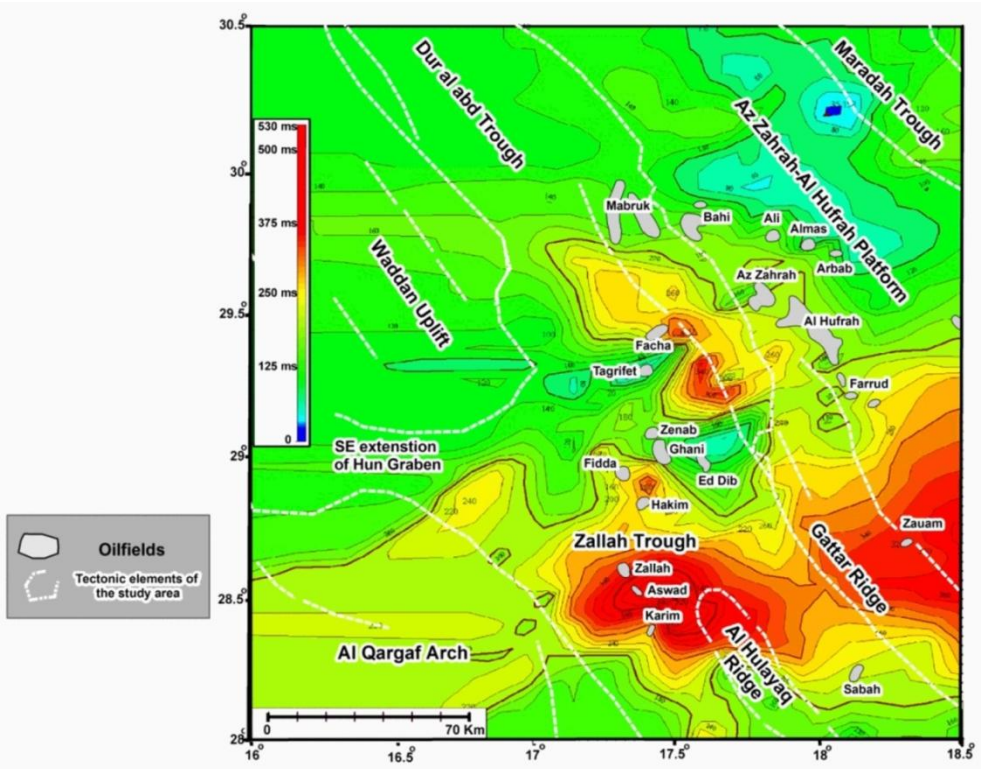


Fig. 6.26 The near top Hon to near top Facha thickness contour map.

6.6.3.2.2 Near top Hon to near top Facha (Late Lower Eocene to Early Upper Eocene)

The same procedure was used to create the near top Hon to near top Facha (Middle Eocene) isopach map (Fig. 6.26). This isopach map (Fig. 6.26) shows the distribution of Middle Eocene sediments (including the Hon Evaporites) in the study area. These sediments are distributed throughout most of the study area concentrated mainly in the Zallah Trough, Dur al Abd Trough, and southern Az Zahrah-Al Hufrah Platform. They range in thickness in these areas from 396m (1300') -732m (2400'), 335m (1100')-488m (1600'), and 366m (1200')-549m (1800') respectively. The thickening of this unit can probably be attributed to the extent of the rifted areas during the time of deposition. It thins towards the northern half of the map where it is not more than 183m (600') in thickness.

6.7 Summary

This chapter addresses the interpretation and summarizes results of a study of the seismic data made accessible to the project. The objective of this chapter was to gain a better understanding of regional structural and stratigraphic relationships.

This chapter is based on the interpretation of approximately 5000 km of 2D seismic data with various spacings available mainly in the eastern half of the study area supported by about 300 wells which imported into the study area database. Evaluation of the seismic data showed that the near top Hon and near top Sirte (near base Kalash) seismic markers held the most promise as regional markers.

An extensive evaluation of the major fault intersections on the regional time markers and the ground surface was undertaken. Nine sub-populations of major normal faults have been identified in the study area, distinguished by the size of the faults and the period of time during the rift phase when they were active.

Based on all the interpreted seismic and well-based geological cross sections the study area seems to be more tectonically and structurally complicated to the south. The resulting increasing number of the faults has led to more tectonic blocks being defined in the south.

Many time, isochron, and velocity structural maps were constructed on the main regionally extensive time markers. (i.e. Hon, Zelten, Dahra, and base Kalash) to define the main structural trends across the study area between the Late Cretaceous, the start of main rift phase and the Late Eocene post rift phase.

The dominant faults picked on the seismic data are normal faults trending north-northwest to south-southeast and northwest to southeast, dipping mainly southwest or northeast towards the basin. The central part of the area is characterized by a major north-northwest to south-southeast-trending elongate low representing the Zallah Sub Basin (Trough). It is cut in places by an important set of northeast trending faults that segment the Trough into more depocenters. The interpreted major faults also show an en-echelon style that might reflect oblique extension. Some folds have been identified in the study area parallel to the major faults are interpreted to have been either generated by compaction in the troughs or they may have connected with subsidence movements during the filling of the Sirt Basin.

Based on the interpretation of the seismic reflection data used in this study; the following points can be made:

1. The identification of faults from seismic and their orientation in plan view for the key mapped horizons has shown several prospective structural trends and provided a better definition of the boundaries of the major tectonic elements of the study area.
2. All the identified faults show vertical displacment across the sequence with different throws at different time intervals.
3. Most of the identified faults started appear to have larger displacements and that decline upsection. These decreases accompanied by thickening of sedimentary layers in the hanging walls of the faults, are due to syn-sedimentary fault growth.
4. In all figures used in this section there is characteristic of syn-tectonic growth strata in the hanging-wall for Upper Cretaceous time constrained by the reflection data.
5. It seems that most of the faults initiated at the study area boundaries and then propagated towards the centre of the area as indicated by a different throw history of the intra-basin faults compared to those at the margins.

CHAPTER 7: PALEOSTRESS ANALYSIS

7.1 Introduction

Faulting is the brittle response of rocks to tectonic stresses. During the 20th century geologists sought to understand the origin and evolution of faults, and the tectonic history of faulted regions, by relating fault orientation and slip direction to the state of stress in Earth's crust (e.g. Anderson, 1942; Price, 1966; Voight, 1966; Mandl, 1988). The geometrical properties of faults and their movements are thought to be controlled by the nature of the active stresses. Paleostress analysis is the name popularly given to the estimation of principal stress orientation and ratios from data consisting of the orientation of fault planes and their corresponding slip direction indicators. A key understanding of tectonic events in studied areas was the work of Wallace (1951) and Bott (1959), who assumed that slip on a plane occurs in the direction of the maximum resolved shear stress. Changes of stress field can cause new fault formation or the reactivation of older ones and multiple striations on some fault surfaces indicate this reactivation has occurred. The mechanism of this process is complicated by many factors such as the variability of the stress field in geological time, the precision of measurements, the production of spurious solutions, etc (Fry, 1999; Yamaji, 2000; Shan et al., 2004a).

Data from faults observed at surface outcrops are also frequently incomplete. Faults cutting young non-indurated sediments may not produce clear linear structures (Hirono, 2000). In any many cases the fault zone may be subject to erosion, making observation of fault surface and slip lineations impossible. In the case of buried faults, three-dimensional (3D) seismic surveys may allow fault plane orientations to be recorded though their associated slip directions remain unknown.

Field data required for paleostress analysis are the dip direction/dip angle for planes and trend/plunge for lineations. These data are normally either produced directly from field measurement of faults and their associated striations or indirectly from the first motions of earthquakes. Valid dip directions/trends (strike) are 0–359º counted clockwise from north, the dip angle/plunge must be between 0 and 89º, measured in down plunge direction. For faults, dip direction/dip of the fault plane and trend/plunge of the fault lineation have to be recorded and ideally the relative sense of slip (normal/reverse/strike-slip) determined from kinematic indicators. A wide variety of

kinematic indicators have been reviewed by Price and Cosgrove (1990), Hancock (1985), Petite (1987) and Cloetingh (1992) among others.

One of the most important issues in paleostress inversion studies is to date the constructed stress configurations. This may be achieved by dating the stratigraphical horizons involved in the faulting and the relationship between sedimentation and tectonics (Angelier, 1984).

In many geological cases it is not straightforward from outcrop observation to determine whether the rocks have been deformed by a single event or in multiple stages under possibly different orientations of the main stress field. Data from faults observed at surface outcrops are also frequently incomplete. To identify multiple stress regimes that occurred at different times, previous studies have classified minor faults into homogeneous subsets at the outcrop scale based on their apparent relative ages (e.g., Angelier et al., 1986; Choi et al., 2001; Viola et al., 2009).

Some of the features of minor faults are useful in distinguishing different fault sets, including the age of the rocks affected by a certain deformation event (Choi et al., 2001; Vandycke and Bergerat, 2001; Yamaji, 2000), the characteristics of syn-sedimentary faults (e.g., fault drag) (Choi et al., 2001; Vandycke and Bergerat, 2001), the geometrical relationships between geological structures (Angelier et al., 1986; Vandycke and Bergerat, 2001), the occurrence of multiple striations on a single fault plane (Rossetti et al., 2000; Storti et al., 2001), and the characteristics and mineralogy of veins (Choi et al., 2001; Viola et al., 2009). Therefore, these criteria are not always applicable because of a lack of suitable outcrop data. These arguments have been discussed in detail, for example, by Dupin et al. (1993), Pollard et al. (1993), Twiss and Unruh (1998), Watterson (1999), Tikoff and Wojtal (1999), Marrett and Peacock (1999).

The reconstruction of paleostress tensors includes two distinct stages: (1) a detailed field analysis of many sites, where each site generally consists of a population of several tens of measurements in a small area, mainly faults with slickenside lineations, bedding planes, tension gashes and joints. The aim of the field analysis is to identify the faults belonging to single tectonic events resulting from the same paleostress field. and (2) the numerical processing of fault populations selected and measured in the field which is based on the principle of fault-slip data inversion first solved by Carey and Brunier (1974). The assumption is made that observed fault slip and calculated shear stress

should be similar in orientation and sense for each fault of the population moving independently under a single stress regime. Because data consist of orientations and senses, and not magnitudes, the result is the reconstruction of a reduced stress tensor (Angelier, 1989) with the determination of the principal stress axes α1, α2 and α3 orientation, and of the ratio Φ of principal stress differences [Φ =(σ2-σ3)/(σ1-σ3); (with σ1 > σ2 > σ3), (Angelier,1984, and 1989).

The stress regime is defined by the nature of the vertical stress axes:
1) Normal faulting when σ2 is the maximum horizontal stress axes (σ2 SHmax) and σ1 is vertical,
2) strike-slip faulting when σ1 is the maximum horizontal stress axes (σ1 SHmax) and when σ2 is vertical and
3) thrust/reverse faulting when σ1 is the maximum horizontal stress axes (σ1 SHmax) and σ3 is vertical.
The stress regimes also vary as a function of the stress ratio Φ: radial extension (σ1 vertical, $0 < \Phi < 0.25$), pure extension (σ1 vertical , $0.25 < \Phi < 0.75$), transtension (σ1 vertical , $0.75 < \Phi < 1$ or σ2 vertical , $1 > \Phi > 0.75$), pure strike-slip (σ2 vertical , $0.75 > \Phi > 0.25$), transpression (σ2 vertical , $0.25 > \Phi > 0$ or σ3 vertical, $0 > \Phi > 0.25$), pure compression (σ3 vertical, $0.25 < \Phi < 0.75$), and radial compression (σ3 vertical , $0.75 < \Phi < 1$) (Delvaux et al., 1997).
The orientation of the principal stresses and the stress difference ratio (Φ) are determined by selecting those measurements of small faults with obvious sense of movement (i.e. slickolites and mineral steps).
Many computer programs have been produced to plot and analyze orientation data (e.g. Charlesworth et al., 1989; Griffis, et al., 1985; Guth, 1987; Diggle and Fisher, 1985; Pecher, 1989; Pilant, 1989; Starkey, 1977). Generally, such programs have been written to satisfy specific needs of the authors and most require specialized input data format. In addition, limitations of programs have been put on the style or quality of the output.

7.2 Data processing and results

7.2.1 Stress inversion techniques

In this study palaeostress orientations and principal stress ratios have been calculated using standard inversion methods in MyFault™ (v. 1.03) stereonet software, produced by Pangaea Scientific Limited. MyFault is an easy-to-use Windows application for analyzing fault and slip geometry and estimating the stresses that lead to the formation

of these structures. Until now, researchers performed these operations using a variety of different tools, each requiring its own special data formats. MyFault combines them into one unified application. Further, because of the effort necessary to prepare the data files, researchers cannot easily compare calculated stresses using different methods. In MyFault this can be done with a simple click of the mouse.

MyFault processes field slickenside measurements, earthquake nodal solutions and P-T axes data and gives a large variety of formats for entering the values. You can even mix formats and data types in the same data file.

7.2.2 Fault geometry analysis

MyFault™ can make fully customizable scatter plots, stereonets, histograms, rose diagrams and Mohr diagrams, choosing which features or variables to plot, both measured and computed, including the results of the stress analysis. It can examine the interrelationships between features, their statistical properties and orientation distribution. All the plot characteristics can be saved as templates to standardize presentations, in addition, MyFault create plots automatically when a new data file is loaded.

7.2.3 Stress analysis

MyFault™ calculates the stresses that may have produced the faults using one of 5 published methods of stress inversion. MyFault lets the user switch easily between the various methods and compare the results. Each method has its own set of assumptions and procedures which may or may not be valid for a particular field situation. All methods use the same data set, user interface and calculation options, although some methods may have additional options particular to themselves (MyFault software manual).

7.2.3.1 Simple shear tensor average (Sperner et. al., 1993)

This method is one of five inversion methods which is offered by the MyFault™ program and allows a quick and easy comparison between different methodologies, each of which is based on different assumptions. Automatically, every fault dataset is run through each methodology (provided data numbers are sufficient) in order to assess any mismatches in the resulting palaeostress orientation calculations. In this method, a simple shear stress state is assumed for each fault, with the intermediate principal stress lying in the fault plane perpendicular to the slip direction. The individual stress tensors

can then be averaged together to give an estimate of the collective stress tensor. The angle between the maximum principal stress and the fault plane can be varied to search for the minimum deviation between the faults in the set; MyFault™ automatically scans between 0 and 45°. The method assumes that slip occurs in the same direction as when the fault was first formed, and it does not allow for an estimate of the intermediate principal stress. Its average value will tend to lie close to 0.5, where the maximum and minimum principal stresses are normalised to 1 and 0, respectively. As such, in all the inversion methods detailed here, the stress ratio: (intermediate-minimum) / (maximum-minimum) is equal to the intermediate stress. The uncertainties in these quantities are estimated using the bootstrap resampling method (as is the case for all the methods described). For each calculation, MyFault randomly samples the record set, choosing the same number of records for the new set as were in the original. Since the sampling is random, there will necessarily be duplication of one or more of the original records. It then computes the principal stress tensor for each resampled set and computes its tensor distance from the principal stress tensor of the full original record set (Michael, 1987a).

7.3 Testing regional tectonic models

A goals for this study was to collect data for a new fault analysis in the study area, but unfortunately, due to the lack of security and stability in Libya during this period, this has been replaced by an analysis of measurements previously obtained by Abadi (2002) for the Hun Graben, of the western Sirt Basin (Fig. 7.1) and Gamberlu (2007) for the region of Jifarah Basin and Jabal Nafusah Uplift of northwestern Libya (Fig. 7.2) as a test of the prevailing tectonic models.

Anketell (1996) suggested a model of a dextral dilatation jog that was responsible for the shaping of the Sirt Basin (Fig. 7.3). This model involves normal faulting and formation of fault-related folds under the conditions of interaction between the South Cyrenaica Fault in the north and the southern Sirt basement shear zone in the south. In such a way, a block-faulted geometry characterized by numerous grabens and intervening horsts was produced (Goudarzi and Smith, 1978; van Houten, 1983; Anketell, 1996).

In this model, the main deformational event is related to a NE–SW extensional stress field occurred during Palaeogene–Lower Miocene and was followed by basin inversion

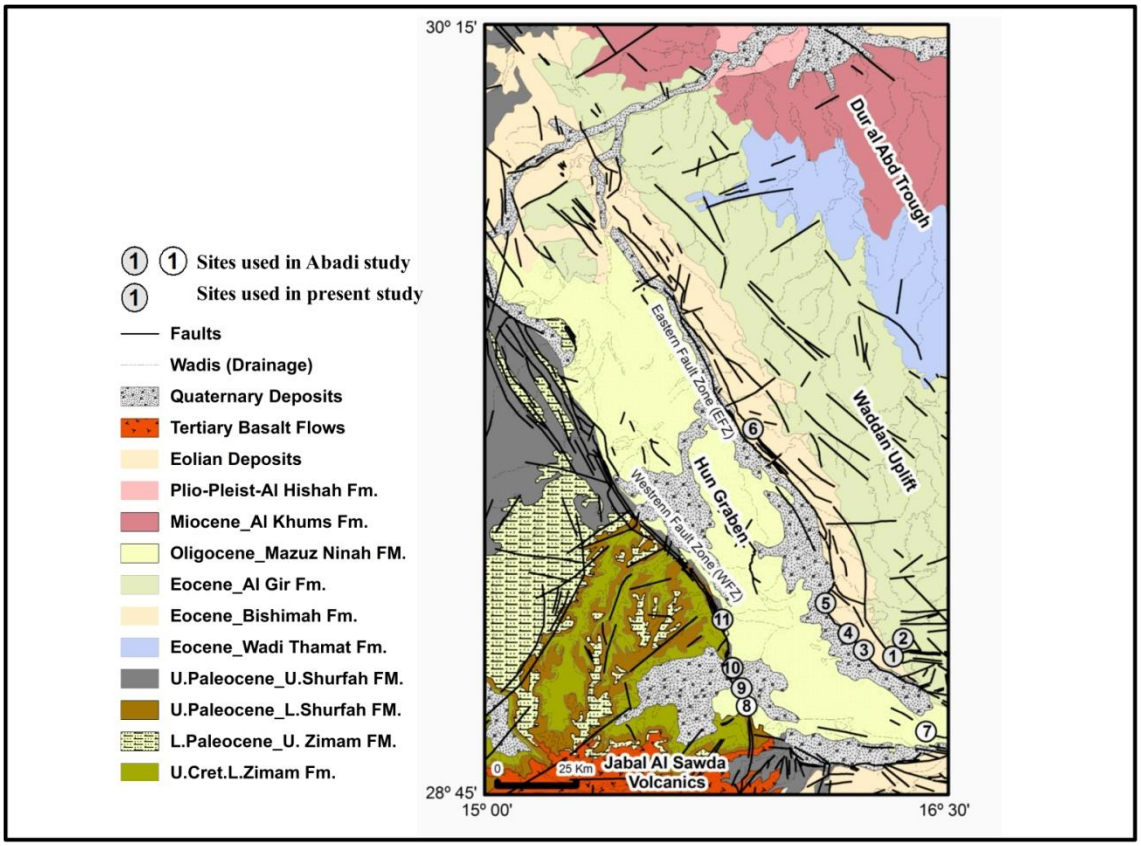


Fig. 7.1 Geological map of Hun Graben (after Abdshakor and Shagroni, 1984)

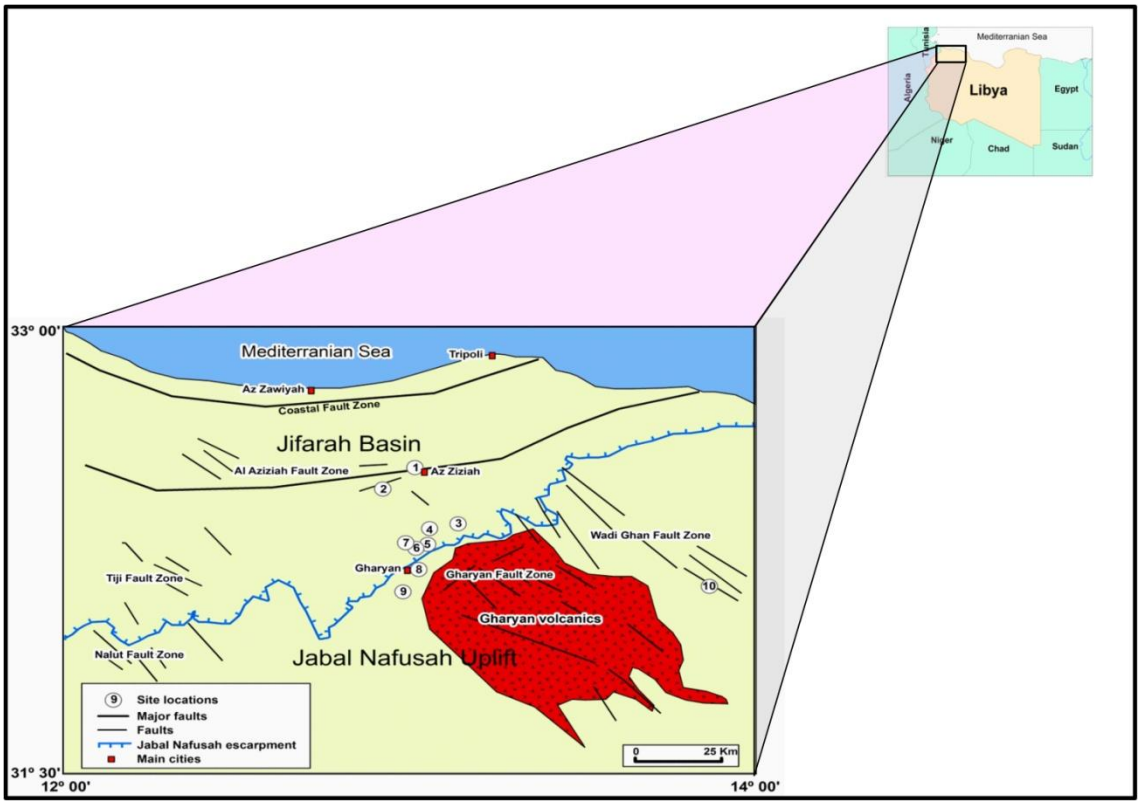


Fig. 7.2 Generalized tectonic map for the region of Jifarah Basin and Jabal Nafusah Uplift of northwestern Libya showing major structural features and location of the sites ues in this study.

and activation of magma tectonic lineaments of the reactivated older faults of the Tibesti-Tripoli Arch (Cvetkovic et al, 2010).

These faults were reactivated under conditions of Late Miocene–Pliocene–Quaternary stress field of NW–SE compression and perpendicular tension (Schafer et al., 1980) and they controlled the basaltic magmatic activity.

A slight change in the stress field orientation toward ENE–WSW and E–W directions, from the Sirt Basin toward the Abu Tumayam Trough, were a consequence of the pre-existing basement structures (Fodor et al., 2005; Peregi et al., 2003, and Marovic´, 2007). After the Burdigalian, the western part of the Sirt Basin area was deformed in a stress field of NW–SE compression and perpendicular tension (Schafer et al., 1980). These terrains of western part of Sirt Basin could have been subjected to inversion, uplifting and the accompanying erosion since that time. Older deposits (Eocene and Oligocene) occur in the north, while younger sediments (Lower Miocene) are in the south, which indicates a southward tilting of the whole area.

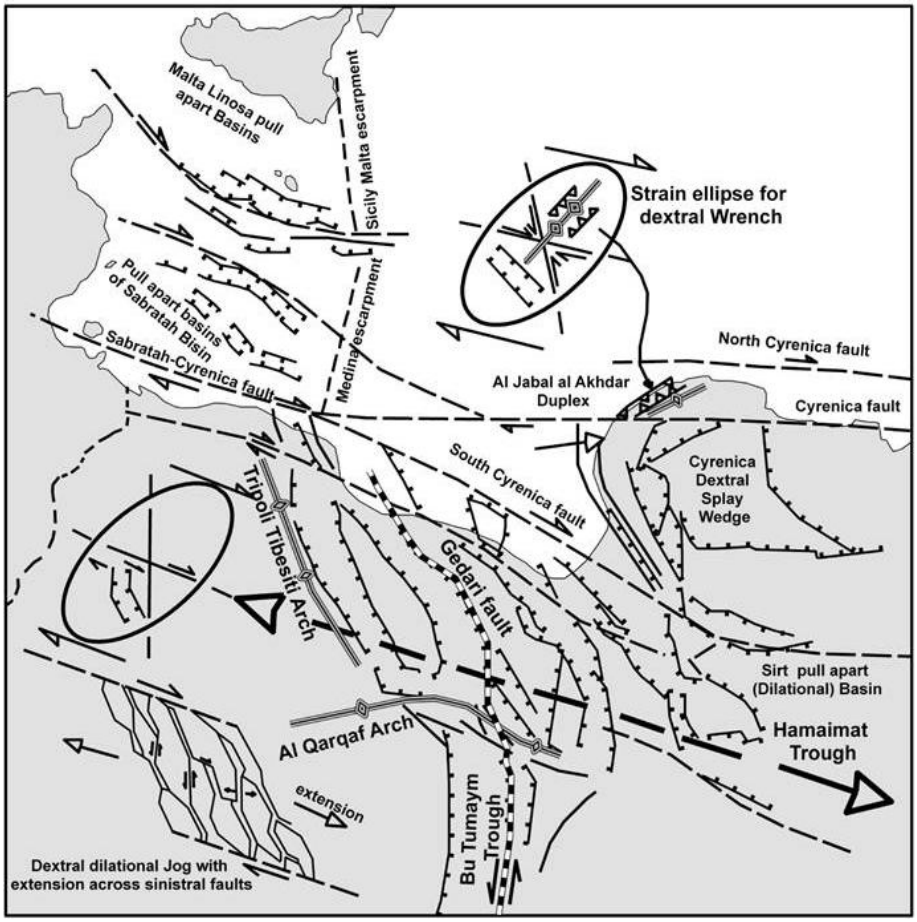


Fig. 7.3 Interpretation of Sirt Basin relative to the Sabratah Basin and Cyrenaican Platform. (Modified after Anketell, 1996).

The western part of Hun Graben consists of flat terrain, that is slightly undulating but gently dipping to the northeast. The sediments in this zone are from the Paleocene to

recent (Fig. 7.1) except in the southern part, where basalt flows from Jabal Assawda can be found. The eastern area is hilly terrain terminating at the western margin in a steep scarp, while a regional dip NE-NNE is observed. Undulations and gentle dome like structures are noticed in the eastern region belonging to the Sirt Basin area. The direction of the faults adjacent to the graben area is usually in the basic structural direction of NNW-SSE to NW-SE. The dominant trends of the faults show that the graben-forming forces have probably acted with a slight variation of orientation on both edges and reflect the regional structure of the Al Qargaf Arch in the southern part (Abdshakoor and Shagroni, 1984). The west boundary of the Hun Graben featured in the fault zone consists of several subparallel faults accompanied by brecciated zones. In fact the nature and origin of the Hun Graben is controversial. Klitzsch (1970) suggested that the tectonic development of the Hun Graben started prior to the Cretaceous and that the western boundary of the graben is Paleocene in age. However, Cepek (1979) inferred that the graben is probably Oligocene in age.

In contrast to the Sirt Basin, the Jifarah Basin in northwestern Libya (Fig. 7.2) is bounded by the Nafusah Uplift to the south and the offshore Sabrath Basin to the north. The Jifarah Fault is part of the Sabratah-Cyrenaica wrench zone, (Fig. 7.3) which marks the boundary between the relatively stable shelf to the south and the unstable continental margin to the north. The Mesozoic basin-fill of the Jifarah Basin was affected by syn-depositional faulting during the Triassic and by shearing during the Neocomian which reflected major tectonic activity along the southern margin of Tethys. The structure of the Jifarah Basin was studied by Anketell and Ghellali (1991). They demonstrated that the dominent fault directions in the Mesozoic section are east-west and NNW-ESE with an en echelon arrangement which they interpreted as riedel shears and imbricate fan splays formed as a result of strike slip movement on the South Atlas-Jifarah dislocation. Riedel shears are slip surfaces formed during the early stages of shearing. They developed a model which suggested an analogy between the imbricate fan splays visible in the Wadi Ghan area south of Al Aziziyah with the strikingly similar fault trends in the Sirt Basin, and attributed both to strike-slip faulting associated with underlying basement dislocations.

Generally, the region is comprised of gently dipping Mesozoic limestone with shale and sandstone overlain unconformably by Tertiary and Quaternary deposits (Anketell and Ghellali, 1991).

The Nafusah Uplift is a major east-west ridge which separates the Ghadamis Basin from the Jifarah Basin. It extends for 400km from Misratah to the Tunisian border, and continues in Tunisia as the Dahar Uplift and in Algeria as the Talemzane Arch. It is bounded to the north by the Jifarah Fault and Jifarah Basin and to the south by the Ghadamis Basin. The southern margin is also partially faulted. During the Early Palaeozoic the area of the Nafusah Uplift formed part of the Ghadamis Basin and a thick sequence of Palaeozoic rocks was deposited.

Sedimentation continued until the Palaeocene, but the basin was caught up in the Eocene tectonism which reactivated the Nafusah Uplift and introduced a new generation of faulting in the Jifarah Basin (El-Hinnawy, and Cheshitev, 1975). Eocene tectonism also led to the production of basaltic sills and flows near Gharyan, and the volcanic activity has continued until recent times. A major escarpment formed along the line of the Jifarah Fault and Jurassic and Triassic rocks outcrop both on the escarpment and on the Jifarah Basin. Extensive pre-Miocene erosion removed much of the Mesozoic sediments from the basin, and the pre-Miocene subcrop shows a complex pattern.

The purpose of the paleostress analysis carried out in this chapter is to delineate the kinematic evolution of these regions and to identify any relationship to their tectonic evolution. Also the datasets used allowed us to test the Anketell and Ghellali (1991) and Anketell (1996) models.

7.3.1 Previous results from the Hun Graben, western Sirt Basin

In the original work of Abadi (2002), fault-slip data were measured at three areas within the Hun Graben fault zones (Fig 7.1). One was along the East Fault Zone of Hun Graben (EFZ), where measurements were made at six different locations over about 50 km. Two data sites (sites 1 and 2) were located in NE oriented road cuts perpendicular to the EFZ scarp. These outcrops are made of dolomitic limestone of the Paleocene Shurfah Formation and of chalky limestone and dolomitic limestone of the Eocene Bishimah Formation (Abdshakoor and Shagroni, 1984). The four other sites are located along the main EFZ (Fig. Fig 7.1). Site 3 (Fig 7.1) is located in a N-S trending fault zone that contains high-angle normal faults, with the downthrown block always to the west.

Abadi (2002) stated that the width of the EFZ is more than 10 m and the distance between the faults a few centimetres only and the main trend is 350°/90°. These outcrops are made of silicified limestone, dolomitic, chalky and gypsiferous marly

limestone, and gypsum of the Eocene Al Jir Formation. The other data sites were observed in gullies.

The second group of sites of Abadi, (2002) measurements were collected from four locations along the West Fault Zone (WFZ), in outcrops of the Paleocene Shurfah and Zimam Formations (Fig 7.1). For the third area, data were collected from only one location in the central southeastern corner of the graben (GC). The outcrop is made up of calcareous clay, occasionally gypsiferous of the Oligocene Ma'zul Ninah Formation.

Abadi, (2002) confirmed that most of the faults observed correspond to minor structures with displacement ranging from several centimetres to several metres and the sense of movement was identified using the slickenlines and other associated structures. He found that about 90% of the observed faults are dominant normal faults (oblique dip-slip component), with their pitch ranging from 60° to 90° and their dip ranging from 70° to 90° (high-angle normal faults). Faults with a strike-slip component were also observed where most of them have oblique slip, with their pitch ranging from 20° to 40°, but some were pure strike-slip faults, with a pitch less than 20° and dip greater than 70°.

The paleostress analysis study carried out by Abadi (2002) suggested evidence for four stress field orientations in the Hun Graben and by inferred that this could be extended over large parts of the Sirt Basin.

These tensor phases are:

(1) A WNW-ESE trending dextral strike-slip regime, recorded only on the WFZ where the minimum stress axis σ3 lies horizontal and corresponds to the minimum horizontal stress and the maximum stress axis σ1 is also horizontal whilst the σ2 is subvertical. The orientation of the principal stresses are: σ1=099°/20°, σ2=252°/68°, σ3=006/9° and the stress ratio was Φ=0.480. Abadi (2002) believed that because this phase was encountered in Danian units but not found in the other units that were examined, an Early Paleocene (Danian) age is assigned to this phase.

(2) A NNW-SSE direction extensional regime was obtained from the Paleocene and Eocene rocks outcropping along the EFZ. The orientation of the mean regional principal stresses are: σ1=002°N/71°, σ2=245°N/09°, σ3=152°N/17° and stress the ratio Φ = 0.240 where (σ1 subvertical, σ3 subhorizontal, $0.174 \leq \Phi \geq 0.431$. The youngest unit that recorded this phase is the Al Jir Formation (Lower Eocene), therefore Abadi (2002) assumed that this deformational phase operated

until Lower Eocene time.

(3) An ENE-WSW direction extension regime, from tensors obtained from five stations, the youngest of which were located in the Oligocene clay and gypsum outcrops at the southeastern end of the Hun Graben (location 7 in Fig. 7.1). The orientation of the mean regional principal stresses are: σ1=046°N/82°, σ2=170°N/04°, σ3=261°N/06° and stress the ratio Φ =0.266. This Phase 3 consists of a group of tensors with σ1 subvertical, σ3 subhorizontal and $0.278 \leq \Phi \geq 0.284$. The orientation of the horizontal component of each site is almost perpendicular to the NNW-SSE faults.

(4) A NNE-SSW direction extension regime was recorded from six stations with age up to Oligocene that show NE-SW extension was distributed along both the EFZ and WFZ. The orientation of the mean regional principal stresses are: σ1=342°N/77°, σ2=111°N/08°, σ3=152°N/17° and the stress ratio Φ =0.343. The regional orientation of stress (σ3) and stress ratio (Φ) in the EFZ and WFZ are similar and trending 199°N/08° and 020°N/07° respectively which he explained it as both fault zones have undergone the same deformation. The orientation of the horizontal component (σ2) is oblique to the NW-SE structural trend of the main fault zones (EFZ and WFZ).

Abadi (2002) in his study is suggesting that the NE-SW stress regime may have led to the collapse of the Sirt Arch during the Late Cretaceous and the reactivation of pre-existing Precambrian basement faults led to rifting and continued subsidence during Paleocene and Early Eocene. On the other hand strike-slip deformation, with σ1 WNW-ESE and σ3 NNW-SSE, might have been active during the Late Cretaceous and Early Paleocene rifting.

7.4 The present study results

Data from nine sites were made available to the present study (Abadi Pers. Comm) from the east and west margins of the Hun Graben and 150 fault slip data were used for the calculations. Measurements were made at six different locations over about 50 km along the East Fault Zone of the Hun Graben (EFZ). Two data sites (sites 1 and 2) were located in NE oriented road cuts perpendicular to the EFZ scarp. These outcrops are made of dolomitic limestone of the Paleocene Shurfah Formation and of chalky limestone and dolomitic limestone of the Eocene Bishimah Formation (Abdshakoor & Shagroni, 1984). The four other sites are located along the main EFZ (Fig 7.1). Site 3 of these locations (Fig 7.1) is located in a N-S trending fault

zone (high-angle normal faults), with the downthrown block always to the west.
The West Fault Zone (WFZ) by 3 sites (7-9) all on the main fault in outcrops of the Paleocene Shurfah and Zimam Formations (Fig 7.1). The measured fault slips were obtained from outcrops which made of the Paleocene and the Eocene sedimentary sequences (Abdshakoor & Shagroni, 1984) which means the measured fault slips might belong to these ages or later.

7.4.1 Inversion procedures

In total, 150 faults with good kinematic indicators were recorded (Fig 7.1), which can be used for kinematic inversion. MyFault™ stereonet software, produced by Pangaea Scientific Ltd., was used for kinematic analysis.
Two separate steps for sorting the fault data into populations for inversion analysis have been applied during the present study. The first step simply uses the entire unsorted data set (i.e., all 150 fault and fault striae), while the second (step 2), required manual sorting and separate analysis of the data into fault systems.

In step 1, after input of the raw data, data files were corrected to ensure that all striae lie perfectly on their respective fault planes (i.e., no angular mismatch). To do this, fault strikes were rotated along the common plane and because the collected data were measured using dip directions the data strikes where changed to a range from 0 to 360º to compute the stress tensor using the MyFault software. Those faults with high misfit angles (>40º) relative to the inversion result were rejected and the inversion rerun. This procedure was repeated and the stress tensor was recomputed again only for 124 faults.

In step 2, we formed data sets according to the geographic position of the study sites. The Hun Graben depression acted as a dividing line between the eastern (EFZ) and western (WFZ) groups of data sets. The aim of this step was to get enough data to compute paleostress tensors independently between the EFZ and WFZ of the Hun Graben fault system. Splitting the data up by area may be geologically more meaningful than analysing the data by the age of the rocks in which the faults are found as Abadi (2002) had done. The justification for this different approach is that strike-slip and dip-slip normal faults may well be the same age if the area has experienced transtensional deformation (De Paola et al 2006)

7.4.2 Whole Hun Graben

To determine the bulk brittle tectonics in the Cenozoic sediments and eliminate local deviations, all measurements were initially processed as one dataset.

In the bulk inversion of all the fault data (step 1) three separate sets of paleostress axes derived, and one for each fault system analyzed. The resultant paleostress tensor for the whole area was grouped according to the orientation of the principal stress axes. (i.e., system 1 Left normal dip-slip, system 2 Normal dip-slip, and system 3 Left Normal strike-slip faults; Figs 7.1, 4, 5, and 6). On the basis of the orientation relation of the structure and tensors, it appears to be possible to correlate a specific paleostress tensor with a specific rift structure. The parameters of the reduced tensor for the investigated area are illustrated in Table (1) showing the principal stress and the value of Φ which expresses a linear relation between the principal stress directions.

System 1: Left normal dip-slip

A NNE-SSW direction left normal dip-slip extension regime recorded from 66 measurements in the study area (Fig. 7.4 and Table 1). This slip type represents about 55% of total fault slip measurements. It gives the maximum principal stress axis (σ1) 71º/ 80º, as subvertical, whilst the intermediate principal stress axis (σ2) 296º/7º, and the minimum principal stress axis (σ3) 205º/7º; correspond to horizontal stress with stress ratio (Φ) equals 0.28.

The tensor belongs to a left normal dip-slip extension regime with a rake ranging between 51º - 80º (Threet, 1973). It indicates WNW-ESE compression and NNE-SSW extension.

System 2: Normal dip-slip

The second stress tensor recorded from fifty measurements in the study area (Fig. 7.5 and Table 1) represents about 40% of total fault slip measurements. It is characterized by a vertical, maximum principal stress axis (σ1) 356º/ 81º, and a horizontal stress intermediate principal stress axis (σ2) 115º/4º, and the minimum principal stress axis (σ3) 205º/7º; with stress ratio (Φ) equals 0.32.

This tensor belongs to pure normal dip-slip regime, with a rake ranging between 81º - 100º and indicates WNW-ESE compression and NNE-SSW extension.

System 3: Left normal strike-slip faults

A NNE-SSW strike-slip stress tensor was recorded from only six measurements in the study area (Fig. 7.6 and Table 1) represents about 5% of total fault slip measurements. The minimum stress axis σ3 lies horizontal and corresponds to the minimum horizontal stress and the maximum stress axis σ1 is also horizontal whilst the σ2 is subvertical. The orientation of the stress and stress ratio are: σ1 =103°/15°, σ2=289°/75°, σ3=194°/1° and Φ=0.58.

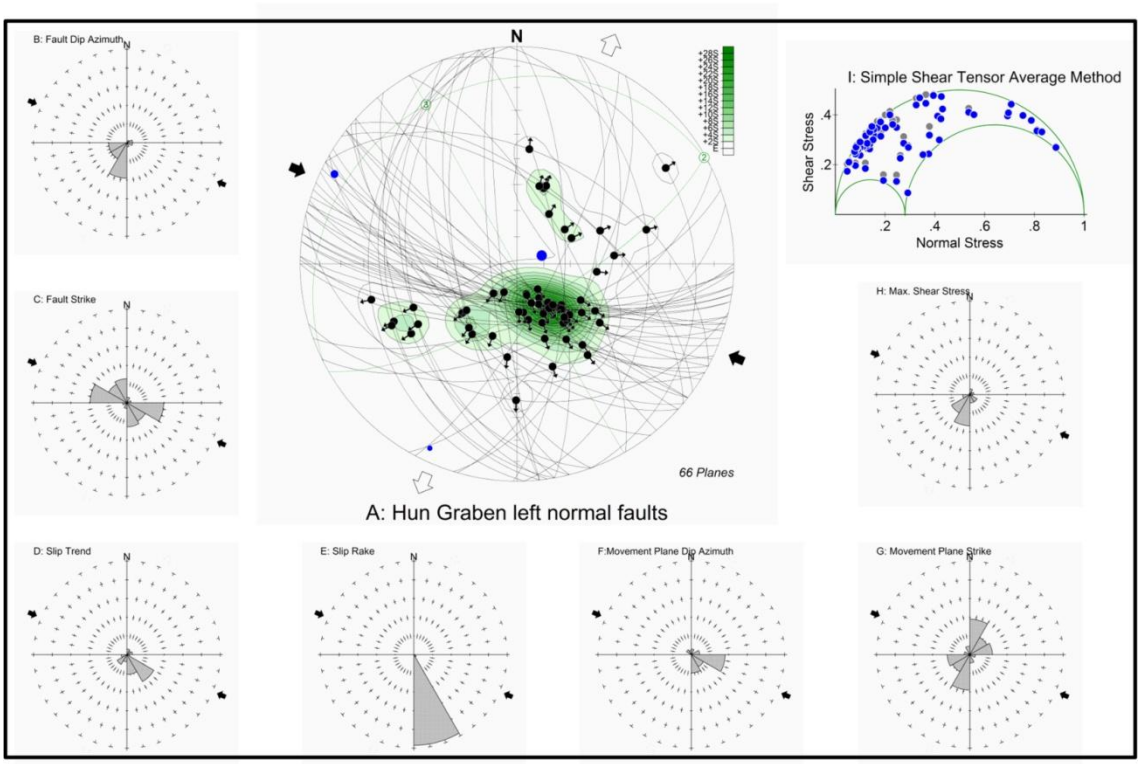


Fig. 7.4 Results of different stress phases for the Hun Graben. Field data diagram are Schmidt's projections of lower hemisphere. A: System 1: Left normal dip-slip. Faults are great circles, slickenside lineations are dots with arrows indicating the sense of motion of the hanging wall. Computed stress axes are represented as large blue dot (σ1), medium blue dot (σ2) and small blue dot (σ3). Large divergent white arrows indicate the horizontal extensional stress direction (σ3) whilst large convergent black arrows indicate maximum principal stress axis (σ1). Rose diagrams for the structures observed Hun Graben. The radius of the rose corresponds to the class with the highest frequency as represented in the figure (B to I).

Area of study	Tensor type	No. Of measured faults	Stress ratio (Φ)	Principal stress axis			% total measured faults	Regional principal stress orientations
				σ1	σ2	σ3		
Whole area	Left normal Fault	66	0.28	71°/ 80°	296°/7°	205°/7°	55	NNE-SSW extension
	Normal dip-slip	50	0.32	356°/ 81°	115°/4°	205°/7°	40	NNE-SSW extension
	Left Normal strike-slip faults	10	0.58	103°/15°	289°/75°	194°/1°	5	NNE-SSW extension
East fault zone (EFZ)	Left normal Fault	119	0.32	43°/ 82°	293°/3°	202°/7°	68	NNE-SSW extension
	Normal dip-slip						48	
	Left Normal strike-slip faults						4	
East fault zone (EFZ), sites 3,4,5,and 6	Left normal Fault	46	0.28	284°/ 82°	161°/4°	71°/6°	46	90% NNE-SSW extension and 10% NNW-SSE extension
	Normal dip-slip						50	
	Left Normal strike-slip faults						4	
West fault zone (WFZ)	Left normal Fault	10	0.62	101°/ 81°	320°/7°	229°/5°	50	NNE-SSW extension
	Normal dip-slip						20	
	Left Normal strike-slip faults						30	

Table 7.1 Results of the reduced Paleostress tensors from fault-slip data of the Hun Graben.

This tensor belongs to pure strike-slip regime, with a rake ranging between 0º - 10º and indicates WNW-ESE compression and NNE-SSW extension giving left lateral or sinistral kinematics.

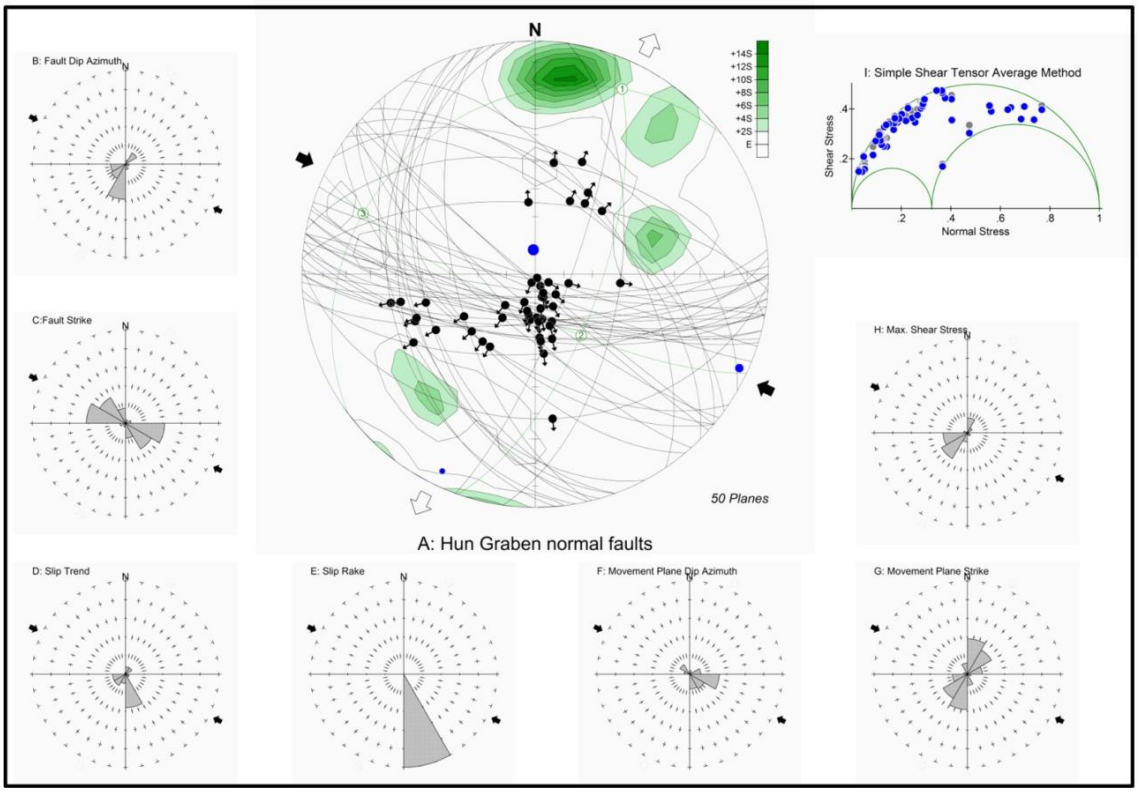


Fig. 7.5 Results of different stress phases for the Hun Graben. Field data diagram are Schmidt's projections of lower hemisphere. A: System 2: Normal dip-slip. Faults are great circles, slickenside lineations are dots with arrows indicating the sense of motion of the hanging wall. Computed stress axes are represented as large blue dot (σ1), medium blue dot (σ2) and small blue dot (σ3). Large divergent white arrows indicate the horizontal extensional stress direction (σ3) whilst large convergent black arrows indicate maximum principal stress axis (σ1). Rose diagrams for the structures observed Hun Graben. The radius of the rose corresponds to the class with the highest frequency as represented in the figure (B to I).

7.4.3 Paleostress tensor analysis along Eastern Fault Zone (EFZ):

About 119 fault slip measurements were recorded along the Eastern Fault Zone of Hun Graben (EFZ). The orientation of the mean regional principal stresses and stress ratio (Fig. 7.7 and Table 1) indicates WNW-ESE compression and NNE-SSW extension where characterized by a vertical, maximum principal stress axis (σ1) 43º/ 82º, and a horizontal stress intermediate principal stress axis (σ2) 293º/3º, and the minimum principal stress axis (σ3) 202º/7º; with stress ratio (Φ) equals 0.32. In terms of fault slip type this region is dominated by about 56% of left normal movement (rake: 51º - 80º), and 40% of normal fault slip (rake: 81º - 100º), whilst left strike-slip stress (rake: 0º - 10º) represents only 4%. This means that the EFZ of the Hun Graben seems to have moved mainly perpendicular to the EFZ scarp rather than other directions.

Measurements from sites 3, 4, 5, and 6 on the EFZ scarp show the orientation of the mean regional principal stresses is split into two extension directions (Fig. 7.8 and Table 1): firstly NNW-SSE compression and ENE-WSW extension, secondly ENE-WSW compression and NNW-SSE extension. The maximum principal stress axis (σ1)

284º/ 82º, is vertical, whilst the intermediate principal stress axis (σ2) 161º/4º, and the minimum principal stress axis (σ3) 71º/6º; correspond to horizontal stress with stress ratio (Φ) equal to 0.28 and dominated by a normal slip faults. It means that these tensors maybe responsible for producing the conjugate NE and NW left normal-slip faults.

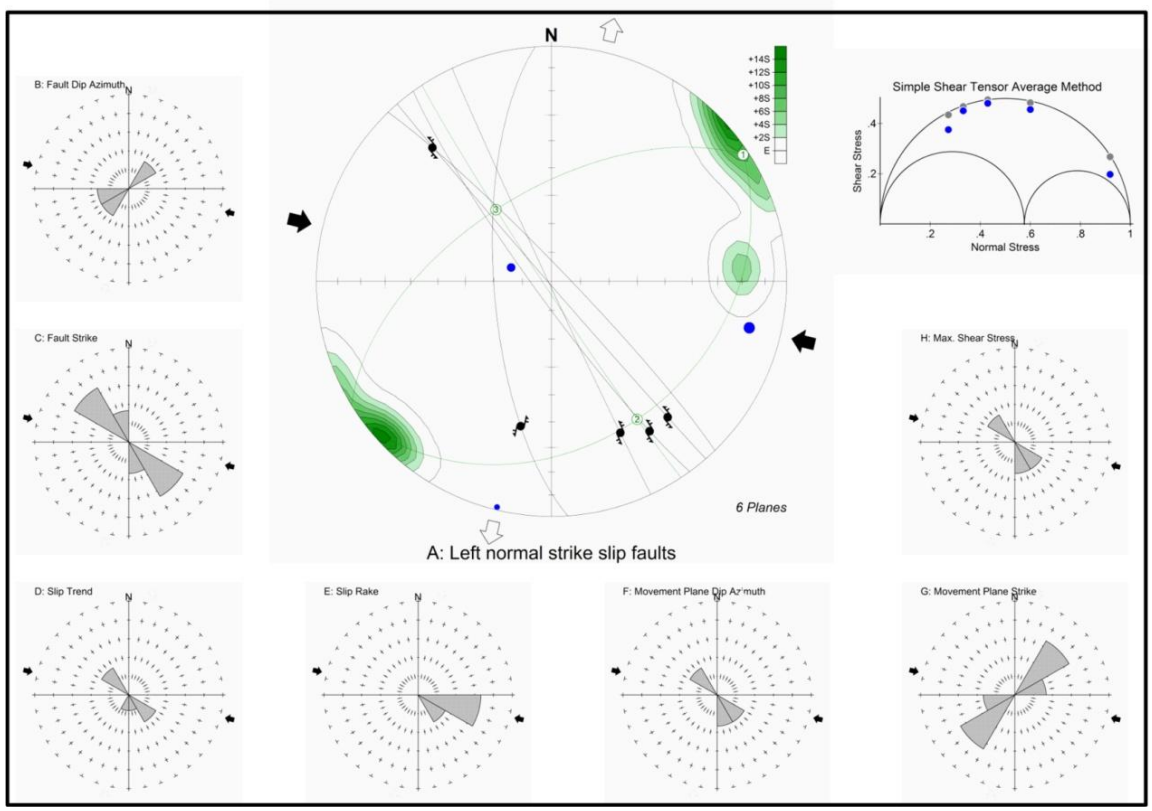


Fig. 7.6 Results of different stress phases for the Eastern Fault Zone (EFZ) of Hun Graben. Field data diagram are Schmidt's projections of lower hemisphere. A: System 3: Left Normal strike-slip faults . Faults are great circles, slickenside lineations are dots with arrows indicating the sense of motion of the hanging wall. Computed stress axes are represented as large blue dot (σ1), medium blue dot (σ2) and small blue dot (σ3). Large divergent white arrows indicate the horizontal extensional stress direction (σ3) whilst large convergent black arrows indicate maximum principal stress axis (σ1). Rose diagrams for the structures observed Hun Graben. The radius of the rose corresponds to the class with the highest frequency as represented in the figure (B to I).

7.4.4 Paleostress tensor analysis along West Fault Zone (WFZ)

Only 10 fault slip measurements were recorded along West Fault Zone of Hun Graben (WFZ) were made at 3 different locations over WFZ scarp (Fig. 7.9 and Table 1). In terms of fault slip type this region is dominated by about 50% of left lateral movement, and 30% of left normal strike slip, whilst normal fault slip stress represents only 20%.

The orientation of the mean regional principal stresses and stress ratio indicates NW-SE compression and NE-SW extension where characterized by a vertical, maximum principal stress axis (σ1) orientated 101º/ 81º, with a horizontal stress

intermediate principal stress axis (σ2) 320º/7º, and a minimum principal stress axis (σ3) was 229º/5º; with stress ratio (Φ) equals 0.62. In terms of fault slip type this region is dominated by about 67% of left lateral movement, and 48% of normal fault slip, whilst strike-slip stress represents only 4%.

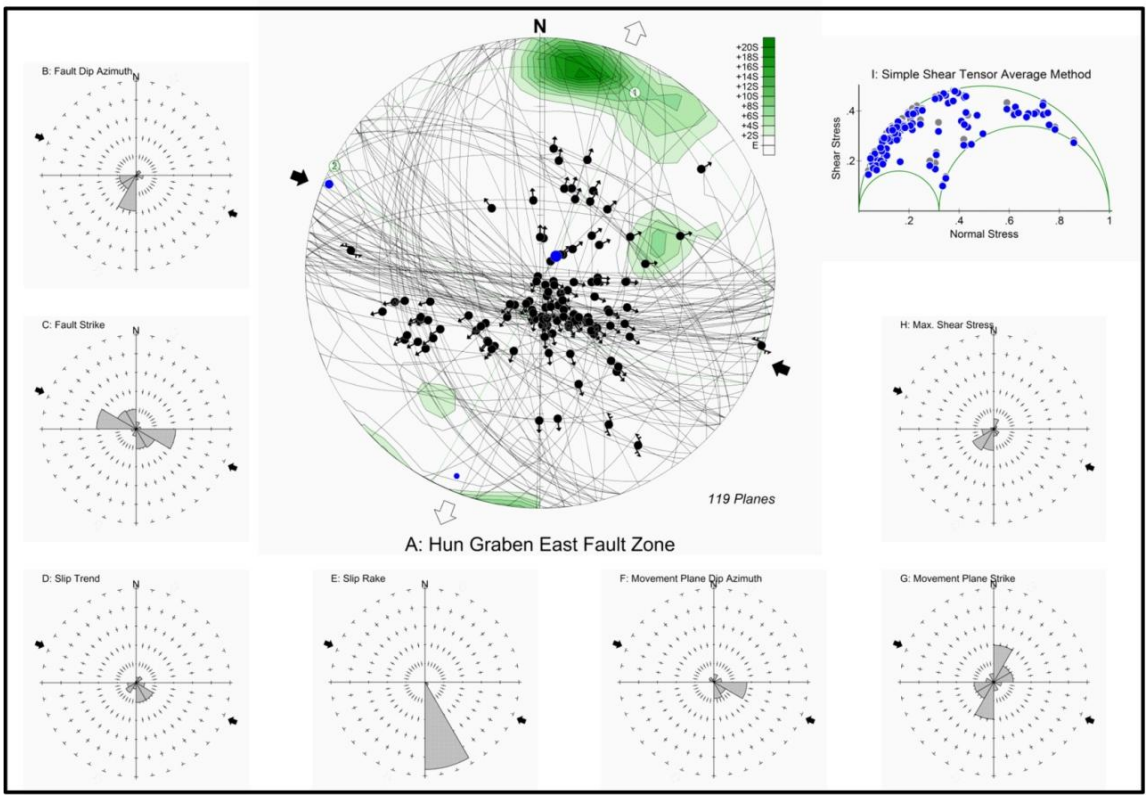


Fig. 7.7 Results of different stress phases for the Eastern Fault Zone (EFZ) of Hun Graben. Field data diagram are Schmidt's projections of lower hemisphere. A: Left Normal strike-slip faults . Faults are great circles, slickenside lineations are dots with arrows indicating the sense of motion of the hanging wall. Computed stress axes are represented as large blue dot (σ1), medium blue dot (σ2) and small blue dot (σ3). Large divergent white arrows indicate the horizontal extensional stress direction (σ3) whilst large convergent black arrows indicate maximum principal stress axis (σ1). Rose diagrams for the structures observed Hun Graben. The radius of the rose corresponds to the class with the highest frequency as represented in the figure (B to I).

7.4.5 Summary and discussion of Hun Graben

150 fault planes with their slickenlines were selected from the east and west margins of the Hun Graben from the western Sirt Basin. In general most of the faults observed correspond to minor structures with displacement ranging from several centimetres to several metres. Various types of faults (left normal faults, normal faults, and strike-slip faults) were observed, but about 56% of the observed faults are predominantly left normal faults (oblique dip-slip component), with their pitch (rake) ranging from 51º to 80º and their dip ranging from 70° to 90° (high-angle

normal faults). A NNE-SSW direction and WNW-ESE compression extension regime was inferred from 66 measurements in the study area.

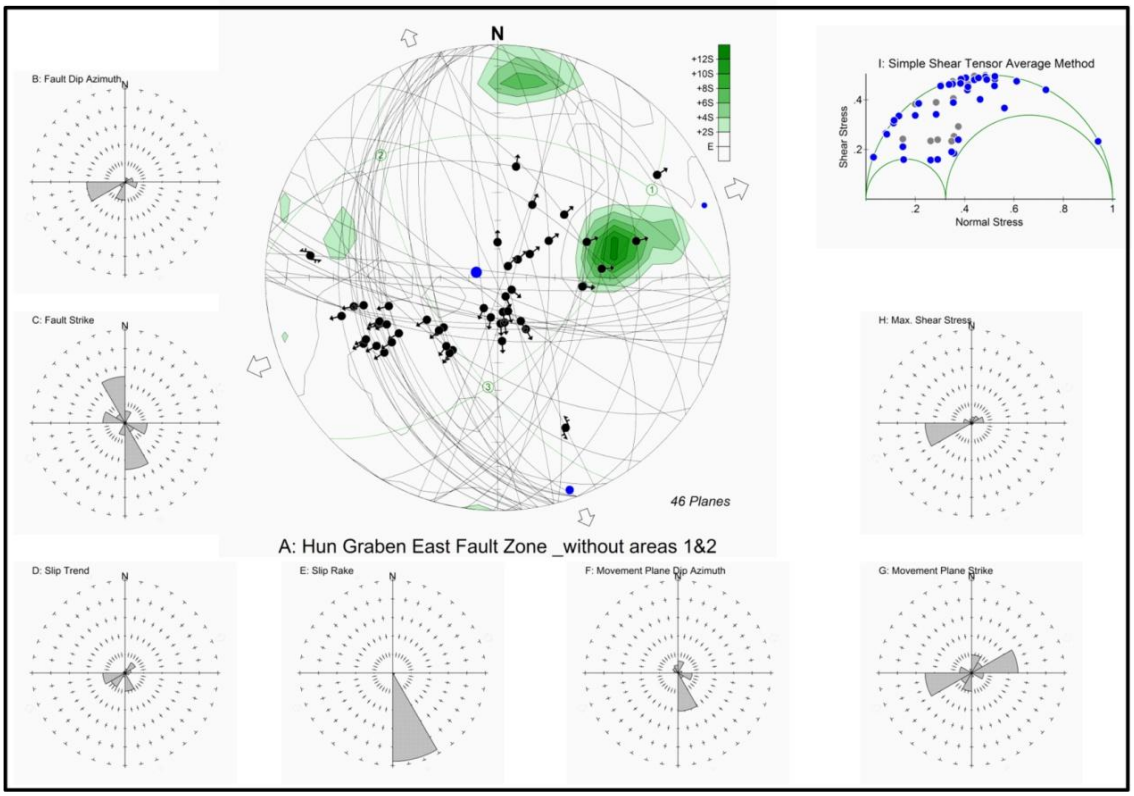


Fig. 7.8 Results of different stress phases for the Hun Graben. Field data diagram are Schmidt's projections of lower hemisphere. A: The Eastern Fault Zone (EFZ) of Hun Graben without area 1&2. Faults are great circles, slickenside lineations are dots with arrows indicating the sense of motion of the hanging wall. Computed stress axes are represented as large blue dot (σ1), medium blue dot (σ2) and small blue dot (σ3). Large divergent white arrows indicate the horizontal extensional stress direction (σ3) whilst large convergent black arrows indicate maximum principal stress axis (σ1). Rose diagrams for the structures observed Hun Graben. The radius of the rose corresponds to the class with the highest frequency as represented in the figure (B to I).

Fifty measurements from normal faults were recorded from the study area (Fig. 7.5 and Table 1) and represents about 40% of total fault slip measurements with a rake ranging between 81º - 100º indicating WNW-ESE compression and NNE-SSW extension. Sinistral strike-slip faults are less abundant than normal faults representing about 5% of the total measured faults with a rake ranging between 0º - 10º and indicates WNW-ESE compression and NNE-SSW extension.

This interpretation implies that the dominant directions of extension average N20-25°E in the Hun Graben with minor predicted directions of extension averaging N10-15°W at the eastern margin (EFZ) showing that the σ3 directions has rotated counterclockwise from NNE–SSW to NNW–SSE. It seems that two principal extensions have affected the graben, one of which is perpendicular (transverse) to the basin axis to give the normal

faults whilst the 2nd is oblique to the axis and responsible for the left normal and strike slip faults that mainly appear along the western margin of the Hun Graben.

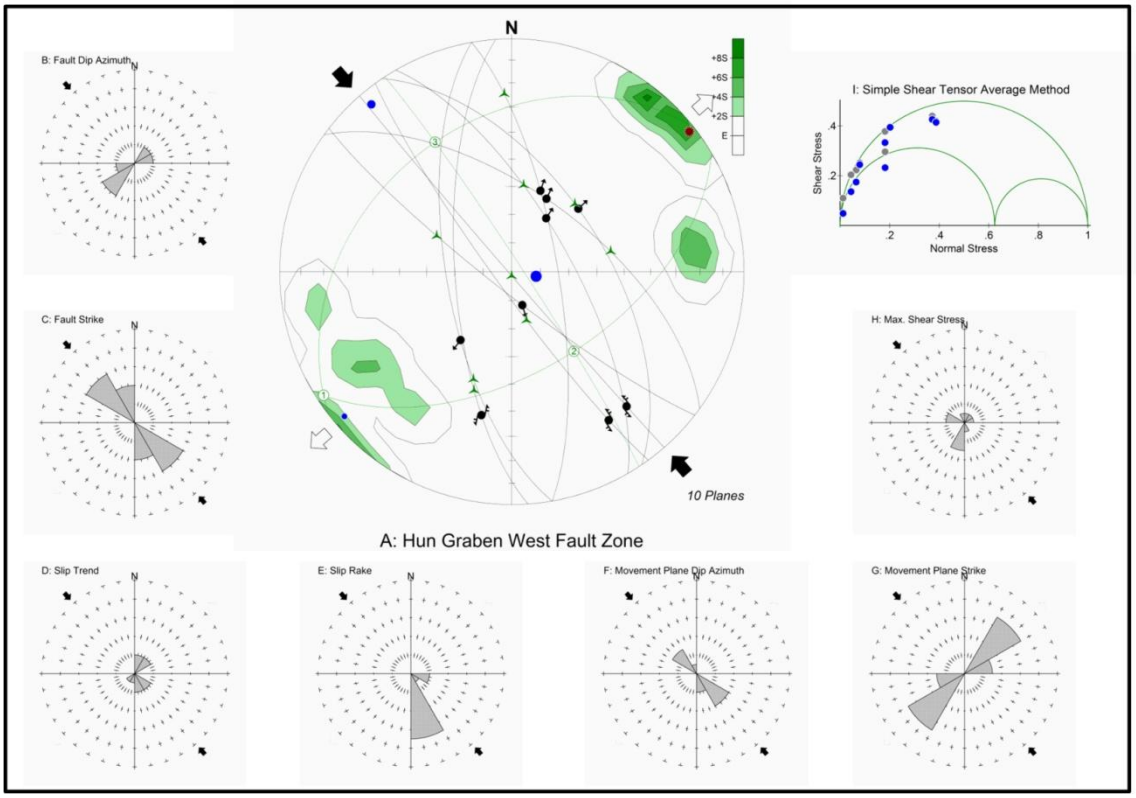


Fig. 7.9 Results of different stress phases for the Hun Graben. Field data diagram are Schmidt's projections of lower hemisphere. A: The West Fault Zone (WFZ) of Hun Graben without area 1&2. Faults are great circles, slickenside lineations are dots with arrows indicating the sense of motion of the hanging wall. Computed stress axes are represented as large blue dot (σ1), medium blue dot (σ2) and small blue dot (σ3). Large divergent white arrows indicate the horizontal extensional stress direction (σ3) whilst large convergent black arrows indicate maximum principal stress axis (σ1). Rose diagrams for the structures observed Hun Graben. The radius of the rose corresponds to the class with the highest frequency as represented in the figure (B to I).

The directions of extension computed from fault slip data sets are remarkably homogeneous in all sites (Figs. 7.4-9). These major faults controlled the geometry of the Hun Graben and reflects the regional NNE–SSW extension that has rotated anti-clockwise toward NNW–SSE directions superimposed with transtension which were a consequence of the pre-existing basement structures (Fodor et al., 2005; Peregi et al., 2003, and Marovic´, 2007) described in many studies (Schafer et al, 1980; Abadi, 2002).

Oblique extension in the Tunisia-Libya seismic zone could be regarded as internal deformation of the African plate and represented as a clockwise rotation of the Ionian Sea region north of this zone at rate - 0.2° Myr-1 around a pole at 28° N, 20°E relative to the stable interior of the African plate (Samir Bouaziz et al, 2002).

On other hand rift systems that undergo extension oblique to the basin bounding faults commonly show complex multimodal fault patterns (e.g., Withjack and Jamison, 1986; Clifton et al., 2000; Dewey, 2002; De Paola et al., 2005a, 2005b). As the extension directions calculated in Hun Graben appear slightly oblique to the trend of the Hun Graben bounding faults, it is likely that this area has undergone transtensional deformation.

Regional extension related to the subsidence of the NW–SE elongated Sirt Basin structures that was active during the Late Cretaceous extends north westward to the offshore basins. The Late Cretaceous extensions evidenced in north central Libya is characterized by a mainly NE–SW to E–W component. This Late Cretaceous normal faulting affected the whole North African margin, forming NW–SE to NNW–SSE striking basins. Such a NE–SW extension was active eastward in the Sirt basin (Baird et al., 1996), and offshore in the Tarabulus basin and in the Pelagian shelf (Anketell, 1996).

The WNW-ESE compression and NNE-SSW extension suggested by this study is consistent with progressive collisional coupling of Africa and Europe, under approximately northwest–southeast compressional stresses during the Late Eocene, (Ziegler et al., 1998; Cloetingh et al., 2005). During this time in the Sirt Basin, a thick succession of postrift sediments were being deposited from the Late Eocene until the Miocene whilst in the western part of the basin, large parts of the Tertiary sequence were been eroded (e.g., Gumati and Schamel, 1988), which is contemporaneous with the widespread volcanic activity. In addition, volcanic activity occurred immediately west of the Sirt Basin (Al Haruj volcanics) mainly as an outcome of the intersection of differently oriented fracture zones (Al Qargaf and Tripoli-Tibesti arches) but possibly also affected by the intersection of NNE-SSW and NNW-SSE extension which is the outcome in this work. This volcanic episode was widespread in east and northwest Africa (Abadi, 2008) and has a range of age dates, suggesting early Eocene to Pliocene (Wilson and Guiraud, 1992).

Dextral strike-slip movement along the main Europe-Africa plate margins along the Sabratah-Cyrenaica fault system may have caused the renewed rifting and further extension of the Sirt Basin and east-west–oriented basins in Egypt (Anketell, 1996, Guiraud et al., 2001) and would be compatible with north-northeast–south southwest extensional stresses.

The rejuvenation of strike-slip faults displacements, under fluctuating stress fields, facilitated the vertical migration of hydrocarbons (Guiraud and Bosworth, 1997). This interpretation is in agreement with Eocene–present-day paleostress analysis in the Hun Graben although the strike-slip faults and palaeostress changes are certainly present but play a minor role which represent only 5% of the total measured faults as shown in this study.

The western edge of the Sirt basin, including the Hun Graben, has been one of the most seismically active regions in Libya throughout historic time (Suleiman, and Doser, 1995). This was manifest as a complex series of strike-slip earthquakes along the eastern boundary fault of the graben in 1935.

7.5 Northwest Libya (Jifarah Basin and Nafusah Uplift)

The aim for this part of the study was to examine the Mesozoic fault kinematics in another basement province outside the Sirt Basin. Provided the faults are of similar age, any differences in basement influence compared to the Sirt Basin should be reflected in different fault geometries and kinematics. Anketell and Ghellali (1991) demonstrated that this area is dominated by east-west and NNW-ESE fault directions in the Mesozoic section with an en echelon arrangement, which they interpreted as Riedel shears and imbricate fan splays formed as a result of strike slip movement on the South Atlas-Jifarah dislocation. They developed a model which suggested an analogy between the imbricate fan splays visible in the Wadi Ghan area south of Al Aziziyah with the strikingly similar fault trends in the Sirt Basin, and attributed both to strike-slip faulting associated with underlying basement dislocations.

Both sites 1 and 2 (Fig. 7.2) are located in Al Aziziah area belonging to the Jifarah coastal plain, which is bounded to the south by the escarpment of the Jabel Nafusah Uplift, a rocky plateau that dips gently southwards towards the Sahara desert and faces north to the Mediterranean Sea. It represents a down-faulted terrace on the continental margin.

The Jifarah Basin was affected by syn-depositional faulting during the Triassic and by shearing during the Neocomian which reflects major tectonic activity along the southern margin of Tethys. The Al ziziyah fault zone is one of four east-west trending fault zones (coastal, Al ziziyah, Tiji and Nalut) that affected the trend of basement fractures in the Jifarah region and was controlled by the Hercynian “Jeffara flexure” Anketell and Ghellali (1991).

The sites 3 & 4 (Fig. 7.2) are located on the escarpment of the Jabel Nafusah Uplift in two outcrops of the middle Triassic Kurush Formation and the upper Triassic of the Abu Ghaylan Formation. The Jabal Nafusah Uplift is a major east-west ridge which separates the Ghadamis Basin from the Jifarah Basin. It is bounded to the north by the Jifarah Fault and the Jifarah Basin and to the south by the Ghadamis Basin. The Hercynian orogeny inverted the northern Ghadamis Basin into a prominent east-west arch which was extensively eroded during the Permian, exposing the Precambrian core of Pharusian rocks in the area.

Another five sites numbered 5 to 9 (Fig. 7.2) in the Gharyan fault zone (GFZ) were studied in rocks of the Abu Ghaylan Formation, comprising the Upper Jurassic Kikla Sandstone as well as the youngest outcrops of the Nalut, the Sidi Al Said and the Qaser Tighrinah Formation which are mainly dolomitic limestones of Upper Cretaceous formations on the highest elevations in the area.

The southeast areas of Gharyan were covered by basalt sheets forming flat and broad plains forming dark hills made of phonolite and basalt which were a result of the tectonic events produced in the Jabal Nafusah in the post-Cretaceous.

This area is represented by the Gharyan-Tarhuna region is highly affected by tectonic events which resulted in normal faults belonging to the trending of NW-SE, directions (El-Hinnawy, and Cheshitev, 1975; and Ghellali, 1977).

Site 10 (Fig. 7.2) is located in the eastern portion of the study area refered to as Wadi Ghan Fault Zone on a plateau which is made up of mainly hard and dolomitic limestone of upper Cretaceous age. Previous paleostress results (Gamberlu, 2007) from the fault zone showed an ESE-WNW extension and NNE-SSW directed compression directions which resulted in the volcanic intrusion and activities in this area and was responsible for the existence of compressional fractures as well. This trend of faulting is characterised by its large throws exposed over a long extent, and it is clearly observed in the field, it runs parallel to the main tectonic line of the Jabal uplift and its associated faults (El-Hinnawy, and Cheshitev, 1975).

This analysis performed by Gamberlu (2007) was carried out on a group of data collected from the two main fault systems that trend perpendicular to each other (Fig. 7.2), the first fault system was the E-W trending Al Azizyah fault system observed in two localities within the Jifarah basin. The first locality was along the Al Azizyah fault zone (AZFZ), where the measurements were taken from two different stations in the Al Azizyah area (Fig. 7.2). The second location was from the south of Al Azizyah city at

Al Azizyah quarry in the Ras Allefa area, where a well-exposed normal fault planes exists along with igneous dikes. Both sites are in the Al Azizyah formation made of limestone and dolomitic limestone of the Middle to Upper Triassic age.

The second set of measurements were taken from Nafusah Uplift along the Gharyan fault Zone (GFZ) in outcrops of the middle Triassic Kurush Formation in two outcrops and the upper Triassic of the Abu Ghaylan Formation from four outcrops. Another four sites of the Abu Ghaylan Formation as well as the youngest outcrops of (the Nalut, the Sidi Al Said and the Qaser Tighrinah) upper Cretaceous formations; the last site measured was the upper Jurassic Kikla sandstone Formation. In all locations, the faults measured vary in scale from centimetres to more than ten metres.

Gamberlu (2007) has collected about 200 faults with slip orientations measured in this study area. She found that more than 92% of the measured data were normal faults with range of dip from (25˚ to 90˚) while their pitch angle ranges from (7˚ to 90˚) although (80%) of the pitches are more than (75˚). Three strike slip faults were detected with pitch angle between (7˚- 25˚) and dips greater than (75˚).

From these fault data, results from a paleostress analysis by Gamberlu, (2007) provided two stress field orientations for this area of northwest Libya. The paleostress tensor of the whole area was grouped according to the orientation of the principal stress axes and the relative order of fault motion. On the basis of the orientation relation of the structure and tensors, it appears to be possible to correlate a specific Paleostress tensor with a specific rift structure.

Phase 1: represents the tensor inversion direction of WNW-ESE extension regime measured along Gharyan fault system where σ1 is sub-vertical, and σ3 is sub horizontal, and this movement is recorded in the upper Triassic of the Abu Ghylan carbonate rock.

Phase 2: demonstrates the results obtained from thirteen stations, where the tensor inversion shows ENE-SWS extension direction regime. The orientation of the mean regional principal stresses axes σ1 lies nearly vertically and σ3 is horizontal. The fault slip data related to this phase was measured in mid-upper Triassic age rocks.

7.6 The present study results

Data from ten sites were made available to the present study from northwest Libya (Jifarah Basin and Nafusah Uplift) and 200 fault slip data were used in the calculation

(Fig. 7.2). Sites 1 and 2 were measured in the Jifarah Basin along the Al Azizyah fault zone (AZFZ), whilst sites 3 and 4 were located on the Jabal Nafusah escarpment fault zone (JEFZ). The sites 5 to 9 measurements were taken from Jabal Nafusah Uplift along the Gharyan fault Zone (GFZ) whilst site 10 is located on the eastern side of Jabal Nafusah Uplift along the Wadi Ghan fault Zone (WGFZ).

7.6.1 Inversion Procedures

The same procedures used in the Hun Graben analysis have been applied to data from this area using My Fault TM stereonet software and data sorting.

7.6.2 Whole study area

In the bulk inversion of all fault data (step 1) three separate sets of paleostress axes can be derived, one for each fault system analyzed. The resultant paleostress tensor for the whole area was grouped according to the orientation of the principal stress axes (i.e., system 1 right normal dip-slip, system 2 Normal dip-slip, and system 3 Left Normal strike-slip faults which are very rare and neglected (Figs 7.10 -11 and Table 7.2). On the basis of the orientation relationships between the structures and tensors, it appears possible to correlate a specific paleostress tensor with a specific rift structure. The parameters of the reduced tensor for the investigated area are illustrated in table (7.2) showing the principal stress and the number for Φ which expresses a linear relation between the principal stress directions.

System 1: Normal dip-slip

The stress tensor recorded from ninety six measurements in the study area (Fig. 7.10 and Table 2) represents about 71% of total fault slip measurements. It is characterized by a vertical, maximum principal stress axis (σ1) orientated 42°/ 86°, and a horizontal stress intermediate principal stress axis (σ2) 285°/2°, and the minimum principal stress axis (σ3) 195°/4°; with stress ratio (Φ) equals 0.14.

This tensor belongs to a pure normal dip-slip regime, with a rake ranging between 81º - 100º and indicates extension in a NNE-SSW (N12°E) direction and less well developed in the WNW-ESE (N102°E) direction.

System 2: Right normal dip-slip

Predominantly NNE-SSW (N25°E) extension and less WNW-ESE (N115°E) compression regime recorded from thirty nine measurements in the study area (Fig. 7.11 and Table 2). This slip type represents about 29% of total fault slip measurements. It gives a maximum principal stress axis (σ1) orientated 96º/76º, as subvertical, whilst the intermediate principal stress axis (σ2) 299°/13°, and the minimum principal stress

axis (σ3) 208°/5°; correspond to horizontal stress with stress ratio (Φ) equals 0.28. The tensor belongs to a right normal dip-slip fault regime with a rake slip direction ranging between 101º - 130º (Threet, 1973). It indicates a NNE-SSW (N25°E) extension and WNW-ESE (N115°E) compression regime.

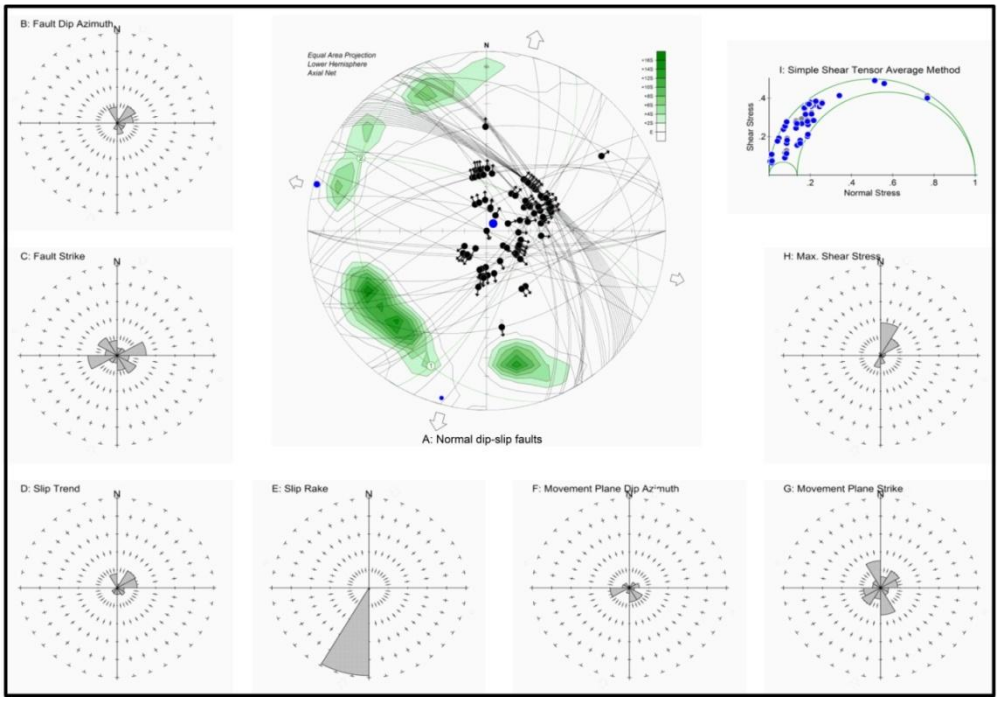


Fig. 7.10 Results of different stress phases for northwest Libya (Jifarah Basin and Nafusah Uplift). Field data diagram are Schmidt's projections of lower hemisphere. A: System 1: Normal dip-slip. Faults are great circles, slickenside lineations are dots with arrows indicating the sense of motion of the hanging wall. Computed stress axes are represented as large blue dot (σ1), medium blue dot (σ2) and small blue dot (σ3). Large divergent white arrows indicate the horizontal extensional stress direction (σ3) whilst large convergent black arrows indicate maximum principal stress axis (σ1). Rose diagrams for the structures observed northwest Libya (Jifarah Basin and Nafusah Uplift). The radius of the rose corresponds to the class with the highest frequency as represented in the figure (B to I).

7.6.3 Paleostress tensor analysis along Al Azizyah fault zone (AZFZ), site 1 & 2

About 13 fault slip measurements were recorded along the Al Azizyah fault zone (AZFZ) (Fig. 7.12 and Table 2) were made at two different locations. The first area was along the Al Azizyah fault zone (AZFZ), where the measurements were taken and the second stop was south of Al Azizyah city at Al Azizyah quarry in the Ras Allefa area.

The orientation of the mean regional principal stresses and stress ratio indicates N-S to NNE-SSW (N2°E) and minor E-W to WNW-ESE (N92°E) extensions characterized by a vertical, maximum principal stress axis (σ1) 345°/ 81°, and a horizontal stress intermediate principal stress axis (σ2) 210°/6°, and the minimum

principal stress axis (σ3) 119°/6°; with stress ratio (Φ) equals 0.02. In terms of fault slip type this region is dominated by about 69% of normal fault slip, and 23% of left strike-slip movement, whilst right normal faults slip stress represents only 8% and represents only less than 2% from the whole study area.

Area of study	Tensor type	No. Of measured faults	Stress ratio (Φ)	Principal stress axis			% total measured faults	Regional principal stress orientations
				σ1	σ2	σ3		
Whole area	Right normal Fault	39	0.28	96°/ 76°	299°/13°	208°/5°	29	Predominantly NNE-SSW (N25°E) extension and less WNW-ESE (N115°E) compression
	Normal dip-slip	96	0.14	42°/ 86°	285°/2°	195°/4°	71	Predominantly NNE-SSW (N12°E) and less WNW-ESE (N102°E) extensions
Al Azizyah fault zone (AZFZ), site 1&2	Right normal Fault	13	0.02	345°/ 81°	210°/6°	119°/6°	8	Predominantly N-S to NNE-SSW (N2°E) and less E-W to WNW-ESE (N92°E) extensions
	Normal dip-slip						69	
	Left strike slip Fault						23	
Jabal Nafusah escarpment fault zone (JEFZ), sites 3&4	Right normal Fault	43	0.25	88°/ 81°	316°/6°	226°/7°	33	Predominantly NE-SW (N42°E) and less NW-SE (N132°E) extensions
	Normal dip-slip						67	
Gharyan fault zone (GFZ), sites 5 to 9	Right normal Fault	73	0.32	123°/ 89°	275°/1°	5°/1°	26	Predominantly N-S to NNE-SSW (N5°E) extension andless E-W to WNW-ESE (N95°E) compression
	Normal dip-slip						74	
Wadi Ghan fault zone (WFZ), site 10	Normal Fault	15	0.32	43°/ 82°	293°/3°	202°/7°	67	Predominantly WNW-ESE (N109°E) extension and less NNE-SSW (N19°E) compression
	Compression fracture						33	

Table 7.2 Results of the reduced Paleostress tensors from fault-slip data of northwest Libya (Jifarah Basin and Nafusah Uplift).

As shown in figure 7.10 and table 7.2 we can find left strike-slip movement only in this part of area study which very rare and neglected.

7.6.4 Paleostress tensor analysis of Jabal Nafusah escarpment fault zone (JEFZ), sites 3 & 4

Forty three fault slip measurements were recorded along Jabal Nafusah escarpment fault zone (JEFZ), from two different locations over the scarp (Fig. 7.13 and Table 2). In terms of fault slip type this region is dominated by about 67% normal slip faults, and 33% right normal slip faults.

The orientation of the mean regional principal stresses and stress ratio indicates predominantly NE-SW (N42°E) and minor NW-SE (N132°E) extensions with a vertical, maximum principal stress axis (σ1) 88°/ 81°, and a horizontal stress intermediate principal stress axis (σ2) 316°/6°, and the minimum principal stress axis (σ3) 226°/7°; and a stress ratio (Φ) that equals 0.25.

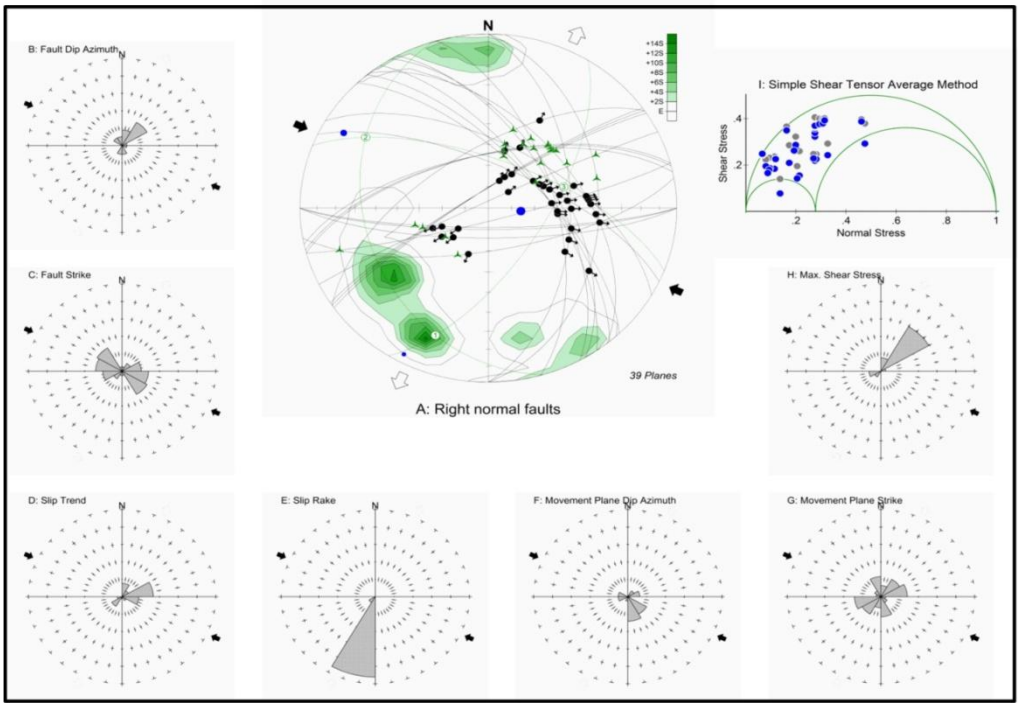


Fig. 7.11 Results of different stress phases for northwest Libya (Jifarah Basin and Nafusah Uplift). Field data diagram are Schmidt's projections of lower hemisphere. A: System 2: Right normal dip-slip. Faults are great circles, slickenside lineations are dots with arrows indicating the sense of motion of the hanging wall. Computed stress axes are represented as large blue dot (σ1), medium blue dot (σ2) and small blue dot (σ3). Large divergent white arrows indicate the horizontal extensional stress direction (σ3) whilst large convergent black arrows indicate maximum principal stress axis (σ1). Rose diagrams for the structures observed northwest Libya (Jifarah Basin and Nafusah Uplift). The radius of the rose corresponds to the class with the highest frequency as represented in the figure (B to I).

7.6.5 Paleostress tensor analysis of Jabal Nafusah uplift along Gharyan fault zone (GFZ), sites 5 to 9

Over Jabal Nafusah uplift along Gharyan fault zone (GFZ), seventy three fault slip measurements were recorded from five different locations (Fig. 7.14 and Table 2). The orientation of the mean regional principal stresses and stress ratio indicates predominantly N-S to NNE-SSW (N5°E) extension and minor E-W to WNW-ESE (N95°E) compression where characterized by a vertical, maximum principal stress axis (σ1) 123°/ 89°, and a horizontal stress intermediate principal stress axis (σ2) 275°/1°, and the minimum principal stress axis (σ3) 5°/1°; with stress ratio (Φ) equals 0.32. In terms of fault slip type this region is dominated by about 74% normal slip faults, and 26% of right normal slip faults.

7.6.6 Paleostress tensor analysis of Jabal Nafusah uplift along Wadi Ghan fault zone (WFZ), site 10

Fifteen fault slip measurements were recorded along the Wadi Ghan fault zone (WFZ) at one location (Fig. 7.15 and Table 2). In terms of fault slip type this region is

dominated by about 67% of normal slip faults, and 33% of compression fracture regime.

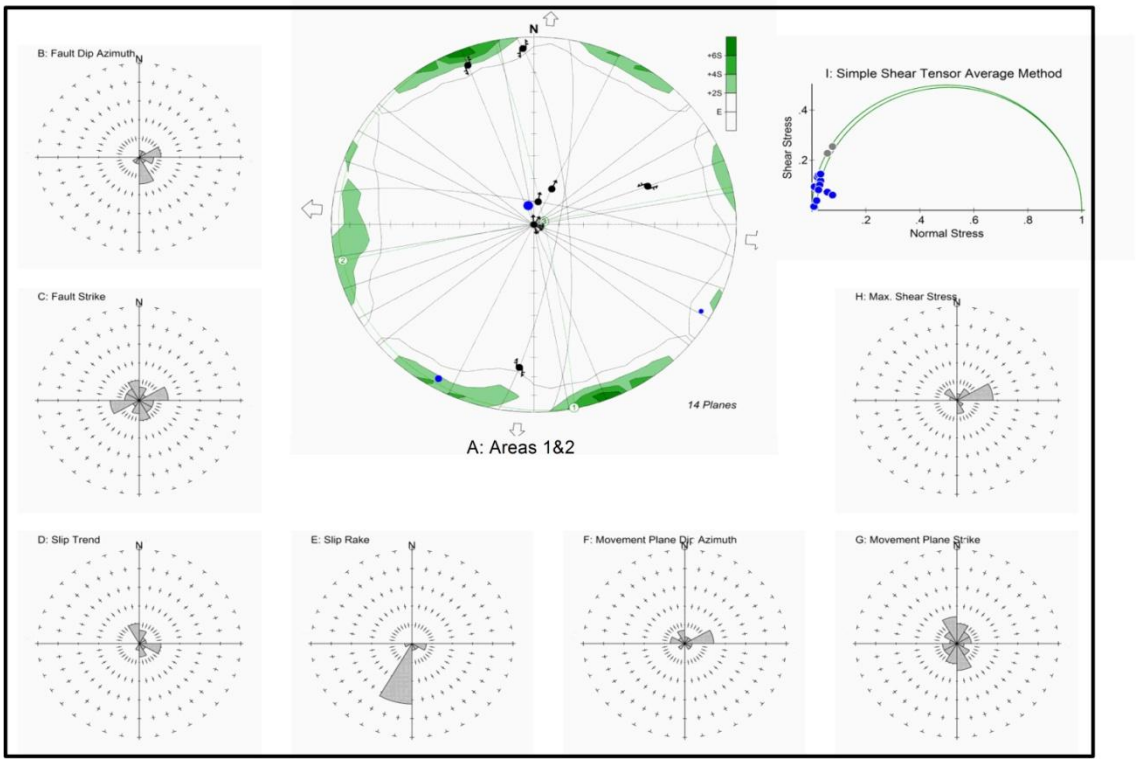


Fig. 7.12 Results of different stress phases for northwest Libya (along Al Azizyah fault zone (AZFZ), site 1&2, Jifarah Basin). Field data diagram are Schmidt's projections of lower hemisphere. A: areas 1&2. Faults are great circles, slickenside lineations are dots with arrows indicating the sense of motion of the hanging wall. Computed stress axes are represented as large blue dot (σ1), medium blue dot (σ2) and small blue dot (σ3). Large divergent white arrows indicate the horizontal extensional stress direction (σ3) whilst large convergent black arrows indicate maximum principal stress axis (σ1). Rose diagrams for the structures observed northwest Libya (Jifarah Basin and Nafusah Uplift). The radius of the rose corresponds to the class with the highest frequency as represented in the figure (B to I).

The orientation of the mean regional principal stresses and stress ratio indicates predominantly WNW-ESE (N109°E) extension and minor NNE-SSW (N19°E) compression with a vertical, maximum principal stress axis (σ1) 43°/ 82°, and a horizontal stress intermediate principal stress axis (σ2) 293°/3°, and the minimum principal stress axis (σ3) 202°/7°; with stress ratio (Φ) equals 0.32.

7.7 Summary and discussion of northwest Libya

200 fault planes with their slickenlines were selected on from northwest Libya (Jifarah Basin and Nafusah Uplift) for analysis.

In general most of the faults observed correspond to minor structures with displacement ranging from several centimetres to several metres. Various types of faults (normal faults, right normal faults, and a rare left strike-slip faults) were observed, but about 71% of the observed faults are predominantly normal faults, with their rake ranging from 51º to 80º and their dip ranging from 70° to 90° (high-

angle normal faults). A NNE-SSW (N12°E) and minor WNW-ESE (N102°E) extension regime was recorded from ninety six measurements in the study area.

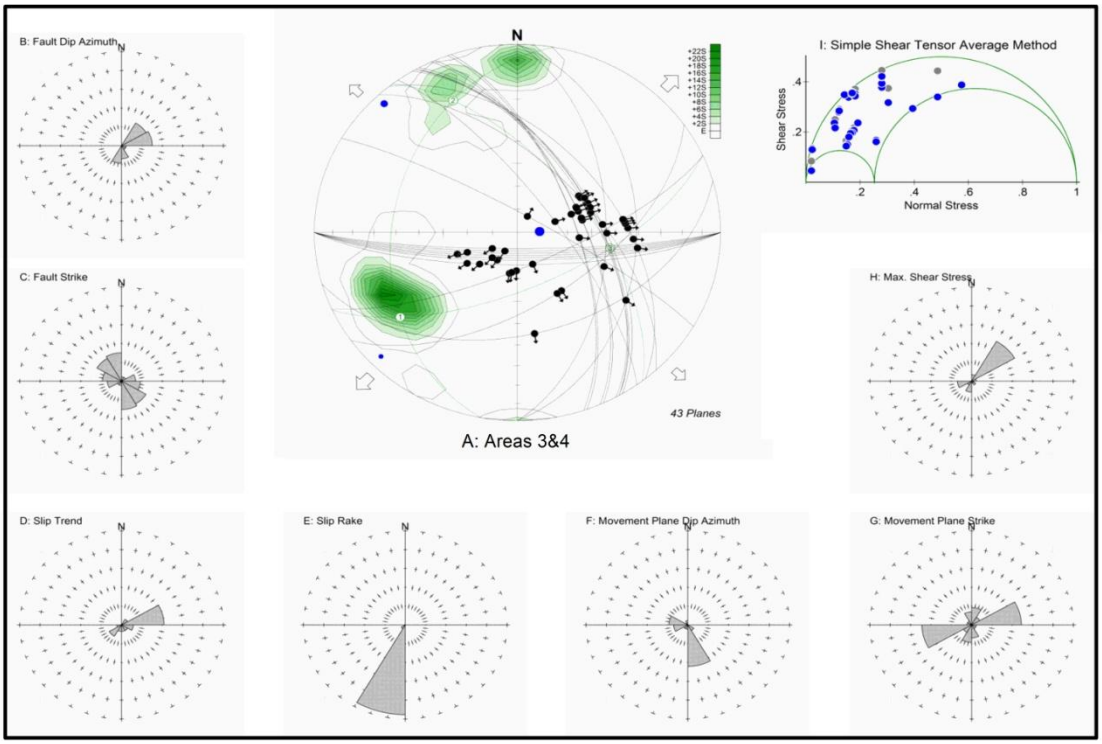


Fig. 7.13 Results of different stress phases for northwest Libya (Jifarah Basin and Nafusah Uplift). Field data diagram are Schmidt's projections of lower hemisphere. A: areas 3&4. Faults are great circles, slickenside lineations are dots with arrows indicating the sense of motion of the hanging wall. Computed stress axes are represented as large blue dot (σ1), medium blue dot (σ2) and small blue dot (σ3). Large divergent white arrows indicate the horizontal extensional stress direction (σ3) whilst large convergent black arrows indicate maximum principal stress axis (σ1). Rose diagrams for the structures observed northwest Libya (Jifarah Basin and Nafusah Uplift). The radius of the rose corresponds to the class with the highest frequency as represented in the figure (B to I).

Right normal slip faults are less abundant than normal faults representing about 29% of the total measured faults with a rake ranging between 101º - 130º and indicates predominantly NNE-SSW (N25°E) extension and minor WNW-ESE (N115°E) compression.

It is clear from this study that the area is predominantly characterized by NNE-SSW directions of extension ranging from N12°E to 25°E with lesser expected ENE-WSW directions of extension averaging N102°E where the σ3 directions rotate clockwise from NNE–SSW to ENE-WSW. The area was also affected by minor ENE-WSW direction of compression which led to the development of the right normal faults.

Paleostress results from this study has showed that the Gharyan region has experienced extension orientated in a NNE-SSW direction and ESE-WNW compression which might have resulted from volcanic intrusion, doming and folding where the beds at

Gharyan area are highly inclined due to the presence of the Gharyan dome, and they are arranged into hog-backed ridges around the dome centre (Gray, 1971).

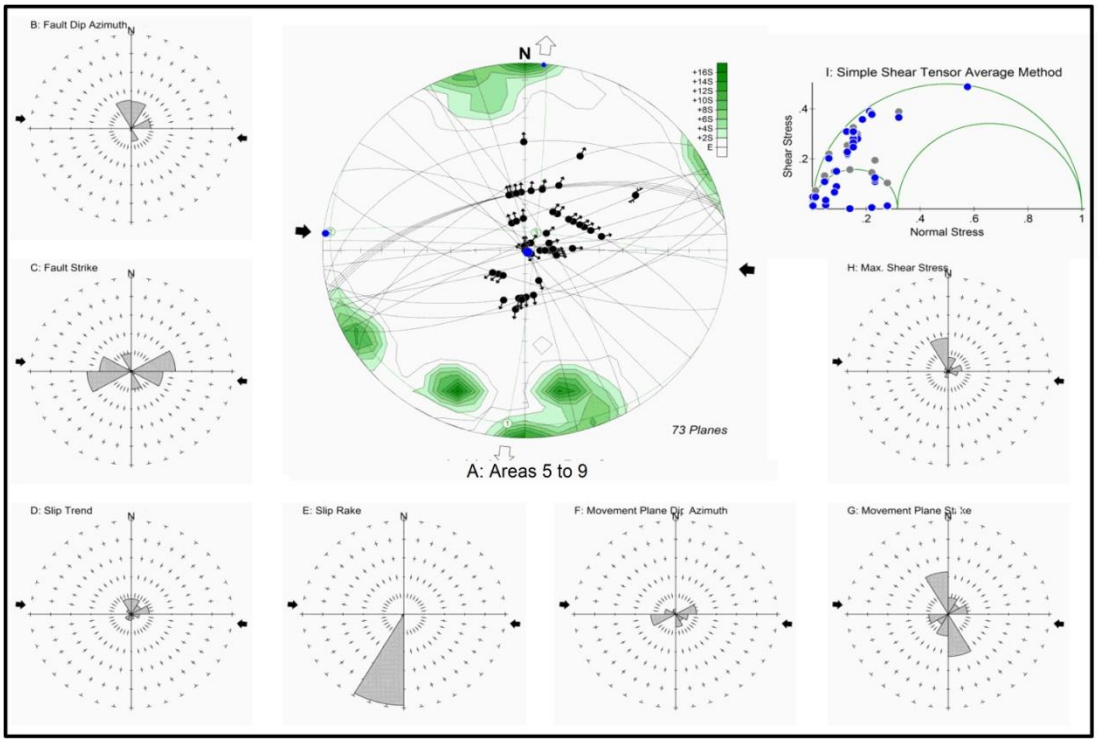


Fig. 7. 14 Results of different stress phases for northwest Libya (Jifarah Basin and Nafusah Uplift). Field data diagram are Schmidt's projections of lower hemisphere. A: areas 5 to 9. Faults are great circles, slickenside lineations are dots with arrows indicating the sense of motion of the hanging wall. Computed stress axes are represented as large blue dot (σ1), medium blue dot (σ2) and small blue dot (σ3). Large divergent white arrows indicate the horizontal extensional stress direction (σ3) whilst large convergent black arrows indicate maximum principal stress axis (σ1). Rose diagrams for the structures observed northwest Libya (Jifarah Basin and Nafusah Uplift). The radius of the rose corresponds to the class with the highest frequency as represented in the figure (B to I).

7.7.1 Extension regimes

The tectonic regime for the whole area is characterized by NNE-SSW extension with a lesser ESE-WNW component (Fig. 7.16) and represents the tensor inversion direction of:

a) Pure extension N-S to NNE-SSW (N2°E) and less E-W to WNW-ESE (N92°E) extensions NNE-SSW extension regime located mainly in the Jifarah Plain (Fig. 7.10 & 17 / Table 2).
b) NE-SW (N42°E) and less NW-SE (N132°E) extensions of Jabal Nafusah escarpment fault zone (JEFZ)
c) N-S to NNE-SSW (N5°E) extension of Jabal Nafusah Uplift along Gharyan fault zone (GFZ),
d) WNW-ESE (N109°E) extension of Jabal Nafusah Uplift along Wadi Ghan fault zone (WFZ)

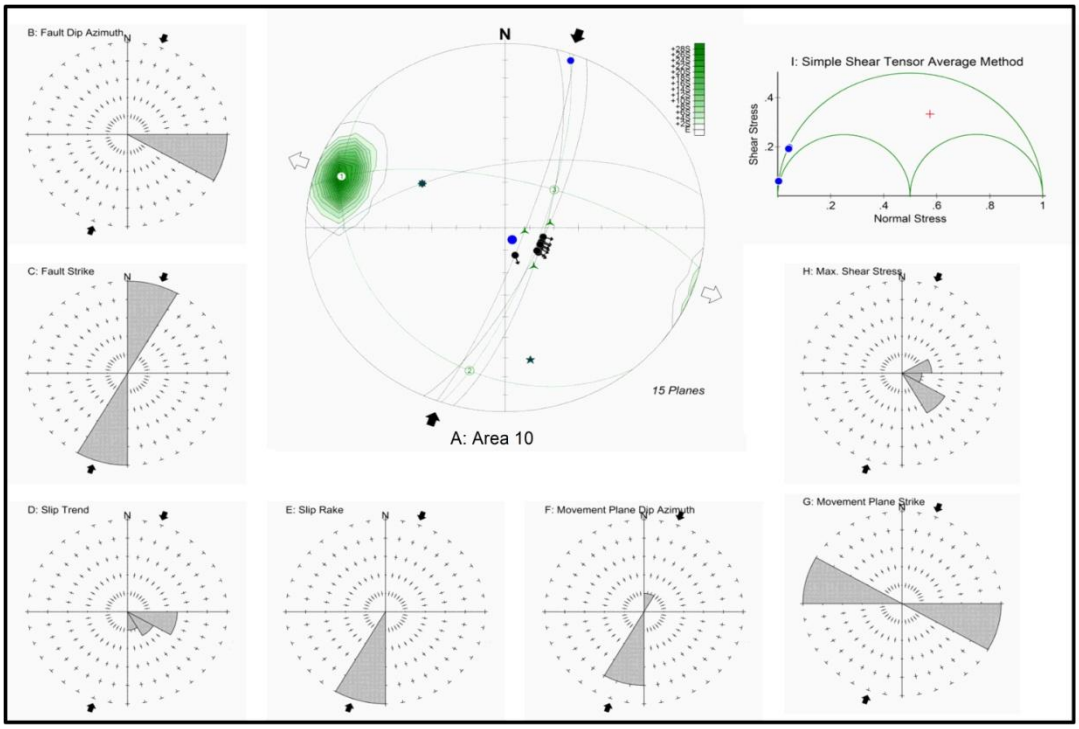


Fig. 7.15 Results of different stress phases for northwest Libya (Jifarah Basin and Nafusah Uplift). Field data diagram are Schmidt's projections of lower hemisphere. A: area 10. Faults are great circles, slickenside lineations are dots with arrows indicating the sense of motion of the hanging wall. Computed stress axes are represented as large blue dot (σ1), medium blue dot (σ2) and small blue dot (σ3). Large divergent white arrows indicate the horizontal extensional stress direction (σ3) whilst large convergent black arrows indicate maximum principal stress axis (σ1). Rose diagrams for the structures observed northwest Libya (Jifarah Basin and Nafusah Uplift). The radius of the rose corresponds to the class with the highest frequency as represented in the figure (B to I).

7.7.2 Compressional regime

This tectonic regime is restricted mainly on the Jabal Nafusah Uplift area as (Fig. 7.17) E-W to WNW-ESE (N95°E) compression along Gharyan fault zone (GFZ), and NNE-SSW (N19°E) compression along Wadi Ghan fault zone (WFZ).

This paleostress analysis results and the previous studies supports the suggested original view that these E-W and NW-SE trending structural trends are related to the Albian tectonic event, the Jurassic or Upper Cretaceous (Anketell and Ghellali, 1991).

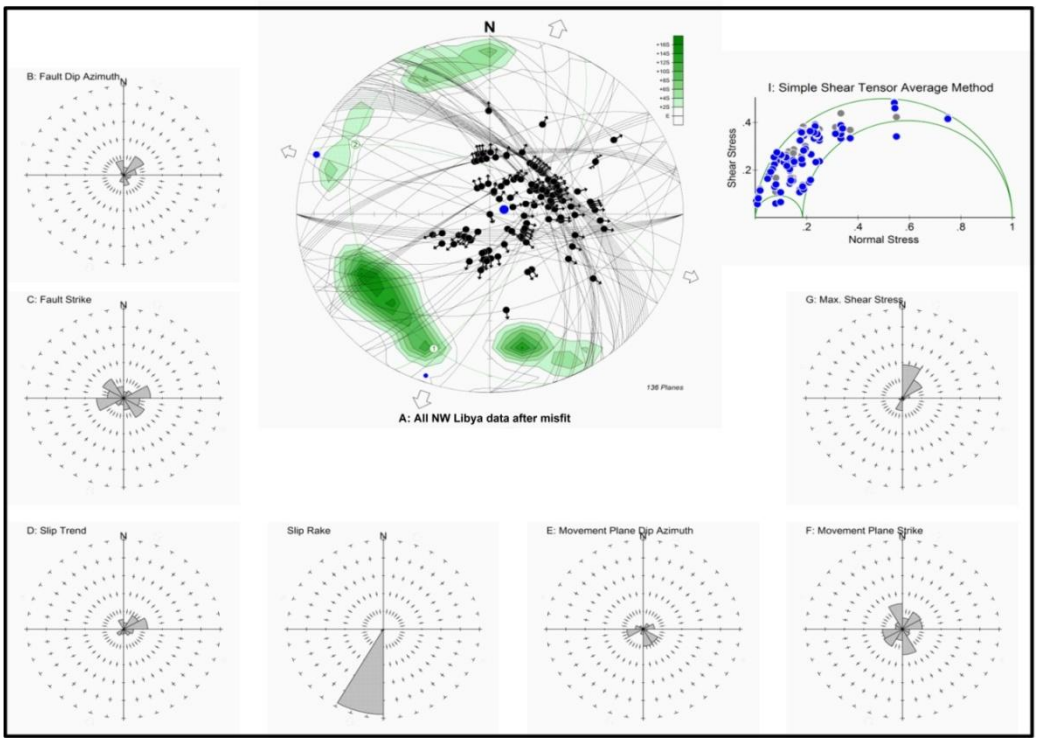


Fig. 7.16 Results of different stress phases for northwest Libya (Jifarah Basin and Nafusah Uplift). Field data diagram are Schmidt's projections of lower hemisphere. A: All NW Libya data after misfit. Faults are great circles, slickenside lineations are dots with arrows indicating the sense of motion of the hanging wall. Computed stress axes are represented as large blue dot (σ1), medium blue dot (σ2) and small blue dot (σ3). Large divergent white arrows indicate the horizontal extensional stress direction (σ3) whilst large convergent black arrows indicate maximum principal stress axis (σ1). Rose diagrams for the structures observed northwest Libya (Jifarah Basin and Nafusah Uplift). The radius of the rose corresponds to the class with the highest frequency as represented in the figure (B to I).

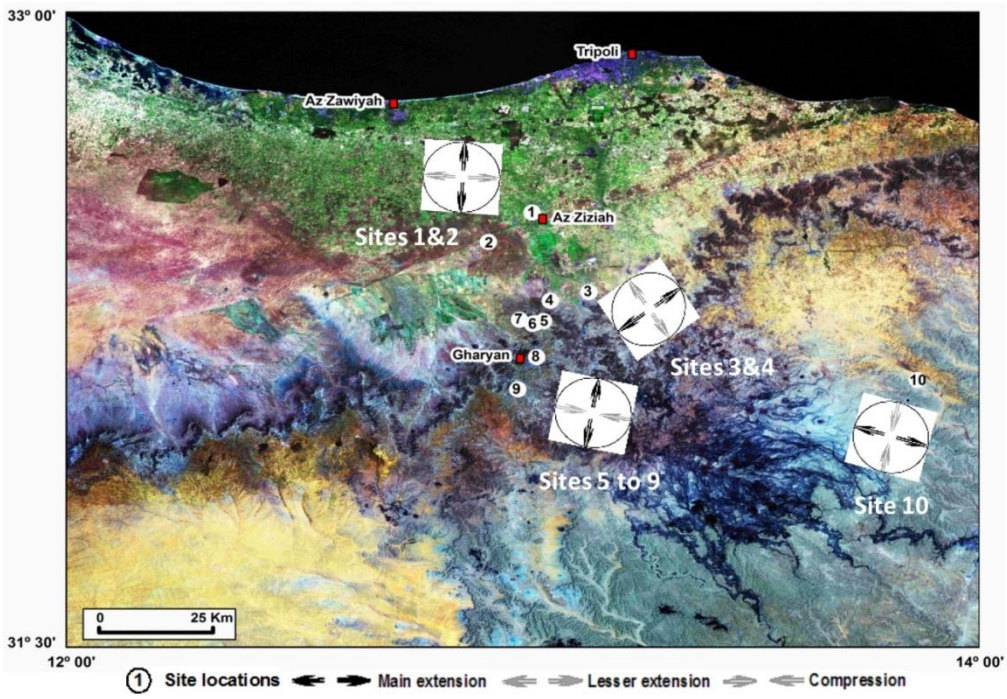


Fig. 7.17 The identified phases of the pure extension and compression for northwest Libya over the satellite (MrSid) imagery.

7.8 Summary

One of the most important issues in paleostress inversion studies is to date the constructed stress configurations. This may be achieved by dating the stratigraphical horizons involved in the faulting and the relationship between sedimentation and tectonics In this study palaeostress orientations and principal stress ratios have been calculated using standard inversion methods in MyFault™ (v. 1.03) stereonet software, produced by Pangaea Scientific Limited.

In general most of the faults observed in the Hun Graben and northwest Libya (Jifarah Basin and Nafusah Uplift) correspond to minor structures with displacement ranging from several centimetres to several metres. Various types of faults (normal faults, left normal faults, right normal faults and strike-slip faults) with their rake ranging from 51º to 80º and their dip ranging from 70° to 90° (high-angle normal faults) are present. A NNE-SSW directed extension regime with WNW-ESE compression is recorded by most of the measurements in the study area.

The directions of extension computed from fault slip data sets are remarkably homogeneous in all sites. The WNW-ESE compression and NNE-SSW extension resulted from this study is consistent with progressive collisional coupling of Africa and Europe, being under approximately WNW-ESE reactivated compressional stresses during Late Eocene-aged.

In the Hun Graben about 56% of the observed faults are predominantly left normal faults (oblique dip-slip component), whilst in Northwest Libya (Jifarah Basin and Nafusah Uplift) right normal slip faults represent about 29% of the total measured faults with a rake ranging between 101º - 130º and indicates predominantly NNE-SSW (N25°E) extension and less WNW-ESE (N115°E) compression.

However 71% of the observed faults are predominantly normal faults where the compressional regime is restricted mainly on the Jabal Nafusah Uplift area as E-W to WNW-ESE (N95°E) compression along Gharyan fault zone (GFZ), and NNE-SSW (N19°E) compression along Wadi Ghan fault zone (WFZ).

It is clear from this study that the two areas are predominantly characterized by NNE-SSW directions of extension ranging from N12°E to 25°E with lesser component of ENE-WSW.

CHAPTER 8: DISCUSSION

8.1 Introduction

This chapter brings together the main findings of each of the different strands of the thesis. The combination of several geological and geophysical methods (remote sensing interpretation, borehole data analysis, extensive seismic reflection profiles and maps, and paleostress analysis), have proved particularly useful in identifying various surface and subsurface regional and local structures in the study area. It is clear that uncertainties in interpretation from any one method are reduced by this combined approach.

In the following sections, the structural history, tectonic subsidence and rifting history, basin evolution are discussed in turn. The findings of this study have implications for the Sirt rift basin infill, Mesozoic rifting in the context of the break-up of Gondwana, the relationship, a geometric and kinematic model of NW Libya in the context of regional tectonics of the northern African platform and nearby European plate boundaries, and finally the petroleum prospectivity of the western Sirt Basin. For each of these topics, information is taken primarily from the findings and results of each chapter, with an effort to weave these into a coherent story and to provide some synthesis between the different parts.

8.2 Major structural elements in the western Sirt Basin

The main structure of the western part of Sirt Basin is characterised by a strong NNW-SSE structural grain (Fig. 8.1 and see Chapters, 4, 5, and 6). The area has also been divided into a number of structural domains based on the surface structures expressed on satellite imagery. The structural domains generally show good correlation with regional sub-surface structural features defined by seismic and borehole data (Chapters 5 and 6). A finding of this study is that the location of structural elements on the Tectonic Elements Map (Mouzughi, and Taleb, 1981 and published sources) appears to be over simplified, particularly the location of major bounding faults compared to the structures interpreted from the satellite imagery and seismic data.

It is also clear from this study that the western Sirt region has been the subject of multiple tectonic episodes. In common with other basins in North Africa it underwent extension during the Early Cretaceous. It was followed by a rotation in the extension direction and the formation of different populations of faults during the phases of

extension that occurred since the Early Cretaceous. This anticlockwise extension rotation indicated by thick sediments of Lower Cretaceous as evidenced by the isopach maps (Fig 5.3-8) that were constructed from the borehole data.

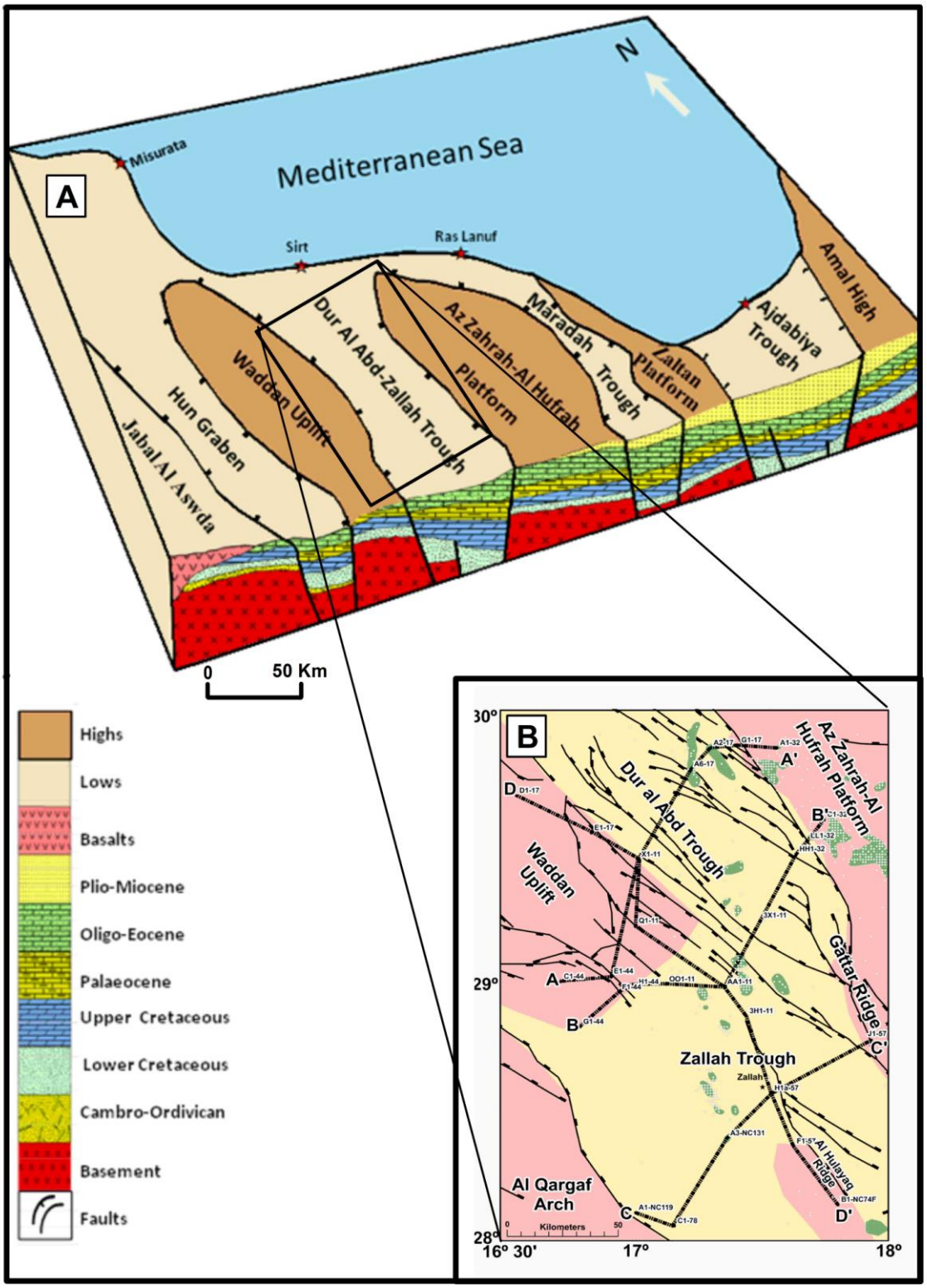


Fig. 8.1 (A) Schematic E-W cross section of Sirt Basin. (B) Overview structural map of the central part of the study area showing the major faults and the main structural domains. For cross sections see fig. 8.2

A structural trend that is orientated NNE-SSW, then N-S and NNW-SSE direction is evident during the Upper Cretaceous phase, followed by NW-SE-trending during the Paleocene and Eocene when a thick stratigraphic interval of sediments were deposited (Fig. 5.3-8). The main faults in the study region show a segmented fault pattern with up to tens of kilometres in length, NW-SE and N-S to NNE-SSW striking extensional fault systems formed at both the rift borders, and within the rift basin (Fig. 4.1-4.4 and 6.1). These segmented structures define the geometry of the main tectonic elements in the Sirt Basin. Deformation of this fault network resulted in a complex structural history that led to the formation of several fault-bounded geomorphological elevated blocks and depressions (Fig. 4.18) and the characteristic rhomboidal or zigzag map patterns. Each block is asymmetric, bounded on one side by a major NW trending border fault system with large throws from approximately 300 to 1000 m with a dominant stratal dip direction toward the border fault system. The extensional tectonism that formed these blocks and depressions began in the Early Cretaceous and created a wide variety of structures, many of which have become effective hydrocarbon traps. In cross-section view, (Fig. 5.7 and 8.2) the centre of the study area is characterized by a series of SW and NE dipping, planar to near-planar domino-style extensional faults. Most of the major fault systems seem to have formed during a rift climax phase (Cowie et al., 2005) during the Upper Cretaceous depositing a maximum of 850 m of sedimentary rocks in the trough regions compared to very thin occurrences or an absence on the platforms (Fig. 5.1). Later movements, though minor, occurred during the Paleocene and reactivated mainly during Eocene. The en-echelon and offset nature of fault segments shown in figures (4.2-4, 5.3-6, and 6.14-19) are a common feature of rifting of an oblique basement fabric, and has been documented from the North Sea and in analogue modeling of oblique rifting (McClay & White 1995). The en-echelon nature of the NNW-SSE to NW-SE trending faults in the study area suggests that the extension direction was slightly oblique to reactivated Paleozoic basement fabrics trending NNW-SSE as explained mainly in chapters 4 and 7, however this level of detail cannot be resolved in the seismic data.

The main boundaries of the geomorphological elevated blocks and depressions of the study area are defined by the Gedari fault, the Qarat Ash Shush fault, east Dur al Abd Trough fault, east Az Zahrah-Al Hufrah Platform fault, east Mabrouk Area fault, east Waddan Uplift fault, west Al Hulayq Ridge fault, and the Western Range fault. These structures also act as boundaries dividing the main structural elements into a number of internal sub-blocks.

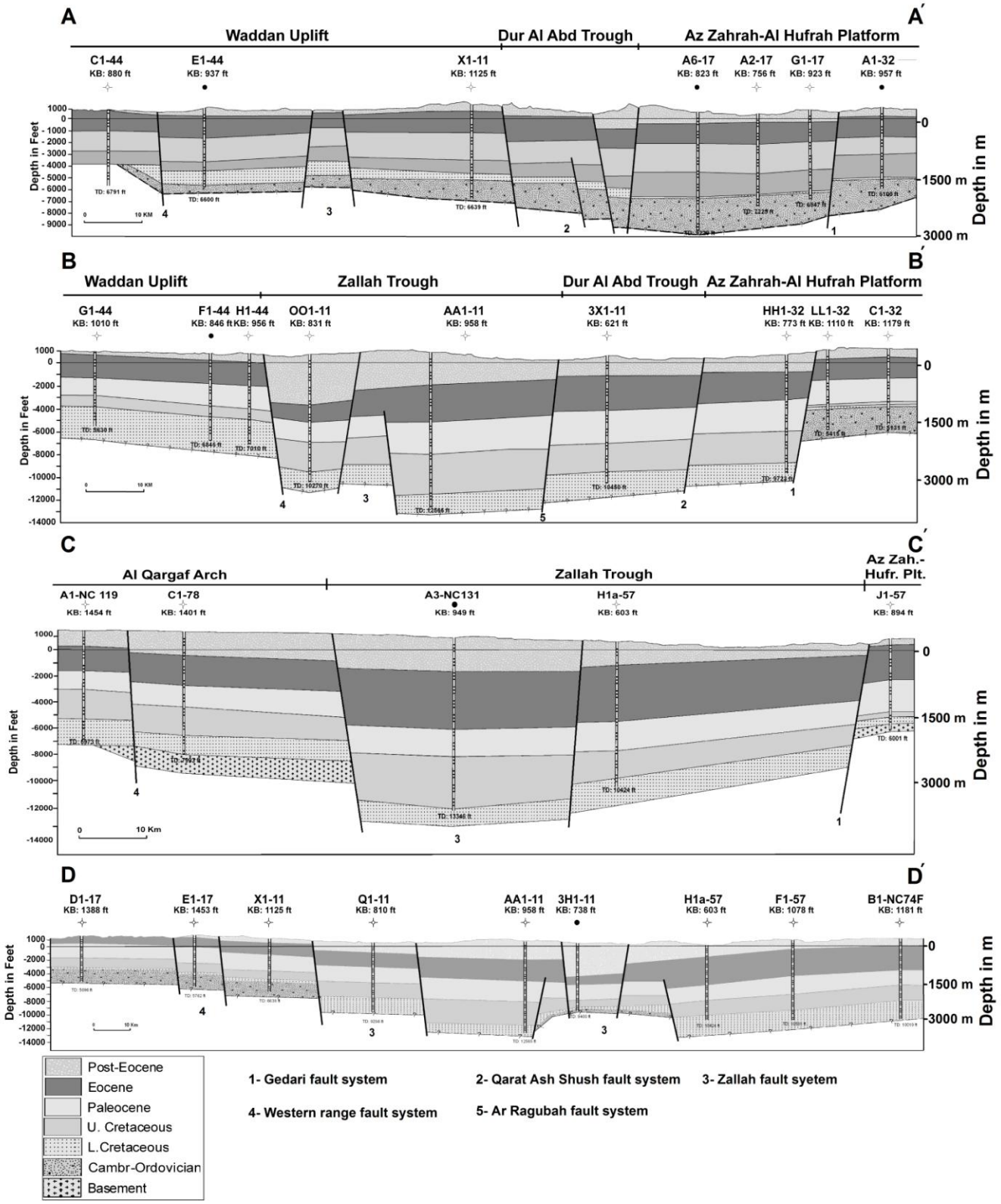


Fig. 8.2 Geological cross sections through the Zallah-Dur Al Abd Trough constrained by well data showing the tectonic evolution of the study area. Note the numerous faults, with only the larger ones shown here, demonstrating the distributed nature of deformation in the trough. Dramatic thickening of the Upper Cretaceous strata indicates that the rifting was most active at this time, followed by a period of Paleocene downwarping subsidence. For location see Fig. 8.1. Cross-sections labelled as aa', bb', and cc' were constructed perpendicular to the main structural elements of the study area with same horizontal scale, and are displayed with differnt vertical exaggeration whilst dd' oriented parallel to the boundary fault (longitudinal section).

The major Late Cretaceous fault in our study area (the Gedari fault system) possibly continues to the north and may also belongs to a family of NNW-SSE basement shears which cross the Saharan Platform to the south parallel to Paleozoic structural trends (Guiraud et al., 1987; Klitzsch, 1970).

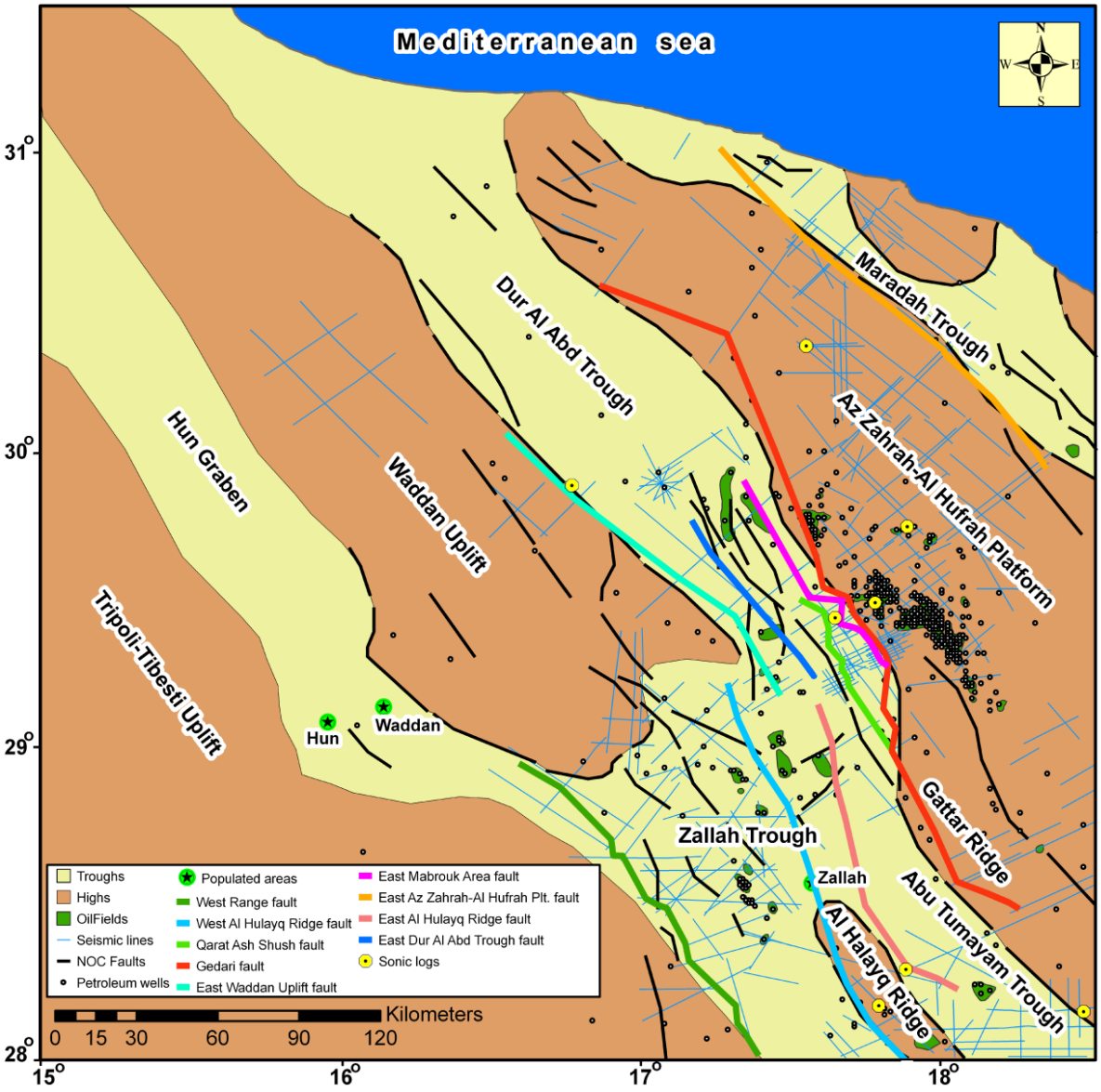


Fig.8.3 Illustrates the main boundaries of the geomorphological elevated blocks and depressions of the study area are defined by major faults interpreted from seismic data.

8.3 Fault and fold geometries,

In the hangingwalls adjacent to the major faults in our study area, the beds are inclined forming synclines trending parallel to sub-parallel to the main faults (Fig. 4.7). Many folds within the study area are located sub-parallel to and are bounded by NNE-SSW trending cross fault zones. Rift-related faulting within the study area fault block is also associated with ductile deformation as indicated by the kilometre-scale folds (Fig. 4.7b). If they are synchronous these parallel folds and the Eocene strike-slip reactivation (Fig.

4.11) of many of the faults can be explained as a result of a partitioning of WNW inducing compressional stress where the closing of Tethys (NE-SW stress) induced folds and, lateral movement of African sub-plates and induced sinistral strike-slip faults (Anketell and Kumati, 1991b). The evidence for strike-slip deformation is supported in this thesis by:- 1) the remote sensing interpretation – the en echelon structures above and, 2) the paleostress analysis in Chapter 7 that is discussed below.

This strain partitioning is likely to have been induced by the obliquity between the pre-existing normal fault trends and the post-Eocene compression direction that was probably induced by Eurasian/Afro-Arabian collision (Schafer et al, 1980; Anketell and Kumati, 1991b; Anketell and Ghellali, 1991). Such partitioning is typical of mildly compressional deformation in many settings (e.g. Holdsworth et al. 2002).

Minor folding observed in the area is also likely to be due to ductile deformation in a relay ramp formed between two overlapping faults (Fig. 4.11). This kind of folding is characterized by structural highs in the overlapped zone. Folds associated with relay ramps are related to segmented en echelon faults, and are frequently seen in the southeastern part of the area. However, the anticlines that are present adjacent to the major boundary faults that show Middle Eocene fold cores flanked by U. Eocene sediments and others by Oligocene cores flanked by Miocene are a result of the post-Miocene regional compression discussed in the previous section. Many other faults and fault-related folds (drag-folds) are typically narrow asymmetric monoclinal structures and the larger very low amplitude, periclinal folds. The period of folding is connected with subsidence movements during the filling of the Sirt Basin. Some of the very open fold structures could be due to compaction of sediments in troughs, which supplement the tectonic folding (Vesely, 1985) where the sedimentary sequences are mildly undulated into synclines and anticlines and the en echelon nature of the boundary faults that many of these traps are formed.

In contrast if there is a variation in thickness and compaction potential of a sequence, loading by later deposits will give rise to spatially varying amounts of compaction. Both the thickness and structure of the later sequence will be controlled by the underlying geology in the absence of any active tectonics. Buried tilted fault blocks in a rift basin often produce large anticlinal closures in the post-rift section that may form traps for hydrocarbons (Sclater and Christie, 1980, Fowler and Yang, 1998, and Bahr, et al. 2001). In addition compaction over a buried hill, carbonate reef also produces traps on a smaller scale.

The seismic reflection data for the study area with a constrained stratigraphy has the potential to resolve the history of displacement accumulation on active faults on timescales that shed light on cycles of tectonic activity.

The interpretation of a large volume of two-way time seismic data has allowed to the construction of long regional seismic cross sections and resultant time structure contour and thickness maps, thus, allowing to observe structural and stratigraphic relationships on a regional scale. Generally speaking and as illustrated, display of the seismic and well data together strengthens the interpretation of both. Subtle, uninterpreted faults indicated by the well data can be interpreted on the seismic data, and changes in the patterns in the seismic data can influence the stratigraphic interpretation of the well data. Based on all the interpreted seismic and well-based geological cross sections the study area seems to be more tectonically and structurally complicated to the south. The resulting increasing number of the faults has led to the identification of more tectonic blocks to the south. The Waddan Uplift, Dur al abd Trough, and Az Zahrah-Al Hufrah Platform are intersected on cross section A-A' (Fig. 6.6, 6.7 and 8.2) in the northern part of the area. Waddan Uplift, Zallah Trough, the Dur al Abd Trough, and Az Zahrah-Al Hufrah Platform on cross section B-B' (Fig. 6.8, 6.9 and 8.2) in the central part of the area. The (Al Qagaf Arch) Al Harug Al Aswad Uplift, Zallah Trough, Al Halayq Ridge, Abu Tumayam Trough and Gattar Ridge or southwestern fringe of Az Zahrah-Al Hufrah Platform is intersected on cross section C-C' (Fig. 6.10, 6.11 and 8.2) to the south of the area. Conversely, the strike-parallel cross section D-D' (Fig. 6.12, 6.13 and 8.2) shows that most reflectors are generally flat lying and the stratigraphy has approximately constant thickness with faults that mainly occur below base Kalash horizon (remind reader of age) indicating that along strike the basin is less complicated than across-strike. Also the general structure of the study area is illustrated by normal faults that are approximately symmetrically distributed around the main structural elements extend up to the surface and by inference the main phase of active extension must be Late Cretaceous.

Many of these faults clearly offset or disrupt most of the sedimentary sequence particularly near base Kalash indicating that they penetrate deep into the section, probably into Precambrian rocks where the basement directly underlies this horizon mainly in the footwalls. Some folds have been identified in the study area parallel to the major faults are interpreted to have been either generated by compaction in the troughs

or they may have connected with differential subsidence movements during the filling of the Sirt Basin.

The Gedari fault seems to be the master fault in the study area where it vertically displaces and horizontally extends the whole sedimentary sequence imaged in the seismic data from the Upper Cretaceous until the Eocene. It is clear that the vertical displacement of the Gedari fault is dominant in the rift development except during the deposition or post deposition of Sirte Shale of Upper Cretaceous age when the horizontal displacement is the greatest value.

The second fault in terms of the magnitude of the displacement is the East Waddan Uplift fault although all other faults have already initiated, it shows larger amounts of vertical displacement during the Late Upper Cretaceous, comparatively, acting as an antithetic western boundary fault that formed after the master Gedari Fault. During the Paleocene, the East Mabrouk and West Al Halayq Ridge faults became dominant with the exception of the Middle Paleocene when the Qarat ash Ahush fault is dominant apart from the Gedari fault.

Based on what the interpretation of the seismic reflection data used in this study; the following points can be made:

6. The identification of faults from seismic and their orientation in plan view for the key mapped horizons has shown several prospective structural trends and provided a better definition of the boundaries of the major tectonic elements of the study area.
7. All the identified faults show vertical displacment across the sequence with different throws at different time intervals.
8. Most of the identified faults started appear to have larger displacements and that decline upsection. These decreases accompanied by thickening of sedimentary layers in the hanging walls of the faults, are due to syn-sedimentary fault growth.
9. In all figures used in this section there is characteristic of syn-tectonic growth strata in the hanging-wall for Upper Cretaceous time constrained by the reflection data.
10. It seems to be that most of the faults initiated at the study area boundaries and then propagated towards the centre of the area indicated by a different throw history of the intra-basin faults compared to those at the margins which seems to be initiated earlier as shown in figures 6.6-13.

8.4 Rift basin infill model for the NW Sirt Basin

The stratigraphy of many continental rift basins shows a vertical transition from an early fluvial, shallow lake, or shallow-marine succession to a deep lake or deep-marine succession (Lambiase and Bosworth, 1995). Here, we compare the stratigraphic sequence determined from boreholes with the four-fold division of rift evolution suggested by Prosser (1993). The four stages are rift initiation, rift climax, immediate post-rift, and late post-rift which we suggest corresponds to the second, third, fourth and fifth combined, and sixth phases respectively in our study area.

1. During rift initiation, deposits are often continental in nature with sedimentation rate greater or equal to subsidence and this agrees with our interpretation of Lower Cretaceous initial rifting in the study area (Fig. 5.3 and 5.8). In general, the Nubian Formation is speculated to be of Lower Cretaceous age in the Sirt Basin (Barr and Weegar, 1972; Banerjee, 1980; Butt, 1986). It is a continental siliciclastic sequence composed of three lithologic units. The lower and upper units comprise non-marine argillaceous sandstones while a middle unit that includes mainly greenish gray shales.
2. The rift climax phase is the time of maximum fault throw rate and sedimentation is outpaced by subsidence. As a result, most of the basin has been drowned either in a lacustrine or a marine setting. Sediments deposited are primarily fine-grained with the exception of coarser grained talus and fan deposits derived from the upthrown footwall. In the study area this coincides with accelerating rifting and rapid subsidence in the troughs resulting in thick deep marine sediments (e.g. shales of Campanian age) that are missing or very thin on the platforms (see Fig. 5.1).
3. The immediate post-rift stage marks the end of active tectonism and fault displacement. Sedimentation in this stage is associated with basin infill in a generally coarsening-upward succession. Structures in the study area were relatively inactive during the Paleocene with basin down-warping forming a structural sag during thermal subsidence with only minor reactivation or rejuvenation of tectonic activity on Upper Cretaceous faults. This phase was dominated by the deposition of shallow marine carbonates and was followed by fault reactivation that became stronger than during the Paleocene time as indicated by the accumulation of a huge thickness of evaporites and dolomites of Late Eocene age.

4. Late post-rift is related to the final infilling of the basin with the erosion of the footwall highs and general peneplanation of the surrounding area. In our study area this phase is characterized by formation of NNW-SSE striking anticlines reflecting slight inversion of the central study area, erosion of most Post-Eocene sediments and finally the extrusion of the extensive (8-2 Ma) Al Harug Al Aswad basalts. These crop out in the southern part of the basin accompanied by post-rift tilting related to Alpine tectonic pulses.

It should also be noted that, based on the borehole data used in this study, Upper Paleozoic- and Lower Mesozoic- age sedimentary rocks are largely absent suggesting that the area was domed, faulted and eroded during Late Mesozoic by the creation of Sirt Arch (Aliev et al., 1971; Burollet et al., 1978; Boote et al., 1998). However, it must be acknowledged that most wells do not reach the basement and do not penetrate the whole Palaeozoic section, and as a result, the presence or absence of these sediments is inferred across the trough (Fig. 8.4).

8.4.1 Mesozoic rifting and continental break-up

8.4.1.1 Permo Triassic rifting

In this section, the relationship between the Sirt Basin rift development, as exemplified in the study area and the break-up of Gondwana is discussed. The structural evolution of the West-Central African rift system, the South and Central Atlantic, and the Tethys and Indian Oceans are also considered. Gondwana break-up (Guiraud and Bellion, 1995) was initiated during the Permo-Triassic (Aliev et al, 1971; Burollet, et al., 1978; Boote, et al., 1998) and ultimately created the present-day African continental margins. A series of intra-continental rift basins, located mainly on older (Late Proterozoic) shear zones (Janssen et al., 1993) were formed along what became the eastern margin of the Atlantic Ocean and the southern margin of Tethys Ocean (Mengoli and Spinicci, 1985; Guiraud, 1998). This phase of basin development was associated with the separation of northwest Africa from North America, during the Late Triassic-Early Jurassic as a result of the opening of the Central Atlantic (Klitgord and Schouten, 1986) and mid-Jurassic crustal separation between North Africa and Europe (Ziegler, 1988, 1992).

The North African continental margin and that of northwest Arabia record a change from being convergent associated with the closure of the Paleotethys, to a passive margin, and then the initial opening of Neotethys during the Permian (Wilson & Guiraud, 1998, Şengör, 1979; Stampfli et al., 2001; and Garfunkel, 2004). Neotethys underwent a complicated evolution in which several discrete blocks separated from

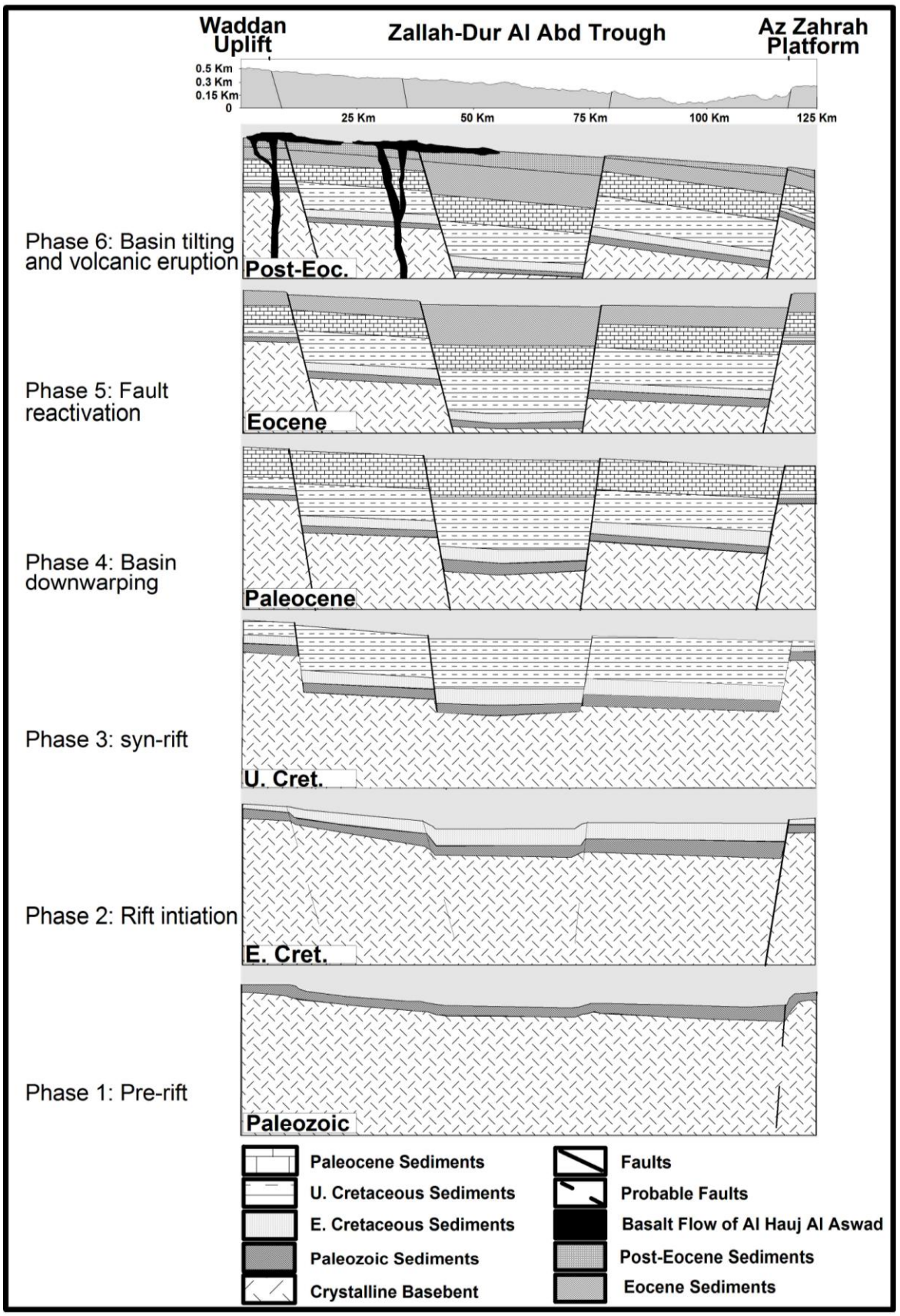


Fig. 8.4 Polyphase tectonic model for the study area shows the structural development and basin evolution of the area. This model is based on borehole data that were selected along fences perpendicular to the main structural elements of the study area. Well-bore penetrations for the Paleozoic section are relatively few and this has had to be inferred.

Africa, e.g., Apulia which rifted from Libya, leaving what is now the Bay of Sirt. It has been suggested that the northern Libyan margin basins formed from Permian times along the offshore domain and mainly from the Cretaceous times in the onshore domain (Shegewi, 1992; Dercourt et al., 1993; Anketell, 1996) and this is consistent with the NW Libya structures that mentioned in Chapter 7. During Triassic times, the Maragh Trough in the eastern Sirt Basin, and the south-western margin of the Cyrenaica Platform formed as incipient rifts, (Table 8.1) and were a prelude to the main rifting of the Sirt Basin (Guiraud and Bellion, 1995). These basins formed on a margin that contained pre-existing NE-trending basement structures of the Hercynian Orogen, such as the Sirt Arch in which an older Paleozoic section was folded, uplifted, and eroded (Aliev et al., 1971; Burollet et al., 1978; Boote et al., 1998). These incipient rifts were E-W to NE-SW trending formed by an interaction of N-S extension and NE-SW trending basement fabrics. This forms the foundation upon which the overall picture of extensional tectonics and rapid subsidence linked to the Cretaceous Pan-African rifting is constructed (Van Der Meer & Cloetingh, 1993; Guiraud and Bosworth, 1997, Selley, 1997; Gras and Thusu, 1998).

8.4.1.2 Cretaceous rifting

Our stratigraphic thickness maps (Fig. 5.3-6) show an anticlockwise rotation of the basin axis through time from NE-SW (Early Cretaceous) through N-S (Upper Cretaceous) to NW-SE (Paleocene and Eocene). A pole of rotation at 27°18' relative to Africa has been proposed by Fairhead (1988) to explain the opening of the south Atlantic; extension of the rifts; and strike-slip displacements on the Benue and Central African shear systems during the Early Cretaceous (130-119 Ma). Rotation about this pole would have facilitated N-S extension along the incipient North Africa continental margin (Guiraud and Maurin, 1992) at this time.

Several authors have discussed the relationship between the development of Late Mesozoic rift basins, the opening of the South Atlantic and their location along Pan-African fractures (Pindel and Dewey, 1982; Fairhead, 1988; Unternehr et al., 1988; Fairhead and Binks, 1991). They describe different episodes of rifting, formed under a constant north or northeast-trending extensional stress, as being responsible for the opening of all basins during the Early Cretaceous evolution of the South and Equatorial Atlantic domains.

Furthermore, Guiraud and Maurin (1992) concluded that from the Neocomian to Early Aptian roughly E-W and NW-SE trending troughs (Upper Benue, N. Cameroon, S.

Chad, Sudan etc.) opened in response to a N-S extensional regime in Central Africa while in Western Africa the N-S trending trans-Saharan fault zone acted as a sinistral wrench. From Middle Aptian to Late Albian times and into the Upper Cretaceous (Guiraud et al, 1987 and Anketell, 1996) large northwest trending troughs (E. Niger, Sudan, Sirt, etc.) opened in response to a northeast extensional regime while the Central African fault zone (from Benue to Sudan) exhibited strike-slip movements, generating pull-apart basins (Guiraud, & Maurin, 1992). In the study area (Fig. 5.3), a trough trending NNE-SSW was formed after an older E-W (Late Jurassic/Triassic?) trough and before a younger NW-SE (Late Cretaceous) African trough, which probably opened during the Early to Late Aptian.

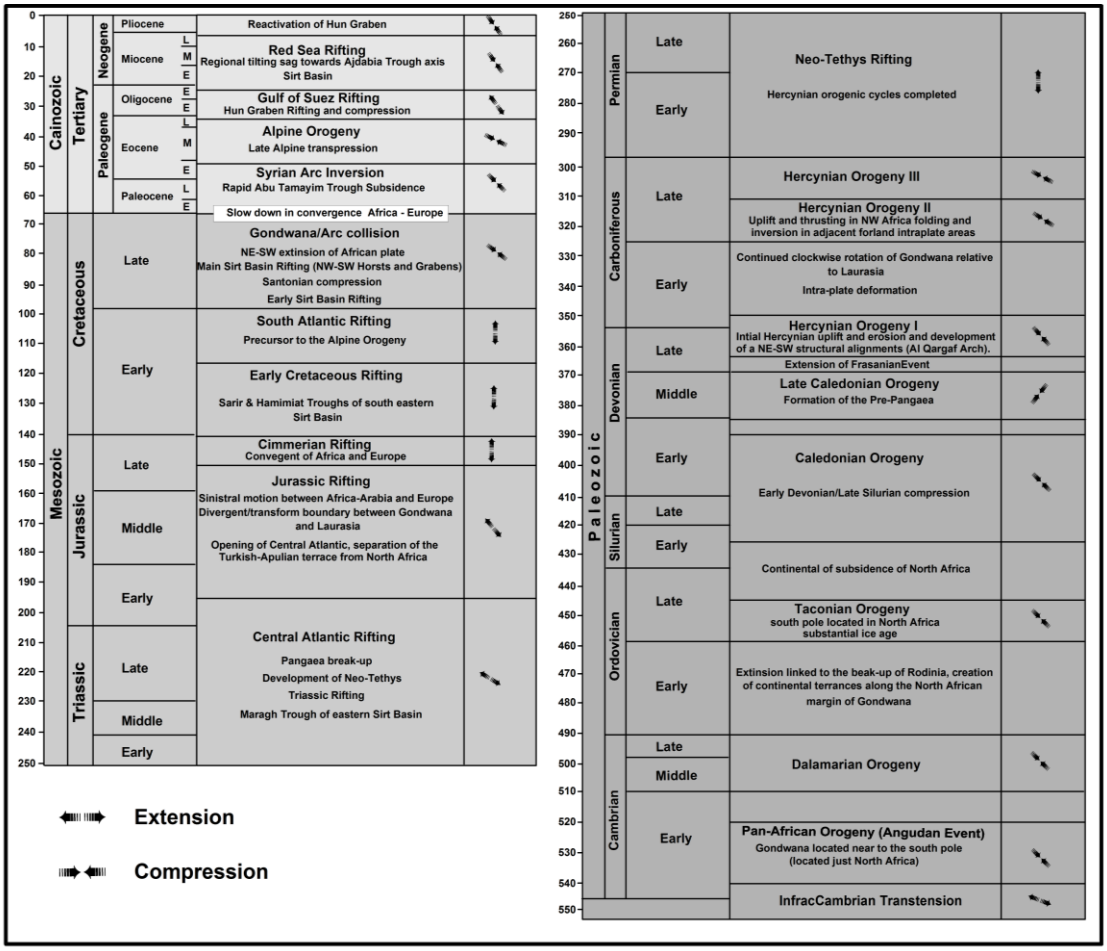


Table 8.1 Tectonosedimentary events and its influence on Sirt Basin (modified after Fairhead, and Green, 1989, Fairhead, and Binks, 1991, Guiraud, and Maurin, 1992, and Anketell, 1996).

Rifting in North Africa can be also correlated with similar deformation in the southern Palmyrides, and other structures in Lebanon and farther south, (Brew et al. 2001) when between the Jurassic and Early Cretaceous, the fault activity shows a clear migration to the NE. Furthermore, a shift in the dominant orientation of the major faulting is apparent, suggesting a similar anticlockwise reorientation in overall extension direction

from roughly NW–SE to roughly north–south. This has been attributed to a reorientation of forces imposed by oblique subduction in the NeoTethys Ocean to the NE of Arabia (e.g. Lovelock 1984). Brew et al. (2003) relate this episode of extension throughout Syria to a renewed period of extension interpreted in the eastern Mediterranean that was invoked by mentioned by Robertson & Dixon (1984). Litak et al. (1997) believe that the majority of the Euphrates fault system activity in NE Syria occurred during the Campanian and Maastrichtian which is consistent with the observations in our study area.

(AGOCO 1980) believes that the earliest faulting in the Sirt Basin occurred in the Hameimat-Sarir troughs and commenced in Neocomian times, trending E-W and WNW-ESE. Anketell (1996) suggested that an array of roughly E-W trending basement faults have controlled fragmentation of the craton/plate margin along a Sabratah-Cyrenaica Shear Zone (Fig. 7.3). This structure possibly forms the eastern extension of the South Atlas Shear Zone and may continue further east along the Egyptian coast into the Levant. These shear zones were in turn strongly influenced by Hercynian structural trends (Anketell, 1996). This hypothesis, although difficult to test, to a certain extent is in agreement with the subsurface (well) data, where we see a thick Lower Cretaceous sequence in the study area implying Early Cretaceous basin had a NNE-SSW trend (Fig. 5.3). This local sub-basin formed at the same time as a second phase of faulting in the Sarir-Al Hameimat that reactivated the fault blocks and led to the development of an important intra-Aptian unconformity (Rossi et al., 1991). These faults lie immediately north of the WNW-ESE basement fault zone along an arcuate continuation of the Hercynian Al Qargaf Arch postulated to underlie the southern margin of the Sirt Basin (Anketell, 1996). This Early Cretaceous NNE-SSW trend found in the study area (Fig. 5.3) is a possible extension of Abu Tumayam Trough which for its most part is obscured by the Al Haruj lava field and was largely inherited from the structural grain of the Tibisti-Sirt Uplift (a Paleozoic trend?).

The basement control hypothesis is to recognize that the trend of the structure is similar to that of NNE trending dilational jog arrays as suggested by Anketell (1996) and the western Sirt was rifted by sinistral transtension in response to the same stress field which developed the Sirt faults (Fig. 7.3).

In summary, analysis of the depositional sequence and subsidence history of the region suggests that the troughs were initiated as WNW-ESE trending rifts prior to the NW-SE fault complexes that created the main troughs of the Sirt Basin. This work suggests a rotation of the Sirt Basin axis from the Early Cretaceous to the Late Cretaceous, and

hence the later NE-SW directed Upper Cretaceous extension that created the main NW-SE trending trough was superimposed on a Lower Cretaceous NNE-SSW trending trough. This evolution of the Sirt Basin coincides with North and Central Africa beginning a clockwise rotation, under the influence of forces related to the opening of the South Atlantic (Guiraud and Maurin, 1992), followed by left lateral wrenching between the southern European microplates and North Africa (Pawellek, 2009). This rotation of the extension direction and/or the North and central Africa plates was generated by the event that separated South America from West Africa, (Binks and Fairhead, 1992).

In terms of areal extent, the thick layer of deep marine shales marks the peak of intraplate, African rifting in the Campanian (Guiraud et al., 1992; Bosworth, 1992). The consistency of onset of Campanian rifting across diverse tectonic terranes indicates that this rifting event was passive in nature, and driven by transmitted plate boundary forces rather than by local upwelling of mantle plumes (Binks and Fairhead, 1992). Although Van Houten (1983) thought that the Sirt Basin may have developed when Mesozoic drift of the African plate put north-central Libya over a fixed mantle hotspot in Early Cretaceous time (140 to 100 Ma).

8.4.1.3 Latest Cretaceous and Cenozoic evolution: thermal sag, fault reactivation and inversion.

The Syrian arc fold system formed during the Late Cretaceous convergence between the Afro-Arabia and Eurasia plates that followed the opening of the South Atlantic ridge. This regional compressive regime is present throughout the eastern Mediterranean region from Syria (Palmyrean Chain) across Palestine and Northern Sinai, to the Western Desert of Egypt and possibly into the Sirt Basin. It has been suggested that this compression (Table 8.1) caused the inversion of the Al Jabal al Akhdar Trough in Cyrenaica with folding about NNE-SSW axes (Rohlich, 1991; Anketell and Ghellali, 1991) reflecting the marked change in tectonic style which took place in the Santonian throughout the Mediterranean region and Africa (Sander, 1970; Guiraud et al., 1992). However, the Sirt Basin is characterized by major rifting during most of Upper Cretaceous. Tectonic models for the evolution of the Mediterranean suggest also that left-lateral motion between Europe and Africa continued up to 80 Ma, then ceased due to collision between Anatolia and Arabia, (Biju Duval et al. l977).

In Paleocene times (between 67–55 Ma), Africa had almost stopped moving relative to Europe, (Rosenbaum et al 2002) resulting in a relatively inactive structural period with basin down-warping forming a structural sag (Hallet, 2002) characterized by the highest

regional subsidence rates in the study area. At this time of warm oceans and generally high sea levels, a vast epicontinental sea formed far inside the African continent (Guasti & Lüning, 2009) extending further than the Late Cretaceous seas. In the study area, both the troughs and the platforms subsided uniformly and rapidly throughout the Palaeocene as there is little change in thickness across the main structural features. A weak fault reactivation is recorded during the Paleocene but became stronger during Eocene times as recorded by differences in thickness of the Hon evaporates. Fig. 4.10 shows the sinistral strike slip faults that have been suggested by Anketell and Kumati (1991b) to have been the result of major sinistral strike-slip reactivation of the basement faults of the NW-trending Gedari fault. The event is manifest through-out our study area as a marked unconformity, with the topmost Eocene deposits resting on faulted earlier Eocene sequences (Anketell, 1996). Borehole records show a thick stratigraphic interval was deposited in the main depocentre trending NW-SE during this time (Fig. 5.6) suggesting a short, intense period of Middle/Late Ecocene rifting resulted in an abrupt deepening of the basin and finally deposition of Late Eocene evaporites and dolomite of Gir Formation. This difference in thickness of of Late Eocene evaporites and dolomite of Gir Formation could be related to flow within salt rather than faulting or combination and no evidence has been found to confirm this fact eithr from this study or from previous works on this area although it shown using paleostress data in chapter 7 and discussed late on in section 8.4.0. Major sinistral strike-slip reactivation of NW-SE trending faults during the Late Eocene records more rapid movement of the Arabian-Nubian block about the Western block resulting from slowing down of the latter due to its continuing collision with Europe (Anketell, 1996). These faults are identified clearly in the study area particularly adjacent to the eastern boundary of Qarat Ash Shush fault system (Fig. 4.10).

Oligocene time was characterized by creation of anticlines that are difficult to recognize at the map scales. They exhibit a NNW-SSE strike, and show Oligocene cores flanked by Miocene outcrop indicating a pre-Middle Miocene gentle compression. This slight inversion of the central study area was a result of a stress normal to it, i.e. approximately NNE-SSW (Schafer et al, 1980). The study area was tilted towards east-northeast (Fig. 8.4), towards the axis of Sirt Basin; interpreted to have taken place as a result of the compressional stresses that had affected Sirt Basin during the Late Eocene possibly driving the latest stage of regional minor subsidence (van der Meer and Cloetingh, 1993). On the Az Zahrah-Al Hufrah Platform pre-Oligocene ENE tilting

resulted in an angular unconformity with progressive stripping of Upper Eocene beds towards the southwest (Anketell, 1996). Exceptionally, rapid subsidence was recorded in the adjacent Hun Graben and northern parts of the Ajdabiya Trough in the western and eastern parts of the study area respectively.

The basin tilting was followed by the basin inversion and activation of magma tectonic lineaments which formed the most recent tectonic development of the area, the Al Harug Al Aswad basalts (Farahat et al. 2009; Cvetkovic´et al. 2010), that record a post-rift tilting in the study area and its effect is seen across the whole Sirt Basin and may be caused by Alpine-related tectonic pulses in the post-Eocene resulted in northward tilting of the basin. This episode (Bumby & Guiraud, 2005) relates directly to the evolution of the Red Sea-Gulf of Aden system that took place between the Late Eocene and Early Miocene, (Table 8.1) and was associated with the breakup of Arabia from Northeast Africa (Binks and Fairhead, 1992).

8.5 Hun Graben and northwest Libya (Jifarah Basin and Nafusah Uplift) relationship

The northwest Libya structures trends represent the remnants of reactivated structures that formed under the stress regimes generated during the tectonic evolution of North Africa. Late Permian–Middle Triassic dextral (clockwise) motion of Africa relative to Eurasia created a westward-narrowing wedge-shaped arm of the paleo-Tethys (Robertson and Dixon, 1984) and the Permian clastic deposition dominated in the Jifarah Basin. The area became a stable platform from the Late Cretaceous to the Miocene. Downwarping in the Miocene resulted in the deposition of Miocene sediments (Tawadros, 2001)

Capitanio et al.2012 pointed out that the progressive closure of the Ionian basin and the pull of subducting Hellenic slab have conferred complex deformation along the Libyan margin during the Paleocene, with inversion in the NW Libya (Tripolitania) and Cyrenaica bordering the subsiding domain of the Sirte Basin (van der Meer & Cloetingh 1993; Abadi et al. 2008; Bosworth et al. 2008; Capitanio et al. 2009).

In general most of the faults observed in the Hun Graben and northwest Libya (Jifarah Basin and Nafusah Uplift) (Fig. 8.5) correspond to minor structures with displacement ranging from several centimetres to several metres. Various types of faults (normal faults, left normal faults, right normal faults and strike-slip faults) with their rake ranging from 51º to 80º and their dip ranging from 70° to 90° (high-

angle normal faults) are present. A NNE-SSW directed extension regime with WNW-ESE compression is recorded by most of the measurements in the study area.
The directions of extension computed from fault slip data sets are remarkably homogeneous in all sites. The WNW-ESE compression and NNE-SSW extension resulted from this study is consistent with progressive collisional coupling of Africa and Europe, (Table 8.1) being under approximately WNW-ESE reactivated compressional stresses during Late Eocene-aged (Ziegler et al., 1998; Cloetingh et al., 2005) Alpine deformation (Table 8.1).
In the Hun Graben (Table 7.1) about 56% of the observed faults are predominantly left normal faults (oblique dip-slip component), whilst in Northwest Libya (Jifarah Basin and Nafusah Uplift) right normal slip faults represent about 29% of the total measured faults with a rake ranging between 101º - 130º and indicates predominantly NNE-SSW (N25°E) extension and less WNW-ESE (N115°E) compression (Table 7.2).
However 71% of the observed faults are predominantly normal faults where the compressional regime is restricted mainly on the Jabal Nafusah Uplift area as E-W to WNW-ESE (N95°E) compression along Gharyan fault zone (GFZ), and NNE-SSW (N19°E) compression along Wadi Ghan fault zone (WFZ).

The combination of dip slip normal faulting resulted from a horizontal NE-SW trending σ3 axis and a vertical σ1 axis and the left normal and strike slip faults might correspond to an overall transtensional movements in the formation of Hun Graben and extends to Whole Sirt Basin.

It is clear from this study that the two areas are predominantly characterized by NNE-SSW directions of extension ranging from N12°E to 25°E with lesser component of ENE-WSW direction of extension with an average N102°E where the σ3 directions rotate clockwise from NNE–SSW to ENE-WSW in northwest Libya (Jifarah Basin and Nafusah Uplift). It seems also that the area was affected by minor ENE-WSW direction compression which led to the development of the right normal faults. However in the Hun Graben, minor expected directions of extension may average NNW-SSE where the σ3 directions rotate counterclockwise from NNE–SSW to NNW–SSE. Anketell and Ghellali, 1991, Anketell, 1996, and Abadi, 2002 and 2008 thought that the western Sirt Basin boundary along Hun Graben indicative for regional extension is related to the subsidence of the NW–SE elongated Sirt Basin structures active during Late Cretaceous and extended north westward to the offshore basins in the Sabratah

Basin and in the Pelagian shelf (Fig. 7.3) which means that these area are might be related to each other in their original formation.

The Hun Graben boundaries are formed by segmented faults. The origins of this segmentation and segment boundary zones are often attributed to the influence of basement structure (e.g., Davison, 1997; Clemson et al., 1997). It thought that such segmentation reflects along-strike changes in the orientation of pre-existing structures in the underlying continental basement (McClay & White, 1995).

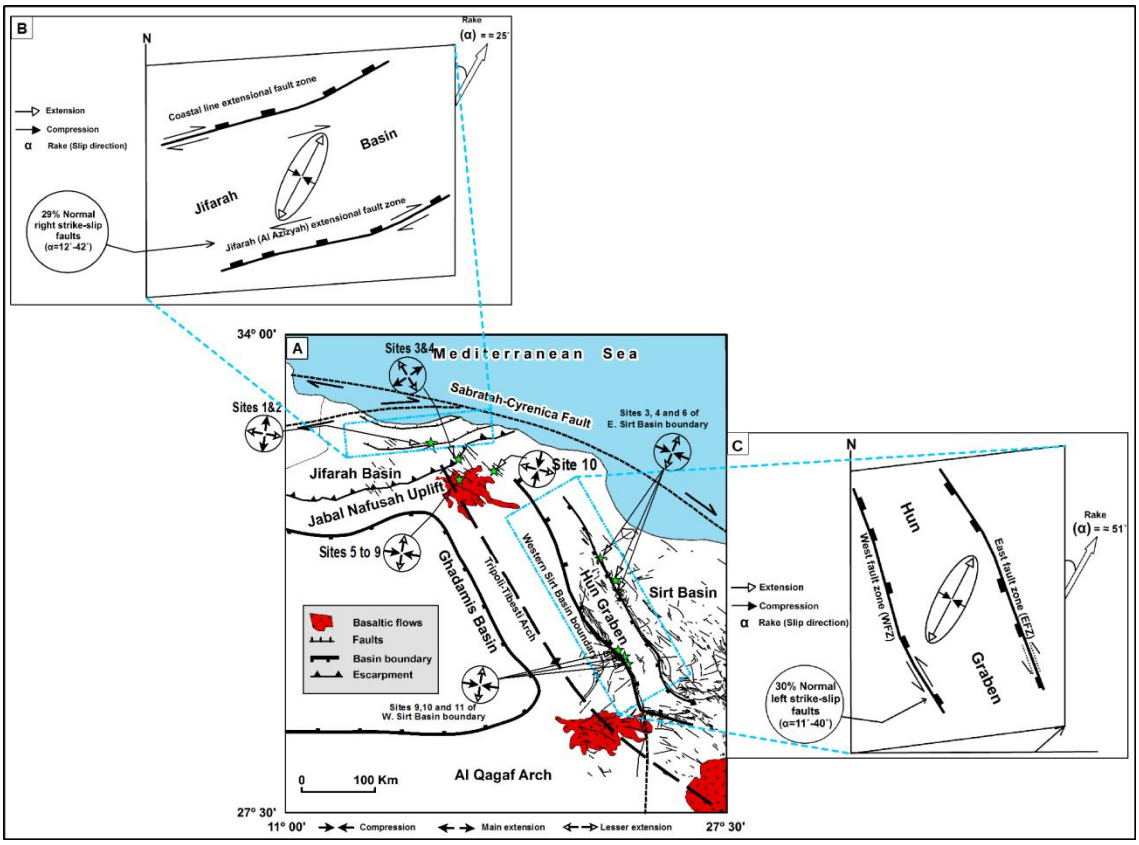


Fig. 8.5 (A) Map shows the location of the studied areas and the orientation of maximum horizontal extension of the Jifarah Basin and Jabal Nafusah Uplift. (B) Plan view of structural styles and geometries of associated minor structures of the Jifarah Basin and summarizing corrections due to obliquity between maximum horizontal extensional strain and Jifarah Basin extensional fault zone trends in order to estimate true regional extension. It shows the homogeneous transtension zones with divergence angles α=25˚ and about 29% are normal right strike-slip faults in the Jifarah Basin with divergence angles α=12˚-42˚. (C) Plan view of structural styles and geometries of associated minor structures of Hun Graben and summarizing corrections due to obliquity between maximum horizontal extension strain and Hun Graben margin trends in order to estimate true regional extension. It shows the homogeneous transtension zones with divergence angles α=51˚ along the eastern fault zone (EFZ) and about 30% are normal left strike-slip faults along the wastern fault zone (WFZ) with divergence angles α=11˚-40˚. Transtension (0_ < α < 90˚) where pure shear coaxial extension (α = 90˚) and noncoaxial wrench simple shear (α = 0˚) and extension-dominated transtension (20˚ < α < 90˚) (Modified from De Paola et al., 2005a). Note: Withjack and Jamison (1986) show that during oblique rifting the orientation of maximum horizontal extension strain is controlled by α, the angle between the rift trend and the direction of displacement.

A consequence of this model is that if such pre-existing structures undergo reactivation then they will often be significantly oblique to the direction of regional extension. This leads to the development of zones of oblique extension or transtension on what would otherwise be a simple extensional margin (Dewey, 2002; Morley et al., 2004) and is manifest in the Hun Graben as extension-dominated transtension (Fig. 8.5b).

Withjack and Jamison (1986) show that during oblique rifting the orientation of maximum horizontal extension strain is controlled by α, the angle between the rift trend and the direction of displacement. The structural styles and geometries of the Hun Graben resulted from the obliquity between maximum horizontal extensional strain and underlying structural trends led to regional extension of homogeneous transtensional zones with divergence angles α=51˚-80˚ along the eastern fault zone (EFZ) forming about 30% normal left strike-slip faults along the western fault zone (WFZ) with divergence angles α=11˚-40˚ (Fig. 7.18b). Transtension is defined by $0^\circ < \alpha < 90^\circ$ where pure shear coaxial extension $\alpha = 90^\circ$ and noncoaxial wrench simple shear $\alpha = 0^\circ$ and extension-dominated transtension $20^\circ < \alpha < 90^\circ$ (De Paola et al., 2005a).

8.6 Geometry and kinematic model for the NW Libya in response to Hun Graben, W. Sirt Basin

The Jifarah Basin (Fig. 8.5a) by extensional dextral strike-slip faults that are considered as part of the Sabratah-Cyrenaica wrench zone (Anketell and Ghellali, 1991), and represents a down faulted terrace on the boundary between the relatively stable shelf to the south and the unstable continental margin to the north. The Jifarah dextral strike-slip faults underlie the Jifarah Basin and extends westwards into southern Tunisia.

The Jifarah Basin has undergone a complex and polyphase structural history since Carboniferous time (Burollet and Desfoges,1982; Ben Ayed, 1986). It has been affected by multiple episodes of tectonism, including a late Paleozoic collision with Laurasia and subsequent early Mesozoic rifting associated with the opening of the Tethyan Ocean (Memmi et al., 1986; Gabtni, 2006). The combined effect of several tectonic phases (Taconic, Caledonian, Hercynian, Austrian, and Alpine (Late Cretaceous–Early Eocene)) on the Jifarah area has been the production of a large sedimentary basin (the Jifarah Basin).

The Mesozoic basin-fill of the Jifarah Basin was affected by normal faulting during the Triassic and by alignment as NW–SE-trending (Fig. 8.5a), in Tunisia, to E–W-trending,

in Libya as a collapsed block faulting formed during the Late Cretaceous and Cenozoic by extensional faulting, which is overlain by Tertiary and Quaternary sediments (Benton et al., 2000).

Anketell and Ghellali, (1991) demonstrated that the dominant fault directions in the Mesozoic section in this area are east-west and NNW-ESE with an en echelon arrangement which they interpreted as riedel shears and imbricate fan splays formed as a result of strike-slip movement on the South Atlas-Jifarah dislocation. This direction played a major role during the Cretaceous–Paleocene development of the Sirt Basin, which is characterized by a NE–SW direction of extension (Jongsma et al., 1985; Klett, 2001). However, the Jifarah fault system is inherited from a long history and acted likely as a transform direction during the lower Mesozoic (Burollet, 1991; Piqué et al.,2002; Lazzez et al., 2008). The Jifarah fault which borders the Jabal Nafusah Uplift from the north was reactivated during the mid-Tertiary in response to the closing of Tethys (Memmi et al., 1986; Gabtni, 2006) accompanied by production of basaltic sills and flows near Gharyan formed by Eocene tectonism, and this volcanic activity has continued until recent times.

In the Sirt Basin, after initial Cretaceous rifting, major subsidence was achieved in the Paleocene under shallow marine conditions that lasted until the Late Eocene (Goudarzi 1980; Anketell 1996; Baird et al. 1996; van der Meer & Cloetingh 1993; Guiraud & Bosworth 1997). Subsidence occurred during Palaeogene–Neogene deformation which reactivated the Hun Graben buried structures, as indicated by the close distribution around the N140ºE trend in Palaeogenic rocks north of Bu Njem (Capitanio et al 2012).

Capitanio et al (2012) have found evidence of Pliocene deformation along a belt stretching from the Jabal Al Khums (eastern Jifarah Basin) region to Jabal As Sawda, in the southern Hun Graben, where volcanism and reactivation of normal faults suggest a NE-directed extension. In addition Argnani (1993) and Capitanio et al (2012) believe that NW Libya (Jifarah Basin and the Nafusah Uplift) and the Hun Graben are compatible with age and trends of the Sicily Channel rift zone (Finetti, 1984), a deformational belt that developed across the Maghrebian chain whilst the rest of Sirt Basin extensional structures formed in response to the strong slab-pull gradients at the central Mediterranean subduction margin which followed the progressive closure of the oceanic basin. Paleostress analysis of west and central Libya (Schafer et al. 1980) and rift-related volcanism in the Zallah Trough, aged 6–0.2 Ma (Ade-Hall et al. 1974;

Farahat et al. 2009; Cvetkovic´ et al. 2010), support the idea that this regime has been continuous from the Pliocene to today and extends far deeper in the African Plate than that indicated by seismicity studied by Westaway 1990 and Serpelloni et al. 2007 (Capitanio et al 2012).

A new kinematic and structural conceptual model is proposed here for the evolution of NW Libya (Jifarah Basin and the Nafusah Uplift) and Hun Graben. It seems that the Al Aziziah E–W fault system plays a major role controlling the north tilting of the Jifarah block faulting as well as its sedimentary infilling. These E–W faults running along the Jifarah Basin represent inherited structural features in relation to deep faulting in the Paleozoic substratum.

Many hypotheses have been proposed to explain the evolution of NW Libya (Jifarah Basin and the Nafusah Uplift) in respect to Hun Graben. The results of an integrated study of the Mesozoic tectonic evolution of the region based on a reassessment of paleostress data and results of satellite image interpretation alongside with subsurface data. In the new structural hypothesis, the Jifarah Basin of NW Libya is interpreted as resulting from large scale block extensional faulting, mainly controlled by inherited E–W major faults, the Al Aziziah fault system. These E–W faults running along the Jifarah Basin may represent inherited structural features in relation with deep faulting in the Paleozoic substratum. This rifting that occurred during the late Triassic up to the end of the early Jurassic, is part of a general East Mediterranean block tilting has been mainly active during the late Triassic and Liassic (Raulin et al., 2011). During the Eocene time these E–W faults in the Jifarah Basin underwent a compressional stress trending approximately WNW-ESE as a result of the convergence between Africa and Eurasia that began in the Late Cretaceous, about 90 Ma ago that led to the formation of dextral strike-slip movements as shown in fig. 8.5b, whilst the Hun Graben fault system which result from the reactivated Cretaceous faults running in NW-SE direction under similar compressional stress formed the sinistral strike-slip and normal fault movements as shown in fig. 8.4c. Sinistral strike-slip movements are clearly documented in this work further east and south of the Hun Graben in satellite image interpretation (Fig. 4.9 and 4.10) and seismic data where major faults branch out into smaller faults (columns C, D, E, F, G, and part of H Fig. 6.6) reminiscent of a flower structures such has often been shown to be associated with strike-slip faulting (Harding, 1985). Another example is represented by the heavily fractured area in the Dur al Abd Trough (centred on column F in Fig. 6.8) displaying a number of NE- and SW-dipping faults, without a clear

change of throw at all depths and is likely to be another zone of wrench tectonics. Also a clear displacement is distributed among several fault strands that are seen to coalesce at depth suggesting a typical ‘flower structure’ located at the middle point of column A (Fig. 6.10). It can be argued that this deformation is of the correct age, geometry and kinematics to be equivalent to the reactivated deformation in the Hun graben.

Capitanio et al (2012) have found evidence of Pliocene deformation along a belt stretching from the Jabal Al Khums (eastern Jifarah Basin) region to Jabal As Sawda, in the southern Hun Graben, where volcanism and reactivation of normal faults suggest a NE-directed extension.

The reactivation can be broadly constrained by the age of the volcanic centre of Jabal As Sawda on the southern border of the Hun Graben, that is coeval to the Gharyan event. This reactivation of Cretaceous lineaments (Goudarzi 1980) in the Hun Graben, is also in general agreement with the NW-trend of joints in the Nafusah Uplift, revealed mainly in Wadi Ghan area (Fig. 8.5a) coeval with volcanism by 6 Ma. The reactivation of faults is recorded as far south as the Zallah Trough, where continental rifting-related volcanism in the Jabal Al Haruj is coeval to volcanism in the Hun Graben and near Gharyan in the Jabal Nafusah Uplift (Capitanio et al 2012; Ade-Hall et al. 1974).

8.7 Surface and sub-surface structure correlation and their petroleum prospectivity.

Most of the oil in the Sirt Basin is derived from Campanian age organic-rich black Sirt Shale (El Alami, et al., 1989, Hallet, 2002). The main structural features of the study area are considered important conduits for oil migration from the source kitchen to the trap. The Sirt shale entered the early phase of oil generation during the mid-Eocene and reached peak generation during the Oligocene (Brennan, 1992 and Roohi, 1996a).

Most oil fields are similarly located on structural highs associated with normal faults and rely on upthrown closure against those faults. Based on the interpretation of well and seismic data, the resultant depth maps on the base Kalash, top Dahra, top Zelten and top Hon show numerous fault bounded trends that have potential for containing structural closures prospective for hydrocarbons. Well and seismic control, however, are too widely spaced to define actual prospects. Inspection of the structure thickness maps (Chapter 5) and seismic structural time and isochrones maps (Chapter 6) reveal that this productive trend follows the fault trends discussed, as well as the rift axis.

In addition, some larger fields generally are located near the deepest part of the Zallah Trough suggest that the location of productive fields is largely governed by the

thickness and maturity of synrift source rocks. Also many oil fields of limited areal extent, but significant productivity, are due to the extremely numerous minor faults around the Zallah Trough oil fields and the relatively undeformed sealing lithology that exists above good reservoir rocks.

Peak oil generation is Late Eocene-Oligocene with migration during the Late Oligocene-Miocene. Due to major subsidence and eastward tilting of the basin from the mid-Eocene (Roohi, 1996a), oil migration from the source kitchen to the traps in the west Sirt Basin has been principally from northeast to southwest. Resulting in hydrocarbons migrating onto adjacent platforms via fault conduits on the eastern boundary faults of the platforms. Westward migration then occurred until a trapping configuration was encountered. Hydrocarbons frequently migrated as far as the western margin of platforms.

The Hun graben appears to be an Oligocene age structure and it appears that the hydrocarbon prospectivity of the Hun Graben should be considered as poor due to the lack of reservoir and source rocks. To date no major oil shows have been found in the Sirt Basin west of the Zallah Trough. A significant source kitchen is present in the northern Zallah Trough and between the Mabruk and Az Zahrah fields, but peak maturity is only present in the Az Zahrah area and is only early mature to the north. (For more detail see chapter 3).

The Dur al Abd Trough can be visualized as a structural saddle in the area to the north of the deeper Zallah Trough and mapping at the various horizons identified in seismic data supports this observation. Remote sensing imagery combined with surface geology, seismic and borehole data show that the trough dips towards the northeast. There is also a predominant northwest to southeast trend for the faults and fractures. The northeastern part of the trough contains a large syncline-anticline pair in which the north plunging nose of the anticline represents the northern end of the Az Zahrah-Al Hufrah Platform. Several wells have been drilled in the Dur al Abd Trough, but with no success to date.

The Az Zahrah-Al Hufrah Platform is very favorably situated for entrapment of hydrocarbons as attested to by the numerous oil and gas fields located on the high. Interpretation of the remote sensing images combined with surface geologic data show a predominance of mainly northwest oriented lineaments (i.e., faults and fractures). The interpreted faults from seismic data coincide fairly closely with the major lineaments from the remote sensing images. Also present on the remote sensing images and surface geology map over the Az Zahrah-Al Hufrah Platform are several fold structures. For example, there is a major anticlinal axis at the north end of the platform that continues

southwards to the Az Zahrah-Al Hufrah fields. This fold axis is also present on several structure maps such as the top Hon, top Dahra and top Zelten formations. Although the fold axis appears continuous, it may actually be arranged en echelon and, therefore, contain separate closures that could be prospective.

In the Zallah Trough, the remote sensing and surface geology show a predominance of northwest trending faults and associated folds in the area north of the surface volcanic rocks of the Zallah Trough. The interpreted faults from seismic data also closely approximate the imagery results. In fact, the seismic data also shows a continuation of these fault trends in the area beneath the surface volcanics as well. The integrated datasets used in this study indicate some highs and lows, most probably related to the small grabens and horst blocks.

Structural traps are dominant in the Zallah Trough and mainly related to Eocene deformation and all have good surface expressions on the satellite imagery. Most traps occur in the heavily faulted western side of the basin.

Some exploration leads can be revealed in the study area which are primarily structural traps with a related surface and subsurface expression as interpreted from the satellite imagery, seismic and borehole data. These leads have been identified based on surface four-way closure such as at the southern end of the Waddan Uplift. The southeast part and southern most edge of the uplift, however, have sufficient seismic data and do in-fact indicate some major faults to support a boundary in these areas. On the other hand, prospectivity of the southern part of the uplift is considered to be more favorable because of a thicker Tertiary and Cretaceous sedimentary section that contains reservoirs and seals, apparent fault-associated traps and nearness to the mature source rocks situated in the adjoining Zallah Trough. The structure is along strike from surface closures associated with the Al Hulayq Ridge and the Karim, Aswad and Zallah oil fields. The southeastern side of the Waddan Uplift as interpreted from data used is appears as a down faulted trap-door type structure that would be dependent on the western bounding fault being a sealing fault. Migration would be up-dip from the Zallah Trough. Also the western margin or crest of the northeast tilted Gattar Ridge where the Paleocene carbonates are likely to be highly fractured due to the proximity of the western boundary fault. Due to the amount of downthrow across the Az Zahrah-Al Hufrah Platform bounding fault to the east, the structure would probably require oil migration from the Zallah Trough.

CHAPTER 9: CONCLUSIONS AND FUTURE WORK

9.1 Conclusions

The architecture and structural evolution of the Sirt Basin is typical of a rift-basin located within Pan-African zones of lithospheric weakness that define intraplates on the African continent. Extension commenced as early as the Late Jurassic and continued into the Tertiary, however the basin records a complex history of extension interrupted by compressional, and strike-slip phases. It is clear that the sequence records a regional response that was clearly related to the breakup of Gondwanaland and shares similar tectonic histories and styles to those of major Central and western African basins.

Based on borehole data the study area can be subdivided into six rifting phases with significant rifting in the Early Cretaceous, related to the opening of the South and Equatorial Atlantic, culminating in a Late Cretaceous syn-rift sedimentary basin formed by intense normal faulting and graben formation. Faulting essentially ceased by the Paleocene as down-warping formed a thermal sag basin that overlies the graben system.
Generally the Mesozoic sediments rocks show stronger lateral and vertical variations in thickness and lithology compared to the overlying Tertiary sediments. The synrift units are thin to absent on adjacent platforms throughout synrift sedimentation. A short episode of renewed rifting occurred in the Eocene and was then ended with uplift and compression during the Oligocene/Miocene and lastly eastward tilting and volcanic eruptions. Fault reactivation has been recognized by differences in thickness of some rock units compared with other stratigraphic units.
The study area has been subjected to multiple tectonic episodes. In common with other basins in North Africa it underwent extension during the Early Cretaceous. Unlike other basins' this was followed by a rotation in the extension direction and the formation of a separate population of faults during a second minor extensional episode in the Eocene time).
Analysis of fault geometries, fault kinematics and sedimentation patterns indicates that our study area is composed of a segmented fault pattern with NNW-SSE to NW-SE and N-S to NNE-SSW striking steeply dipping normal fault systems with relatively large throws in the northwestern part of the study area. These trends reflect pre-existing basement fabrics and older Pan-African shear zones that have been reactivated to form the rift borders under ENE- WSW directed extension. Many surface structural features interpreted from satellite images confirm sinistral strike-slip deformation has been

superimposed on the rift basin. These faults dissect the study area into geomorphological elevated blocks and depressions: the Facha graben, Ar Ramlah Syncline, Gattar Ridge, Al Hulayq Ridge, Zallah sub-basin and Ma‘amir graben.

Many folds in the hangingwalls to the main faults can be explained as a result of a partitioning likely to have been induced by the obliquity between the pre-existing normal fault trends and the Eocene compression direction. Folds associated with relay ramps related to segmented en echelon faults, are frequently seen in the southeastern part of the area.

Based on all the interpreted seismic and well-based geological cross sections trending NE-SW the study area seems to be more tectonically and structurally complicated to the south. The resulting increasing number of the faults has is reflected in more tectonic blocks to the south. Conversely, the strike-parallel cross section NW-SE shows the most of the reflectors are generally flat lying and approximately constant thickness and faults are mainly occur below the base Kalash horizon indicate that the strike direction cross section (NW-SE) is most likely less complication of NE-SW trending cross sections. Most of the identified faults seem to be clearly offset or disrupt most of the sedimentary sequence particularly the near base Kalash reflector indicating that they penetrate deep into the section, probably into Precambrian basement. The basement in many of the footwalls directly underlies this horizon. The Gedari fault seems to be the master fault in the study area where it vertically displaces and horizontally extends the whole sedimentary sequence from Upper Cretaceous to the Eocene.

The development of antithetic faults in the hanging wall to the western margin of the Az Zahrah-Al Hufrah Platform defining a synformal structure at shallow level gives the impression that flower structures are developed.

Paleostress analysis utilized in this study showed that the Northwest Libya (Jifarah Basin and Nafusah Uplift) and Hun Graben areas are predominantly characterized by NNE-SSW directions of extension ranging from N12°E to 25°E with lesser component of ENE-WSW direction of extension with an average N102°E where the σ3 directions rotate clockwise from NNE–SSW to ENE-WSW in Northwest Libya (Jifarah Basin and Nafusah Uplift).

The new proposed model based on the paleostress analysis in this study suggests that during the Eocene time these E–W faults in the Jifarah Basin underwent a compressional stress trending approximately from a WNW-ESE as a result of the convergence between Africa and Eurasia that began in the Late Cretaceous, about 90

Ma ago that led to the formation of dextral strike-slip movements whilst the Hun Graben fault system which result from the reactivated Cretaceous faults running in NW-SE direction under similar compressional stress formed the sinistral strike-slip and normal fault movements. This led to the development of zones of oblique extension or transtension on what would otherwise be a simple extensional margin which manifested mainly in Hun Graben as extension-dominated transtension.

Sinistral strike-slip movements are clearly documented in this work further east and south of the Hun Graben in satellite image interpretation and seismic data where major faults branch out into smaller faults reminiscent of a flower structures such has often been shown to be associated with strike-slip faulting.

Some exploration leads have been revealed in the study area which is primarily structural traps with a related surface and subsurface expression as interpreted from the satellite imagery, seismic and borehole data. In Zallah Trough the integrated used data indicate some highs and lows, most probably related to the small grabens and horst blocks.

Most oil fields are similarly located on structural highs associated with normal faults and rely on upthrown closure against those faults.

9.2 Future work

Further work is required in the study area as a part of Sirt Basin to understand the effects of the tectonic processes on its formation and occurrence of the hydrocarbon deposits.

It can be concluded from the diversity of geological opinion that there is still a debate regarding the tectonic evolution of the Sirt Basin mainly for two reasons:-

- The present seismic data which characterized by the absence of deep seismic reflection and refraction data do not reveal seismic events below the Middle Cretaceous; it is not possible to deduce in full the history of the basin structures and their stages of development prior to Middle Cretaceous times, and,
- The absence of deep drilled well reaching to the basement where the Pre-Cretaceous sediments have been penetrated by only a few wells particularly in deep trough areas.

Therefore, the study area requires future geological and geophysical investigations, and to substantiate the interpretation made in this study, further deep drilling, combined with high resolution 3D seismic acquisition of deep reflection and refraction seismic

survey, with the objectives to constrain the geological model of the Sirt Basin evolution is needed particularly in the deep trough area. Additional key well data and seismic data, especially in the area of the Waddan Uplift and Hun Graben, would provide a much better understanding of the stratigraphic and structural aspects. This additional data would also serve to further reduce the level of uncertainty concerning the hydrocarbon potential in this area.

For a detailed surface investigations:

- A more detailed structural interpretation of higher resolution satellite imagery (possible even stereo imagery) should be made of existing oil fields to use as structural analogues for evaluating new exploration leads. This study could be combined with a more rigorous analysis of available seismic and Potential Fields data.

- The general good correlation between the surface and subsurface structure suggests that field investigation for hydrocarbon micro-seepage may prove useful, especially in the vicinity of major faults.

- An extensive field programme should be performed to examine the kinematic relationships of particular faults and fault zones interpreted in the study area. This would help to provide information on the relative timing of fault movement, the sense of displacement and possible indication of hydrocarbon seepage. It is also useful to further evaluation for any identified leads in this study.

APPENDIX 1

Teknica seismic data reprocessing

One of the objectives of the project was to determine if reprocessing of the seismic data would improve the data quality with the goal being improved structural definition and enhancement of stratigraphic aspects. Therefore, at the start of the project and as part of the initial seismic data review, Teknica performed data reprocessing on the following six (6) seismic lines (total of about 123 km) received from Zuetina:

1. Line V-54-74C
2. Line NC74A-76-V30
3. Line NC74B-78V59
4. Line NC74F-84-816
5. Line NC74F-85-832
6. Line NC74F-87-929

The seismic data was received as paper copies and was then scanned to obtain digital SGY files necessary for seismic testing. Post stack processes such as deconvolution and migration were investigated to determine their usefulness in improving the interpretability of seismic data. Results of the processing indicated that data quality improvement was minimal and did not justify the extra costs required for additional processing of seismic lines. As a result, no more reprocessing has been done to-date.

Mis-tie derived seismic interpretation problems

As the 2D seismic interpretation progressed, it became clear that the diverse nature of the seismic acquisition and overall processing parameters was impeding accurate correlations of seismic markers, making the well-to-seismic and seismic-to-seismic correlation complicated. This was partly due to large mis-ties arising from the different datum static correction methods used for the different surveys. A further complication was the presence of major geologic structural features at the tie points. Therefore, Teknica decision was made to systematically diminish the mis-ties due to datum statics to an acceptable level.

While some mis-tie reduction could be achieved through expensive digital seismic reprocessing, the high volume of seismic data (264 lines or 6573 km) of records, dictated a quicker, less arduous and expensive method be used, even if the overall

solution was slightly less precise than the reprocessing option. An additional objective was that the mis-tie reduction process should not introduce any artificial structure into the reflector patterns, by altering the local dips. These requirements were met in the mis-tie methodology used in the study.

General overview of mis-ties

Interpreters of 2D seismic reflection data characteristically use the match of qualitative character/appearance and quantitative reflection time values at line intersections to validate and check their work. Ideally, reflection time values measured along 2D seismic lines will be exactly the same (within some small noise level's, standard deviation), or will tie at line intersections. This is usually the case for lines from the same survey. However, the differences in reflection response and line mis-ties invariably increase when the surveys are of different vintages and conducted with different surveying, acquisition and processing parameters and methods. Major factors that contribute to 2D seismic mis-ties are:

1. **<u>Data acquisition</u>**

Many of the following aspects related to data acquistion can be minimized in the data processing stage (usually by careful deconvolution):

a. *Instrumentation:* Different recording systems have different phase and amplitude responses as a function of frequency.

b. *Sources:* Different energy sources, the accuracy of their near-source measurement and other parameters will produce different outgoing wavelets and the corresponding records.

c. *Receivers:* The responses of geophones (and hydrophones and accelerometers) vary depending on their natural frequencies. Recording is also dependent on array configuration, near surface conditions, ground coupling (in land data); or streamer depth and feathering (in marine surveys). If feathering (or a crooked line layout of land data) occurs then the CMP position is not strictly a common point, but a patch which varies in area as a function of record time. This is because the deep data incorporates the full offset range, while the shallow data contains only the short-offset traces. Consequently when this data is tied, it will only be correct for the unstacked zero-offset traces. Therefore, the stacked data will be smeared, especially if one or more lines have a dip component, resulting in a reflection time mis-tie.

2. ***Positioning****:* Older, pre-Global (Satellite) Positioning System (GPS) land and marine surveys are not as accurately located as the more recent ones. Consequently, tie points between surveys that cannot be absolutely calibrated to topography/bathymetry, and satellite positions may not in fact be where they are shown. This effect will introduce mis-ties because reflection times are not being measured at the same location. Commonly, if good quality topographic maps and bathymetric charts are available, the geophysicist can before, or during, the interpretation stage adjust the seismic lines' shot point locations using the contoured values from these maps and charts (as well as those from the initial reflector maps), to eliminate many of these mis-ties. Lines that go through well locations may use these elevations to "anchor" some of their shot point locations, provided of course that the wells were also accurately surveyed

3. Processing

It is well known that seismic processing is a highly interpretive procedure involving the application of many varying parameters which can change the character (wavelet) and time values of the final seismic section. These parameters include the following (note, static and residual static corrections will be discussed later):

a. *Deconvolution and Phase Shifting:* The objective of many processing programs is to generate a zero-phase seismic section, usually by the application of a deconvolution operator. The result of this operation is approximately zero-phase, but the approximation deteriorates or is less effective with older data and technology. If, at the tie point the lines are not identical in appearance (i.e., amplitude, zero-phase and frequency derived), the picked values may be different and a mis-tie will occur. This can be partially compensated for by filter cross-equalization (i.e., estimating an average wavelet for the two lines and applying a special filter derived from it to the two lines), or, as has been done for many years, by "phase rotation," during which an approximate constant phase shift is applied to all of the data's frequencies. This procedure changes the reflectors' appearance while (usually) also moving the reflection times up or down by as much as 0.030 second's and thereby facilitating line ties.

b. *Stacking Velocity*: The reflector appearance and event reflection time on a seismic section are highly dependent on the stacking velocities chosen and their number/spatial density. Often, in order to suppress multiples, the optimum

stacking velocities for the primary data are slightly changed and, hence, the final sections are not perfectly stacked.

c. *Normal Moveout Stretch:* The nature of the mute program that is applied before stack will affect the frequency content and character of the resulting stacked traces, and, in turn, the picked reflection times, thus contributing to mis-ties.

d. *Migration and Crooked-Line Surveys:* During migration, the positioning of any final section's reflection point is a function of the dip of the horizons and the interpreted velocity field. In 3D data sets, all relevant dip information is available and the velocity field is usually quite dense, so the migrated reflections points are positioned relatively accurately and diffractions collapse to a point. However, with 2D data migration process can only migrate the line components, even if the line is straight (worse with crooked line surveys). Therefore, intersections of migrated strike and dip 2D lines in highly structural areas (e.g. Sirt Basin) will rarely tie accurately.

e. *Frequency Filters*: In areas characterized by complex reflections, (i.e. due to thin beds, lithological changes, fractures, etc.) the appearance and resolution of the reflectors will be drastically altered by the filters applied. Generally, the higher the frequency content of the data, the better the resolution (i.e., resolution ≈ dominant wavelength /4 ≈ bed velocity / (4x dominant frequency)) resulting in geological accuracy and consistency of picked times. Mixed surveys using different band pass filters will, therefore, have resolution related mis-ties.

f. *Seismic Section Display Polarity:* Unless polarity is precisely known, the interpreter may attempt to correlate lines of different polarities resulting in mis-ties of at least one half of a reflector cycle.

4. Static corrections

The purpose of static corrections is to time shift the seismic data to a common datum. The selection of the correction method, the correction velocities, and the raw times can be very interpretive. Differences in equipment acquisition parameters, and processing and used between surveys will generate mis-ties.

Static corrections are usually applied in the following two steps:

a. *Datum Static Corrections:* This is the major contributor to mis-ties. Mis-tie errors can be generated by datum static corrections if the velocity information is insufficient or inaccurate for the near-surface layers. Moreover, if the Reference

Datum Plane is above the ground surface, and mathematical sign conventions are not meticulously followed, mis-tie errors can be generated in the calculations.

The wrong Elevation (or Replacement) Velocity used in the correction through the weathered layer can lead to long-wavelength (i.e., low frequency) artificial time structure anomalies, especially if the velocity used along the line is not changed as a function of the geologic conditions. Within a survey, these anomalies may not generate significant mis-ties, but they will at line intersections with other surveys that use different constant or varying replacement velocities, even if the datum of the second survey is identical to the first.

b. *Residual Static Corrections:* These corrections are necessary to remove short wavelength residual anomalies remaining after the application of the Datum Static Corrections. Generally, they improve the CMP stack and produce only minor changes in the structural configuration at depth.

The accurate estimation and application of datum and residual static corrections is a large and complex subject (Cox 1999) and, if not accurately done, can result in line mis-ties between different seismic surveys and even within the same 2D survey.

In summary, the elimination, or at least minimization, of mis-ties has always been an important initial corrective step in seismic interpretation and structural mapping, but it has also become a vital step in modern seismic stratigraphic interpretation and attribute/coherence analyses. After all of the physical and geological factors described above have been carefully compensated, a small amount of "random noise related errors", will remain in any survey to produce residual mis-ties. This "noise" can make interpretation difficult, and the problem worsens when surveys of different vintages and parameters are mixed.

Any remaining "residual" mis-ties have usually been further reduced by the application of various statistical, least-mean-square (LMS) curve fitting and contouring methods, along the seismic profiles and / or over the map area.

Seismic survey static correction parameters: The datum plane and elevation or replacement velocity

When two or more surveys are merged, the mis-tie problem is exacerbated if each survey has been corrected to a different Datum Plane (i.e., the reference surface from which survey reflection times are measured) or by using different Replacement or Elevation Velocities. This reference datum plane is usually selected so that:

1. It is just below, or near the bottom of the weathered layer.

2. The spatial changes in velocity below the datum are slow and smooth (i.e., it is approximately an iso-velocity surface).
3. It is usually a horizontal surface, but can also be a tilted or contour surface.
4. Reductions to this level minimize local topographic and near-surface effects (i.e., seismic times and velocities are referred to this plane as if the signal source and geophones have been located on this plane and as if no low-velocity layer exists).

The datum static corrections also require that the near surface seismic times be adjusted up or down to the Datum Reference Plane from the base of the weathered layer, using a correction velocity normally called the Replacement Velocity (sometimes the Datum, or Elevation or Sub-weathering Velocity). This Velocity usually is:

1. The velocity within the weathered layer.
2. Considered to be constant (or very slowly varying) along the seismic line. This implies that it is only slightly affected by changes in local geology.
3. A vertical velocity (i.e., it is used to correct times along almost vertical ray paths).
4. Usually (but not always) annotated on the final paper section either as a profile, values printed along the line, or as a constant value on the header (along with the selected Datum Reference Plane). Unfortunately this vital information is sometimes left off of paper sections and almost always omitted from "modern, improved" seismic, transmitted solely on 8 mm digital tape.
5. Easily "spot checked" with a hand calculator if the seismic section has a known datum plane, a ground elevation profile, a profile of the static correction that was applied and (helpful, but not essential) the residual static profile remaining after the application of the static profile. Using these, the equivalent Replacement Velocity at those traces with 0 msec residual static can be calculated and, if necessary, an approximate average Replacement Velocity estimated for the entire line. This technique proved essential in our work on those lines that did not use (or list) an average Replacement Velocity in their field static correction computations.
7. Empirically verifiable by comparing the shapes of subsurface structures with surface features located above them. If they correlate, either directly or inversely, then there is possibly a problem with the chosen replacement velocity, which may be either too low or too high.

The datum plane adjustment algorithm (with examples)

When several vintages of seismic surveys are to be combined for a single interpretation, it will be necessary to use a common Reference Plane (Seismic Datum) to enable concurrence of reflection times wherever different studies overlap.

The procedure is normally one of simply backing out the original correction applied, in order to restore the original reflection time to surface, and then to calculate a new correction to adjust the reflection time to the reference datum used for the study.

Usually the selected reference plane is flat, but where the study extends over a wide area having appreciable changes in surface elevation, the reference datum may be a smoothly contoured image mimicking surface topography in order to minimize the amount of adjustment.

When the original field data is available for processing, elevation corrections are separately applied to compensate for the elevation at the source, for the downgoing signal, and at the geophone received station for the upgoing signal.

For the more common case, when the only data format available is the finished processed section, it is assumed that each seismic trace has been fully corrected to its position on the seismic section, and a single two-way correction can be applied.

Let:

E_s = Elevation of the Surface

E_x = Elevation of the Reference Plane for Line X

E_r = Elevation of the Reference Plane

V_x = Line X Correction Velocity

V_r = Reference Correction Velocity

Then: (Observing Signs)

$$T_r = T_x + 2\left(\frac{E_s - E_x}{V_x}\right) - 2\left(\frac{E_s\ E_r}{V_r}\right)$$

$$= T_x + 2\left(\frac{(Es - Ex)}{V_x} - \frac{(E_s - E_r)}{V_r}\right)$$

or

$$T_r = T_x + \Delta t$$

Where $$\Delta t = 2\left(\frac{(Es - Ex)}{V_x} - \frac{(E_s - E_r)}{V_r}\right)$$

1. The Elevation Velocity for each seismic line is a constant (i.e., it does not change as the near surface geology varies). This is usually a valid assumption, but where Elevation Velocities varied moderately along the line (and were not noted), these can be estimated and an average velocity "back calculated".
2. The Elevation Velocity is a constant from the surface to the Datum Plane (i.e., it incorporates both the weathering and the near-top, sub-weathering layer velocities).
3. The Elevation Velocity and the seismic wave ray paths are vertical in the weathered layer and at the top of the sub-weathered layer.

For land seismic surveys the surface elevation E is a variable for each seismic trace and consequently, the time shift (Δt) becomes a dynamic shift along any line. Therefore the elevation must be known for each trace position. At tie points the surface elevation of any two lines should be identical (or close enough to average). Isolated lines and surveys can be shifted to the regional datum plane accurately using these equations.

Due to the wide variation in datum planes and correction velocities between the several surveys consolidated into the present study, Δt corrections to bring all data to a common reference plane varied from –200 msec to +200 msec. However, it should be remembered that all corrections are only close approximations, a function of the survey's acquisition and processing parameters so unless they are identical for two surveys the actual "picked" reflection time may be slightly different on each line.

Summary of mis-tie resolution

A detailed review of Mis-Tie Resolution procedures may be found in Appendix 5.1.

1. All of the 2D seismic lines made available for project interpretation were shifted to new regional standards of 200 m ASL (Datum Plane) and 2000 m/s (Elevation / Replacement Velocity). This eliminated many of the observed seismic mis-ties and reduced most to less than 25 msec. Prior to this few of the mis-ties were as small as this and many were in the 100-200 m sec. range.
2. The dynamic time shift method developed for this mis-tie minimization study did not appear to introduce any false structural anomalies into the reflection time sections. However, further analyses including detailed time structure mapping are needed to confirm this, and will be accomplished later in the project.

3. A topographic map detailing the ground elevation of the Western Sirt Basin (seismic) Project area, to an accuracy of ± 5 m, has been constructed for the solution of the seismic mis-tie problem. The data for this map was derived from a mixture of wells, seismic, field topographic surveys and satellite observations.
4. The results of the analysis of the datum planes and elevation velocities used by the operating companies were mapped out. These two "blob" maps, of the 13 Datum Plane areas and the 10 Elevation Velocity areas, are expected to be useful initial tools for companies new to exploration in Libya, and in the process of planning future seismic programs within this part of the WSB.

Mis-tie recommendations

1. Ensure that all information necessary to ensure the rapid and accurate interpretation of the data will be included in future seismic data transmittals. The information received for all of the stacked seismic sections should include a complete record of the surveying, acquisition and processing parameters used.
2. The Mis-tie Minimization Technology developed for this project should be used routinely, where appropriate, as a tool to detect and eliminate poorly interpreted seismic reflectors.

REFERENCES

Abadi, A.M., 2002. Tectonics of the Sirt basin. Inferences from tectonic subsidence analysis, stress inversion and gravity modeling. *PhD thesis*, Vrije University, Amsterdam, the Netherlands, 187 pp.

Abadi, A.M., van Wees, J.D., van Dijk, P.M., Cloetingh, S.A.P.L., 2008. Tectonics and subsidence evolution of the Sirt Basin, Libya. *Am. Ass. Petrol. Geol. Bulletin* 92, 993–1027.

Abdalla, A.A., and Stewart, R.R., 1990. Traveltime inversion and reflection processing of cross-hole seismic data: Expanded Abstracts, *SEG meeting*, San Francisco.

Abdshakoor, A. and Shagroni, Y. 1984. Sheet Hun (NH 33-11), Geological Map of Libya, scale 1:250,000, Explanatory Booklet, *Industrial Research Centre*, Tripoli.

Abugares, Y.I. 1996. Sedimentology and hydrocarbon potential of the Gir Formation, Sirt Basin, Libya. *First Symposium on the Sedimentary Basins of Libya,Geology of the Sirt Basin*, vol. 2. *(eds. M.J. Salem,A.S. El Hawat, A.M. Sbeta)*, Elsevier, Amsterdam, p.45-64.

Ade-Hall, J. M., Reynolds, P. H., Dagley, P., Mussett, A. E., Hubbard, T. P. & Klitzsch, E. H. 1974. Geophysical studies of North African Cenozoic volcanic areas: I. Haruj Assuad, Libya. *Canadian Journal of Earth Sciences*, 11, 998–1006.

AGOCO (Arab Golf Oil Company), 1980. Geology of a stratigraphic giant - the Messlah oilfield. In *The Geology of Libya* Volume II, Salem, M. J. and Busrewil, M. T. (eds.), Academic Press, London. 521-536.

Ahlbrandt, T.S., 2001. The Sirte Basin province of Libya–Sirte-Zelton total petroleum system, *U.S. Geological Survey Bulletin* 2202-F, 29p.

Aliev, M., A.At Lasoussine, N., Avrov, V., Aleksine, G., Barouline, G., Lakovlev, B., Korj, M., Kouvykine, V., Mazanov, V., Medvedev, E., Mkrtchiane, O., Moustafinov, R., Oriev, L., Oroudjeva, D., Oulmi, M. and Saad, A., 1971. Geological structure and estimation of oil and gas in the Sahara in Algeria. *Altamira-Rotopress*, S.A., 265p

Ambrose, G., 2000. The geology and hydrocarbon habitat of the Sarir Sandstone, SE Sirt Basin, Libya: *Journal of Petroleum Geology*, 23, 165-191.

Anderson, E.M. 1942. *The dynamics of faulting and dyke formation with application to Britain*. Oliver Boyd, Edinburgh.

Angelier, J. 1989. From orientation to magnitudes in paleostresses determinations using fault slip data. *J. Struct. Geol*. 11:37-50.

Angelier, J., 1984. Tectonic analysis of fault slip data sets. *J. Geophys. Res*. 89 (B7), 5835–5848.

Angelier, J., Barrier, E., Chu, H.T., 1986. Plate collision and paleostress trajectories in a fold-thrust belt: the foothills of Taiwan. *Tectonophysics* 125, 161-178.

Angelier, J. 1989. From orientation to magnitudes in paleostresses determinations using fault slip data. J. Struct. Geol. 11:37-50.

Anketel, J.M. 1996. Structural History of the Sirt Basin and its relationships to the Sabratah Basin and Cyrenaican Platform, Northern Libya. *In The Geology of Sirt Basin*

Volume II, Salem, M.J., El-Hawat, A.S. and A.M. Sbeta (eds), Elsevier, Amsterdam. 57-87.

Anketell, J.M. and Ghellali, S. 1991. A paleogeologic map of the Pre-Tertiary surface in the region of the Jifarah Plain and its implication to the structural history of the northern Libya. *In The Geology of Libya* Volume VI, Salem, M.J., Sbeta A.M. and Bakbak M.R. (eds),.2381-2406.

Anketell, J.M. and Kumati, S.M. 1991a. Sedimentary history of the Asiyah Formation – Upper Eocene of Al Hufrah area, Western Sirt Basin, G.S.P.L.A.J. *In The Geology of Libya* Volume V, Salem, M.J. and M.N. Belaid (eds), 1883-1906.

Anketell, J.M. and Kumati, S.M. 1991b. Structure of Al Hufrah Region – Western Sirt Basin, G.S.P.L.A.J. *In The Geology of Libya* Volume V, Salem, M.J. and M.N. Belaid (eds), 2353-2370.

Argnani, A. 1993. Neogene basins in the Strait of Sicily (central Mediterranean): tectonic setting and geodynamic implications. In: Boschi, E., Mantovani, E. & Morelli, A. (eds) *Recent Evolution and Seismicity of the Mediterranean Region*. Springer, Berlin, 173–187.

Assaf, H.S. 1991. Folding structure in the Basement rocks of the Jabal Nuqay area, southern Libya. *Third Symposium on the Geology of Libya,* vol. 6 *(eds. MJ.Salem, A.M. Sbeta and M.R. Bakbak),* Elsevier, Amsterdam, p. 2287-2294.

Bahr, D. B., Hutton, E. W., Syvitski J. P., and Pratson, L. F. 2001. Exponential approximations to compacted sediment porosity profiles, Computers & Geosciences, 27, 691-700.

Baird, D. W., Aburawi, R. M., and Bailey, N. J. L. 1996. Geohistory and petroleum in the central Sirt Basin. In: *The Geology of the Sirt Basin*, Vol. 3. Salem, M. J., Busrewil, M. T., Misallati, A.A., and Sola M.A. (eds) Elsevier, Amsterdam,.3-56.

Banerjee, S. 1980. Stratigraphic lexicon of Libya. *Department of Geological Researches and Mining Bulletin* No. 13, 300p.

Baric, G., Spanic, D, and Maricic, M. 1996. Geochemical characterization of source rocks in the NC-157 block (Zaltan Platform), Sirt Basin. *First Symposium on the Sedimentary Basins of Libya,Geology of the Sirt Basin,* vol. 2. *(eds. M.J. Salem,A.S. El-Hawat and A.M. Sbeta),* Elsevier, Amsterdam, p. 541-553.

Barr, F.T. and Weegar, A.A. 1972. Stratigraphic nomenclature of the Sirte Basin, Libya. *The Petroleum Exploration Society of Libya,* 179p.

Bellini, E. and Massa, D. 1980. A stratigraphic contribution to the Palaeozoic of the southern basins of Libya. *Second Symposium on the Geology of Libya.* vol. 1 *(eds. M.J. Salem and M.T. Busrewil),*Academic Press, London,p. 3-56.

Ben Ayed, N., 1986. Evolution tectonique de l'avant pays de la chaıˆne alpine de Tunisie du de´but du Me´sozoı¨que a` l'Actuel. The`se Doc. Etat, *Univ. Paris Sud*, France, 328 pp.

Ben-Avraham, Z., 1992. Development of asymmetric basins along continental transform faults, *Tectonophys*., 215, 209-220.

Benfield, A.C. and Wright, E.P. 1980. Post-Eocene sedimentation in the eastern Sirt Basin, Libya. *Second Symposium on the Geology of Libya,* vol. 2 *(eds. M.J. Salem and M.T. Busrewil),* Academic Press, London, p. 463-500.

Benton, M., Bouaziz, S., Buffetaut, E., Martill, D., Ouaja, M., Soussi, M., Trueman, C., 2000. Dinosaurs and other fossil vertebrates from fluvial deposits in the Lower Cretaceous of southern Tunisia. *Paleogr. Palaeoclim. Palaeoecol*. 157, 227–246.

Bezan, A.M. 1996. The Paleocene sequence in Sirt Basin. *In The Geology of Sirt Basin* Volume I, Salem, M.J., Mouzughi, A.J. and O.S. Hammuda (eds), Elsevier, Amsterdam, 97-117.

Biju-Duval. B. Dercourt, J. and LePichon. X. 1977. From the Tethys Ocean to the Mediterranean sea: A plate tectonic model of the evolution of the Western Alpine system. In: B. BiJu-Duval and L. Montadert (eds). *Int. Symp. Structural History of the Mediterranean Basins* (Split. Yugoslavia).

Binks, R.M., and Fairhead, J.D., 1992. A Plate Tectonic Setting for Mesozoic Rifts of West and Central Africa: *Tectonophysics*, 213, 141-151.

Bishop, M. S., 1960. Subsurface mapping: *New York, John Wiley and Sons*, p. 67, 91-98.

Boote, D. R., Clark-Lowes, D.D., Traut, M.W., 1998. Palaeozoic petroleum systems of North Africa, in D. S. MacGregor, Moody, R.T.J., Clark-Lowes, D.D., ed., *Petroleum Geology of North Africa*, London, Geological Society Special Publication, 132, 7-68.

Boote, D.R.D., A.Dardour, P.F.Green, J.D.Smewing & F.Van Hoeflaken. 2008. Burial and unroofing history of the baseTanezzuft 'hot' Shale source rock, Murzuq Basin, SW Libya: new AFTA constraints from basin margin outcrops. *4th Sedimentary Basins of Libya Symposium: the Geology of Southern Libya,* 17-20th November 2008, Tripoli, Libya (in press)

Bosworth, 1992. Mesozoic and early Tertiary rift tectonics in East Africa, *Tectonophysics* **209**, 115–137.

Bosworth, W., El-Hawat, A. S., Helgeson, D. E. & Burke, K. 2008. Cyrenaican 'shock absorber' and associated inversion strain shadow in the collision zone of NE Africa. *Geology*, 36, 695–698.

Bosworth, W., Huchon, P., and McClay, K., 2005. The Red Sea and Gulf of Aden basins: *Journal of African Earth Sciences*, 43, 334-378.

Bott, M.H.P., 1959. The mechanics of oblique-slip faulting: *Geological Magazine*, v. 96, p. 109-117.

Brady, T.J., Campbell, N.D.J., and Maher, C.E. 1980. Intisar 'D' oil field, Libya. In: *Giant oil andgas fields of the decade 1968-1978. (ed. M.T.Halbouty).* Mem. Amer. Assoc. Pet. Geol. No. 30, p. 843-861.

Brennan, 1992. Raguba Field – Libya. In: Treatise of Petroleum Geology. *Atlas of oil and gas fields,* Structural Traps VII (complied by Beaumont, E. A. and Foster, N. H.) *Am. Assoc. Pet. Geol*., pp.267-289.

Brew, G., Barazangi, M., Al-Maleh, K. & Sawaf, T. 2001. The tectonic and geologic evolution of Syria. *GeoArabia*, 6, 573–616.

Brew, G., Best, J., Barazangi, M., and Sawaf, T. 2003. Tectonic evolution of the NE Palmyride mountain belt, Syria: the Bishri crustal block. *Journal of the Geological Society, London*, 160, 677–685.

Brugman, W.A. and Visscher, H. 1988. Permian and Triassic palynostratigraphy of northeast Libya. In: *Subsurface palynostrati-graphy of northeast Libya,(eds. A. El-*

*Arnauti, B. Owens and B. Thusu).*Research Centre, Garyounis University, Benghazi, p. 157-170.

Brugman, W.A., Eggink, J.W., and Visscher, H. 1985. Middle Triassic (Anisian-Ladinian) palynomorphs. In: *The palynostratigraphy of north-east Libya (eds. B. Thusu and B. Owens). Journ. Micropalae-ontology,* vol. 4, p. 107-112. BUROLLET, P.F. 1960. Libye. *Lexique Stratigraphique International, Afrique (dir. R. Furon) Fascicule IVa.*Congres Geologique International, Cent. Nat. Rech. Sci. Paris, 62p

Bumby, A.J., and Guiraud, R., 2005. The geodynamic setting of the Phanerozoic basins of Africa: *Journal of African Earth Sciences*, 43, 1-12.

Burke, K., and J. Dewey, 1974. Two plates in Africa during Cretaceous: *Nature,* 249, 313-316

Burollet, P.F. 1960. Libye. *Lexique Stratigraphique International, Afrique (dir. R. Furon) Fascicule IVa.* Congres Geologique International, Cent. Nat. Rech. Sci. Paris, 62p.

Burollet, P.F. 1963. Reconnaissance geologique dans le sud-est du bassin de Kufra. *First Saharan Symposium.* Rev. Inst. Fran. Pet. special volume, p. 219-227.

Burollet, P.F., 1991. Structures and tectonics of Tunisia: *Tectonophysics,* v. 195, p. 359–369.

Burollet, P.F., Desfoges, G., 1982. dynamique des bassins néocrétacés en Tunisie in Livre Jubilaire Gabriel Lucas. *Mém. Géol. Univ. Dijon,* 381–389.

Burollet, P.F., Mugniot, J.M., and Sweeney, P., 1978. The geology of the Pelagian block—The margins and basins off southern Tunisia and Tripolitania, in Nairn, A.E.M., Kanes, W.H., and Stehli, F.G., eds., *The ocean basins and margins: New York, Plenum Press,* 4B, 331– 359.

Busrewil, M. T., Oun, K. M. and Haman, M., 2009. Neoproterozoic-Lower Cretaceous Tectono-sedimaentary Evolution of the Sirt Basin, Libya. *Third Sedimentary Basins of Libya: The Geology of East Libya,* vol. IV. *(eds. M.J. Salem, A. Al-Arnauti and A. El sogher),* Elsevier, Amsterdam, p. 251-268.

Butt. A.A. 1986. Upper Cretaceous biostratigraphy of the Sirte Basin. Northern Libya. *Rev. Paleobiol.* 5(2).175-191.

Campbell, C.J. 1991. The golden centuiy of oil 1950-2050. *Kluwer Academic Publishers*, Dordrecht, 345p.

Capitanio, F. A., Faccenna, C. & Funiciello, R. 2009. Opening of Sirte Basin: result of slab avalanche? *Earth and Planetary Science Letters*, 285, 210–216.

Capitanio F. A., Faccenna C., Funiciello R. & Salvini F., 2012. Recent tectonics of Tripolitania, Libya: an intraplate record of Mediterranean subduction. *Geological Society, London, Special Publications* 2011, v.357; p319-328.

Carey, E., Brunier, B., 1974. Analyse theorique et rumerique d'un modele mecanique elementaire applique a l'etude d'une population de failles. Comptes Rendus Hebdomadaires des Seances de l'Academie des Sciences, Serie D: *Sciences Naturelles* 279 (11), 891–894.

Cepek, P. 1979. Sheet Al Qaryat ash Sharqiyah (NH 33-6), Geological Map of Libya, scale 1:250,000, Explanatory Booklet, *Industrial Research Centre*, Tripoli.

Charlesworth, H., Cruden, D., Ramsden, J., and Huang, Q., 1989., ORIENT: an interactive FORTRAN-77 program for processing orientations on a microcomputer: *Computers & Geosciences*, v. 15, no. 3, p. 275 293.

Chiu, S. K., and Stewart, R. R., 1987. Estimating P-wave anisotropy using multi-offset VSP and surface seismic data: Presented at Can. *Soc. Explor. Geophys. Nat. Conv*. (abst. VELa-I), Calgary.

Choi, P.Y., Kwon, S.K., Hwang, J.H., Lee, S.R., An, G.O., 2001. Paleostress analysis of thePohang-Ulsan area, Southeast Korea: tectonic sequence and timing of blockrotation. *Geosciences Journal* 5, 1-18.

Clemson, J., J. Cartwright, and J. Booth (1997). Structural segmentation and the influence of basement structure on the Namibian passive margin, *J. Geol. Soc.* London, 154, 477 – 482.

Clifford, H.J., Grund, R. and Musrati, H. 1980. Geology of a stratigraphic giant: Messla oil field, Libya. In: *Giant oil and gas fields of the decade 1968-1978. (ed. M.T. Halbouty).* Mem. Amer. Assoc. Pet. Geol. No. 30, p. 507-524.

Clifton, A. E., R. W. Schlische, M. O. Withjack, and R. V. Ackermann (2000). Influence on rift obliquity on fault-population systematics: Results of experimental clay models, *J. Struct. Geol*., 22, 1491 – 1509.

Cloetingh, S., Kooi, H., 1992. Intraplate stresses and dynamical aspects of rift basins. *Tectonophysics* 215, 167-185.

Cloetingh, S., Ziegler, P.A., Beekman, F., Andriessen, P.A.M., Matenco, L., Bada, G., Garcia-Castellanos, D., Hardebol, N., Dezes, P. and Sokoutis, D., 2005. Lithospheric memory, state of stress and rheology: neotectonic controls on Europe's intraplate continental topography. *Quaternary Science Reviews*, 24: 241-304

Conant, L. C. and Goudarzi, G. H., (1977). Geological map of Libya 1:2,000,000 (2nd edition): *Industry. Res. Cent*., Tripoli.

Conant, L.C. and Goudarzi, G.H. 1967. Stratigraphic and tectonic framework of Libya. *Bull Amer. Assoc. Pet. Geol* vol. 51, p. 719-730.

Cowie, P. A., Underhill, J. R., Behn, M. D., Lin, J., and Gill, C.E., 2005. Spatio-temporal evolution of strain accumulation derived from multi-scale observations of Late Jurassic rifting in the northern North Sea: A critical test of models for lithospheric extension. *Earth and Planetary Science Letters* 234, 401– 419

Crema, C. 1926. Sulle manifestazioni di idrocarbuii del pozzo artesiano di Sidi-Mesri presso Tripoli. *La Miniera Italiano*, vol 10, p. 49-50.

Cvetkovic´ , V., Toljic´, M., Ammar, N. A., Rundic´, L. & Trish, K. B. 2010. Petrogenesis of the eastern part of the Al Haruj basalts (Libya). *Journal of African Science*, 58, 37–50,

Davison, I. (1997). Wide and narrow margins of the Brazilian South Atlantic, *J. Geol. Soc.* London, 154, 471 – 476.

De Paola, N., Mirabella, F., Barchi, M.R. & Burchielli, F. 2006. Early orogenic normal faults and their reactivation during thrust belt evolution: the Gubbio Fault case study, Umbria-Marche Apennines (Italy). *Journal of Structural Geology* 28(11): 1948-1957.

De Paola, N., R. E. Holdsworth, and K. J. W. McCaffrey (2005a). The influence of lithology and pre-existing structures on reservoir-scale faulting patterns in transtensional rift zones, *J. Geol. Soc.* London, 162, 471 – 480.

De Paola, N., R. E. Holdsworth, K. J. W. McCaffrey, and M. R. Barchi (2005b). Partitioned transtension: An alternative to basin inversion models, *J. Struct. Geol*., 27, 607 – 625.

Delvaux, D. Moeys, R., Stapel, G., Petit, C., Levi, K., Miroshnichenko, A., Ruzchich, V., and San'kov, V. 1997. Paleostress reconstructions and geodynamics of the Baikal region, Central Asia, Part 2. Cenozoic rifting. *Tectonophysics* 282:1-38.

Dercourt, J., Ricou, L. E., and Vrielynck, B., 1993. Atlas Tethys palaeoenvironmental maps: Paris, *Gauthier-Villars*, 307 p.

Dewey, P. C., Ryan, B. F. and Bonnin, J. 1973. Plate tectonics and the evolution of the Alpine systems. *Geological Society of America Bulletin***, 84,** 3,137-80.

Dewey, J. F. (2002). Transtension in arcs and orogens, *Int. Geol. Rev*., 44, 402 – 439.

Dewey, J.F., Helman, M.L., Turco, E., Hutton, D.H.W. and Knott, S.D. 1989. Kinematics of the western Mediterranean. In: *Alpine Tectonics (ed.M.P. Coward, D. Dietrich andR.G. Park),* Geol. Soc. Special Publication No. 45, p. 265-283.

Diggle, P. J., and Fisher, N. I., 1985. SPHERE: a contouring program for spherical data: *Computers & Geosciences*, v. ll, no. 6, p. 725 766.

Dobrin, M. B., 1976. Introduction to geophysical prospecting: McGraw-Hill Book Co.

Drury, S., 2001. Image Interpretation in Geology, *Blackwell Science, Nelson Thornes*, UK, pp. 290

Dupin, J.-M., Sassi,W., and Angelier, J., 1993. Homogeneous stress hypothesis and actual fault slip: A distinct element analysis: *Journal of Structural Geology*, v. 15, p. 1033–1043.

El Hawat, A. and Pawellek, T. (2004). A field guidebook to the geology of Sirt Basin, Libya: from April 27th to May 1st, 2004

El-Alami, M., Rahouma, S. and Butt, a.a. 1989. Hydrocarbon habitat in the Sirte Basin northern Libya. *Pet. Res. Journ.* Tripoli, vol. 1. p. 17-28.

El-Alami, M.A. 1996b. Habitat of oil in Abu Attiffel area, Sirt Basin, Libya. *First Symposium on the Sedimentary Basins of Libya, Geology of the Sirt Basin,* vol. 2. *(eds. M.J. Salem, A.S. El-Hawat and A.M. Sbeta),* Elsevier, Amsterdam, p. 337-348.

El-Hawat, A. 1980a. Carbonate-terrigenous eye he sedimentation and palaeogeography of the Marada Formation (Middle Miocene), Sirt Basin. *Second Symposium on the Geology of Libya,* vol. 2 *(eds. M.J. Salem and M. T. Busrewil),* Academic Press, London, p. 427-448.

El-Hawat, A. 1997. Sedimentary basins of Egypt: an overview of dynamic stratigraphy. In: *Sedimentary Basins of the World (ed. K.J. Hsu), Part 4 African Basins (ed. R.C. Selley).* Elsevier, Amsterdam, chap. 4, p. 39-85.

El-Hawat, A., Missallati, A.A., Bezan, A.M. and Taleb, T.M. 1996. The Nubian Sandstone in Sirt Basin and its correlatives. *First Symposium on the Sedimentary Basins of Libya, Geology of the Sirt Basin,* vol. 2. *(eds. M.J. Salem, A.S. El-Hawat and A.M. Sbeta),* Elsevier, Amsterdam, p. 3-20.

El-Hinnawy, M. and Cheshitev, G. 1975. Sheet Tarabulus (NI 33-13), Geological Map of Libya, scale 1:250,000, Explanatory Booklet, *Industrial Research Centre*, Tripoli.

Eliagoubi, B.A. and Powell, J.D. 1980. Biostratigraphy and palaeoenvironment of Upper Cretaceous (Maastrichtian) foraminifera of northcentral and northwestern Libya. *Second Symposium on the Geology of Libya,* vol. 1 *(eds. M.J. Salem and M.T. Busrewil),* Academic Press, London, p. 137-154.

El-Makhrouf, A.A. 1996. The Tibisti-Sirt orogenic belt, Libya, G.S.P.L.A.J. *First Symposium on the Sedimentary Basins of Libya, Geology of the Sirt Basin,* vol. 3. *(eds. MJ. Salem, M.T. Busrewil, A.A.Misallati and M.J. Sola),* Elsevier, Amsterdam, p. 137-154.

Fairhead, J.D. 1988. Mesozoic plate tectonic reconstructions of the central South Atlantic Ocean. The role of the West and central African rift system. *Tectonophysics* 15, 181–191

Fairhead, J.D. and Green, C. M., 1989. Controls on rifting in Africa and the regional tectonic model for the Nigeria and East Niger rift basins. In: B.R. Rosendahl (Editor), Rifting in Africa. 1. Afr. Earth Sci. Spec. Publ., 8(2-4): 231-249.

Fairhead, J.D., and Binks, R.M., 1991. Differential Opening of the Central and South-Atlantic Oceans and the Opening of the West African Rift System: *Tectonophysics*, 187, 191-203.

Farahat, E. S., Abdel Ghani, M. S., Aboazom, A. S. & Asranc, A. M. H. 2009. Mineral chemistry of Al Haruj low-volcanicity rift basalts, Libya: implications for petrogenetic and geotectonic evolution. *Journal of African Science*, 45, 198–212.

Finetti, I. 1984. Geophysical study of the Sicily Channel Rift Zone. *Bollettino di Geofisica Teorica ed Applicata,* XXXVI, 345–368.

Fodor, L., Turki, S.M., Dalob, H., Al-Gerbi, A., 2005. Fault-related folds and along-dip segmentation of breaching faults: syn-diagenetic deformation in the southwestern Sirt Basin, Libya. *Terra Nova* 17 (2), 121–128.

Fowler, A. C. and Yang, X. S. 1998. Fast and slow compaction in sedimentary basins, SIAM J. Appl. Math., 59, 365-385.

Fraser, W.W. 1967. Geology of the Zelten field, Libya, north Africa. *Proc. 7th World Pet. Cong. Mexico,*Elsevier, Amsterdam, vol. 2, p. 259-264.

Fry, N.1999. Striated faults: visual appreciation of their constraint on possible paleostress tensors. *J. Struct. Geo*., 21, 7-21.

Futyan, A. and Jawzi, A. H., 1996. The hydrocarbon habitat of the oil and gas fields of North Africa with emphasis on the Sirt Basin. In: *The Geology of the Sirt Basin*, II, Salem, M.J. El-Hawat A.S. and Sbeta A.M. (eds.). Elsevier, Amsterdam, 287-308.

Gabtni H., 2006. Caractérisation profonde et modélisation géophysique des zones de transition entre les différents blocs structurauxde la Tunisie centro-méridionale. *Ph.D. Thesis,* University Tunis El Manar, 243 pp.

Gamberlu, L. 2007. Regional Analysis of Jifarah Basin Using Remote Sensing and GIS Techniques. *Unpublished MSc Thesis*. Greenwich University, pp120.

Garfunkel, Z. 2004. Origin of the Eastern Mediterranean basin: a reevaluation. *Tectonophysics*, 391, 11-34.

Ghellali, S. M. 1977. On the geology of eastern Gefara plain, northwest Libya. *Ph.D. thesis*, university of Manchester, England.

Ghori, K.A.R. and Mohammed, R.A. 1996. The application of petroleum generation modelling to the eastern Sirt Basin, Libya. *First Symposium on the Sedimentary Basins*

of Libya, Geology of the Sirt Basin, vol. 2. *(eds. M.J. Salem, A.S. El-Hawat and A.M. Sbeta),* Elsevier, Amsterdam, p. 529-540.

Gillespie, J. and Sanford, R.M. 1967. The geology of the Sarir oilfield, Sirte Basin, Libya. *Proc. 7th World Pet. Cong. Mexico,* Elsevier, Amsterdam, vol. 2, p. 181-193.

Goudarzi, G., Smith, J.P., 1978. Preliminary structure contour map of the Libyan Arab Republic and adjacent areas; 1:2.000, 000. US Geological Survey. *Miscellaneous Geology Investigation MAP* I-350C.

Goudarzi, G.H. 1980. Structure-Libya. *In The Geology of Libya* Volume III, Salem, M.J., Busrewil (eds), *Academic Press, London* p. 879-891.

Gras, R., 1996. Structural style of the southern margin of the Messlah High, in Salem, M.J., El-Hawat, A.S., and Sbeta, A.M., eds., *The geology of Sirt Basin*: Amsterdam, Elsevier, **III**, 201–210.

Gras, R., and Thusu, B., 1998. Trap architecture of the Early Cretaceous Sarir Sandstone in the eastern Sirt Basin, Libya, *in* MacGregor, D.S., Moody, R.T.J., and Clark-Lowes, D.D., eds., Petroleum geology of North Africa: *Geological Society, Special Publication* 132, p. 317–334.

Gray, C. 1971. Structure and origin of the Gharian domes. *First Symposium on the Geology of Libya (ed.C. Gray).* Faculty of Science, University of Libya, Tripoli, p. 310-319.

Griffis, R. A., Gustafson, S. J., and Adams, H. G., 1985. PETFAB: user considerate FORTRAN-77 program for the generation and statistical evaluation of fabric diagrams: *Computers & Geosciences*, v. 11, no. 4, p. 369~409.

Groshong, R. H., Jr. 2006. 3-D structural geology—A practical guide to quantitative surface and subsurface map interpretation: *New York, Springer*, 400 p.

Gruenwald, R. 2001. The hydrocarbon prospectivity of Lower Oligocene deposits in the Maragh Trough, SE Sirt Basin, Libya. *Journ. Pet. Geol.* vol. 24, p.213-231.

Guasti, E., and Lüning, S., 2009. The Paleocene in North Africa – Sea-level Changes and Paleoproductivity in Tunisa, Libya and Egypt Using Microfossils (Extended abstract). *In 4th North African/Mediterranean Petroleum & Geosciences Conference & Exhibition. EAGE*, 2March 2009, Tunisia.

Guiraud R. and Bosworth, W. 1997. Senonian basin inversion and rejuvenation of rifting in Africa and Arabia: synthesis and implications to plate-scale tectonics. *Tectonophysics*, 282, 39-82.

Guiraud R. and Maurin J-CH. 1992. Early Cretaceous rifts of Western and Central Africa: an overview. *Tectonophysics*, 213, 153-168.

Guiraud R., Bellion, Y., 1995. Late Carboniferous to Recent geodynamic evolution of the West Gondwanian cratonic Tethyan margins. In: Nairn, A., Ricou, L.E., Vrielynck, B., Dercourt, J. (Eds.), *The Ocean Basins and Margins 8, the Tethys Ocean. Plenum Press, New York*, 101–124.

Guiraud, R., 1998. Mesozoic rifting and basin inversion along the northern African Tethyan margin: an overview, in D. S. MacGregor, Moody, R.T.J., Clark-Lowes, D.D., ed., *Petroleum Geology of North Africa, London, Geological Society Special Publication*, 132, 217-229.

Guiraud, R., Bellion, Y., Benkhlil, J. and Moreau, C. 1987. Post-Hercynian tectonic in Northern and Western Africa. *Geological Journal*, **22**, 433–466

Guiraud, R., Binks, R.M., Fairhead, J.D., and Wilson, M., 1992. Chronology and Geodynamic Setting of Cretaceous Cenozoic Rifting in West and Central Africa: *Tectonophysics*, 213, 227-234.

Guiraud, R., Issawi, B., Bosworth, W., 2001. Phanerozic history of Egypt and surrounding areas. In: Ziegler, P.A., Cavazza, W., Robertson, A.H.F., Crasquin-Soleau, S. (Eds.), Peri-Tethys Memoir 6: Peri-Tethyan Rift/Wrench Basins and Passive Margins. *Me´moires du Muse´um national d_Histoire naturelle* de Paris 186, pp. 469–509.

Gumati, Y.D. and Kanes, W.H. 1985. Early Tertiary subsidence and sedimentary facies-Northern Sirte Basin, Libya. *The American Association of Petroleum Geologists Bulletin*, 69, 39-52.

Gumati, Y.D., and Nairn, A.E.N., 1991. Tectonic subsidence of the Sirte Basin, Libya: *Jour. Petrol. Geol.*, 14, 93-102.

Gumati, Y.D., and S. Schamel, 1988. Thermal maturation history of the Sirte Basin, Libya: *Jour. Petrol.Geol.*, 11, 205-218.

Gumati, Y.D., Kanes, W.H. and Schamel, S. 1996. An evaluation of the hydrocarbon potential of the sedimentary basins of Libya. *Journ. Pet. Geol.* vol. 19, p. 39-52.

Gurney, J. 1996. Libya; the political economy of oil. *Oxford Institute of Energy Studies.* Oxford University Press. 241p.

Gustafsson, P. 1993. High resolution satellite imagery and GIS as a dynamic tool in groundwater exploration in a semi-arid area. *HydroGIS* 93: *Application of Geographic Information Systems In Hydrology and Water Resources* (proceedings of the Vienna Conferenre, April 1993). IAHS Publ. no. 211, 1993.

Guth, P. L., 1987. MICRONET: interactive equal area and equal angle nets: *Computers & Geosciences*, v. 13, no. 5, p. 541 543.

Hallett, D. 2002. Petroleum Geology of Libya. *Elsevier, Amsterdam*. 503p

Hallett, D. and El Ghoul, A. 1996. Oil and gas potential of the deep trough areas in the Sirt Basin. *In The Geology of Sirt Basin Volume* II, Salem, M.J., El-Hawat, A.S. and A.M. Sbeta (eds), Elsevier, Amsterdam 455-482.

Hamyouni, E. A., 1991. Petroleum source rock evaluation and timing of hydrocarbon generation, Murzuk Basin, Libya: *A case study, in M. J. Salem and M. N. Belaid, eds., Geology of Libya*, p. 183–211.

Hamyouni, E. A., I. A.Amr, M. A. Riani, A. B. El-Ghull, and S. A. Rahoma, 1984. Source and habitat of oil in Libyan basins: Presented at seminar on source and habitat of *petroleum in the Arab countries*, Kuwait, p. 125–178.

Hancock, P.L. 1985. Brittle microtectonics: principles and practice. *Journal of Structural Geology*, 7, 437-457

Harding, T. 1984. Graben hydrocarbon occurrences and structural style. *Bulletin of American Assiciation of Petroleum Geologists*, 68, 333-362.

Harding, T. P. 1983. Divergent wrench fault and negative flower structure, Andaman Sea. In Seismic expression of structure styles: A picture and work atlas, ed. A. W. Bally. *AAPG Studies in Geology Series*, 15. 3:4.2-1-9.

Harding, T. P., and Lowell, J. D., 1979. Structural styles, their plate-tectonic habitats, and hydrocarbon traps in petroleum provinces: *American Association of Petroleum Geologists Bulletin*, 63, 1016–1058.

Harding, T.P., 1985. Seismic characteristics and identification of negative flower structures, positive flower structures, and positive structural inversion. *Bull., Am. Assoc. Petrol. Geol.,* 69, 582-600.

Hintze, W., 1971. Depiction of faults on stratigraphic isopach maps *AAPG Bulletin*, June 1971, v. 55, p. 871-879

Hirono, T. 2000. Determination of slips sense along a fault in an unlithified sediment. *J.Struct. Geol*., 22, 537-541.

Holdsworth, R.E, Tavarnelli, E Clegg, P, Pinheiro, R.V.L, Jones, R.R & McCaffrey, K.J.W 2002. Domainal deformation patterns and strain partitioning during transpression: an example from the Southern Uplands terrane, Scotland. *Journal of the Geological Society* 159(4), 401-415.

Ibrahim, M. W., 1991. Petroleum Geology of the Sirt Group Sandstones, eastern Sirt Basin. In: The *Geology of Libya* III, Salem, M. J., Busrewil, M. T. Ben Ashour A. M. Elsevier, Amsterdam. 2757–2779.

Ivansson, S. (1985). A study of tomographic velocity estimation in the presence of low velocity zones. *Geophysics* 50:969–988.

Iverson, W.P., 1988. Crosswell logging for acoustic impedance: *Pet. Teeh. J*., 75-82.

Janssen, M. E., Stephenson, R.A., Cloetingh, S., 1993. Changes in plate motions and their control on the subsidence of rifted basin in the African plate, in M. *Thorweihe, Schandelmeier, H., ed., Geoscientific research in Northeast Africa,* Rotterdam, Balkema: p. 185-188.

Jerzykiewicz, T., Ghummed, M.A., Abugares, M.M. and Tshakreen S.O., 2002. Evolution of the Western Margin of the Sirt Basin of Libya in Late Cretaceous Time. Abstract, Extended Abstract and Talk at *CSPG Convention in Calgary*, Compact Disc and Abstract Volume, p. 179.

Johnson, B.A. and Nicoud, D.A. 1996. Integrated exploration for Beda reservoirs in the southern Zallah Trough (West Sirt Basin, Libya). *In The Geology of Sirt Basin Volume* II, Salem, M.J., El-Hawat, A.S. and A.M. Sbeta (eds), Elsevier, Amsterdam, 211-222.

Jones, H.L., 1992. Pre-Cretaceous to Early Tertiary geology of the Lehib to Jebel areas, and comparison of relevant strata with Zmam Formation type section, *Wadi Tar. Geological Report* 233. Sirte Oil Company, Libya, 7op.

Jongsma, D., van Hinte, J.E. and Woodside, J.M. 1985. Geologic structure and neotectonics of the North African Continental Margin south of Sicily. *Marine and Petroleum Geology*, 2, pp. 156-178.

Jurak, L., 1985. Sheet Wadi Bu Ash Shaykh (NH 33-12), Geological Map of Libya, scale 1:250,000, Explanatory Booklet, *Industrial Research Centre, Tripoli.*

Kingston, D., C. Dishroon, and P. Williams, 1983a. Global basin classification system: *AAPG Bulletin*, v. 67, p. 2175 – 2193.

Klemme, H.D. and Ulmishek, G.F. 1991. Effective petroleum source rocks of the world: stratigraphic distribution and controlling depositional factors. *Bull.Amer. Assoc. Pet. Geol.* vol. 75, p. 1809-1851.

Klett, T.R., 2001. Total petroleum systems of the Triassic/Ghadames province, Algeria, Tunisia, and Lybia—The Tenezzuft-Oyed Mya, Tanezzuft-Melrhir, and Tenezzuft-Ghadames. *US Geological Survey Bulletin* 2202-C, 22.

Klitgord, K.D. and Schouten, H., 1986. Plate kinematics of the Central Atlantic. In: B.E. Tucholke and P.P. Vogt (Editors), The Western North Atlantic Region. (*The Geology of North America,* M.) *Geol. Soc. Am., Boulder, Colo*., 351-378.

Klitzsch, E. 1963. Geology of the north-east flank of the Murzuk Basin (Djebel ben Ghnema-Dor el Gussa area). *First Saharan Symposium. Rev.* Inst. Fran. Pet. special volume, p. 97-113.

Klitzsch, E. 1971. The structural development of parts of north Africa since Cambrian time. In: C. Gray (ed). *First Symposium on the Geology of Libya Faculty of Science, University of Libya, Tripoli*, 253-262.

Klitzsch, E., 1970. Die Structurgeschichte der Zentralsahara: Neue Erkenntnisse zum Bau und der Palaeogeographie eines Tafellandes. *Geologische Rundschau*, 59 (2), p.459-527.

Knytl, J., Brydle, G. and Greenwood, D. 1996. Tectonic history and structural development of the Kaf-Themar trend of the western Sirt Basin. *First Symposium on the Sedimentary Basins of Libya, Geology of the Sirt Basin,* vol. 3. *(eds. M.J. Salem, M.T. Busrewil, A.A. Misallati and M.J. Sola),* Elsevier, Amsterdam, p. 167-200.

Kumati, S.M., 1981. The geology of the Hofra region, Sirte Basin, Libya (S.P.L.A.J.). Ph.D Thesis. University of Manchester, pp231.

Lambiase, J.J. and Bosworth, W. 1995. Structural controls on sedimentation in continental rifts. In Hydrocarbon habitat in rift basins (Lambiase, J.J. (Ed.). *Geological Society, London, Special Publication* 80, 117-144.

Lazzez, M., Zouaghi, T., Ben Youssef, M., 2008. Austrian phase on the northern African margin inferred from sequence stratigraphy and sedimentary records in Southern Tunisia (Chotts and Djeffara areas). *Tectonics* 340, 543–552.

Le Heron, D. P., & Thusu, B. 2007. Prospects in Libya's mature and frontier basins. *First break* vol. 25 Feb. 2007.

Lewis, C.J. 1990. Sarir Field. In: *Treatise of Petroleum Geology. Atlas of oil and gas fields, Structural Traps H (compiled by E.A. Beaumont and N.H. Foster).* Amer. Assoc. Pet. Geol. p. 253-267.

Litak, R.K., Barazangi, M., Beauchamp, W., Seber, D., Brew, G., Sawaf, T. & Al-Youssef, W. 1997. Mesozoic–Cenozoic evolution of the intraplate Euphrates fault system, Syria: implications for regional tectonics. *Journal of the Geological Society, London*, 154, 653–666.

Lovelock, P.E.R. 1984. A review of the tectonics of the northern Middle East region. *Geological Magazine*, 121, 577–587.

Macgregor, D.S. and Moody, R.T.J. 1998. Mesozoic and Cenozoic petroleum systems of North Africa. In: *Petroleum Geology of North Africa, (ed. D.S. Macgregor, R.T.J. Moody, D.D. Clark-Lowes),* Geol. Soc. Special Publication No. 132, p. 201-216.

Magnier, P. 1969. Etude lithostratigraphique du miocene inferieur du bassin de Syrte (Libye). *Com.Mediterr. Neogene strat. (4th session). Proc. Bologna Mus. Geol*, vol. 35, p. 119-130.

Mandl, G., 1988. Mechanics of Tectonic Faulting. Models and Basic Concepts. Elsevier, Amsterdam.

Mansour, A.T. and Magairhy, LA. 1996. Petroleum geology and stratigraphy of the southeastern part of the Sirt Basin, Libya. *First Symposium on the Sedimentary Basins*

of Libya, Geology of the Sirt Basin, vol. 2. *(eds. M.J. Salem, A.S. El-Hawat and A.M. Sbeta),* Elsevier, Amsterdam, p. 485-528.

Marovic´ , M. 2007. Structural Seting. In: Toljic´ , M., Turki, S. (Eds.), Geological Map of Libya 1:250 000. Sheet Wadi Blhashim (NG 34-1). Explanatory Booklet. *Industrial Research Center,* Tripoli. pp. 109–121.

Marrett, R. and Peacock, D.C.P., 1999. Strain and stress. Journal of Structural *Geology,* 21: 1057-1063.

McClay, K. R., and White, M., 1995. Analogue models of orthogonal and oblique rifting: *Marine and Petroleum Geology*, 12, 137–151.

Megeresi, M.F. and Mamgain, V.D. 1980. The Upper Cretaceous-Tertiary formation of northern Libya. In: Salem, M.J. and Busrewil, M.T. (Eds.). *The Geology of Libya, Academic Press, London,* 1, 91-96.

Meister, E. M., E. F. Ortiz, E. S. T. Pierobon, A. A. Arruda, and M. A. M. Oliveira, 1991. The origin and migration fairways of petroleum in the Murzuq Basin, Libya: An alternative exploration model, *in M. J. Salem, M. T. Busrewil, and A. M. Ben Ashour, eds., The Geology of Libya: Third Symposium on the Geology of Libya*, held at Tripoli, September 27–30, 1987: Amsterdam, Elsevier, v. 7, p. 2725–2742.

Memmi, L., Burollet, P.F., Viterbo, I., 1986. Lexique stratigraphique de la Tunisie, première partie: Précambrien et Paléozoïque. Notes du Service Géologique (Tunisie), No. 53, 64 pp.

Mengoli, S., Spinicci, G., 1985. Tectonic evolution of North Africa (from North Sinai to Algeria), in OAPEC, ed.: *Proceedings of the Seminar on source and habitat of petroleum in the Arab countries*, Oct 1984, 119-174.

Michael, A.J. 1987a. Use of focal mechanisms to determine stress: a control study. *J. Geophys. Res.*, 92, 357-368

Mikbel, S.R., 1979. Structural and configuration map of the basement of east and Central Libya: N. *Jb.Geol. Palaont. Abh*., 158, 209-200.

Montgomery, S.L. 1994. Sirte Basin, north-cetral Libya: prospects for the future. *Petroleum Frontiers, Pet. Inf. Corp., Littleton, Colorado,* vol. 11, no. 1, 94p.

Morley, C.K., 1995. Developments in the Structural Geology of Rifts over the Last Decade and Their Impact on Hydrocarbon Exploration: *Hydrocarbon Habitat in Rift Basins*, 1-32

Morley, C. K., C. Haranya, W. Phoosongsee, S. Pongwapee, A. Kornsawan, and N. Wonganan 2004. Activation of rift oblique and parallel pre-existing fabrics during extension and their effect on deformation style: Examples from the rifts of Thailand, *J. Struct. Geol.,* 26, 1803 – 1829.

Mouzughi, A. J. and Taleb, T.M., 1981. Tectonic elements of Libya, 1:2000,000. National Oil Corporation, Libay.

Parsons, M.G., Zagaar, A.M. and Curry, J.J. 1980. Hydrocarbon occurrences in the Sirte Basin, Libya. in Facts and principles of world petroleum occurrence, A.D. Miall (ed), *CSPG Memoir* 6, 723-732.

Pawellek, T. 2009. From thin section to discovery: the Upper Satal in the central Sirte Basin (north-central Libya) - a success story: *In the Geotectonic research* 96, 87-100.

Pawellek, T., 2007. A field guidebook to the geology of Sirt Basin, Libya. Gutenberg Press, Malta pp. 1-102. *RWE fieldtrip guidebooks*. Tripoli.

Pecher, 1989. Schmidtmac--a program to display and analyze directional data. *Computers & Geosciences* Vol. 15, No. 8, pp. 1315-1326, 1989

Peregi, Zs., Less, Gy., Konrád, Gy., Fodor, L., Gulácsi, Z., Gyalog, L., Turki, S. M., Suwesi, S. KH., Sherif, K., Dalub, H., 2003. Geological Map of Libya 1:250 000. Sheet Al Haruj al Abyad (NG 33-8). Explanatory Booklet. *Industrial Research Center*, Tripoli, 250 p.

Petite, J.P., 1987. Criteria for the sense of movement on fault surfaces in brittle rocks. *Journal of Structural Geology* 9, 597-608.

Pickford, M., 1991. Biostratigraphic correlations of the Middle Miocene mammal locality of Jabal Zaltan, Libya. In: The geology of Libya. M.J. Salem, A.M. Sbeta & M.R. Bakbak (eds), 1483-1490.

Pilant, W. L., 1989. A PC-interactive stereonet plotting program: *Computers & Geosciences,* v. 15, no. 1, p. 43-58.

Pindell, J., and Dewey, J.F. 1982. Permo-Triassic reconstruction of western Pangea and the evolution of the Gulf of Mexico/Caribbean region: *Tectonics*, 1, 179-211.

Piqué, A., Tricart, Guiraud, P., Laville, R.E., Bouaziz, S., Amrhar, S.M., Aït Ouali, R., 2002. The Mesozoic–Cenozoic Atlas belt (North Africa). *Geodyn. Acta* 15, 159–208.

Pollard, D.D., Saltzer, S.D. and Rubin, A.M., 1993. Stress inversion methods: are they based on faulty assumptions? *Journal of Structural Geology*, 15(8): 1045-1054.

Pratsch, J.C., 1991. Vertical hydrocarbon migration; a major exploration parameter: *Journal of Petroleum Geology*, v. 14' p. 429–444.

Price, L.C., 1980. Utilization and documentation of vertical oil migration in deep basins: *Journal of Petroleum Geology*, v. 2, p. 353–387.

Price, N.J., 1966. Fault and Joint Development in Brittle and Semi-brittle Rock. *Pergamon*, London.

Price, N.J., Cosgrove, J. W., 1990. Analysis of geological structures. Cambridge University Press, Cambridge, 502pp *Remote Sensing*, 18, No.6, p 1233-1244.

Prosser, S., 1993. Rift-related linked depositional systems and their seismic expression, in Williams, G. D., and Dobb, A, eds., Tectonics and seismic sequence stratigraphy: *Geological Society [London] Special Publication* 71, 35–66.

Rajesh, H.M., 2004. Application of remote sensing and GIS in mineral resource mapping - An overview: *Journal of Mineralogical and Petrological Sciences*, 99, p. 83-103.

Raulin, C., de Lamotte, D. F., Bouaziz, S., Khomsi, S., Mouchot, N. Ruiz, G., and Guillocheau, F. 2011. Late Triassic–early Jurassic block tilting along E–W faults, in southern Tunisia: New interpretation of the Tebaga of Medenine. *Journal of African Earth Sciences* 61 (2011) 94–104).

Roberts, J.M. 1970. Amal field, Libya. In: *Geology of giant petroleum fields, (ed. M.T. Halbouty). Mem. Amer. Assoc. Pet. Geol*. No. 14, p. 438-448.

Robertson Research Group, 1989. Petroleum Geochemical Evaluation of the Western Sirt Basin, Libya. Project No. RGPD/889/Ic/25285, Prepared for Mobil Oil Libya.

Robertson, A.H.F. & Dixon, J.E. 1984. Aspects of the geological evolution of the Eastern Mediterranean. In: Dixon, J.E. & Robertson, A.H.F. (eds) The Geologic

Evolution of the Eastern Mediterranean. *Geological Society, London, Special Publications*, 17, 1–74.

Rohlich, P.,1991. Tectonic development of Al Jabal al Akhdar, in Salem, M. J., and Busrewil, M. T., eds., *The geology of Libya*, 3: London, Academic Press, 923–931.

Roohi, M., 1996a. A geological view of source-reservoir relationships in the western Sirt Basin, *in* M. J. Salem, A. S. El-Hawat, and A. M. Sbeta, eds., *Geology of the Sirt Basin:* Amsterdam, Elsevier, v. 2, p. 323–336.

Roohi, M., 1996b. Geological history and hydrocarbon migration pattern of the central Az Zahrah–Al Hufrah platform, *in* M. J. Salem, A. S. El-Hawat, and A. M. Sbeta, eds., *Geology of the Sirt Basin*: Amsterdam, Elsevier, v. 2, p. 435–454.

Rosenbaum, G. Lister G. and Duboz, C., 2002. Relative motions of Africa, Iberia and Europe during Alpine orogeny, *Tectonophysics* 359

Rosendahl, B. R., 1987. Architecture of continental rifts with special reference to east Africa: *Annual Review of Earth and Planetary Sciences*, 15.

Rossetti, F., Storti, F., Salvini, F., 2000. Cenozoic noncoaxial transtension along thewestern shoulder of the Ross Sea, Antarctica, and the emplacement of McMurdodyke arrays. *Terra Nova* 12, 60-66.

Rossi, M. E., Tonna, M., and Larbash, M., 1991. Latest Jurassic–Early Cretaceous deposits in the subsurface of the eastern Sirt basin (Libya): Facies and relationships with tectonics and sea-level changes. *In The geology of Libya*, 6, Salem, M. J., Sbeta, A. M., and Bakbak, M. R., eds.,: Elsevier, Amsterdam, 2212–2225.

Rusk, D. C., 2001. Libya: Petroleum potential of the underexplored basin centers—A twenty-first-century challenge, *in* M.W. Downey, J. C. Threet, and W. A. Morgan, eds., Petroleum provinces of the twenty-first century: *AAPG Memoir* 74, p. 429–452.

Said, M. 1981. Sheet Bunjim (NH 33-7), *Geological Map of Libya, scale 1:250,000, Explanatory Booklet,* Industrial Research Centre, Tripoli.

Samir Bouaziz, Eric Barrier, Mohamed Soussi, Mohamed M. Turki d, He´di Zouari, 2002. Tectonic evolution of the northern African margin in Tunisia from paleostress data and sedimentary record. *Tectonophysics* 357 (2002) 227– 253

Sander, B., 1970. In: An Introduction to the Study of Fabrics of Geological Bodies, *Pergamon Press, Oxford (English edition).*

Sandford, R.M., 1970. Sarir oil field, Libya—Desert surprise, *in* Halbouty, M.T., ed., Geology of giant petroleum fields: *American Association of Petroleum Geologists Memoir* 14, p. 449–476.

Schäfer, K., Kraft, K.H, Hausler H. and Erdman, J. 1980. In situ stresses and paleostresses in Libya. In: N.J. Salem and M.T. Busrewil, Editors, *Geology of Libya, Al-Fateh Univ, Tripoli* (1981), 907–922.

Schroter, T. 1996. Tectonic and sedimentary development of the central Zallah Trough Western Sirt Basin, Libya. In: *The Geology of Sirt Basin* III, Salem, M.J., Busrewil, M.T., Misallati, A.A. and M.A. Sola (eds), Elsevier, Amsterdam 155-166.

Sclater, J.G. & Christie, P.A.F. 1980. Continental stretching: an explanation of the post-mid-Cretaceous subsidence of the Central North Sea Basin. *Journal of Geophysical Research*, 85, 3711–3739

Selley, R.C. 1971. Structural control of Miocene sedimentation in the Sirte Basin. *First Symposium on the Geology of Libya (ed. C. Gray).* Faculty of Science, University of Libya, Tripoli, p. 99-106.

Selley, R.C., 1997. The basins of Northwest Africa: Structural evolution. In: R. C. Selley (ed.), African Basins. *Sedimentary Basins of the World* 3. Elsevier, Amsterdam, 17-26.

Sengör, A. M. C. 1979. The north Anatolian transform fault: Its age, offset and tectonic significance. *Juurnal of the Geological Societ. J, London*, 136, 269-282.

Serpelloni, E., Vannucci, G. et al. 2007. Kinematics of the Western Africa-Eurasia plate boundary from focal mechanisms and GPS data. *Geophysical Journal International*, 169, 1180–1200.

Shaaban, F.F., and Ghoneim, A.E. 2001. Implication of seismic and borehole data for the structure, petrophysics and oil entrapment of Cretaceous-Palaeocene reservoirs, northern Sirt Basin, Libya. *Journal of African Earth Sciences,* Vol. 33, No 1, PP 103-133, 2001

Shan, Y., Li, Z., Lin, G., 2004a. A stress inversion procedure for automated recognition of polyphase fault/slip data sets. *Journal of Structural Geology* 26 (9), 919-925.

Shegewi,. O.M. 1992. Onshore and offshore basins of northeast Libya: their origin and hydrocarbon potential. In: Ph.D. *Thesis, Univ. South Carolina* (1992), p. 607.

Sperner, B., Ratschbacher L., Ott, R. 1993. Fault-Striae analysis: a Turbo Pascal program package for graphical presentation and reduced stress tensor calculation. *Comp. & Geosci.*, 19(9), 1361-1388.

Stampfli, 2001. In: G. Stampfli, Editor, Geology of the Western Swiss Alps, *A Guide-book, Mémoires de Géologie (Lausanne)* 36 (2001) 195 pp.

Starkey, J., 1977. The contouring of orientation data represented in spherical projection: *Can. Jour. Earth Sciences*, v. 14, no. 2, p. 268-277.

Stewart, R.R., 1990. Exploration seismic tomography: Fundamentals:Continuing Education Course Notes, *Society of Exploration Geophysicists*.

Storti, F., Rossetti, F., Salvini, F., 2001. Structural architecture and displacementaccommodation mechanisms at the termination of the Priestley Fault, northernVictoria Land, Antarctica. *Tectonophysics* 341, 141-161.

Suleiman, A.S. and. Doser, D.I. (1995). The seismicity, seismotectonics and earthquake hazards of Libya, with detailed analysis of the 1935 April 19, *M* = 7.1 earthquake sequence. *Geophys. J. Znt.* (1995) 120,312-322

Tawadros, E.E. 2001. Geology of Egypt and Libya. A.A. Balkema, Rotterdam, 468p.

Thomas, D. 1995a. Geology, Murzuk oil development could boost SW Libya prospects. *Oil and Gas Journ.* vol. 93, no. 10, p. 41-46.

Thomas, D. 1995b. Exploration limited since '70s in Libya's Sirte Basin. *Oil and Gas Journ.* vol. 93, no. 11, p. 99-104.

Threet, R.L., 1973. Classification of translational fault slip: *Geological Society of America Bulletin,* v. 84, p. 1825-1828.

Thusu, B., 1996. Implication of the discovery of reworked and in situ late Palaeozoic and Triassic palynomorphs on the evolution of Sirt Basin, Libya, in: Salem, M.J.,

Mouzughi, A.J., and Hammuda, O.S., eds., *The geology of Sirt Basin*; I.: Elsevier, Amsterdam, 455-474.

Tikoff, B., and S. F. Wojtal, 1999. Displacement control of geologic structures: *Journal of Structural Geology*, v. 21, p. 959 – 967.

Twiss R.J. & Unruh, J.R. 1998. Analysis of fault slip inversions: Do they constrain stress or strain rate? *Journal of Geophysical Research* 103, 12205-12222.

Unternehr, P., Curie, D., Olivet, J.L., Goslin, J. Beuzart, P., 1988. South Atlantic fits and intraplate boundaries in Africa and South America, *Tectonophysics*, **155**, 169–179.

Van de Weerd, A.A., Ware, P.L.G., 1994. A review of the east Algerian Sahara oil and gas province (Triassic, Ghadames and Illizi basins). *First Break* 12, 363–373.

Van der Meer, F. & Cloetingh, S. 1996. Intraplate stresses and the subsidence history of the Sirt Basin. *In the Geology of the Sirt Basin*, III, M.J. Salem, M.T. Busrewil, A.A. Misallati, & M.J. Sola (eds.), Elsevier, Amsterdam 211-230.

Van der Meer, F. and Cloetingh, S., 1993. Intraplate stresses and the subsidence history of the Sirte basin (Libya). *Tectonophysics*, 226, 37–58.

Van, Dijk P.M. and Eabadi A.M. 1996. Relay growth faulting and contemporaneous drape folding of the Ma'zul Ninah Formation in the southern extension of the Hun Graben, Western Sirt Basin, Libya. In: *The Geology of Sirt Basin* **III**, Salem, M.J., Busrewil, M.T., Misallati, A.A. and M.A. Sola (eds), Elsevier, Amsterdam 155-166.

Van Houten, F.B. 1980. Latest Jurassic-early Cretaceous regressive facies, northeast Africa craton. *Bull. Amer. Assoc. Pet. Geol.* vol 64, p. 857-867.

Van Houten, F.B., 1983. Sirte Basin, north-central Libya: Cretaceous rifting above a fixed mantle hotspot? *Geology*, 11, 115-118.

Vandycke, S., Bergerat, F., 2001. Brittle tectonic structures and palaeostress analysisin the Isle of Wight, Wessex basin, southern U.K. *Journal of Structural Geology* 23, 393-406.

Vesely, J., 1985. Sheet Zallah (NH 33-16), Geological Map of Libya, scale 1:250,000, Explanatory Booklet, *Industrial Research Centre, Tripoli*.

Viola, G., Ganerod, G.V., Wahlgren, C.H., 2009. Unraveling 1.5 Ga of brittle deformationhistory in the Laxemar-Simpevarp area, southeast Sweden: a contributionto the Swedish site investigation study for the disposal of highlyradioactive nuclear waste. *Tectonics* 28.

Viterbo, I. 1969. Lower Cretaceous charophyta from the subsurface 'Nubian complex' of the Sirte Basin, Libya. *Proc. 3rd Afr. Micropal. Colloq,* Cairo, p. 393-402.

Voight, B., 1966. Beziehung zwischen großen horizontalen Spannungen in Gebirge und der Tektonik und der Abtragung. In: Proc. 1st Congr. *Int. Soc. Rock Mech*., vol. 2, pp. 1e56. Lisbon.

Waddams, F.C. 1980. The Libyan oil industry. Croom Helm, London. 338p.

Wallace, R.E., 1951. Geometry of shearing stress and relation to faulting. *Journal of Geology* 59, 118- 130.

Walsh, J.J. and Watterson, J. 1987. Distribution of cumulative displacement and of seismic slip on a single normal fault surface. *J. Struct. Geol*., 9 (1987), pp. 1039–1046

Watterson, J. 1999. The Future of Failure: Stress or Strain?. *Journal of Structural Geology* 21, 939-948.

Wennekers, J.H.N., Wallace, F.K. and Abugares, Y.I. 1996. The geology and hydrocarbons of the Sirt Basin: a synopsis. *First Symposium on the Sedimentary Basins of Libya, Geology of the Sirt Basin,* vol. 1. *(eds. M.J. Salem, A.J. Mouzughi and O.S. Hammuda),* Elsevier, Amsterdam, p. 3-56.

Westaway, R. 1996. Active tectonic deformation in the Sirt basin and its surroundings. *First Symposium on the Sedimentary Basins of Libya, Geology of the Sirt Basin,* vol. 3. *(eds. M.J. Salem, M.T. Busrewil, A.A. Misallati and M.J. Sola),* Elsevier, Amsterdam, p. 89-100.

Williams, J.J. 1972. Augila field, Libya: depositional environment and diagenesis of sedimentary reservoir and description of igneous reservoir. In: *Stratigraphic oil and gas fields; classification exploration methods and case histories (ed. R.E. King).* Amer. Assoc. Pet. Geol. Mem. 16, p. 623-632.

Wilson M., and Guiraud R. 1992. Magmatism and rifting in Western and Central Africa from Late Jurassic to Recent times. *Tectonophysics* 213:1–23.

Wilson, B.M; Guiraud, R 1998. Late Permian to Recent magmatic activity on the Africa-Arabian margin of Tethys, In: MacGregor, D.S., Moody, R.T.J. and Clark-Lowes, D.D. (Ed) *Petroleum Geology of North Africa*, *Geological Society of London Special Publication*, **132**, 231-263.

Withjack, M. O., and W. R. Jamison 1986. Deformation produced by oblique rifting, *Tectonophysics*, 126, 99 – 124.

Yamaji, A., 2000. The multiple inverse method: a new technique to separate stresses from heterogeneous fault-slip data. *Journal of Structural Geology* 22 (4), 441e452.

Zhu, X., and McMechan, G.A., 1988. Acoustic modeling and migration of slacked cross-hole data: *Geophysics* 53, 492-500.

Ziegler, P.A., Van Wees, J.D., and Cloetingh, S., 1998. Mechanical controls on collision-related compressional intraplate deformation: *Tectonophysics*, v. 300, p. 103–129.

Ziegler, P. A., 1988. Evolution of the Arctic–North Atlantic and the western Tethys: *American Association of Petroleum Geologists Memoir* 43, 198 p.

Ziegler, P.A., 1992. Plate-Tectonics, Plate Moving Mechanisms and Rifting: *Tectonophysics*, 215, 9-34.

Zinati M. S., and Roohi, M. 2007. Late Tertiary Subsidence and Tilting in the Sirt Basin and their Seismic Signatures. *Pet. Res. Journ. Tripoli,* vol. 20, p. 59-76.